

**I. A STUDY OF THE DYNAMICS OF TRIPLET EXCITONS  
IN MOLECULAR CRYSTALS**

**II. AN INVESTIGATION OF DELAYED LIGHT EMISSION  
FROM Chlorella Pyrenoidosa**

Thesis by

Eldon Bruce Priestley

In Partial Fulfillment of the Requirements

For the Degree of

Doctor of Philosophy

California Institute of Technology

Pasadena, California

1970

(Submitted September 8, 1969)

To My Father and Mother



## ACKNOWLEDGMENTS

I wish to express my sincere appreciation to Professor G. Wilse Robinson, my research advisor, for his continued advice and encouragement throughout the course of the research described in this thesis.

Special thanks also goes to Drs. A. Haug and B. E. Kohler who, each in his own unique way, contributed so greatly to my scientific understanding and education. I have many fond memories of the hours spent in collaboration with both Alfred and Bryan.

I am indebted to Dr. P. L. Fehder for his expert counsel, always cheerfully given whenever a breakdown in communications occurred between myself and the computer.

The experimental work undertaken could not have been completed were it not for the extraordinary competence of the staffs of the Instrument and Glassworking Shops in the Chemistry Department at Caltech. Particular mention must be made of Bill Scheulke, Villy Jorgenson and Learco Minghetti whose assistance on so many occasions was absolutely indispensable.

The superb secretarial skills of Adria Larson eased the burden of manuscript preparation and correspondence, for which I am indeed grateful. I also wish to thank Joyce Lundstedt for the splendid job she did of typing this thesis.

Financial support from the California Institute of Technology during my four year stay is gratefully acknowledged.

Finally, and most important of all, I wish to thank my wife, Fern, for her continual encouragement and warm affection which contributed immeasurably to the success of my graduate career.

## ABSTRACT

### I. PREAMBLE AND SCOPE

Brief introductory remarks, together with a definition of the scope of the material discussed in the thesis, are given.

### II. A STUDY OF THE DYNAMICS OF TRIPLET EXCITONS IN MOLECULAR CRYSTALS

Phosphorescence spectra of pure crystalline naphthalene at room temperature and at 77° K are presented. The lifetime of the lowest triplet  $^3B_{1u}$  state of the crystal is determined from measurements of the time-dependence of the phosphorescence decay after termination of the excitation light. The fact that this lifetime is considerably shorter in the pure crystal at room temperature than in isotopic mixed crystals at 4.2° K is discussed, with special importance being attached to the mobility of triplet excitons in the pure crystal.

Excitation spectra of the delayed fluorescence and phosphorescence from crystalline naphthalene and anthracene are also presented. The equation governing the time- and spatial-dependence of the triplet exciton concentration in the crystal is discussed, along with several approximate equations obtained from the general equation under certain simplifying assumptions. The influence of triplet exciton diffusion on the observed excitation spectra and the possibility of using the latter to investigate the former is also considered. Calculations of the delayed

fluorescence and phosphorescence excitation spectra of crystalline naphthalene are described.

A search for absorption of additional light quanta by triplet excitons in naphthalene and anthracene crystals failed to produce any evidence for the phenomenon. This apparent absence of triplet-triplet absorption in pure crystals is attributed to a low steady-state triplet concentration, due to processes like triplet-triplet annihilation, resulting in an absorption too weak to be detected with the apparatus used in the experiments. A comparison of triplet-triplet absorption by naphthalene in a glass at 77° K with that by naphthalene- $\underline{h}_8$  in naphthalene- $\underline{d}_8$  at 4.2° K is given. A broad absorption in the isotopic mixed crystal triplet-triplet spectrum has been tentatively interpreted in terms of coupling between the guest  $^3B_{1u}$  state and the conduction band and charge-transfer states of the host crystal.

### III. AN INVESTIGATION OF DELAYED LIGHT EMISSION FROM Chlorella Pyrenoidosa

An apparatus capable of measuring emission lifetimes in the range  $5 \times 10^{-9}$  sec to  $6 \times 10^{-3}$  sec is described in detail. A cw argon ion laser beam, interrupted periodically by means of an electro-optic shutter, serves as the excitation source. Rapid sampling techniques coupled with signal averaging and digital data acquisition comprise the sensitive detection and readout portion of the apparatus. The capabilities of the equipment are adequately demonstrated by the results of a determination of the fluorescence lifetime of 5,6,11,12-tetraphenyl-

naphthacene in benzene solution at room temperature. Details of numerical methods used in the final data reduction are also described.

The results of preliminary measurements of delayed light emission from Chlorella pyrenoidosa in the range  $10^{-3}$  sec to 1 sec are presented. Effects on the emission of an inhibitor and of variations in the excitation light intensity have been investigated. Kinetic analysis of the emission decay curves obtained under these various experimental conditions indicate that in the millisecond-to-second time interval the decay is adequately described by the sum of two first-order decay processes. The values of the time constants of these processes appear to be sensitive both to added inhibitor and to excitation light intensity.

## TABLE OF CONTENTS

| SECTION | TITLE   | PAGE |
|---------|---|------|
| I.      | PREAMBLE AND SCOPE . . . . .  | 1    |
|         | References . . . . .  | 8    |
| II.     | A STUDY OF THE DYNAMICS OF TRIPLET EXCITONS<br>IN MOLECULAR CRYSTALS . . . . .          | 9    |
| A.      | THE PHOSPHORESCENCE SPECTRUM OF PURE<br>CRYSTALLINE NAPHTHALENE . . . . .               | 10   |
|         | 1. Introduction . . . . .   | 11   |
|         | 2. Kinetic Analysis . . . . .   | 12   |
|         | 3. Experimental . . . . .   | 15   |
|         | 4. Results . . . . .  | 17   |
|         | a. Phosphorescence Spectra . . . . .  | 17   |
|         | b. Triplet Exciton Decay Characteristics . . . . .                                      | 26   |
|         | c. Impurity Effects . . . . .   | 36   |
|         | 5. Discussion . . . . .   | 37   |
|         | 6. Addendum . . . . .   | 39   |
|         | References . . . . .  | 42   |
| B.      | DIFFUSION OF TRIPLET EXCITONS IN<br>CRYSTALLINE NAPHTHALENE AND<br>ANTHRACENE . . . . . | 46   |
|         | 1. Introduction . . . . .   | 47   |
|         | 2. Theoretical . . . . .  | 48   |

| SECTION | TITLE  | PAGE |
|---------|--|------|
|         | a. The Semi-Infinite-Crystal Diffusional Model . . . . .                                 | 49   |
|         | b. The Finite-Crystal Diffusional Model . . . . .  | 52   |
|         | c. The Finite-Crystal Annihilation Model . . . . .                                       | 54   |
|         | d. The Finite-Crystal Diffusional Annihilation Model . . . . .                           | 56   |
| 3.      | Experimental . . . . .   | 57   |
|         | a. The Apparatus . . . . .   | 57   |
|         | b. The Experimental Procedure . . . . .  | 57   |
|         | c. Sample Preparation . . . . .  | 58   |
| 4.      | Results . . . . .  | 59   |
|         | a. Naphthalene . . . . .   | 59   |
|         | b. Anthracene . . . . .  | 72   |
|         | c. The Spectral Distribution of the Exciting Light . . . . .                             | 72   |
| 5.      | Discussion . . . . .   | 77   |
| 6.      | Conclusions . . . . .  | 79   |
|         | References . . . . .   | 80   |
| C.      | ON THE APPARENT ABSENCE OF TRIPLET-TRIPLET ABSORPTION IN PURE ORGANIC CRYSTALS . . . . . | 82   |
|         | 1. Introduction . . . . .  | 83   |
|         | 2. Experimental . . . . .  | 84   |
|         | a. The Apparatus . . . . .   | 84   |
|         | b. The Experimental Procedure . . . . .  | 87   |

| SECTION | TITLE   | PAGE |
|---------|---|------|
|         | c. Sample Preparation . . . . .   | 90   |
| 3.      | Results . . . . .   | 91   |
|         | a. Naphthalene- $\underline{h}_8$ in 3-Methylpentane at 77° K . .                 | 91   |
|         | b. Naphthalene- $\underline{h}_8$ in Naphthalene- $\underline{d}_8$ at 4.2° K . . | 91   |
|         | c. Pure Crystalline Naphthalene . . . . .   | 95   |
| 4.      | Discussion . . . . .  | 95   |
|         | a. Naphthalene- $\underline{h}_8$ in 3-Methylpentane at 77° K . .                 | 97   |
|         | b. Naphthalene- $\underline{h}_8$ in Naphthalene- $\underline{d}_8$ at 4.2° K . . | 98   |
|         | c. Pure Crystalline Naphthalene . . . . .   | 100  |
| 5.      | Conclusions . . . . .   | 100  |
|         | References . . . . .  | 102  |
| III.    | AN INVESTIGATION OF DELAYED LIGHT EMISSION  |      |
|         | FROM <u>Chlorella Pyrenoidosa</u> . . . . .                                       | 106  |
| A.      | MEASUREMENT OF RAPID PHOTOPROCESSES   |      |
|         | USING A MODULATED cw LASER . . . . .  | 107  |
| 1.      | Introduction . . . . .  | 108  |
| 2.      | Principle of Operation . . . . .  | 110  |
| 3.      | Excitation System . . . . .   | 115  |
| 4.      | Signal Detection and Readout System . . . . .                                     | 118  |
| 5.      | Performance . . . . .   | 120  |
|         | a. Sample Preparation . . . . .   | 121  |
|         | b. Lifetime Determination . . . . .   | 122  |
| 6.      | Data Analysis for Arbitrary Decay Kinetics . . .                                  | 126  |
| 7.      | Conclusions . . . . .   | 127  |
|         | References . . . . .  | 128  |



| SECTION | TITLE   | PAGE |
|---------|---|------|
| B.      | THE DECAY KINETICS OF DELAYED EMISSION<br>FROM <u>Chlorella Pyrenoidosa</u> IN THE MILLI-<br>SECOND-TO-SECOND TIME INTERVAL . . . . . | 131  |
| 1.      | Introduction . . . . .  | 132  |
| 2.      | Experimental . . . . .  | 134  |
| a.      | Materials . . . . .   | 134  |
| b.      | Apparatus . . . . .   | 135  |
| 3.      | Results and Discussion . . . . .  | 135  |
|         | References . . . . .  | 143  |
| IV.     | APPENDICES . . . . .  | 145  |
| A.      | EXPERIMENTAL . . . . .  | 146  |
| 1.      | Equipment . . . . .   | 146  |
| a.      | Variable Speed Phosphoroscope . . . . .   | 146  |
| b.      | Coolable Photomultiplier Housing . . . . .  | 154  |
| c.      | Optical Bench Support Assembly . . . . .  | 154  |
| d.      | Light Tunnel Assembly . . . . .   | 159  |
| e.      | Rotary Refractor Plate Assembly . . . . .   | 170  |
| 2.      | Procedures . . . . .  | 175  |
| a.      | Purification of Anthracene . . . . .  | 175  |
| b.      | Purification of Naphthalene . . . . .   | 180  |
| B.      | CONCERNING THE DECAY KINETICS OF EXCITED<br>STATES . . . . .  | 183  |
| 1.      | Continuous Excitation . . . . .   | 184  |
| 2.      | Periodic Excitation . . . . .   | 186  |
| 3.      | Conclusions . . . . .   | 190  |

| SECTION | TITLE   | PAGE |
|---------|---|------|
| C.      | NUMERICAL METHODS . . . . .   | 198  |
| 1.      | Initialization of Lifetime Data . . . . .   | 198  |
| 2.      | Fitting a Kinetic Scheme to the Data . . . . .  | 199  |
| 3.      | Solution of the Triplet Excitation Diffusion<br>Equation . . . . .                          | 200  |
| 4.      | Calculation of the Delayed Fluorescence and<br>Phosphorescence Excitation Spectra . . . . . | 203  |
| 5.      | Fitting the Calculated Excitation Spectra to<br>those Obtained Experimentally . . . . .     | 204  |
|         | References . . . . .  | 206  |
| D.      | PROGRAM LISTINGS . . . . .  | 207  |
| V.      | PROPOSITIONS . . . . .  | 254  |

**PART I**

**PREAMBLE AND SCOPE**

The first part of this thesis describes several experiments aimed primarily at providing a better understanding of the dynamics of triplet excitons in organic molecular crystals.<sup>1-4</sup> The processes of particular interest are those associated either directly or indirectly with the existence of these mobile, neutral, electronically excited triplet states of the crystal. In fact, it is principally the mobility of triplet excitons that gives rise to much of the interesting excitation dynamics, unique to the crystalline state, with which we shall be concerned. Consequently, considerable emphasis is placed on room temperature measurements since at temperatures in this range the excitons are essentially free, whereas at low temperature they are effectively immobilized due to complicated trapping effects. Only brief mention is made of the process of generating triplet excitons, the principal concern being with what befalls them after they are already in existence. Specifically, the processes of first-order radiative decay (phosphorescence), second-order radiative annihilation (delayed fluorescence), absorption of additional light quanta by the triplet excitons (triplet-triplet absorption) and energy transfer (diffusion) are each considered at length. Also finding their way into the discussion are the ever-present, if somewhat less exciting, nonradiative decay mechanisms (quenching).

Naphthalene was chosen as the model system for most of the experiments although anthracene was employed occasionally. Both molecules have  $D_{2h}$  symmetry, crystallize in the monoclinic system with space group  $C_{2h}^5$  and have two molecules per unit cell, so that

almost all of the concepts applicable to one apply equally well to the other.

A brief summary of the basic concepts of exciton theory, as it applies to molecular crystals,<sup>1,4</sup> is presented here to provide a background for the more detailed discussions of various aspects of the theory that appear in subsequent sections. Molecular crystals are held together by weak Van der Waals forces, making it possible to regard the intermolecular interactions as a small perturbation on the oriented array of molecules. Due to these small but finite intermolecular forces, it is impossible to construct a stationary state for a perfect crystal in which one particular molecule is excited. Rather, the correct zero-order states for a crystal with one quantum of excitation correspond to a delocalization of the energy over the entire crystal. It is convenient to describe the quantum of excitation as an exciton of momentum  $\hbar\vec{k}$  which propagates through the crystal with a velocity determined by the magnitude of the intermolecular interactions. Also dependent upon the magnitude of these interactions is the extent to which the molecular energy levels are altered in the crystal. When the intermolecular interactions are weak, as they are in molecular crystals, the electronic energy levels of the crystal are traceable to parent molecular levels. Consequently, there is a one-to-one correspondence between the excited states of the free molecule and the neutral exciton states of the crystal. It is therefore a convenient and commonly accepted practice to label each of the crystal exciton states by the symmetry designation of the parent energy level of the free molecule.

Using this designation we identify the ground state ( $^1A_g$ ), the lowest excited singlet state ( $^1B_{2u}$ ) and the lowest excited triplet state ( $^3B_{1u}$ ) of naphthalene. The  $^1A_g - ^1B_{2u}$  and  $^1A_g - ^3B_{1u}$  energy intervals, averaged over the two Davydov components in both cases, are  $31,554 \text{ cm}^{-1}$  and  $21,209 \text{ cm}^{-1}$ , respectively. The corresponding energy separations,  $^1A_g - ^1B_{1u}$  and  $^1A_g - ^3B_{1u}$ , in crystalline anthracene are  $25,400 \text{ cm}^{-1}$  and  $14,750 \text{ cm}^{-1}$ , respectively.

The Hamiltonian for a crystal containing  $N$  unit cells and  $h$  molecules per unit cell can be written in the form

$$\mathcal{H} = \sum_{\mu=1}^h \sum_{k=1}^N H_{k\mu} + \sum_{k\mu < \ell\nu} V_{k\mu, \ell\nu} \quad (1)$$

where the double indices  $k\mu$  and  $\ell\nu$  label different molecules,  $H_{k\mu}$  is the Hamiltonian for an isolated molecule and  $V_{k\mu, \ell\nu}$  is the pairwise intermolecular interaction. Since the coupling between molecules is small compared to the intramolecular interactions, the Heitler-London formalism may be used. The ground state of the crystal, then, has the form

$$\Psi^0 = \mathcal{A} \prod_{k\mu=1}^{Nh} \phi_{k\mu}^0 \quad (2)$$

where  $\phi_{k\mu}^0$  are the ground state antisymmetrized wave functions of the individual molecules and  $\mathcal{A}$  is the antisymmetrization operator permuting electrons between the molecules.

The symmetry adapted wave functions corresponding to the  $f$ th excited state of the crystal are given by

$$\Psi_i^f = \frac{1}{\sqrt{h}} \sum_{\mu=1}^h B_{\mu}^i \Phi_{\mu}^f \quad (3)$$

where

$$\Phi_{\mu}^f = \left(\frac{h}{N}\right)^{\frac{1}{2}} \sum_{m=1}^N \exp(i\vec{k} \cdot \vec{r}_{m\mu}) \psi_{m\mu}^f \quad (4)$$

and

$$\psi_{m\mu}^f = \mathcal{A} \phi_{m\mu}^f \prod_{\nu \neq m\mu} \phi_{\nu}^0 \quad (5)$$

In constructing the exciton states, Eq. (3), use has been made of the fact that the Hamiltonian is characterized by the full symmetry of the crystal, so that each of these states belongs to an irreducible representation of the crystal space group. The coefficients  $B_{\mu}^i$  can be found either by diagonalizing the  $h \times h$  secular determinant or by using the symmetry properties of the group of the wave vector. The functions  $\Phi_{\mu}^f$  are known as one-site excitons and  $\vec{r}_{m\mu}$  is the vector from the origin to the center of molecule  $m\mu$ . We observe that  $\psi_{m\mu}^f$ , representing excitation localized on a single molecule  $m\mu$ , are not eigenfunctions of the crystal Hamiltonian, Eq. (1), because of the pairwise intermolecular interaction term  $V$ .

The exciton states (3) correspond to an elementary excitation modulated by a plane wave, or simply to an elementary excitation moving from site to site in the crystal. A rough estimate of the excitation transfer time  $\tau_t$  between adjacent sites, provided the

magnitude of  $V$  is known, can be obtained from the uncertainty principle,

$$\tau_t \approx \frac{\hbar}{V} \quad . \quad (6)$$

Clearly, the velocity of the exciton is proportional to the pairwise intermolecular interaction  $V$ . Finally, we note that if the "elementary excitation" mentioned above happens to correspond to an electronic triplet state, the resulting mobile excitation is a triplet exciton whose dynamical properties are the subject of the first part of the thesis.

The remainder of the thesis is concerned with an experimental investigation of the properties of light emitted from Chlorella pyrenoidosa between 10 nsec and roughly 1 sec after termination of the excitation light.<sup>5</sup> Emission occurring in this time interval is customarily qualified by the word "delayed" to distinguish it from "prompt" fluorescence emission which is characterized by a much shorter lifetime, on the order of 1 nsec. All of this emitted light, prompt and delayed, represents excitation energy that is not utilized in the complex photochemical transformations which together constitute the process known as photosynthesis. While this emitted light may be viewed essentially as a useless by-product of photosynthesis, it has been shown to be intimately coupled to the photosynthetic process. Thus, a detailed investigation of the behavior of the emitted light is almost certain to provide valuable insight into the workings of the photosynthetic apparatus. The delayed emission is especially useful



in this respect since much of it is emitted over periods of time characteristic of photochemical reactions. The 2 to 3% total quantum efficiency for emission from Chlorella, though small, is of sufficient magnitude to permit detection of delayed emission, which constitutes only a small fraction of the total emitted light, even at excitation power densities as low as  $1\mu\text{W}/\text{cm}^2$ . Consequently, it is possible to conveniently study the properties of delayed light emission using excitation intensities for which photosynthesis is known to proceed normally.

The measurements described in the latter part of the thesis are the result of an effort to determine the complete time course curve of the emission decay over the region from  $10^{-8}$  sec to 1 sec. Reasonably sophisticated instrumentation is required for this purpose, especially for the measurement of emission decay components lasting less than a microsecond. Up to the time of writing, an apparatus having sufficient time resolution to permit measurement of emission lifetimes anywhere in the range  $5 \times 10^{-9}$  sec to  $6 \times 10^{-3}$  sec has been successfully constructed and tested. Details of this apparatus and its operation are presented. In addition, the interval from 1 msec to 1 sec has been subjected to extensive investigation using a standard phosphoroscope, and the results of these measurements are also discussed.

REFERENCES

1. A. S. Davydov, Theory of Molecular Excitons, trans. M. Kasha and M. Oppenheimer, Jr. (McGraw-Hill Book Company, Inc., New York, 1962).
2. D. L. Dexter and R. S. Knox, Excitons (John Wiley and Sons, Inc., Interscience, New York, 1965).
3. R. S. Knox, Theory of Excitons (Academic Press Inc., New York, 1963).
4. D. P. Craig and S. H. Walmsley, Excitons in Molecular Crystals (W. A. Benjamin Inc., New York, 1968).
5. R. K. Clayton, Molecular Physics in Photosynthesis (Blaisdell Publishing Co., New York, 1965).

**PART II**

**A STUDY OF THE DYNAMICS OF TRIPLET  
EXCITONS IN MOLECULAR CRYSTALS**

SECTION A

PHOSPHORESCENCE SPECTRUM OF PURE  
CRYSTALLINE NAPHTHALENE

The following is the text of a paper published in the  
Journal of Chemical Physics

[E. B. Priestley and A. Haug, J. Chem. Phys. 49, 622 (1968)]

## 1. INTRODUCTION

It is of interest to detect phosphorescence from pure organic molecular crystals since it would provide essentially the first direct means of studying the dynamic properties of the triplet exciton in these systems. In the past, certain characteristics of the triplet state have been inferred from an analysis of the delayed fluorescence,<sup>1,2</sup> considered to arise primarily from the annihilation of two triplet excitons with the subsequent production of a fluorescing singlet exciton. However, it must be realized that at best delayed fluorescence provides an indirect probe, and in this respect may be less relevant than phosphorescence for determining the triplet-state behavior.

Formerly, it has been possible to detect phosphorescence from aromatic hydrocarbons only if the molecules were in the form of isotopic mixed crystals at 4.2° K,<sup>3</sup> or else in rigid glasses at 77° K.<sup>4,5</sup> The apparent absence of pure crystal phosphorescence has indeed been the subject of considerable speculation<sup>1a,6</sup> and, while plausible explanations can be advanced to account for its weakness, there is no reason in principle that actually forbids phosphorescence emission from pure crystals. The question reduces to whether or not the slow phosphorescence emission is detectable in the presence of often overwhelmingly fast processes that rapidly deplete the triplet state non-radiatively.

Recently, several papers have appeared in the literature<sup>7-9</sup> reporting phosphorescence from anthracene crystals at temperatures

ranging from  $4.2^{\circ}$  K to room temperature. There are, however, two main reasons why naphthalene is more suitable for a study of phosphorescence from the crystalline state than is anthracene. First of all, naphthalene can be highly purified by known techniques<sup>10</sup> while no reliable method, aside from extensive zone melting, is known for the purification of anthracene. A more rigorous purification procedure that reduces impurities to about 1 part in  $10^7$  has been developed<sup>10, 11</sup> for benzene and naphthalene. It should be noted that for these molecules even extensive zone melting by itself does not lower the impurity level sufficiently to permit reliable spectroscopic studies of pure crystals. Secondly, the ground state to first triplet state interval is significantly larger in naphthalene ( $21,209\text{ cm}^{-1}$ ) than in anthracene ( $14,750\text{ cm}^{-1}$ ), which, according to the theory of Robinson and Frosch,<sup>12</sup> should result in considerably smaller nonradiative losses from the triplet state in the case of naphthalene. Consequently, one expects the radiative decay to be more intense in naphthalene than in anthracene.

The purpose of this paper is to report the phosphorescence spectrum and also the lifetimes of the phosphorescence and delayed fluorescence decays from pure crystalline naphthalene both at room temperature and at  $77^{\circ}$  K.

## 2. KINETIC ANALYSIS

The rate equation for the concentration of triplet excitons in the crystal is well known<sup>1, 2</sup> and, replacing the source by the initial value condition  $n = n_0$  at  $t = 0$ , can be written

$$-dn/dt = \beta n + \gamma' n^2 - \frac{1}{2} \alpha \gamma' n^2, \quad (1)$$

where  $\beta$  is the unimolecular decay constant ( $\beta^{-1}$  being the triplet state lifetime),  $\gamma'$  is the rate constant for triplet-triplet annihilation, and  $\alpha$  is the fraction of triplet-triplet annihilation events that ultimately gives back triplets.<sup>13</sup> Rewriting Eq. (1) in a slightly different form yields

$$-dn/dt = \beta n + \gamma n^2, \quad (2)$$

where  $\gamma = (1 - \alpha/2)\gamma'$ . Solving Eq. (2) leads to a triplet concentration,

$$n = \beta n_0 / [(\beta + \gamma n_0) \exp(\beta t) - \gamma n_0]. \quad (3)$$

For long times, i. e., for  $t \gg \beta^{-1}$ ,

$$n = \left( \frac{n_0}{1 + (\gamma/\beta)n_0} \right) \exp(-\beta t). \quad (4)$$

If a fraction  $A$  of the first-order decay is radiative, the phosphorescence intensity  $I_p$  is

$$I_p = A\beta n = \left( \frac{A\beta n_0}{1 + (\gamma/\beta)n_0} \right) \exp(-\beta t). \quad (5)$$

Furthermore, assuming that a fraction  $B$  of the triplet-triplet annihilation events result in the production of a fluorescing singlet exciton, we can write for the intensity of delayed fluorescence,

$$I_{df} = \frac{1}{2}(B\gamma)n^2 = \frac{1}{2}(B\gamma) \left( \frac{n_0}{1 + (\gamma/\beta)n_0} \right)^2 \exp(-2\beta t). \quad (6)$$

Evidently, comparing Eqs. (5) and (6), a plot of the logarithm of intensity vs time for phosphorescence and delayed fluorescence should yield slopes that differ by a factor of 2 for times long compared with  $\beta^{-1}$ . Assuming that steady state is reached during the duration of the excitation interval, it can be shown that the initial concentration of triplet excitons  $n_0$  is given by,

$$n_0 = \beta \left( \frac{(1 + 4\gamma k I_0 / \beta^2)^{1/2} - 1}{2\gamma} \right) , \quad (7)$$

where  $k$  is the rate constant for production of triplets and  $I_0$  is the incident light intensity. Combining Eqs. (3) and (5)-(7), we have for  $t=0$ ,

$$(I_{df}/I_p)_{t=0} = (B/4A) [ (1 + 4\gamma k I_0 / \beta^2)^{1/2} - 1 ] . \quad (8)$$

Equation (8) reduces, in the case of low light intensity, to

$$(I_{df}/I_p)_{t=0}^l = (B/2A)(\gamma k I_0 / \beta^2) , \quad (9)$$

and, in the case of high light intensity, to

$$(I_{df}/I_p)_{t=0}^h = (B/2A)(\gamma k I_0 / \beta^2)^{1/2} . \quad (10)$$

The ratio of the delayed fluorescence intensity to the phosphorescence intensity is seen to be dependent on the incident light intensity in both limits.



### 3. EXPERIMENTAL

Light from an Osram 6500-W xenon arc lamp was passed through a 5-cm quartz cell containing a  $\text{NiSO}_4$ - $\text{CoSO}_4$ -water filter solution<sup>14</sup> and the filtered light was used to excite the crystal, located at the center of a cylindrical phosphoroscope. The phosphoroscope was 20 cm in diameter and through reduction pulleys could be operated at several speeds from about 30 to 1725 rpm with less than 2% drift in the frequency. The excitation and observation periods were of equal length and ranged from 0.9 sec at the lowest speed to 15.9 msec at the highest speed. Dead time between excitation and observation varied from 83 to 1.4 msec over the range of phosphoroscope speeds. For spectral measurements the highest speed was used, whereas in the case of lifetime determinations the speed was chosen so as to give excitation and observation intervals equal to more than three lifetimes in all cases.

The crystal emission in the region from 4500 to 5400 Å was passed through Corning glass filters C. S. 3-72 and C. S. 3-73 and focused onto the slit of a Jarrell-Ash Model 82-000, 0.5-m Ebert scanning spectrometer. This instrument was equipped with a grating blazed at 5000 Å in first order, having a reciprocal linear dispersion of 16 Å/mm and effective aperture ratio of f/8.6. The slitwidth was set at 0.4 mm.

Light emerging from the exit slit of the spectrometer was collected on the cathode of a dry-ice cooled EMI 6256 SA photomultiplier by means of appropriate condensing optics. The photomultiplier output was fed into a Victoreen Model VTE-1 electrometer where it was

amplified and the spectrum was recorded on a stripchart recorder.

In determining the lifetime of the emission at a given wavelength, the photomultiplier signal was first amplified to about 1 V and then fed into the time base unit of a Nuclear Data Model ND 180 multi-channel analyzer system operated in the averaging mode. This unit was triggered synchronously with the phosphoroscope by means of the output from a photodiode activated once per revolution at the beginning of the observation period. After averaging the raw signal over  $10^5$  counts, the resulting almost noise-free decay curve was plotted on a Hewlett-Packard model 7590C X-Y recorder.

Measurements, both of the spectrum and of the lifetime, of delayed fluorescence were also made. For these measurements it was necessary only to remove the Corning glass filters C.S. 3-72 and C.S. 3-73.

Great care had to be taken in all experiments to minimize scattered light. To this end the phosphoroscope, spectrometer, and photomultiplier were enclosed in a light-tight box to eliminate scattered light from around the room. Moreover, within the light-tight box, both the excitation light and the emitted light were confined inside metal tubes that also housed the required optics. The following independent checks for scattered light were made both in the presence and absence of the Corning glass filters C.S. 3-72 and C.S. 3-73 to ensure that the precautions taken were sufficient to permit detection of the weak signals. For these checks, an empty sample cell was substituted for the sample in order to simulate the actual experimental conditions as closely as possible.

(1) Kodak 103a-O plates, taken using the second order of a 600-line/mm Bausch & Lomb grating in a 2-m Czerny-Turner mount (effective aperture ratio  $f/11$ ) showed no darkening on exposures up to 1 h.

(2) Not even a dc level was evident when  $10^6$  counts were made with the multichannel analyzer.

(3) Spectrometer traces made by scanning the 0.5-m spectrometer through the spectral region of interest exhibited only a straight baseline.

The crystals were melt grown from naphthalene that had been purified by a process developed in our laboratory and described elsewhere.<sup>10,11</sup> Crystals from three independent purification lots all exhibited similar lifetime and spectral characteristics.

## 4. RESULTS

### a. Phosphorescence Spectra

The phosphorescence spectrum of pure crystalline naphthalene at room temperature and at 77° K is shown in Figs. 1 and 2, respectively. For the purpose of comparison, the phosphorescence spectrum of a  $7.4 \times 10^{-3}$  M solution of naphthalene in 3-methylpentane at 77° K is presented in Fig. 3. The spectra of the glass at 77° K and of the crystal at room temperature are seen to be qualitatively the same except that the maxima of the former are shifted to higher energy by about  $70 \text{ cm}^{-1}$ . All the spectra have been reproduced just as they were

Figure 1. Typical phosphorescence spectrum of pure crystalline naphthalene ( $C_{10}H_8$ ) at 300° K. The sample used in this case had been initially zone-refined (25 passes), twice potassium purified, and then further zone-refined (45 passes). The input range on the electrometer was  $10^{-9}$  A with a 3-sec time constant. Scan rate was 50 Å/min and the photomultiplier was operated at 1600 V.

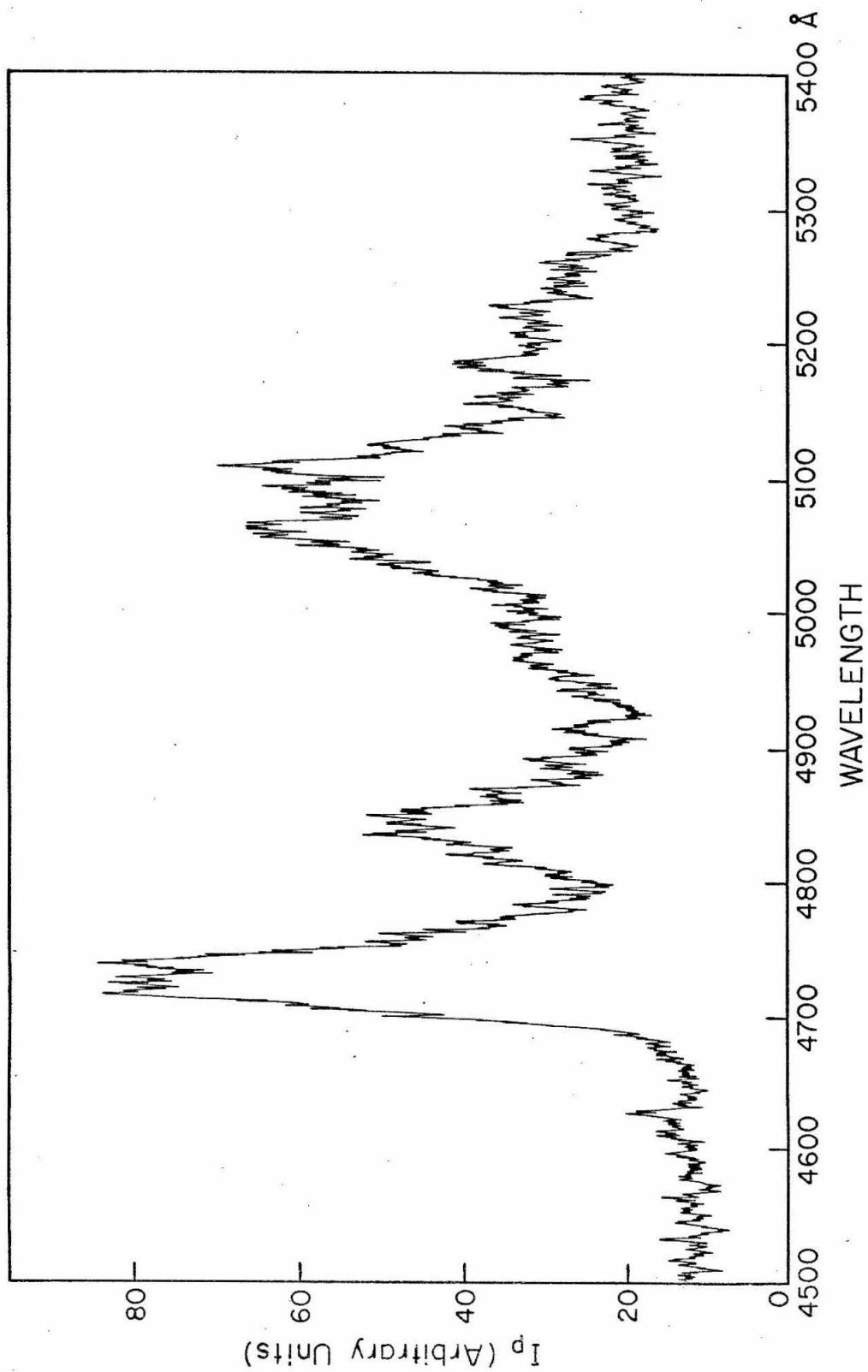


Figure 2. Phosphorescence spectrum of pure crysatlline naphthalene ( $C_{10}H_8$ ) at  $77^\circ K$ . The sample that gave this spectrum had been treated as that in Fig. 1, except it was subjected to 3 potassium treatments and 60 passes in the final zone-refining. Electrometer input range was  $10^{-8}$  A with a 3-sec time constant, the scan rate was 20 Å/min and the photomultiplier was operated at 1900 V. To compare with Fig. 1, peak heights in Fig. 2 must be multiplied by roughly 2.

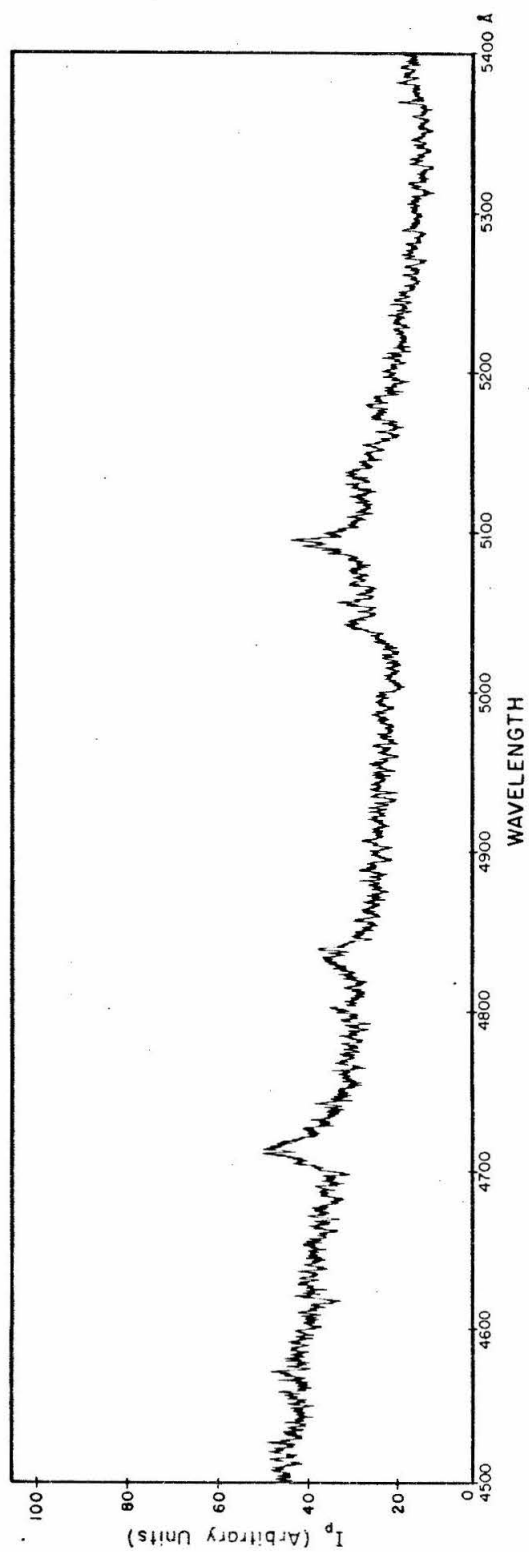
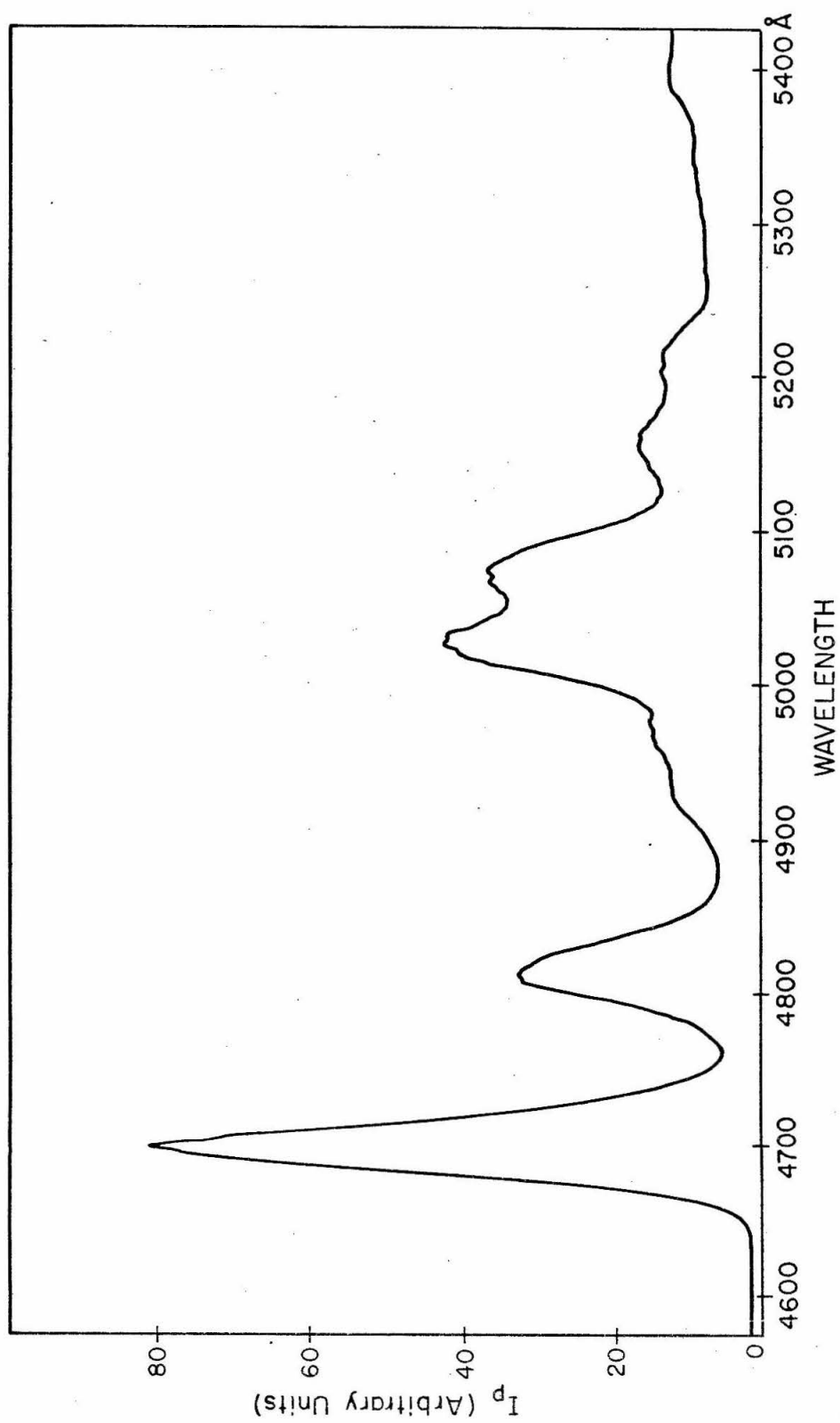


Figure 3. The phosphorescence spectrum of naphthalene in 3-methylpentane ( $7.4 \times 10^{-3}$  M solution) at  $77^\circ$  K. Input range on the electrometer was  $10^{-7}$  A with a 3-sec time constant. Scan rate was 50 Å/min and the photomultiplier voltage was 1300 V.





observed and have not been corrected for photomultiplier or spectrometer response.

Table I summarizes the spectral results and also presents isotopic mixed-crystal phosphorescence data<sup>15</sup> and ground-state vibrational frequencies as determined from gas-phase fluorescence measurements.<sup>16</sup> In view of the fact that the position of the 0, 0 transition as well as the vibrational frequencies are in excellent agreement with the isotopic mixed-crystal data, there can be little doubt that the spectrum is indeed due to naphthalene and not impurities.

With regard to impurities, the position of the 0, 0 of phosphorescence of  $\beta$ -methyl naphthalene, which is known<sup>17</sup> to lie at 4785 Å, is of particular interest since  $\beta$ -methyl naphthalene is one of the most difficult impurities to remove. This is clearly in a region where little or no emission is observed from our crystals. See Fig. 2. One sample did show an unidentified emission line at 5390 Å at 77° K. Since this line did not appear at room temperature and since it was present in only one sample, it is attributed to an impurity. Lipsett and MacPherson<sup>17</sup> also reported having observed emission from naphthalene crystals at this wavelength, and they too assigned it to an unidentified impurity.

Comparing Figs. 1 and 2, it can be seen that the half-intensity width of the 0, 0 transition is 270 cm<sup>-1</sup> at room temperature and narrows to about 75 cm<sup>-1</sup> at liquid-nitrogen temperature. Comparable narrowing of the other peaks is also evident although it is difficult to determine a half-width for these peaks at room temperature due to overlap of two or more vibronic lines. It is seen that the complex

TABLE I. Phosphorescence lines from crystalline naphthalene ( $C_{10}H_8$ ) at 300° and 77° K.

| Pure-crystal phosphorescence <sup>a</sup>  |   |                 |                  |   |                 | Mixed-crystal phosphorescence <sup>b</sup> |                                    |      |                 | Ground-state<br>fundamental<br>vibrational<br>frequencies <sup>c</sup> |
|--|---|-----------------|------------------|---|-----------------|--|------------------------------------|------|-----------------|--|
| 300° K   |   |                 | 77° K            |   |                 |  |                                    |      |                 |  |
| $\lambda$<br>(Å)   | $\nu_{\text{vac}}$<br>(cm <sup>-1</sup> ) | I <sup>d</sup>  | $\lambda$<br>(Å) | $\nu_{\text{vac}}$<br>(cm <sup>-1</sup> ) | I <sup>d</sup>  | $\nu_{\text{vac}}$<br>(cm <sup>-1</sup> )  | $\Delta\nu$<br>(cm <sup>-1</sup> ) | I    | Assignment      |  |
| 4715   | 21 203                                    | 100             | 4714             | 21 207                                    | 100             | 21 208                                     | 0                                  | >90  | 0, 0            | 0  |
| 4812(?)  | 20 776(?)                                 | 40              | 4803             | 20 815                                    | 35              | 20 816                                     | 392                                | 77   | b <sub>1g</sub> | 392  |
|  |   |                 |                  |   |                 | 20 698                                     | 510                                | >90  | b <sub>3g</sub> | 506  |
| 4835   | 20 677                                    | 50              | 4834             | 20 681                                    | 60              | 20 696                                     | 512                                | >90  | a <sub>1g</sub> | 516  |
| 5042   | 19 828                                    | 50              | 5043             | 19 824                                    | 50              |  | 19 826                             | 1382 | >90             | a <sub>1g</sub>  |
| 5060   | 19 757                                    | 70 <sup>e</sup> | 5060             | 19 757                                    | 55 <sup>e</sup> | 19 749                                     | 1459                               | 17   | a <sub>1g</sub> | 1460   |
| 5091   | 19 637                                    | 70              | 5092             | 19 633                                    | >100            | 19 631                                     | 1577                               | >90  | a <sub>1g</sub> | 1579   |
| 5109   | 19 568                                    | 70              | 5100             | 19 602                                    | 45              | 19 579                                     | 1629                               | 80   | b <sub>3g</sub> | 1624   |
| 5130(?)  | 19 488(?)                                 | 30              | 5135             | 19 469                                    | 45              | ...  | ...                                | ...  | ...             | ...  |
| 5182   | 19 292                                    | 40              | 5179             | 19 303                                    | 40              | 19 312                                     | 1896                               | >90  | 1382+512        | ...  |
| 5230   | 19 115                                    | 30              | 5230(?)          | 19 115(?)                                 | <20             | 19 120                                     | 2088                               | 89   | 1577+512        | ...  |
| Broad emission from<br>5400 (18 513 cm <sup>-1</sup> ) to<br>5500 (18 177 cm <sup>-1</sup> ) |   |                 |                  |   |                 | 18 444                                     | 2764                               | >90  | 2×1382          | ...  |
|  |   |                 |                  |   |                 | 18 254                                     | 2954                               | >90  | 1382+1577       | ...  |
|  |   |                 |                  |   |                 |  |                                    |      |                 |  |
|  |   |                 |                  |   |                 |  |                                    |      |                 |  |

<sup>a</sup>Present work.<sup>b</sup>1.0%  $C_{10}H_8$  in  $C_{10}D_8$  measured at 4.2° K; D. M. Hanson and G. W. Robinson (unpub. results).<sup>c</sup>See Ref. 16.<sup>d</sup>Normalized so that the intensity of the 0, 0 is 100.<sup>e</sup>The fact that this line is so intense compared with the 1459-cm<sup>-1</sup> vibration in the mixed crystal raises some doubt as to whether it is actually the 1459-cm<sup>-1</sup> vibration or not.

structure extending from 5000 to 5200 Å in the room-temperature spectrum splits into five reasonably well-defined lines at 77° K. The long-wavelength tail of the delayed fluorescence is responsible for the rising background in the 77° K spectrum.

In order to gain some insight into the relative intensities of delayed fluorescence (df) and phosphorescence (p) in the pure crystal, the complete emission spectrum from 5400 to 3000 Å was recorded both at room temperature and at 77° K. The total integrated intensities, represented by the area under the respective portions of this spectrum, were determined. Under our particular experimental conditions and within experimental uncertainty, the ratio of df:p was found to be approximately 100:1 both at room temperature and at 77° K. As has already been pointed out, this ratio is dependent upon the exciting light intensity. It is apparent from the magnitude of the experimental ratio that the incident light intensity was in the region of applicability of Eq. (10). No correction has been made for photomultiplier or spectrometer response.

#### b. Triplet Exciton Decay Characteristics

The decays of the crystal emission at 5100 Å (phosphorescence region of the spectrum) and 3500 Å (in the region of maximum delayed fluorescence intensity) were followed at 77° K and at room temperature. The room-temperature phosphorescence and delayed fluorescence decay curves are exhibited in Figs. 4 and 5, respectively. It is apparent from Figs. 6 and 7 that for  $t \gtrsim 150$  msec (including the 83 msec dead time between the termination of excitation and initiation

Figure 4. Decay curve of the phosphorescence emission at 5100 Å from pure crystalline naphthalene at room temperature. The sample was that which gave the spectrum shown in Fig. 1.

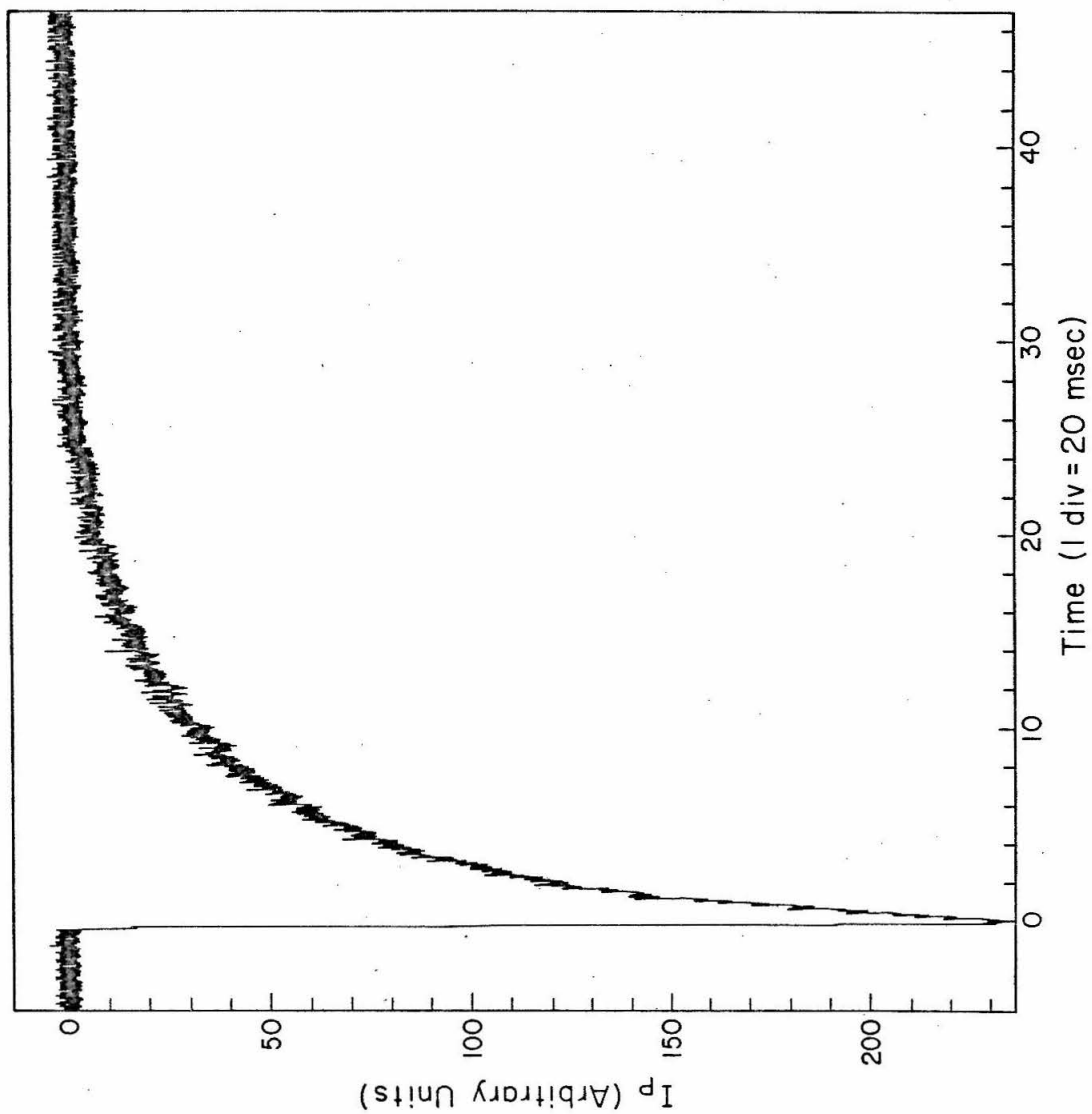
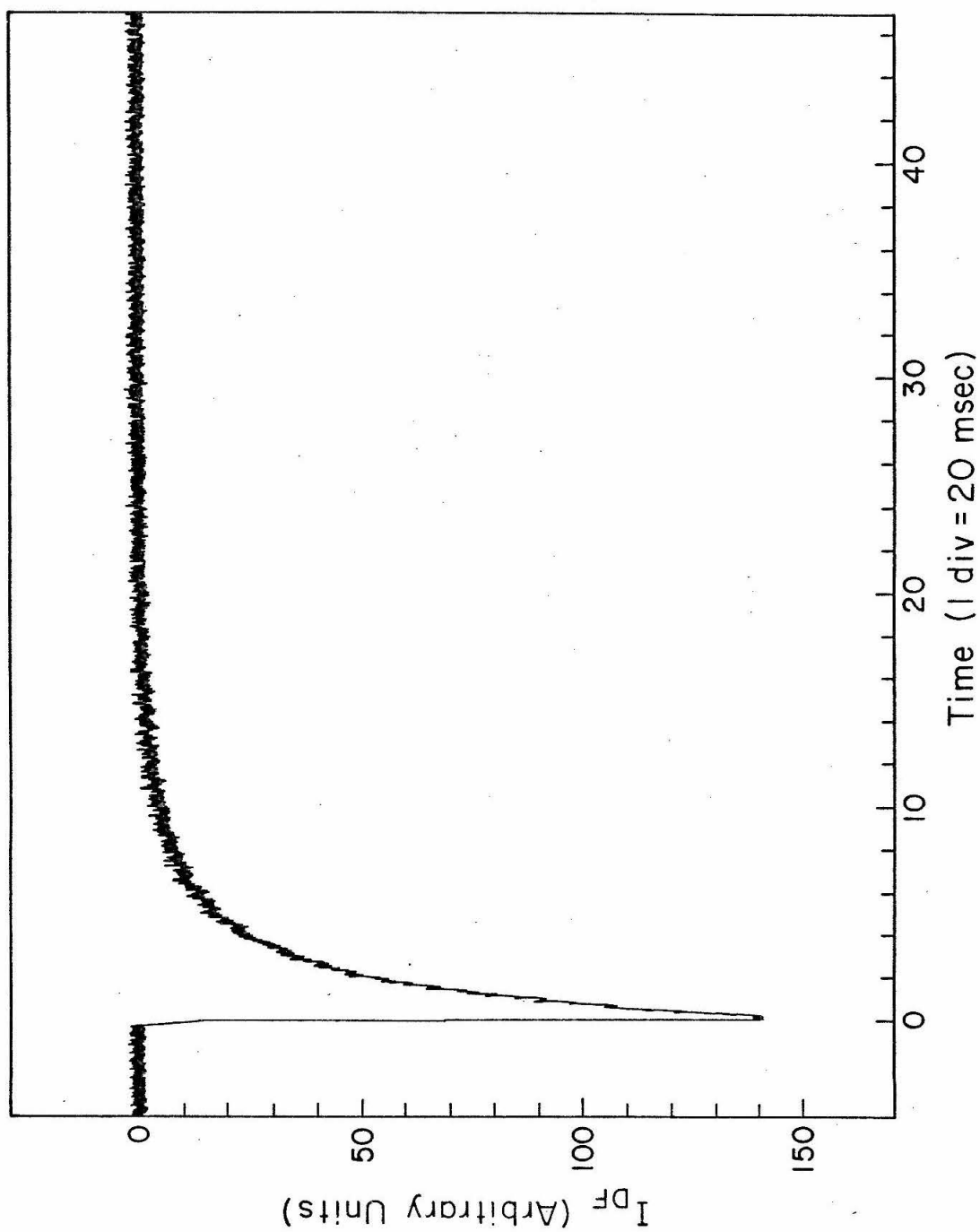


Figure 5. Decay curve of the delayed fluorescence emission at 3500 Å from pure crystalline naphthalene at room temperature. The sample was that which gave the spectrum shown in Fig. 1.





of observation), a plot of the logarithm of the emission intensity vs time becomes exponential for both types of emission. It is also evident from these figures that the initial second-order decay has almost completely died away during the long dead time. Within experimental error, the slopes of the first-order component in the semilogarithmic plots differ by the expected factor of 2, and the lifetime of the triplet exciton [ $\beta^{-1}$  of Eqs. (5) and (6)] evaluated from these slopes is found to be 130 msec.

In order for the slope of the first-order decay component in these semilogarithmic plots to be clearly defined in the case of combined first- and second-order kinetics, it is necessary to follow the decay out to two or three lifetimes. In fact, measuring the decay over a shorter time may result in an apparent dependence of the emission lifetime on the length of the observation interval. This dependence is such that a longer observation interval gives rise to a longer lifetime simply because the instantaneous slope of the semilogarithmic plots decreases with time. Singh *et al.*<sup>2</sup> reported seeing this effect in experiments on anthracene in which the observation period was constant but the delay between laser excitation and observation was varied. Consequently, care must be exercised to ensure that the measured lifetime is independent of the length of the observation period. For phosphoroscope speeds less than about 125 rpm, i. e., for observation intervals longer than approximately 225 msec, the triplet lifetime determined in the present experiments was constant at 130 msec. The experimental error is believed to be no more than  $\pm 15\%$ .

Figure 6. Plot of the logarithm of the emission intensity vs time for the phosphorescence decay curve shown in Fig. 4.

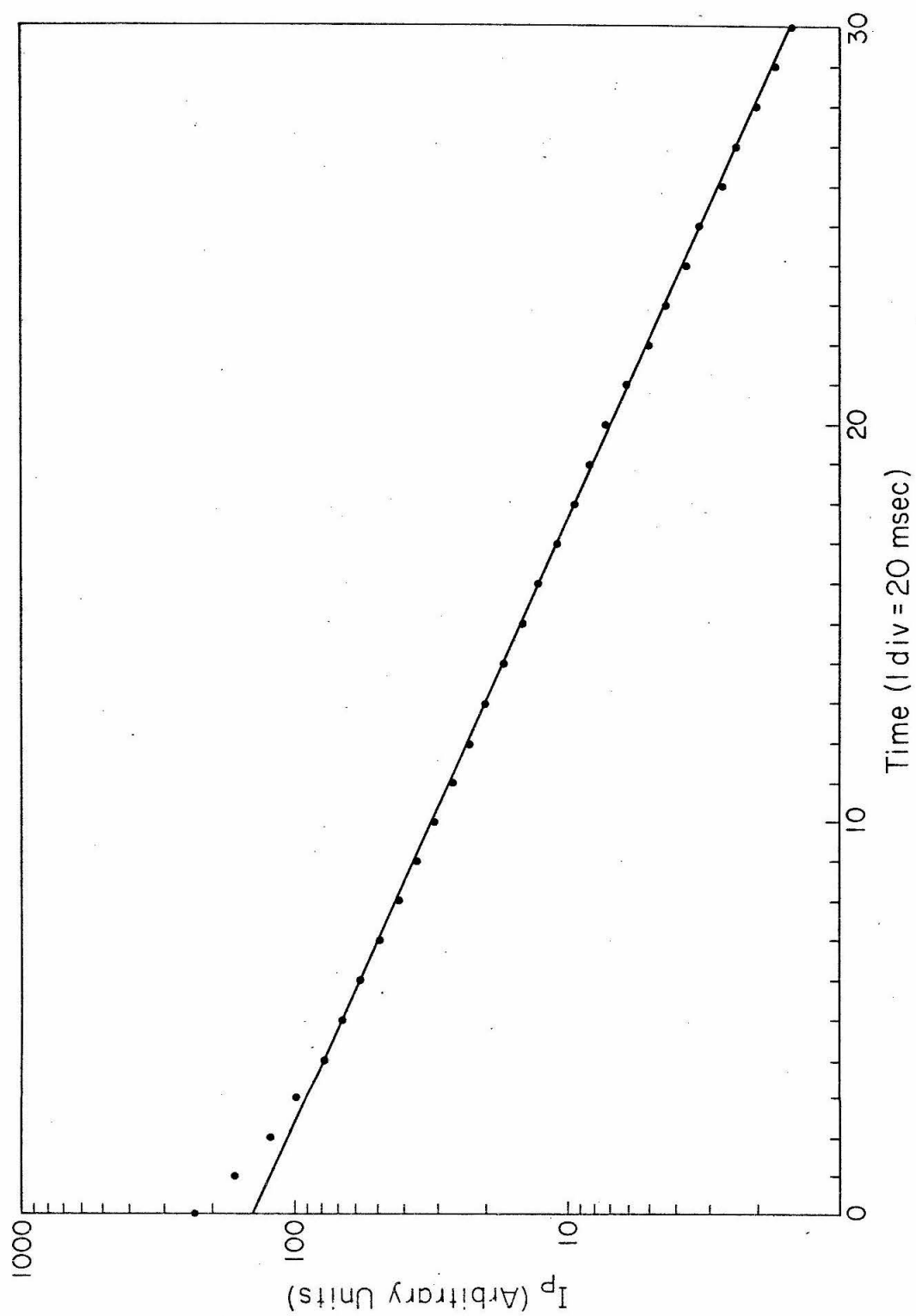
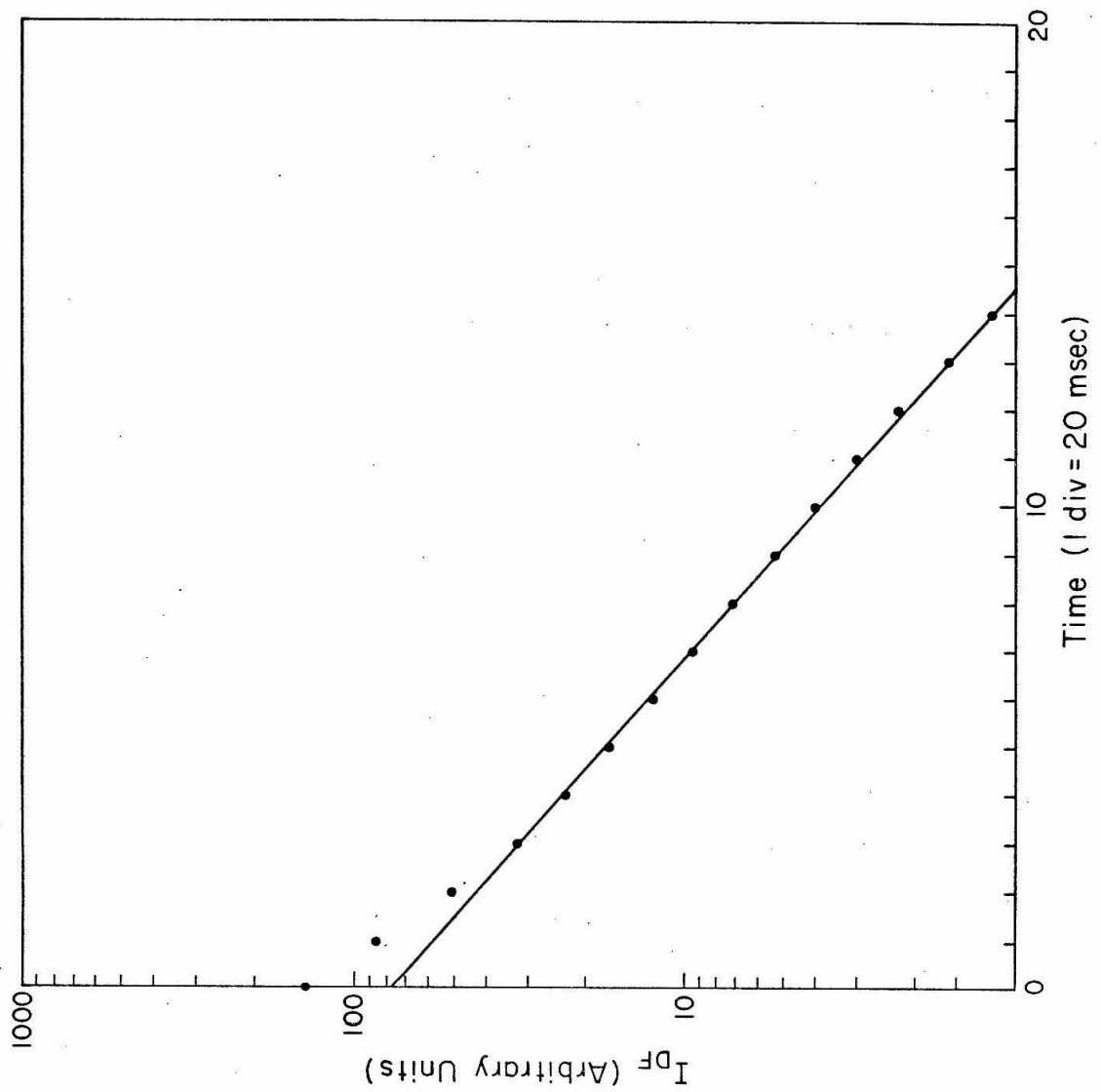


Figure 7. Plot of the logarithm of the emission intensity vs time for the delayed fluorescence decay shown in Fig. 5.



The lifetime measured at 77° K was not significantly different from the 130-msec room-temperature lifetime. There is slight indication that, if anything, the lifetime may be somewhat longer at 77° K than at room temperature.

### c. Impurity Effects

Question may be raised as to whether all the extensive purification was really necessary in light of the relatively high temperatures at which the experiments were carried out. However, a crystal in which  $\beta$ -bromonaphthalene was known to be present as an impurity<sup>18</sup> gave a room-temperature spectrum that, while qualitatively the same as that from the pure samples, differed in several respects. In particular, the emission lines were not as well defined, being somewhat broader and less intense than those from the other crystals under the same conditions. The relative intensities of the lines were also at variance with what was observed from the pure samples. Furthermore, a peak was observed at 4780 Å having an intensity 40% that of the naphthalene 0,0 band at 4715 Å and is believed to be due to phosphorescence from the  $\beta$ -bromonaphthalene.<sup>19</sup> Finally, preliminary results indicate that the lifetime of the triplet exciton is also rather sensitive to impurities that may be present in crystals that have not been carefully purified. Lifetime measurements on an impure crystal,<sup>18</sup> under the same conditions as used to obtain the decay curves shown in Figs. 4 and 5, yielded a value of 30 msec. i. e., a factor of about 4 shorter than the pure crystal value.

While these results are only qualitative, they nevertheless indicate that at least in the case of naphthalene, even for room-temperature studies, it is necessary to purify the crystals rather extensively in order to obtain reliable data. Further experiments are in progress to determine the quantitative dependence of the triplet-state lifetime on the concentration of impurities added under controlled conditions.

## 5. DISCUSSION

The analysis given in Table I of the emission from pure crystalline naphthalene between 4500 and 5400 Å, conclusively demonstrates that this emission originates from the lowest triplet state of the crystal. With the possible exception of the lines at 5060 and 5135 Å, agreement between the present results and the most intense vibronic lines observed in the phosphorescence spectrum of isotopic mixed crystals at 4.2° K is seen to be good. The fact that the 1459-cm<sup>-1</sup> vibration is so weak in the mixed-crystal phosphorescence raises doubt as to whether the intense 5060-Å line in the pure-crystal phosphorescence spectrum is actually the 1459-cm<sup>-1</sup> vibration or not. The high-energy side of the 0,0 transition lies at 4715 Å and this position is virtually independent of temperature. However, the portion of the 0,0 transition to longer wavelength decreases in intensity relative to the 4715-Å peak at dry-ice temperature. At 77° K much of the red portion of the 0,0 emission is lost in the noise.<sup>20</sup> It seems reasonable to interpret this long-wavelength part of the 0,0 band as resulting from transitions involving the radiative decay of a triplet exciton with a simultaneous

increase in the phonon population. This interpretation is substantiated when one considers that: (1) the transition probability for such a process, calculated from a perturbation approach,<sup>21</sup> is expected to increase with increasing temperature; (2) the temperature dependence of this long-wavelength portion of the 0,0 transition follows a trend observed by Colson *et al.*<sup>22</sup> in their studies of exciton band ← exciton band transitions in benzene and naphthalene; and (3) available data<sup>23-25</sup> report optical phonon frequencies ranging from 46 to 146  $\text{cm}^{-1}$  in crystalline naphthalene at room temperature in addition to acoustical phonons whose frequencies in molecular crystals are a factor of 5-10 smaller than the optical phonon frequencies.<sup>26</sup>

Absence of impurity emission at 4.2° K in the phosphorescence region of the spectrum<sup>18</sup> is further proof that the line broadening observed at room temperature is due to an intrinsic property of the naphthalene crystal, i. e., to phonons and not to impurities.

The value of 130 msec for the lifetime of the triplet exciton in pure crystalline naphthalene is considerably longer than the previously reported value of 20 msec.<sup>6</sup> However, it is still roughly an order of magnitude shorter than the triplet-state lifetime of naphthalene in a rigid glass<sup>5, 27</sup> or in a mixed crystal.<sup>28</sup> This could be due to enhancement of nonradiative processes in the pure crystal relative to the glass or mixed crystal. If this is true, the lifetime of the triplet exciton in pure crystalline perdeuteronaphthalene ( $\text{C}_{10}\text{D}_8$ ) might be much longer than 130 msec. Experiments are in progress to determine whether or not a deuterium effect exists.



## 6. ADDENDUM

Since the original work reported in the preceding paper, a crystal has been obtained that had a measured room-temperature triplet-state lifetime of 395 msec, indicating that this crystal had: (1) a higher degree of chemical purity<sup>29</sup>; (2) fewer physical defects; (3) a lower oxygen content; or, perhaps a combination of the three. Even at 395 msec, the lifetime of the triplet state of the pure crystal at room temperature is roughly a factor of 5 shorter than that of naphthalene in a rigid glass<sup>5</sup> or mixed crystal<sup>28</sup> at low temperature. There appears to be good reason for attributing this difference in the triplet-state lifetime of the crystal versus that of the isolated molecule to the mobility of the triplet exciton in the pure crystal. The fact that the excitation can move about in the crystal enhances the "quenching effectiveness" of any quencher present, be it a chemical impurity,<sup>29</sup> oxygen or some physical defect, due simply to the increased probability of the excitation "finding" a site occupied by a quencher.

Results of room-temperature, triplet-state lifetime measurements on a series of chemically mixed crystals of  $\beta$ -methylnaphthalene (BMN) impurity in naphthalene,<sup>30</sup> ranging in concentration from  $10^{-5}$  wt % to 10 wt %, indicate that of the three types of quenchers mentioned above, oxygen is the most important. While there was a general trend toward a shorter triplet lifetime with increasing BMN concentration, there were large fluctuations in the data, i. e., the measured triplet lifetimes did not decrease monotonically with increasing impurity

concentration. These fluctuations were much too large to be accounted for by the experimental uncertainty in BMN concentration; nor could they be satisfactorily explained in terms of variations in the defect content of the crystals. The most likely explanation, then, appears to be that differences in oxygen content from crystal to crystal were responsible for the observed fluctuations in the measured triplet-state lifetimes.

This oxygen could have been introduced via the BMN, which undoubtedly contained a substantial amount of oxygen since it was only zone-refined. One would, however, expect a correlation between the amount of oxygen introduced into a given sample from this source and the BMN concentration of that sample, assuming the oxygen to be uniformly distributed through the zone-refined BMN. This would cause a stronger apparent dependence of triplet lifetime on BMN concentration, but would not cause the sort of fluctuations that were observed. A more likely source of random quantities of oxygen is that liberated during the final process of sealing the crystal tubes and pulling them off the vacuum line. The pressure in the vacuum system was observed to increase by as much as a factor of 10 during this process, indicating the liberation of substantial amounts of some gas. Since it had to pass through a liquid nitrogen trap to reach the pressure gauge, it was apparently not easily condensable, which suggests that it was probably oxygen or perhaps air. The amount of gas liberated varied greatly from crystal tube to crystal tube and depended upon how long the glass was kept heated. In this way, varying amounts of oxygen could have been introduced into the samples; this oxygen then would perturb the

triplet state<sup>11</sup> to a similarly varying degree and give rise to large fluctuations in the measured triplet lifetime.

We conclude that even the longest lifetime measured to date, viz., 395 msec, still does not represent the true triplet exciton lifetime in crystalline naphthalene. Rather, the observed lifetime reflects the fact that the exciton mobility enhances the "quenching effectiveness" of all residual quenchers, of which oxygen is the most important, in the crystal. That the short triplet lifetime in the crystal is not due to enhanced intramolecular radiationless transitions<sup>6</sup> is evidenced by the fact that we observe no significant deuterium effect on the measured lifetime.

REFERENCES

1. See, for example, (a) H. Sternlicht, G. C. Nieman, and G. W. Robinson, J. Chem. Phys. 38, 1326 (1963); 39, 1610 (1963); (b) R. G. Kepler, J. C. Caris, P. Avakian, and E. Abramson, Phys. Rev. Letters 10, 400 (1963).
2. S. Singh, W. J. Jones, W. Siebrand, B. P. Stoicheff, and W. G. Schneider, J. Chem. Phys. 42, 330 (1965), and numerous references cited therein.
3. M. A. El-Sayed, M. T. Wauk, and G. W. Robinson, Mol. Phys. 5, 205 (1962).
4. G. N. Lewis and M. Kasha, J. Am. Chem. Soc. 66, 2100 (1944).
5. V. L. Ermolaev, Usp. Fiz. Nauk 80, 3 (1963) [Sov. Phys. -Usp. 6, 333 (1963)].
6. H. Y. Sun, J. Jortner, and S. A. Rice, J. Chem. Phys. 44, 2539 (1966).
7. D. F. Williams and W. G. Schneider, J. Chem. Phys. 45, 4756 (1966).
8. D. F. Williams, J. Chem. Phys. 47, 344 (1967).
9. H. P. Müller, P. Thoma and G. Vaubel, Phys. Status Solidi 23, 253 (1967).
10. D. M. Hanson and G. W. Robinson, J. Chem. Phys. 43, 4174 (1965).
11. S. D. Colson and E. R. Bernstein, J. Chem. Phys. 43, 2661 (1965); also, Ref. 3.

12. G. W. Robinson and R. P. Frosch, J. Chem. Phys. 37, 1962 (1962); 38, 1187 (1963).
13. Equation (1) is valid in the limit where triplet-triplet annihilation, and not the decay of the bi-exciton intermediate state is the rate-determining process.
14. M. Kasha, J. Opt. Soc. Am. 38, 929 (1948).
15. D. M. Hanson and G. W. Robinson (unpublished results).
16. J. M. Hollas, J. Mol. Spectry. 9, 138 (1962).
17. F. R. Lipsett and G. MacPherson, Can. J. Phys. 44, 1485 (1966).
18. The purity of all samples used was checked by observing the crystal emissions in the singlet and triplet regions of the spectrum at 4.2° K. This was done using a 600-line/mm Bausch & Lomb grating in an f/11, 2-m Czerny-Turner mount using Kodak 103a-O plates. Only one sample showed any emission in the triplet region and it also exhibited extraneous fluorescence lines. The major contaminant present in a concentration estimated to be between 0.1% and 0.01% as determined from these spectra, was found to be  $\beta$ -bromonaphthalene (0,0 at 20 932  $\text{cm}^{-1}$ ). Also present in much smaller quantity in this sample was  $\beta$ -methylnaphthalene (0,0 at 20 905  $\text{cm}^{-1}$ ). One other impure crystal, used only to determine the effect of impurities on the lifetime of the triplet state, also exhibited extraneous fluorescence lines. The nature of these impurities was not determined but it can be safely assumed that they were of the type commonly found in reagent grade naphthalene. The impurity concentration in this crystal is unknown. All the other samples showed only normal fluorescence spectra.

19. J. Sidman, J. Chem. Phys. 25, 229 (1956).
20. Several of the room-temperature spectra exhibited some rather poorly resolved structure in this low-energy portion of the 0, 0 band. In any given spectrum this splitting was not very convincing but, because it appeared in many of the spectra, one tends to believe it is real. Two peaks, one at about  $45\text{ cm}^{-1}$  and another at about  $110\text{ cm}^{-1}$  to lower energy from  $4715\text{ Å}$ , were evident. At dry-ice temperature the intensities of these peaks had dropped to 80% and 65%, respectively, that of the  $4715\text{ Å}$  peak.
21. R. S. Knox, Theory of Excitons (Academic Press Inc., New York, 1963), pp. 144-149, 170.
22. S. D. Colson, D. M. Hanson, R. Kopelman, and G. W. Robinson, J. Chem. Phys. 48, 2215 (1968).
23. A. Kastler and A. Rousset, J. Phys. Radium 2, 49 (1941).
24. D. W. J. Cruickshank, Rev. Mod. Phys. 30, 163 (1958).
25. G. S. Pawley, Phys. Status Solidi 20, 347 (1967).
26. A. S. Davydov, Phys. Status Solidi 20, 143 (1967); A. S. Davydov and E. N. Myasnikov, ibid. 20, 153 (1967).
27. D. S. McClure, J. Chem. Phys. 17, 905 (1949).
28. C. A. Hutchison, Jr. and B. W. Mangum, J. Chem. Phys. 32, 1261 (1960).
29. The word "impurity" is used in a somewhat restricted sense in that it refers only to those molecules of chemical constitution sufficiently similar to that of the host material that they behave as shallow traps.

30. The naphthalene used had a room-temperature, triplet-exciton lifetime of 395 msec; the  $\beta$ -methylnaphthalene, which had been subjected to extensive zone-refining (80 passes) and no further purification, had a triplet-exciton lifetime of  $< 1$  msec. The samples were prepared under a dry nitrogen atmosphere and sealed under vacuum in crystal growing tubes. All crystals were grown from the melt.

**SECTION B**

**DIFFUSION OF TRIPLET EXCITONS IN CRYSTALLINE  
NAPHTHALENE AND ANTHRACENE**



## 1. INTRODUCTION

There has been a great deal of experimental and theoretical activity during the past few years, directed toward gaining a better understanding of the dynamical behavior of triplet excitons in molecular crystals.<sup>1-13</sup> As a result of these investigations, a reasonably complete description of triplet excitons in crystals such as naphthalene and anthracene has emerged. Similarities between crystalline naphthalene and anthracene make it possible to discuss both within the same general theoretical framework. Consequently, both crystals have been used, anthracene to a somewhat greater extent than naphthalene, in experiments concerned with triplet exciton behavior in organic crystals. A recent review by Avakian and Merrifield<sup>14</sup> summarizes the work done on triplet excitons in anthracene crystals. That paper, along with the references cited therein, provides a good survey of the present understanding of triplet exciton behavior in molecular crystals.

One aspect of triplet exciton behavior that has received considerable attention is their ability to move about in the crystal. This motion can be described by a diffusion equation, and several techniques have been devised to measure the diffusion constant and diffusion length of these mobile, neutral, electronically excited triplet states of the crystal.<sup>15-21</sup> The work of Kepler and Switendick<sup>15</sup> and that of Williams and Adolph<sup>16</sup> concerning triplet exciton diffusion in crystalline anthracene is of special interest since part of the present investigation overlaps their experiments.

In the present work the room-temperature excitation spectra<sup>22</sup> of delayed fluorescence and of phosphorescence have been studied both for naphthalene and for anthracene crystals. On the basis of simple theoretical considerations, one would expect a monotonic increase in the integrated emission (phosphorescence or delayed fluorescence) intensity as the wavelength of the excitation light was scanned through the singlet absorption toward higher energy. In contrast to this expectation, the intensity of both types of emission is observed to increase at first, reach a maximum value and then decrease as the wavelength of the excitation light is made shorter. Furthermore, the wavelength at which the maximum in the excitation spectrum occurs depends upon the intensity of the excitation light in the case of delayed fluorescence, but not in the case of phosphorescence. It is with these observations and their possible interpretation in terms of the triplet excitons diffusing to the crystal surface and being quenched there that this paper is concerned.

## 2. THEORETICAL

It has been shown<sup>18,19</sup> that the concentration  $\underline{n}$  of triplet excitons at position  $\underline{\bar{x}}$  and time  $\underline{t}$  at room temperature is governed by the equation

$$\frac{\partial n(\underline{\bar{x}}, t)}{\partial t} = S(\underline{\bar{x}}, t) - \beta n(\underline{\bar{x}}, t) - \gamma' n^2(\underline{\bar{x}}, t) + D \nabla^2 n(\underline{\bar{x}}, t) . \quad (1)$$

The terms on the right-hand side of Eq. (1) represent the source, monomolecular and bimolecular decay and diffusion of the triplet

excitons, respectively. In the above equation,  $\beta$  is the first-order decay constant,  $\gamma'$  is the total second-order annihilation constant and  $D$  is the diffusion constant. Since we will not be concerned with anisotropy<sup>19, 23</sup> in the diffusion, the diffusion constant is taken to be the scalar  $D$  instead of a second rank tensor. In general,  $S(\vec{x}, t)$  may be quite complicated since it includes, in addition to a function describing the incident light intensity, the effects of re-absorption of any emitted light whose wavelength coincides with a strong absorption.

Since Eq. (1) is not amenable to a closed form solution, it is customary to make approximations that reduce it to a more tractable form. The physical model described by the resulting approximate equation depends upon the nature of the approximations made. We consider next several such models, their limitations and the approximations to Eq. (1) that must be made in order to arrive at these models.

#### a. The Semi-Infinite-Crystal Diffusional Model

Approximations to Eq. (1):

- (1) Steady-state excitation  $\Rightarrow (\partial n(\vec{x}, t)/\partial t) = 0$ , so that the triplet exciton density is a function of position only;
- (2) Re-absorption of emitted light is neglected;
- (3)  $S(\vec{x}, t) \equiv m\alpha I_0 \exp(-\alpha x)$  where  $m$  is the intersystem crossing efficiency,  $\alpha$  is the absorption coefficient and  $x$  is the distance into the crystal measured, from the illuminated surface, along the direction of propagation of the exciting light beam, the intensity of which is  $I_0$ ;

- (4) The excitation light intensity is kept sufficiently low to ensure that  $\gamma'n^2(x)$  can be neglected relative to  $\beta n(x)$ ;
- (5) Only diffusion parallel to the x-axis is considered  
 $\Rightarrow \nabla^2 \rightarrow \frac{d^2}{dx^2}$ .

In addition to the above approximations to Eq. (1), the following assumptions are made:

- (1) The crystal is assumed to be semi-infinite in extent; the front surface, lying at  $x=0$ , is the surface upon which the exciting light falls. This is equivalent to requiring the crystal thickness to be large compared to  $\alpha^{-1}$ ;
- (2) Triplet excitons are assumed to be quenched with 100% efficiency at the crystal surfaces.

The resulting diffusion equation has the form<sup>16</sup>

$$0 = m\alpha I_0 \exp(-\alpha x) - \beta n(x) + D \frac{d^2 n(x)}{dx^2} \quad (2)$$

with the boundary conditions  $n(0) = n(\infty) = 0$ .

The physical model described by Eq. (2) is one in which the excitons are quenched at the crystal surfaces so that if they are created within a diffusion length of a surface they can diffuse to that surface and be quenched. Further, the model neglects triplet-triplet annihilation completely. We now proceed to see if this model can even qualitatively account for a maximum in the emission excitation spectra.

The delayed fluorescence intensity as a function of the wavelength of the excitation light is given by

$$I_{df} \sim \gamma \int_0^{\infty} n^2(x) dx \quad (3)$$

$$= \frac{\gamma m^2 I_0}{2\beta^{\frac{1}{2}}} \frac{\alpha}{(\beta^{\frac{1}{2}} + \alpha D^{\frac{1}{2}})^3} \quad \text{for all } \alpha \quad (4)$$

where the solution to Eq. (2) has been used together with Eq. (3) to arrive at Eq. (4). Since any acceptable theory must predict a peak in the excitation spectrum of delayed fluorescence it is necessary that Eq. (4) exhibit a maximum when  $I_{df}$  is plotted versus  $\alpha$ . That this is in fact the case, can be seen most easily by setting the derivative of  $I_{df}$  with respect to  $\alpha$  equal to zero and solving for  $\alpha_{max}$ , the value of the absorption coefficient at the wavelength of the maximum,  $\lambda_{max}$ . We simply state the result,

$$\alpha_{max} = \frac{1}{2} \sqrt{\beta/D} \quad (5)$$

Evidently, the absorption coefficient at  $\lambda_{max}$  and the diffusion constant for triplet excitons are related in a very simple manner within the framework of this particular model. Insofar as the delayed fluorescence excitation spectrum is concerned, the model appears to have the correct qualitative behavior and has in fact been used to arrive at a value for the diffusion constant for triplet excitons in crystalline anthracene at room temperature.<sup>15, 16</sup>

This is essentially as far as either Kepler and Switendick<sup>15</sup> or Williams and Adolph<sup>16</sup> went in their analysis. However, in view of the fact that the phosphorescence excitation spectrum can now be measured, it is of particular interest to investigate the predictions of

the model in that regard. Proceeding as for delayed fluorescence we have

$$I_p \sim \beta \int_0^{\infty} n(x) dx \quad (6)$$

$$= \frac{mI_0}{1 + \alpha\sqrt{D/\beta}} \quad \text{for all } \alpha. \quad (7)$$

Taking the derivative with respect to  $\alpha$  yields,

$$\frac{dI_p}{d\alpha} = - \frac{\beta m I_0 \sqrt{\beta D}}{(\beta + \alpha \sqrt{\beta D})^2}. \quad (8)$$

Inspection of Eq. (8) reveals that  $dI_p/d\alpha$  approaches zero only in the limit as  $\alpha$  approaches infinity. Clearly, Eq. (7) has no maximum and, furthermore, it predicts that the phosphorescence should attain its greatest intensity in the limit as  $\alpha$  tends to zero. This means that when the crystal is not absorbing any excitation light it should be phosphorescing at a maximal rate; the phosphorescence intensity then decreases as the crystal begins to absorb more excitation light, that is, as  $\alpha$  increases. The nature of its own predictions makes the semi-infinite-crystal model highly suspect and one is forced to consider other more realistic models.

#### b. The Finite-Crystal Diffusional Model

Approximations to Eq. (1):

The approximations are identical to those made in Section 2a above.

## Assumptions:

- (1) The crystal is required to be finite in extent; the front surface, lying at  $x=0$ , is the surface upon which the exciting light impinges. The back surface lies at  $x=a$ , that is, the crystal thickness is  $a$ ;
- (2) As in Section 2a above.

Since the approximations to Eq. (1) are unchanged, the appropriate equation is again Eq. (2). The boundary conditions however become  $n(0) = n(a) = 0$  as a result of assumption (1) above. The solution under these conditions is of the form

$$n(x) = c_1 \exp\left[(\beta/D)^{\frac{1}{2}} x\right] + c_2 \exp\left[-(\beta/D)^{\frac{1}{2}} x\right] + \frac{m \alpha I_0}{\beta - D\alpha^2} \exp(-\alpha x) \quad (9)$$

with

$$c_1 = \left( \frac{m \alpha I_0}{\beta - D\alpha^2} \right) \left\{ \exp\left[-(\beta/D)^{\frac{1}{2}} a\right] - \exp(-\alpha a) \right\} / \left\{ \exp\left[(\beta/D)^{\frac{1}{2}} a\right] - \exp\left[-(\beta/D)^{\frac{1}{2}} a\right] \right\}$$

and 
$$c_2 = -(c_1 + c_3), \quad c_3 = \frac{m \alpha I_0}{\beta - D\alpha^2}.$$

Substituting Eq. (9) into Eq. (3) and performing the integral over the range from 0 to  $a$  yields the following expression for the delayed fluorescence excitation spectrum,

$$I_{df} = \gamma c_1^2 \sqrt{D/\beta} \sinh(2a \sqrt{\beta/D}) - \gamma c_3^2 \left\{ \frac{1}{\alpha} \left[ \exp(-2\alpha a) - 1 \right] + \sqrt{D/\beta} \left[ \exp(-2a \sqrt{\beta/D}) - 1 \right] - \frac{4}{\sqrt{\beta/D} + \alpha} \left[ \exp(-\sqrt{\beta/D} a - \alpha a) - 1 \right] \right\}$$

$$\left. \begin{aligned}
& + 2\gamma c_1 c_2 a + 2\gamma c_1 c_3 \left\{ \frac{2 \exp(-\alpha a)}{\beta/D - \alpha^2} \left( \sqrt{\beta/D} \sinh(a\sqrt{\beta/D}) \right. \right. \\
& \left. \left. + \alpha \cosh(a\sqrt{\beta/D}) \right) - \frac{2\alpha}{\beta/D - \alpha^2} - \frac{1}{2} \sqrt{D/\beta} \left[ \exp(-2\sqrt{\beta/D} a) - 1 \right] \right\} \right\} \quad (10)
\end{aligned}$$

Next, Eq. (9) is substituted into Eq. (6) to obtain an expression for the phosphorescence excitation spectrum,

$$I_p = \frac{\beta m I_0}{\beta - D\alpha^2} \left\{ 1 - \exp(-\alpha a) - \alpha \sqrt{D/\beta} \left[ 1 + \exp(-\alpha a) \right] \tanh\left(\frac{a}{2} \sqrt{\beta/D}\right) \right\}. \quad (11)$$

Both Eq. (10) and Eq. (11) exhibit maxima as a function of absorption coefficient. Furthermore, the phosphorescence intensity goes to zero as the absorption coefficient tends to zero, in contrast to the predictions based on the semi-infinite-crystal model.

Evidently, restricting the crystal thickness to a finite value removes the anomalies present in the semi-infinite-crystal model and leads to the prediction of peaks in both the delayed fluorescence and phosphorescence excitation spectra.

### c. The Finite-Crystal Annihilation Model

Approximations to Eq. (1):

- (1) As in Section 2a;
- (2) As in Section 2a;
- (3) As in Section 2a;
- (4) The restriction that  $\gamma n^2 \ll \beta n$  is removed and both terms are kept in the kinetic equation;
- (5) The diffusion term in Eq. (1) is neglected.



Assumptions:

- (1) As in Section 2b;
- (2) Along with the explicit diffusion term, surface quenching of the triplet excitons is ignored.

In this limit, Eq. (1) reduces to

$$0 = m\alpha I_0 \exp(-\alpha x) - \beta n(x) - \gamma' n^2(x) . \quad (12)$$

Despite the lack of an explicit diffusion term in Eq. (12), diffusion has not been totally ignored. Noyes<sup>24</sup> has shown that for the case of isotropic diffusion, the effective second-order rate constant  $\gamma'$  is related to the diffusion constant  $D$  by

$$\gamma' = \frac{2\pi\sigma D}{1 + 2\pi\sigma D/\gamma} . \quad (13)$$

In Eq. (13)  $\sigma$  is the collision diameter and  $\gamma$  the second-order rate constant in the limit where diffusion is not rate controlling, i. e., in the limit where diffusion is rapid compared to the rate of bimolecular annihilation. We observe that for the case of diffusion controlled annihilation, i. e., for  $2\pi\sigma D \ll \gamma$ ,

$$\gamma' \approx 2\pi\sigma D . \quad (14)$$

Eq. (12) can be integrated directly to give

$$mI_0[\exp(-\alpha a) - 1] + \frac{\beta}{\beta_{\text{rad}}} I_p + \frac{\gamma'}{\gamma^{(1)}} I_{\text{df}} = 0 \quad (15)$$

where  $\beta_{\text{rad}}$  is the rate of radiative first-order decay and  $\gamma^{(1)}$  is the

rate of bimolecular production of fluorescing singlet excitons. Based on the present model, a simple relationship of the form of Eq. (15) is expected to exist between the delayed fluorescence and phosphorescence excitation spectra. Equation (15) represents a mathematical statement of the required conservation of excitons and photons.

#### d. The Finite-Crystal Diffusional Annihilation Model

Approximations to Eq. (1):

- (1) As in Section 2a;
- (2) As in Section 2a;
- (3) As in Section 2a;
- (4) As in Section 2c;
- (5) As in Section 2a.

Assumptions:

- (1) As in Section 2b;
- (2) As in Section 2a.

With these approximations and assumptions, the diffusion equation takes the form

$$0 = m\alpha I_0 \exp(-\alpha x) - \beta n(x) - \gamma' n^2(x) + D \frac{d^2 n(x)}{dx^2} \quad (16)$$

with  $n(0) = n(a) = 0$ .

As mentioned in Section 2c, account must be taken of the relationship between  $\gamma'$  and  $D$  since they are not independent. Although Eq. (16) is not the most general equation, it nevertheless contains all the terms appearing in Eq. (1). Unlike the models discussed above,

no assumptions have been made with regard to the relative magnitudes of the individual terms so that this model is physically equivalent to that described by Eq. (1).

### 3. EXPERIMENTAL

#### a. The Apparatus

The experiments were conducted at room temperature using a phosphoroscope described in Appendix A. Light from a 6500 W xenon arc lamp was passed through a 0.5-m Jarrell-Ash Ebert scanning spectrometer and allowed to strike the sample, located at the center of the cylindrical phosphoroscope drum. The spectrometer, which was equipped with a grating having 1180 grooves/mm, blazed at 5000 Å in first order, had a reciprocal linear dispersion of 16 Å/mm at the exit slit and an effective aperture ratio of  $f/8.6$ . The slitwidth was set at 400  $\mu$ . All the light emitted into the solid angle subtended by a lens 4 cm in diameter, located 5 cm from the sample, was collected and focused onto the cathode of a dry-ice cooled EMI 6256 SA photomultiplier. The photomultiplier output was fed into a Victoreen Model VTE-1 electrometer where it was amplified and recorded on a strip-chart recorder. Separation of the delayed fluorescence and phosphorescence light was accomplished with the aid of appropriate Corning glass filters.

#### b. The Experimental Procedure

Phosphorescence and delayed fluorescence are both dependent upon the existence of a non-negligible population of the lowest triplet

state of the crystal. The requisite triplet-state population was provided via direct excitation into the lowest singlet state followed by intersystem crossing to the lowest triplet state. The efficiency with which a given wavelength of excitation light excites triplet states can be determined by measuring the integrated emission (either phosphorescence or delayed fluorescence) intensity due to excitation light of that wavelength. By measuring the integrated emission intensity as the wavelength of the excitation light is scanned through the region of the singlet absorption, one obtains the so-called excitation spectrum of the emission. The excitation spectra reported here were recorded at the highest phosphoroscope speed, *viz.*, 1725 rpm. At this speed, the period of the phosphoroscope is short compared to the emission lifetime, at least in the case of naphthalene, so that the triplet-state concentration can be treated as being effectively constant (see Appendix B).

The wavelength dependence of the excitation light intensity striking the sample was checked using rhodamine B, which has a constant quantum yield from 2000 Å to 6000 Å,<sup>25</sup> in ethylene glycol as a quantum counter.

### c. Sample Preparation

The naphthalene samples were purified by a combination of zone-refining and fusion with potassium metal (Appendix A). Anthracene was chromatographed, reacted with potassium while dissolved in benzene, and finally zone-refined (Appendix A). During both purification processes air was rigorously excluded. All crystals were grown from the melt.

A solution of rhodamine B (3 gm/liter) in ethylene glycol was prepared<sup>25</sup> for use in determining the wavelength dependence of the excitation light intensity at the position of the sample.

#### 4. RESULTS

##### a. Naphthalene

Figures 1 and 2 show the measured phosphorescence and delayed fluorescence excitation spectra, respectively, of pure crystalline naphthalene-d<sub>8</sub> at room temperature. The position of the maximum in the delayed fluorescence excitation spectrum depends upon the intensity of the excitation light; it is observed to shift to the red with increasing intensity. The position of the maximum in the phosphorescence excitation spectrum, on the other hand, is independent of exciting light intensity over the same range of intensities. These results are summarized in Table I. Naphthalene-h<sub>8</sub> crystals exhibit the same characteristics, the only difference being a slight shift in the peak positions.

Figure 3 displays the triplet exciton density, calculated using the model described in Section 2d above, for three different values of the absorption coefficient  $\alpha$  (see Table II). The three curves have been normalized so that their maximum values coincide. Figures 4 and 5 are representative of the phosphorescence and delayed fluorescence excitation spectra calculated from these exciton density distributions. It is evident that the calculated curves have the correct qualitative behavior. However, neither calculated excitation spectrum shows any

Figure 1. The excitation spectrum of the phosphorescence emission from pure crystalline naphthalene- $d_8$  at room temperature. The lower curve was recorded under the following conditions: Corning glass filters, C.S. 3-70 and 3-71, were placed directly over the photomultiplier window, the electrometer input was set at  $10^{-7}$  A full scale with a 0.3 sec time constant, and the scan rate was 50 Å/min. The upper curve was recorded under the same conditions except the electrometer input was set at  $10^{-8}$  A with a 1 sec time constant.

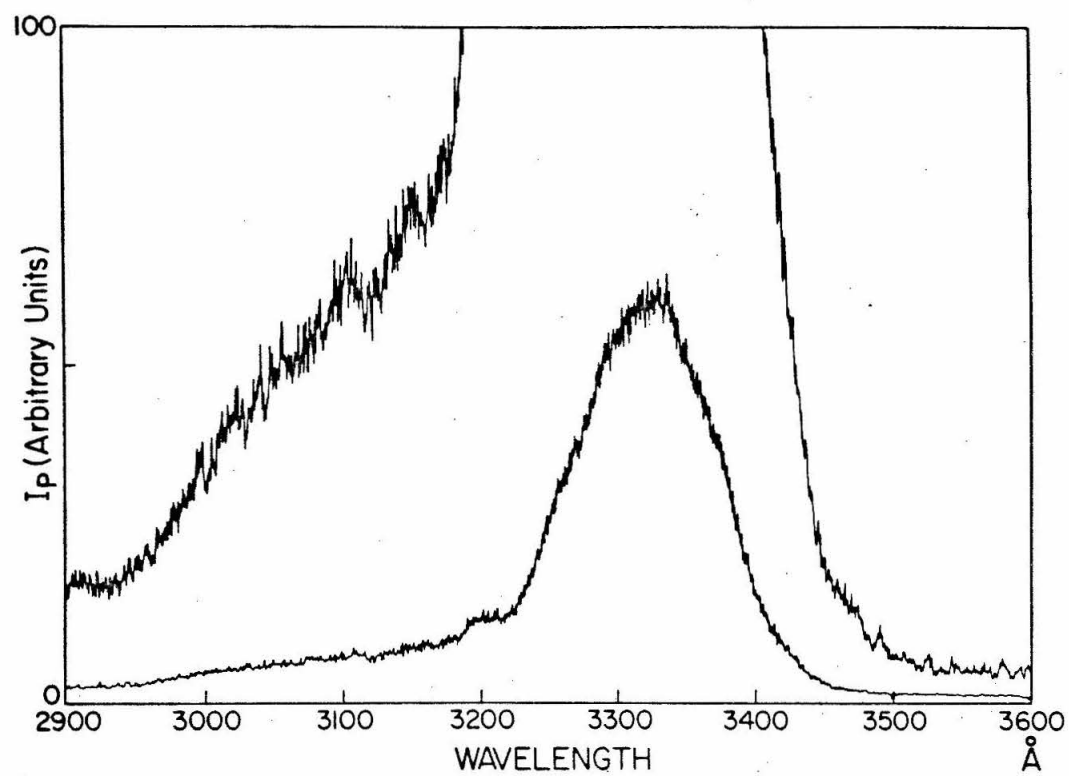


Figure 2. The excitation spectrum of the delayed fluorescence emission from pure crystalline naphthalene- $d_8$  at room temperature. The lower curve was recorded under the following conditions: a Corning glass filter, C.S. 7-54, was placed directly over the photomultiplier window, the electrometer input was set at  $10^{-7}$  A full scale with a 0.3 sec time constant, and the scan rate was 50 Å/min. The upper curve was recorded under the same conditions except the electrometer input was set at  $10^{-8}$  A full scale.



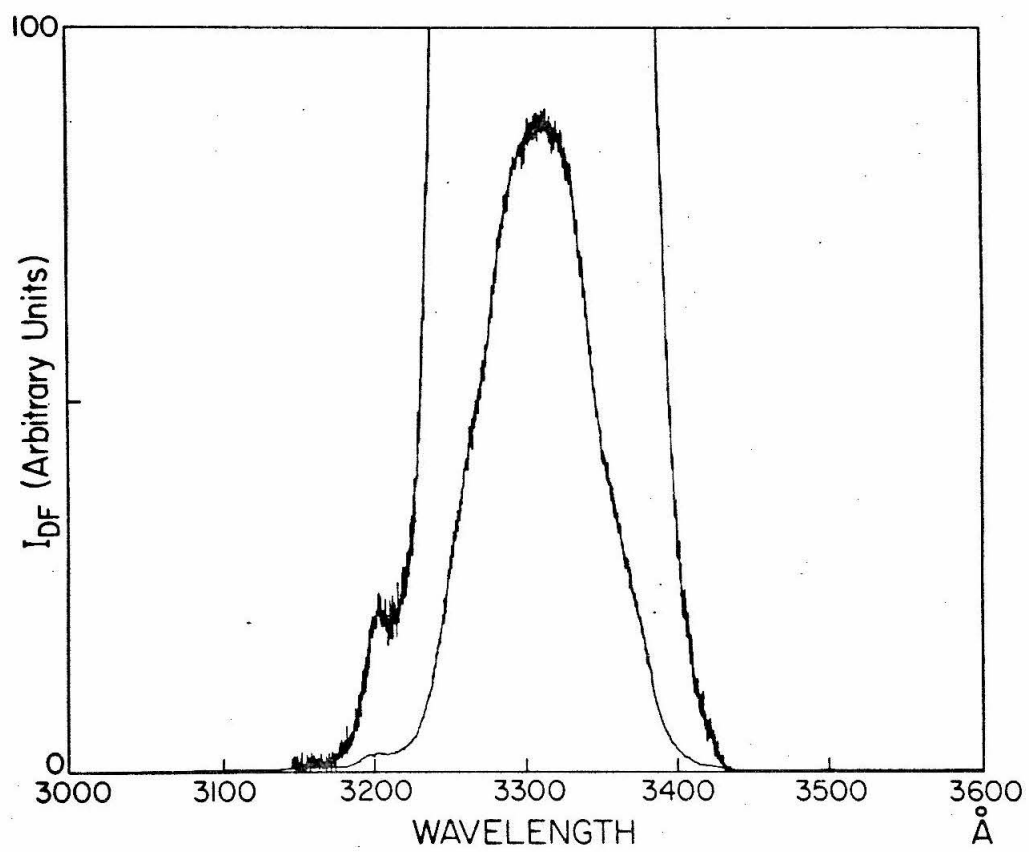


TABLE I. Peak positions in the excitation spectra as a function of excitation light intensity.

| RELATIVE<br>EXCITATION<br>LIGHT INTENSITY | DELAYED<br>FLUORESCENCE<br>PEAK POSITION (Å) | RELATIVE<br>EXCITATION<br>LIGHT INTENSITY | PHOSPHORESCENCE<br>PEAK POSITION (Å) |
|---|--|---|--------------------------------------|
| 1   | 3300   | 1   | 3322                                 |
| 0.21                                      | 3275   | 0.23                                      | 3316                                 |
| 0.05                                      | 3258   | 0.08                                      | 3318                                 |
| 0.01                                      | 3257   | 0.02                                      | 3320                                 |

Figure 3. The triplet exciton density, calculated using the model described in Section 2d, for three different values of the absorption coefficient  $\alpha$ . The three curves have been normalized so their maximum values coincide, in order to facilitate display. In order of increasing absorption coefficient, the calculated values of these maxima are in the ratio 1:9:5. The various parameters were assigned the values:  $\beta = 7.69 \text{ sec}^{-1}$ ,  $\gamma = 10^{-11} \text{ cm}^3 \text{ sec}^{-1}$ ,  $m = 0.3$ ,  $I_0 = 10^{12} \text{ cm}^{-2} \text{ sec}^{-1}$ ,  $D = 10^{-1} \text{ cm}^2 \text{ sec}^{-1}$  and  $\sigma = 10^{-7} \text{ cm}$ . This corresponds to the limit in which diffusion is rapid and the effective second-order constant is just equal to the annihilation rate constant  $\gamma$ . The values of  $\alpha$  used are given in Table II. The crystal thickness was taken to be 0.5 cm.

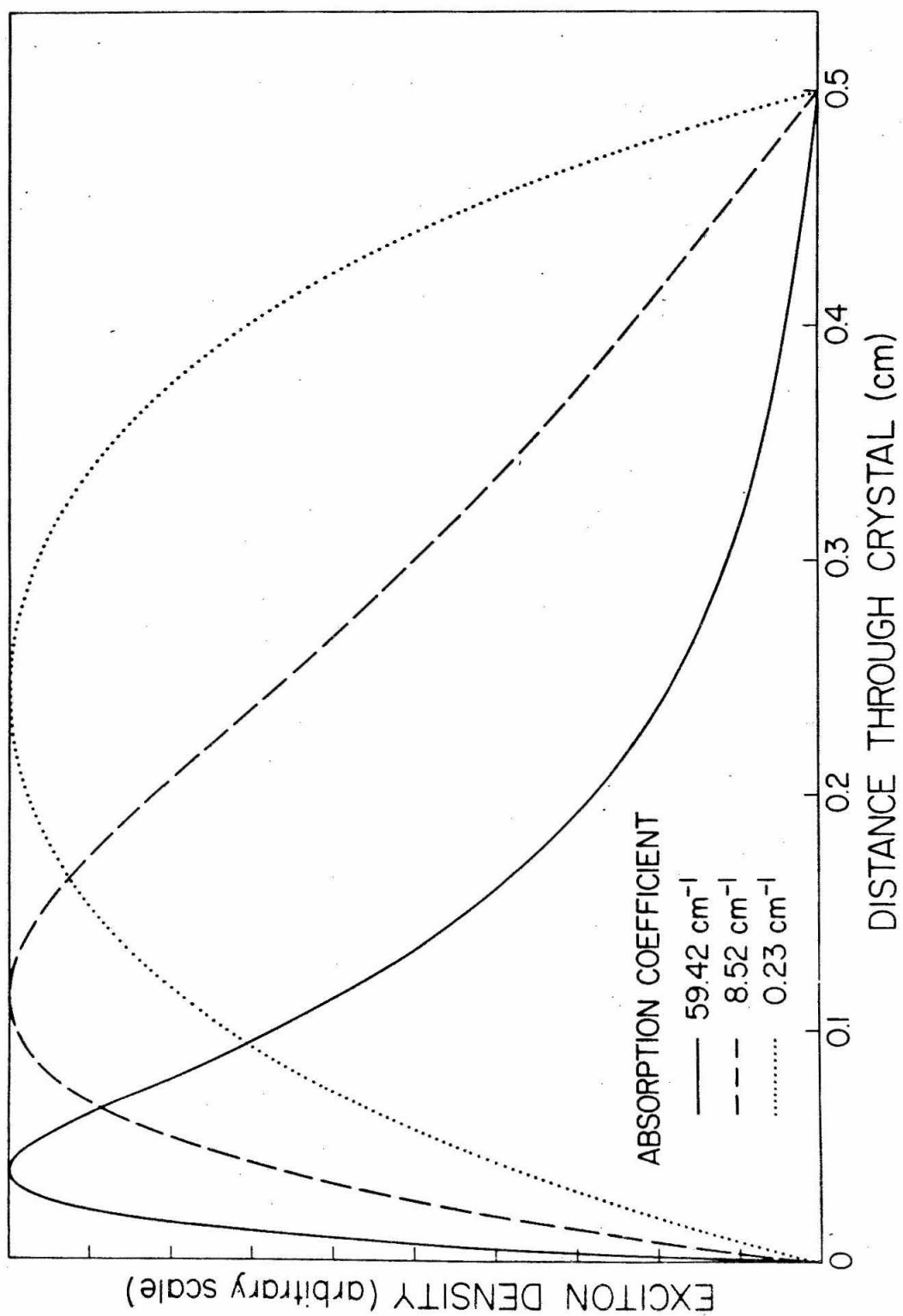


TABLE II. The absorption coefficient for crystalline naphthalene at room temperature. The measurements were made using a 1.0 mm crystal with a Cary Model 14 spectrometer.

| WAVELENGTH ( $\text{\AA}$ ) | ABSORPTION COEFFICIENT ( $\text{cm}^{-1}$ ) <sup>a</sup> |
|-----------------------------|--|
| 3225.0                      | 59.42  |
| 3237.5                      | 59.42  |
| 3250.0                      | 59.42  |
| 3262.5                      | 57.94  |
| 3275.0                      | 46.29  |
| 3287.5                      | 32.70  |
| 3300.0                      | 20.27  |
| 3312.5                      | 11.98  |
| 3325.0                      | 8.52   |
| 3337.5                      | 5.30   |
| 3350.0                      | 2.99   |
| 3362.5                      | 1.61   |
| 3375.0                      | 1.15   |
| 3387.5                      | 0.92   |
| 3400.0                      | 0.46   |
| 3412.5                      | 0.23   |

<sup>a</sup>The experimental uncertainty in these values is believed to be less than 10%.

Figure 4. The phosphorescence excitation spectrum computed from the triplet exciton densities calculated according to the model described in Section 2d. The computed phosphorescence intensities are proportional to  $\int_0^a n_\lambda(x) dx$  where  $a$  is the crystal thickness and  $n_\lambda(x)$  is the triplet exciton density distribution (see Fig. 3) at a particular excitation wavelength  $\lambda$ . A line connecting the computed points has been added to aid in comparing this figure with Fig. 1.

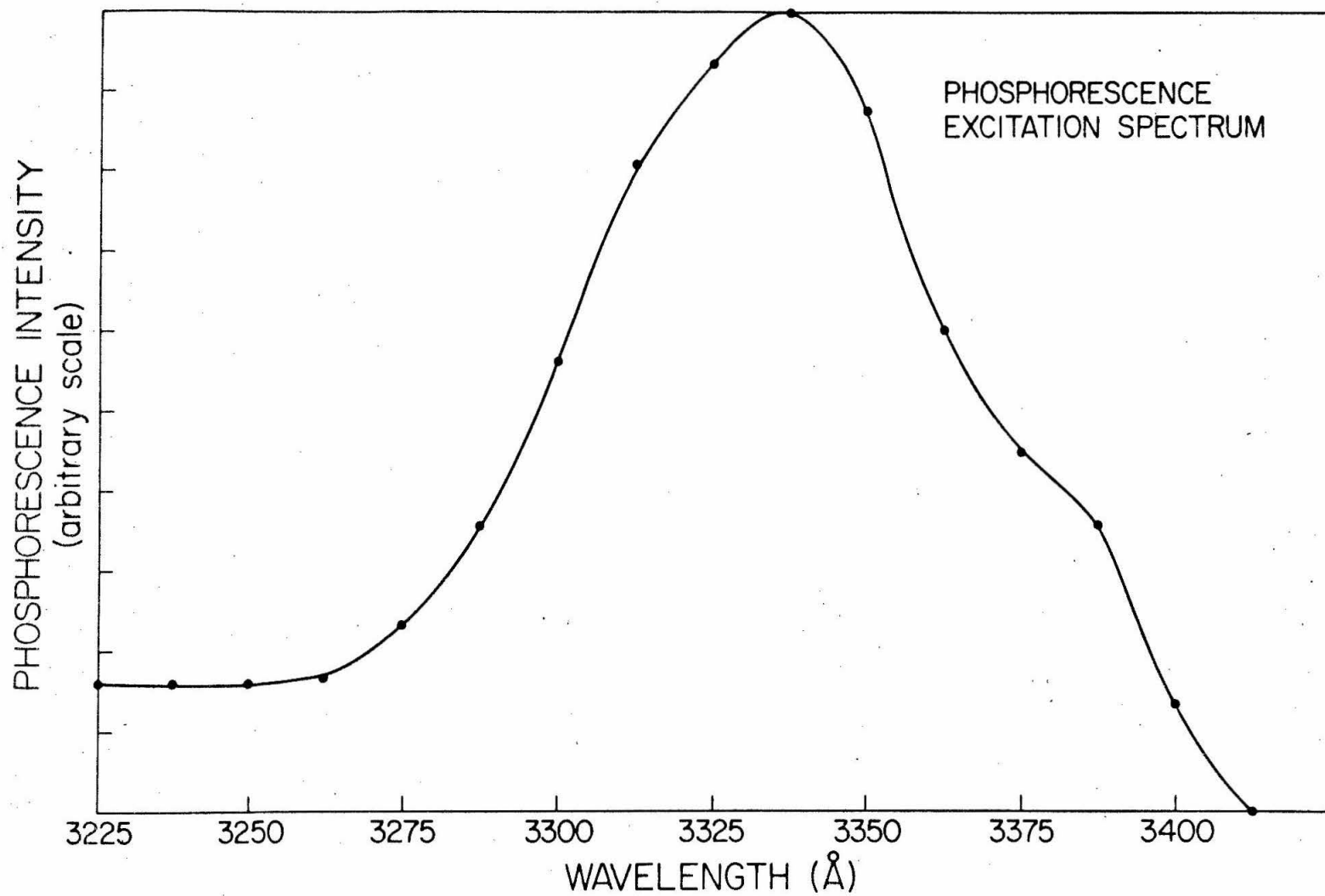
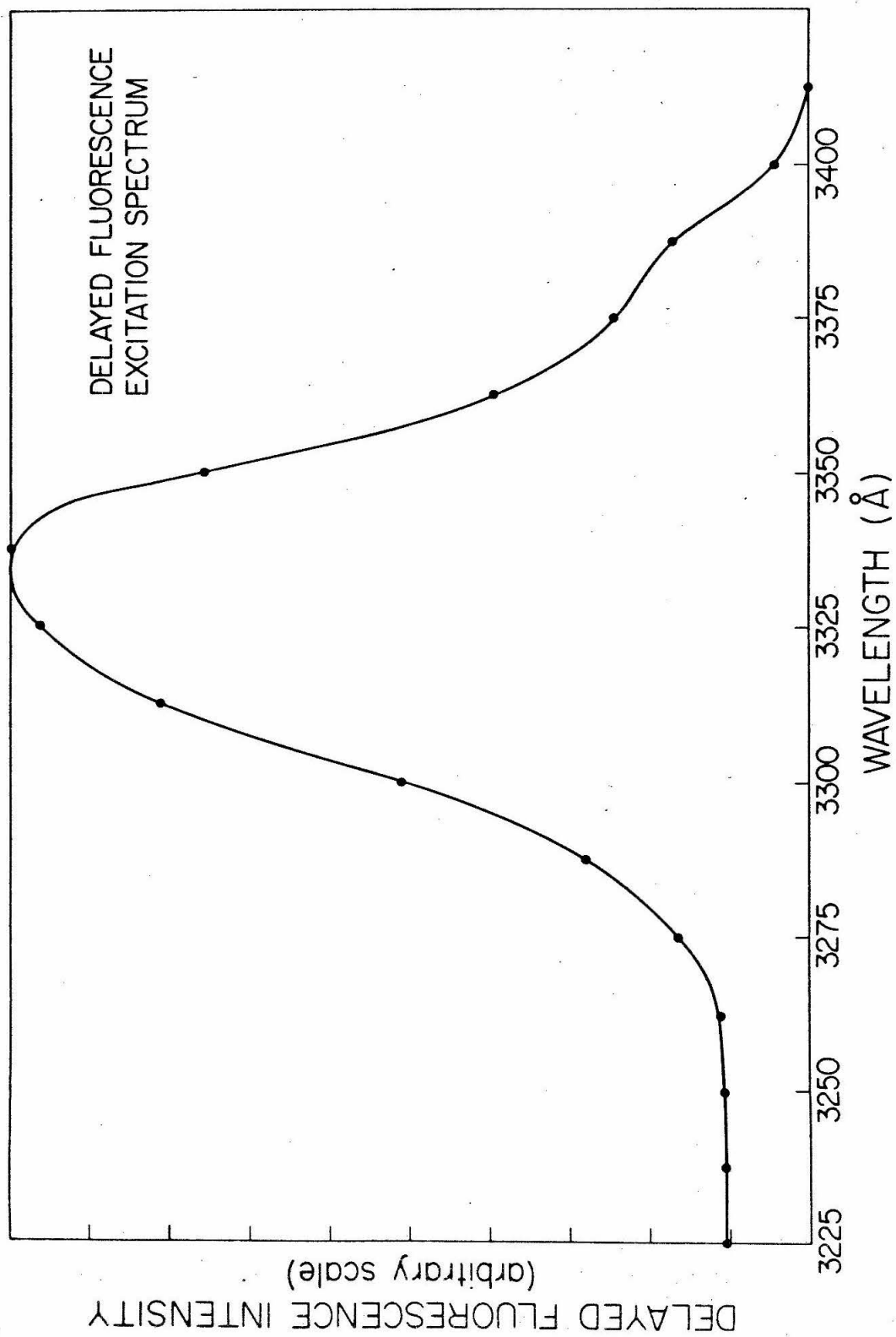


Figure 5. The delayed fluorescence excitation spectrum computed from the triplet exciton densities calculated according to the model described in Section 2d. The computed delayed fluorescence intensities are proportional to  $\int_0^a n_\lambda^2(x) dx$  where  $a$  is the crystal thickness and  $n_\lambda(x)$  is the triplet exciton density distribution (see Fig. 3) at a particular excitation wavelength  $\lambda$ . A line connecting the computed points has been added to aid in comparing this figure with Fig. 2.





dependence upon the excitation intensity with regard to the position of the maximum. The excitation intensity was varied over 6 orders of magnitude in these calculations.

### b. Anthracene

The delayed fluorescence excitation spectrum of crystalline anthracene is shown in Fig. 6. As in the case of naphthalene, the position of the maximum is sensitive to the excitation light intensity. Figure 7 shows the phosphorescence excitation spectrum of anthracene. A study of the excitation intensity dependence of the position of the maximum in this spectrum was not possible with the present experimental setup because of the inherent weakness of the anthracene phosphorescence.

### c. The Spectral Distribution of the Exciting Light

The excitation light intensity at the position of the sample, as a function of wavelength, was determined by replacing the sample with a rhodamine B solution, and recording the rhodamine B emission intensity as the excitation wavelength was scanned through the region of interest. From 4500 Å to 3000 Å, the excitation light intensity was found to be essentially constant; there was a slight decrease in intensity with increasing energy, but certainly nothing sufficient to cause the observed maximum in the excitation spectra. From 3000 Å to higher energy, the intensity of the excitation light was observed to decrease somewhat more rapidly.

Figure 6. The excitation spectrum of the delayed fluorescence emission from pure crystalline anthracene at room temperature. The electrometer input was set at  $10^{-6}$  A full scale with a 0.1 sec time constant, and the scan rate was 50 Å/min.

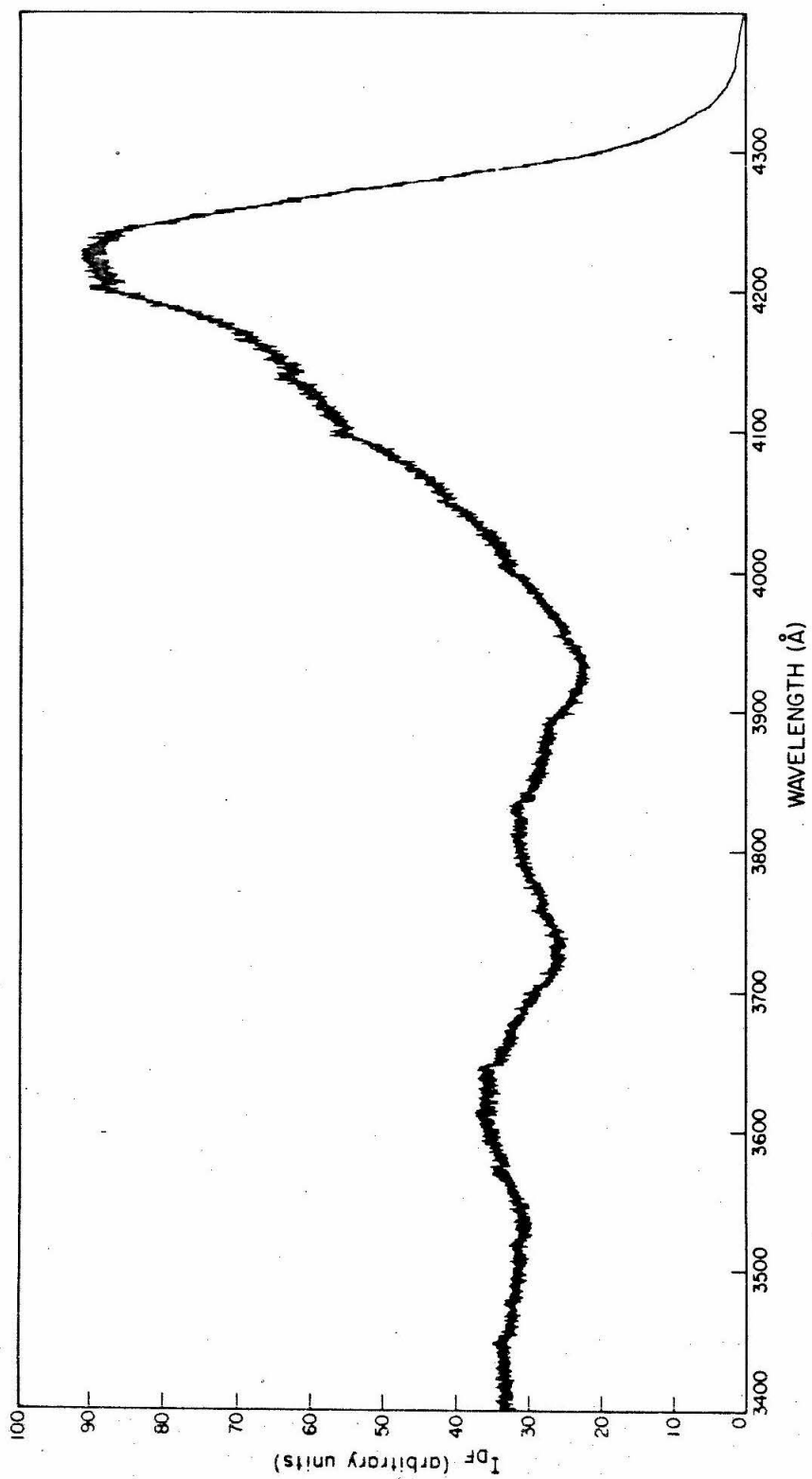
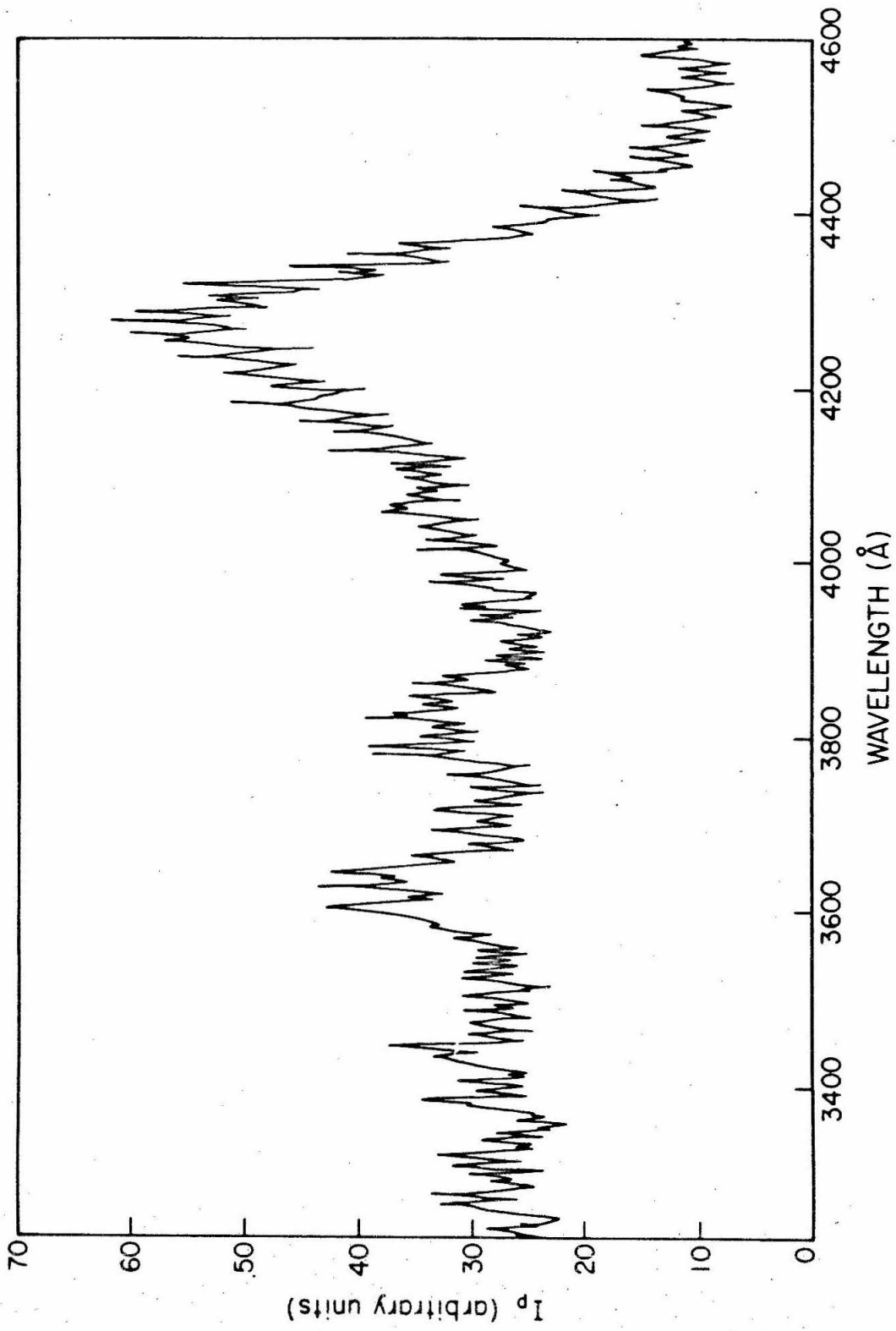


Figure 7. The excitation spectrum of the phosphorescence emission from pure crystalline anthracene at room temperature. A Corning glass filter, C.S. 2-64, was placed directly over the photomultiplier window, the electrometer input was set at  $10^{-9}$  A full scale with a 1 sec time constant, and the scan rate was 125 Å/min.



## 5. DISCUSSION

The semi-infinite-crystal diffusional model (see Section 2a) must be rejected since it predicts incorrect and unphysical behavior as far as the phosphorescence excitation spectrum is concerned. In light of this obvious shortcoming of the model, one is caused to question the validity of the diffusion constant for triplet excitons in crystalline anthracene, determined from the delayed fluorescence excitation spectrum on the basis of this model.<sup>15, 16</sup> The finite-crystal diffusional model (see Section 2b) neglects the effects of triplet-triplet annihilation, an approximation that is probably not valid for our experimental conditions. Consequently, even though preliminary calculations based on this model were reasonably well-behaved, we have made no extensive calculations using the model. The finite-crystal annihilation model (see Section 2c) reduces essentially to a statement of energy conservation, under ideal experimental conditions. In any real experiment there are always complicating factors such as scattered light and the experimental geometry that must be taken into consideration. We conclude then that this particular model is, practically speaking, not of very much use. The remainder of the discussion will therefore be concerned with the finite-crystal diffusional annihilation model (see Section 2d).

We have chosen to make the majority of our calculations using this model since, of the four models discussed in Section 2, it most closely approximates the general picture of triplet exciton dynamics that has emerged over the past few years. All but one of our experimental observations can be accounted for within the framework of this model. The one feature that remains unexplained is the dependence of

the peak position in the delayed fluorescence excitation spectrum on the intensity of the exciting light.

At the outset, it seemed likely that inclusion of the  $\gamma n^2$  term would suffice to explain this effect. However, in retrospect this appears to have been nothing more than a misplaced hope. Apparently, something else is responsible for the failure of the model. On reconsidering the approximations and assumptions that led to the model, the most questionable one would seem to be neglect of re-absorption of the delayed fluorescence emission. The results presented in Table I show that as the excitation intensity is increased, the peak position of the delayed fluorescence shifts toward the red. One might expect this sort of behavior if a large fraction of the total emitted light were of an energy that could be strongly re-absorbed. Clearly, this could only be important for the shortest wavelengths of delayed fluorescence since the absorption coefficient for other wavelengths is extremely small.

Although re-absorption might be responsible for the discrepancy between the observed behavior and that predicted by the model, other possibilities must not be too hastily ruled out. For example, it may be necessary to include in Eq. (1) terms of higher order in the triplet exciton density  $n$ ; these terms could conceivably become important at sufficiently high excitation light intensities. If the answer does not lie in including re-absorption and/or these higher order terms, then it seems likely that something fundamental is lacking in our present picture of triplet exciton dynamics. Until the origin of the discrepancy is thoroughly understood, it will not be possible to make any meaningful



determination of the diffusion constant for triplet excitons from the excitation spectra of the crystal emissions.

## 6. CONCLUSIONS

1. The excitation spectra of phosphorescence and delayed fluorescence from crystalline naphthalene and anthracene have been presented.
2. A model used previously<sup>15, 16</sup> to interpret the delayed fluorescence excitation spectrum of anthracene has been found inadequate to explain the observed phosphorescence excitation spectrum.
3. Calculations of the excitation spectra of naphthalene, based on a more realistic model have been compared with the experimental results.
4. In its present form, the model cannot explain the observed dependence of the position of the maximum in the delayed fluorescence excitation spectrum on excitation light intensity.
5. Suggestions for improving the model have been discussed.

REFERENCES

1. H. Sternlicht, G. C. Nieman and G. W. Robinson, J. Chem. Phys. 38, 1329 (1963); ibid. 39, 1610 (1963).
2. J. L. Katz, J. Jortner, S. -I. Choi and S. A. Rice, J. Chem. Phys. 39, 1897 (1963).
3. R. G. Kepler, J. C. Caris, P. Avakian and E. Abramson, Phys. Rev. Letters 10, 400 (1963).
4. C. A. Hutchison, Jr., Rec. Chem. Progr. 24, 105 (1963).
5. D. M. Hanson and G. W. Robinson, J. Chem. Phys. 43, 4174 (1965).
6. F. R. Lipsett and G. MacPherson, Can. J. Phys. 44, 1485 (1966).
7. D. F. Williams, J. Chem. Phys. 47, 344 (1967).
8. R. C. Johnson, R. E. Merrifield, P. Avakian and R. B. Flippen, Phys. Rev. Letters 19, 285 (1967).
9. R. H. Clarke and R. M. Hochstrasser, J. Chem. Phys. 46, 4532 (1967).
10. R. M. Hochstrasser, J. Chem. Phys. 47, 1015 (1967).
11. S. D. Colson, D. M. Hanson, R. Kopelman and G. W. Robinson, J. Chem. Phys. 48, 2215 (1968).
12. E. B. Priestley and A. Haug, J. Chem. Phys. 49, 622 (1968).
13. B. -S. Sommer and J. Jortner, J. Chem. Phys. 50, 839 (1969).
14. P. Avakian and R. E. Merrifield, Mol. Cryst. 5, 37 (1968).
15. R. G. Kepler and A. C. Switendick, Phys. Rev. Letters 15, 56 (1965).

16. D. F. Williams and J. Adolf, J. Chem. Phys. 46, 4252 (1967).
17. P. Avakian and R. E. Merrifield, Phys. Rev. Letters 13, 541 (1964).
18. V. Ern, P. Avakian and R. E. Merrifield, Phys. Rev. 148, 862 (1966).
19. M. Levine, J. Jortner and A. Szöke, J. Chem. Phys. 45, 862 (1966).
20. P. Avakian, V. Ern, R. E. Merrifield and A. Suna, Phys. Rev. 165, 974 (1968).
21. G. Maier, U. Haeberlen and H. C. Wolf, Physics Letters 25A, 323 (1967).
22. In these experiments, the triplet excitons were generated via the singlet state, i. e., the molecules were first excited into their singlet state and thence to their triplet state by intersystem crossing.
23. V. Ern, Phys. Rev. Letters 22, 343 (1969).
24. R. M. Noyes, "Effects of Diffusion Rates on Chemical Kinetics" in Progress in Reaction Kinetics, G. Porter, Ed. (Pergamon Press, Oxford, 1961), Vol. I, p. 130.
25. W. H. Melhuish, J. Opt. Soc. Am. 52, 1256 (1962).

SECTION C

ON THE APPARENT ABSENCE OF TRIPLET-TRIPLET  
ABSORPTION IN PURE ORGANIC CRYSTALS

## 1. INTRODUCTION

Triplet-triplet absorption in  $\pi$ -electron molecules has received considerable attention over the past several years.<sup>1-32</sup> The earliest study of this type of absorption was made by Lewis *et al.*<sup>1</sup> even before the states involved in the transition had been identified as triplet states by Lewis and Kasha.<sup>2</sup> Numerous other experimental investigations of triplet-triplet absorption have been reported<sup>3-23</sup> during the years since this pioneering work of Lewis and his co-workers.

Triplet-triplet absorption spectra of a large number of  $\pi$ -electron molecules have now been measured under a wide variety of experimental conditions. Perhaps the single most commonly used technique has been to embed the absorbing molecules in a glassy environment (EPA or some hydrocarbon, for example) at 77° K.<sup>4, 16, 18</sup> McClure<sup>3</sup> was the first to make extensive use of this method for obtaining triplet-triplet absorption spectra. The absorption by organic molecules in fluid solutions at room temperature and in the vapor phase at elevated temperatures has also been recorded,<sup>5-7, 9</sup> and it has been shown<sup>10, 11, 17, 21</sup> that triplet-triplet absorption is observable in certain types of mixed molecular crystals where the guest-host energy gap is large. Other studies have been concerned with the pressure dependence,<sup>20</sup> the concentration dependence<sup>15</sup> and the polarization properties<sup>8, 10, 11, 14, 21</sup> of the absorption. Theoretical calculations<sup>24-32</sup> have been found useful especially for predicting the number of allowed transitions, in addition to giving crude estimates of the transition energies.

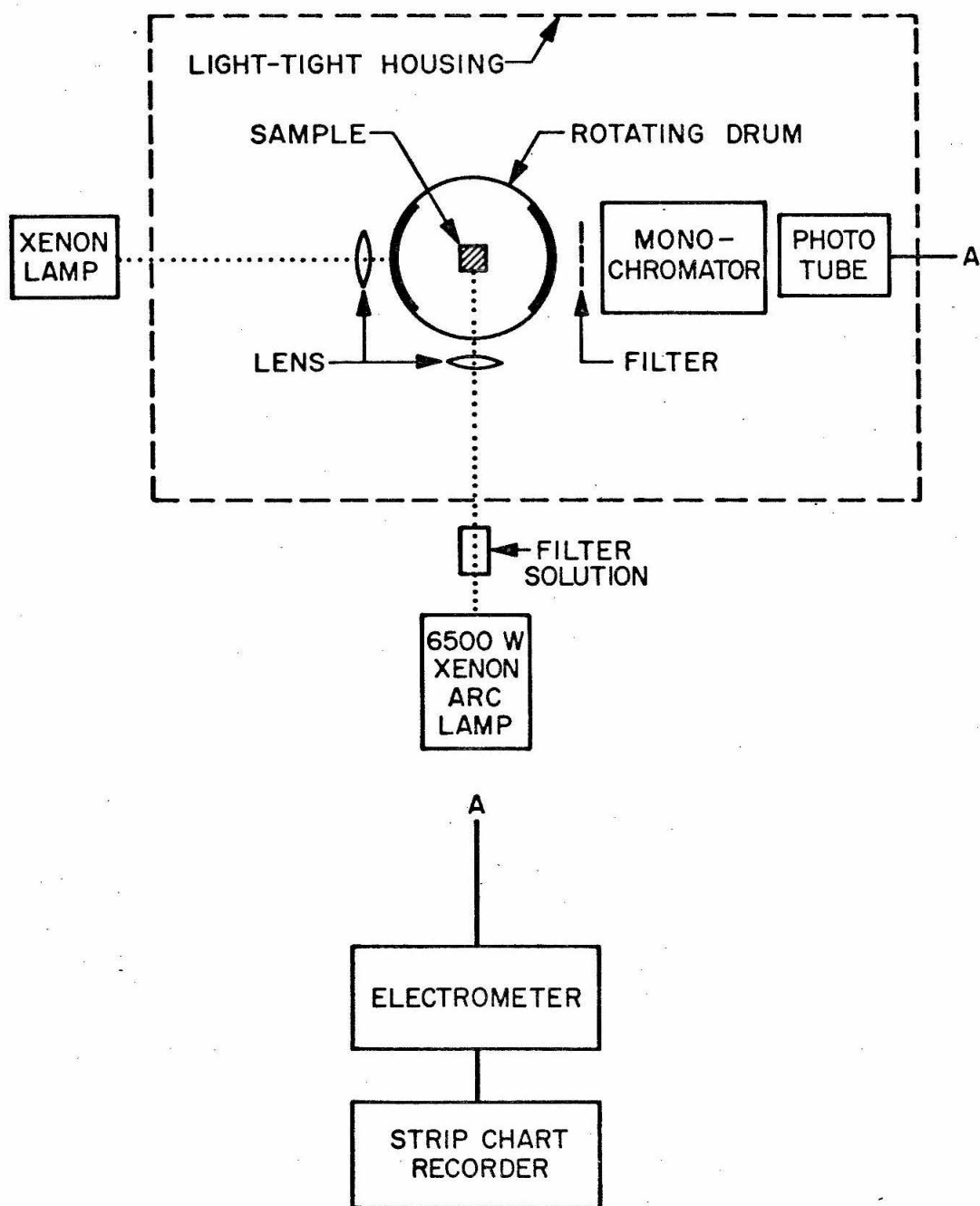
In spite of this vast amount of activity, there has been no report of triplet-triplet absorption in pure crystals or even in isotopic mixed crystals. Although one can immediately point out some obvious reasons why triplet-triplet absorption would be more difficult to detect in such crystals, we were curious to see if there might be some more fundamental reason for the apparent absence of this phenomenon. In addition, if the absorption could be found it would provide yet another method for following the behavior of triplet states in organic crystals. The present paper is therefore concerned with the exact nature of the differences between triplet-triplet absorption in a hydrocarbon glass at 77° K and in an isotopically mixed crystal at 4.2° K. The case of pure molecular crystals is also discussed and experimental data are presented in support of the discussion.

## 2. EXPERIMENTAL

### a. The Apparatus

The experimental arrangement is illustrated schematically in Fig. 1. A rotating cylindrical drum with two opposing slots cut in its circumference provided alternate access to the sample by two light beams positioned at right angles to each other. For the measurements reported herein the drum was rotated at 1725 rpm corresponding to access intervals of approximately 8.2 msec, the slots each subtending an angle of 1.48 radians at the center of the drum. The two light sources were, respectively, a 6500 W xenon arc used to excite the necessary triplet states and a 500 W xenon arc for measuring the

Figure 1. A diagram of the experimental arrangement used to record the triplet-triplet absorption spectra.





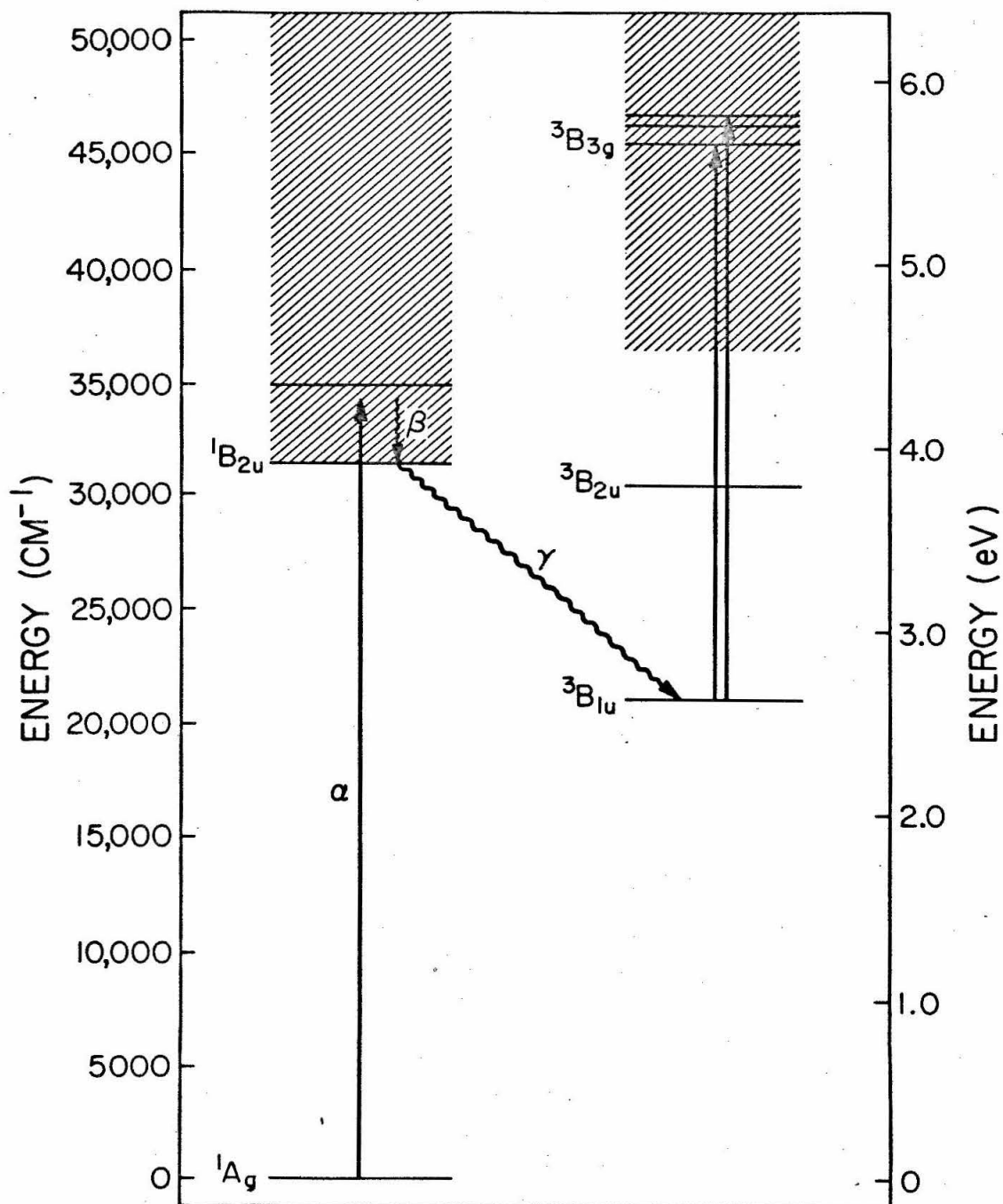
absorption. A 0.5-m Jarrell-Ash spectrometer equipped with a grating having 1180 grooves/mm, blazed at 5000 Å in first order, and a dry-ice cooled EMI 6256 SA photomultiplier was used to scan the spectrum. The spectrometer has a reciprocal linear dispersion of 16 Å/mm at the exit slit and an effective aperture ratio of  $f/8.6$ . The slitwidth was set at  $15\mu$ . The output from the photomultiplier was fed into a Victoreen Model VTE-1 electrometer where it was amplified and recorded on a strip-chart recorder.

### b. The Experimental Procedure

The relevant energy levels of the naphthalene molecule are depicted in Fig. 2. Absorption into the excited singlet manifold (process  $\alpha$ ) is followed by rapid relaxation (process  $\beta$ ) to the lowest excited singlet  $^1B_{2u}$  state. Some of the molecules in this state undergo a radiationless transition (process  $\gamma$ ) to the lowest triplet  $^3B_{1u}$  state thus providing the requisite triplet state population. Absorption from the lowest triplet state to higher triplet states was studied by observing spectral changes correlated with the presence or absence of the exciting light.

Point-by-point determination of the spectrum was found to be the most sensitive method for this sort of absorption measurement. The spectrometer was set at a given wavelength and the photomultiplier output recorded for some specified length of time, alternately with and without the excitation light striking the sample. The transmission of the sample was observed to decrease when the excitation light was allowed to impinge upon it and to return to its original value when the

**Figure 2.** An energy level diagram for naphthalene showing the energy levels of importance in triplet-triplet absorption.



exciting light was blocked. Three measurements of this change were made and the results averaged, after correcting for the wavelength dependence of the system response, to arrive at the magnitude of the absorption at each wavelength. Measurements were made throughout the region extending from 3200 Å (near the singlet absorption edge) to 6000 Å. The interval between successive measurement points varied from 10 to 100 Å so that positions of peaks can be located at best only to within 10 Å. However, since the features in the spectrum seem to be quite broad, this probably is not a serious limitation and will not influence the conclusions to be drawn later in the paper.

Under conditions similar to the actual experimental conditions in all respects except that an empty sample tube replaced the sample, no difference was observed in the transmitted intensity with or without the excitation light on.

### c. Sample Preparation

All crystalline samples were purified by a combination of zone-refining and potassium fusion<sup>33-35</sup> and grown from the melt in sealed quartz tubes. To ensure good thermal contact between the sample and the cryogenic bath when working at 4.2° K, the crystal tubes were broken open by means of a break-seal while submersed in liquid helium.

For the experiments on the glassy state at 77° K, dry 3-methylpentane and zone-refined, potassium-purified naphthalene were used, with special care being exercised in degassing the compounds. The glass was obtained by simply submersing this solution in liquid nitrogen prior to its use in the experiments.

### 3. RESULTS

It was established experimentally, by scanning the region from 4700 Å to 6000 Å with the exciting light on and the spectroscopic light off, that the phosphorescence emission from the samples was of negligible intensity relative to the spectroscopic light so that the triplet-triplet absorption spectrum is in no way complicated by phosphorescence.

#### a. Naphthalene- $\text{h}_8$ in 3-Methylpentane at 77° K

The upper curve in Fig. 3 shows the triplet-triplet absorption spectrum of a  $7.4 \times 10^{-3}$  M solution of naphthalene- $\text{h}_8$  in 3-methylpentane at 77° K. The three transition maxima at 24,089  $\text{cm}^{-1}$ , 25,535  $\text{cm}^{-1}$  and 26,946  $\text{cm}^{-1}$  correspond to previously reported transitions in the triplet-triplet absorption spectrum of naphthalene in other environments.<sup>36</sup> Three new, less intense maxima are evident at 24,993  $\text{cm}^{-1}$ , 26,308  $\text{cm}^{-1}$  and 27,770  $\text{cm}^{-1}$ . Peak positions, relative intensities and spacings between successive maxima in the spectrum are summarized in Table I.

#### b. Naphthalene- $\text{h}_8$ in Naphthalene- $\text{d}_8$ at 4.2° K

The lower curve in Fig. 3 is the triplet-triplet absorption spectrum of an isotopically mixed crystal consisting of 1.0 wt% naphthalene- $\text{h}_8$  in 99.0 wt% naphthalene- $\text{d}_8$  at 4.2° K. The mixed crystal spectrum appears qualitatively the same as the triplet-triplet spectrum of naphthalene in a glass, with the exception of the broad background continuum absorption extending both to higher and lower energy from the principal

Figure 3. The triplet-triplet absorption spectra of naphthalene-h<sub>8</sub> in 3-methylpentane at 77° K and of naphthalene-h<sub>8</sub> in naphthalene-d<sub>8</sub> at 4.2° K.

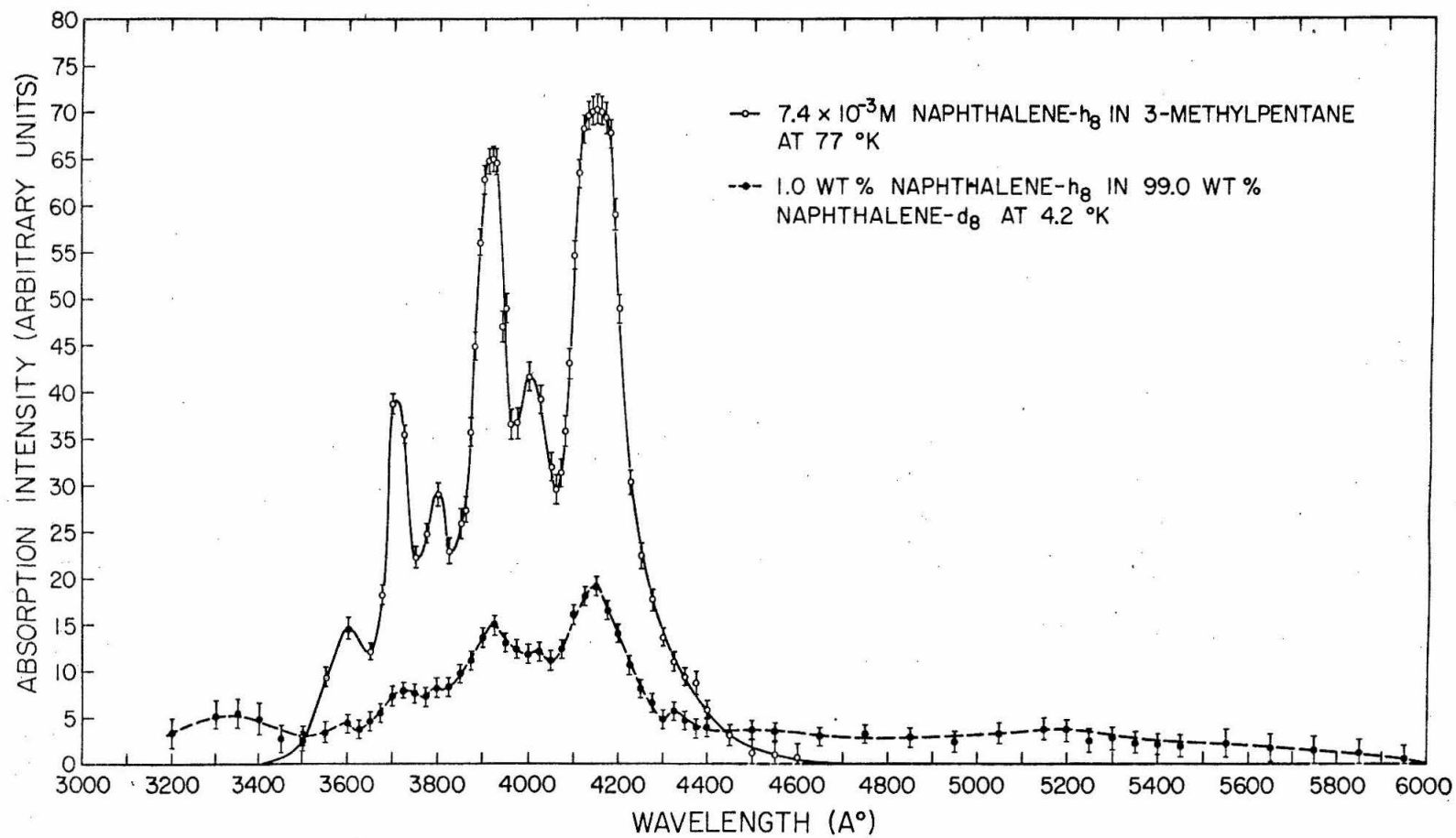


TABLE I. The triplet-triplet absorption spectrum of  
naphthalene- $\underline{h}_8$  in 3-methylpentane at 77° K.

| $\lambda(\text{\AA})^a$ | $\nu_{\text{vac}} (\text{cm}^{-1})$ | $\Delta\nu (\text{cm}^{-1})$ | Intensity <sup>b</sup> |
|-------------------------|-------------------------------------|------------------------------|------------------------|
| 4150                    | 24,089                              | 0                            | 100                    |
| 4000                    | 24,993                              | 904                          | 20                     |
| 3915                    | 25,535                              | 1446                         | 55                     |
| 3800                    | 26,308                              | 2219                         | 15                     |
| 3710                    | 26,946                              | 2857                         | 20                     |
| 3600                    | 27,770                              | 3681                         | 10                     |

<sup>a</sup>Peak positions of the three most intense transitions are accurate to 10 Å. Positions of the other three peaks are accurate to 25 Å.

<sup>b</sup>Normalized so that the most intense peak has an intensity of 100.



spectral features. There is a one-to-one correspondence between the prominent peaks in the spectrum of the mixed crystal and that of the glass. Furthermore, the widths of the features in the spectrum of the glass and of the mixed crystal appear to be about the same. At  $77^{\circ}\text{K}$  the triplet-triplet absorption in the mixed crystal was so weak as to be virtually undetectable with the present apparatus. Table II summarizes the pertinent features in the  $4.2^{\circ}\text{K}$  mixed crystal triplet-triplet absorption spectrum.

#### c. Pure Crystalline Naphthalene

No triplet-triplet absorption could be detected in pure crystalline naphthalene at room temperature,  $77^{\circ}\text{K}$ ,  $4.2^{\circ}\text{K}$  or  $1.8^{\circ}\text{K}$ .

### 4. DISCUSSION

Consider first the relative intensities of the spectra in Fig. 3. Both spectra were recorded using the same overall detection sensitivity so that, if the absorbing species (triplet-state guest molecules) were uniformly distributed through both samples, comparison between the two could be made directly. However, the distribution of excited guest molecules is certainly not uniform in either sample, there being a much higher density of the metastable absorbing species produced in that part of the sample nearest the excitation light. The penetration depth of the exciting light is roughly 1000 times greater in the glass than in the mixed crystal at the solute concentrations used for these experiments. Since the host crystal absorbs strongly in the same spectral

TABLE II. The triplet-triplet absorption spectrum of  
naphthalene- $\underline{h}_8$  in naphthalene- $\underline{d}_8$  at 4.2° K.

| $\lambda(\text{\AA})^a$   | $\nu_{\text{vac}} (\text{cm}^{-1})$ | $\Delta\nu (\text{cm}^{-1})$ | Intensity <sup>b</sup>  |
|---|-------------------------------------|------------------------------|---|
| 4150  | 24,089                              | 0                            | 100   |
| 4025  | 24,838                              | 749                          | c   |
| 3925  | 25,470                              | 1381                         | 60  |
| 3800  | 26,308                              | 2219                         | c   |
| 3725  | 26,838                              | 2749                         | 20  |
| 3600  | 27,770                              | 3681                         | c   |
| Broad absorption extending<br>from 6000 Å to the $^1\text{B}_{2u} - ^1\text{A}_g$<br>absorption edge. |                                     |                              | The total integrated<br>intensity of this<br>band is roughly<br>equal to that of the<br>discrete transitions. |

<sup>a</sup>Peak positions are only accurate to 25 Å.

<sup>b</sup>Normalized so that the most intense peak has an intensity of 100.

<sup>c</sup>It was not possible to get a reasonable estimate for the intensities of these transitions.

region as the guest, as far as its response to the excitation light is concerned, the isotopically mixed crystal behaves just like a pure crystal and most of the light is absorbed very near the surface. At low temperatures a significant fraction of this host excitation is rapidly transferred to the guest molecules<sup>37</sup> so that the resulting distribution of triplet-state guests is essentially identical to the initial host excitation distribution.

Although it is true that the total number of guest molecules excited to the triplet state by the excitation light is considerably greater in the mixed crystal than in the glass, the distribution of these metastable absorbers in the crystal is such that they present a very small optical density to the spectroscopic light beam. Consequently, it is not possible to predict which of the two samples will give rise to the more intense absorption on the basis of the relative numbers of absorbing species alone; rather, the distribution of, as well as the total number of absorbers must be taken into account.<sup>38</sup> The observed absorption intensity due to non-uniformly distributed absorbing species represents a balance between the total number of absorbers and their spatial distribution in the sample. Hence, direct comparison of the relative intensities of the spectra shown in Fig. 3 has no meaning.

a. Naphthalene-h<sub>8</sub> in 3-Methylpentane at 77° K

The three most intense transitions in the triplet-triplet absorption spectrum of the glass form a progression with spacings of 1450 cm<sup>-1</sup> between successive bands. This energy is reminiscent of ground-state totally symmetric carbon-carbon stretching vibrational energies and is

suggestive that such a vibration may be participating in the absorption. These bands are by now quite familiar, having been observed in the triplet-triplet absorption spectrum of naphthalene in a wide variety of environments and using several different experimental techniques.<sup>3-12, 17</sup> Three weaker transitions<sup>39</sup> that appear to form a similar progression characterized by roughly  $1450\text{ cm}^{-1}$  spacings are also evident. There is more uncertainty in the precise positions of these bands due to a lower density of experimental points in the neighborhood of the peaks. This progression is shifted to the blue from that formed by the three most intense bands by some  $800\text{ cm}^{-1}$ . Naphthalene is rich in vibrations having energies of this magnitude and it is likely that these weaker transitions are the result of combination tones involving a symmetric carbon-carbon stretching mode and some other mode, also probably totally symmetric, having an energy of about  $800\text{ cm}^{-1}$ , built on the purely electronic transition. The complete spectrum can thus be interpreted in terms of a single electronic transition with its associated vibrational structure.

b. Naphthalene- $\text{h}_8$  in Naphthalene- $\text{d}_8$  at  $4.2^\circ\text{K}$

The resolved structure in the isotopically mixed crystal triplet-triplet absorption spectrum correlates well with that observed in the glass at  $77^\circ\text{K}$  so that no further discussion of this structure per se is needed. However, the broad background absorption in which the structure appears to be embedded is unique to the mixed crystal spectrum and does merit some additional consideration.

We observe first of all that there are energy states of the crystal, viz., the charge-transfer states and the conduction band, that have no counterpart in the glass. Furthermore, host-guest interactions

are expected to be of similar magnitude to host-host interactions in isotopic mixed crystals since the host and guest molecules have nearly degenerate energy states. Such host-guest interactions can cause mixing of the host and guest zero-order states, so that the correct states of the crystal can be viewed as being partly host and partly guest in character.<sup>40</sup> Consequently, transitions originating on a purely guest energy level will have a non-zero probability of terminating on any level of the proper symmetry that has guest character. This sort of mechanism is proposed to account for the observed triplet-triplet absorption spectrum of naphthalene- $\underline{h}_8$  in naphthalene- $\underline{d}_8$  at 4.2° K. In this particular instance, mixing of the host conduction band and perhaps also the host charge-transfer states with the lowest  $^3B_{1u}$  state of the guest would be necessary.

The conduction band in anthracene has been variously placed at energies ranging from 2.6 eV<sup>41</sup> to 4.9 eV.<sup>42</sup> A value greater than 3.5 eV,<sup>43</sup> perhaps to the order of 4.4 eV,<sup>44</sup> seems to be most probable. The charge-transfer state in anthracene has been reported to have an energy of 3.45 eV.<sup>43</sup> Evidently, the conduction band lies higher in energy than the charge-transfer state in anthracene, a trend that is also observed in tetracene.<sup>43</sup> The charge-transfer state in naphthalene has been placed at  $4.4 \pm 0.2$  eV,<sup>45</sup> so that, on the basis of the anthracene and tetracene results, the conduction band in naphthalene might reasonably be expected to lie at energies on the order of 5 to 6 eV above the ground state.

Recalling that the ground-state to triplet-state energy interval in naphthalene is 2.63 eV, it is evident from Fig. 3 that the continuum

absorption has a threshold at about 4.6 eV and extends to higher energy. The threshold of the absorption lies very close to the position of the charge-transfer state so that participation of this state in the mixing cannot be ruled out. Clearly, the predicted position of the conduction band coincides with the observed continuum absorption.

### c. Pure Crystalline Naphthalene

The absence of any detectable triplet-triplet absorption in pure crystalline naphthalene is probably explained by the lower steady-state concentration of triplet states in the pure crystal compared to that in the mixed crystal. This decrease is due largely to the shorter triplet-state lifetime in the pure crystal.<sup>46</sup> This conclusion is substantiated by the fact that at 77° K triplet-triplet absorption in the isotopically mixed crystal is extremely weak.

## 5. CONCLUSIONS

Differences between triplet-triplet absorption in a hydrocarbon glass at 77° K and in an isotopic mixed crystal at 4.2° K have been discussed. The principle difference is a broad continuum background absorption in the mixed crystal spectrum which is interpreted in terms of host-guest interactions causing mixing between the guest  $^3B_{1u}$  state and host conduction band. At 77° K the absorption in the mixed crystal is too weak to be detected; this is probably due to the lower steady-state concentration of triplet states at 77° K relative to that at 4.2° K. No triplet-triplet absorption was detected in pure samples at

temperatures down to  $1.8^{\circ}$  K presumably because of the small steady-state triplet concentration caused by rapid processes such as triplet-triplet annihilation. If our interpretation of the broad continuum absorption were correct, then for a series of mixed crystals of naphthalene in various host materials having progressively larger host-guest energy separations, one would expect the mixed crystal triplet-triplet spectrum to approach that of naphthalene in a glass at  $77^{\circ}$  K as the energy separation is made very large.

REFERENCES

1. G. N. Lewis, D. Lipkin, and T. T. Magel, J. Am. Chem. Soc. 63, 3005 (1941).
2. G. N. Lewis and M. Kasha, J. Am. Chem. Soc. 66, 2100 (1944).
3. D. S. McClure, J. Chem. Phys. 19, 670 (1951).
4. D. P. Craig and I. G. Ross, J. Chem. Soc. 1954, 1589.
5. G. Porter and M. W. Windsor, Discussions Faraday Soc. 17, 178 (1954).
6. G. Porter and F. J. Wright, Trans. Faraday Soc. 51, 1205 (1955).
7. G. Porter and M. W. Windsor, Proc. Roy. Soc. (London) A245, 238 (1958).
8. M. A. El-Sayed and T. Pavlopoulos, J. Chem. Phys. 39, 834 (1963).
9. G. Porter and F. Wilkinson, Proc. Roy. Soc. (London) A264, 1 (1964).
10. R. M. Hochstrasser and S. Lower, J. Chem. Phys. 40, 1041 (1964).
11. D. P. Craig and G. Fischer, Proc. Chem. Soc. 1964, 176.
12. S. Siegel and K. B. Eisenthal, J. Chem. Phys. 42, 2494 (1965).
13. I. A. Zhmyreva, V. P. Kolobkov, and S. V. Volkov, Opt. Spectrosc. 20, 162 (1966).
14. K. B. Eisenthal, J. Chem. Phys. 46, 3268 (1967).
15. T. N. Bolotnikova and T. M. Naumova, Opt. Spectrosc. 23, 206 (1967).



16. R. Astier and Y. Meyer, J. Chim. Phys. 64, 919 (1967).
17. D. P. Craig and G. Fischer, Trans. Faraday Soc. 63, 530 (1967).
18. B. R. Henry and M. Kasha, J. Chem. Phys. 47, 3319 (1967).
19. The Triplet State, A. B. Zahlan, Ed. (Cambridge University Press, London, England, 1967). Several articles dealing with different aspects of triplet-triplet absorption are contained in this book.
20. M. Nicol and J. Somekh, J. Opt. Soc. Am. 58, 233 (1968).
21. R. M. Hochstrasser and A. P. Marchetti, Chem. Phys. Letters 1, 597 (1968).
22. E. J. Land, Proc. Roy. Soc. (London) A305, 457 (1968).
23. J. S. Brinan, J. Chem. Phys. 49, 586 (1968).
24. R. Pariser, J. Chem. Phys. 24, 250 (1956).
25. D. R. Kearns, J. Chem. Phys. 36, 1608 (1962).
26. L. Goodman and J. R. Hoyland, J. Chem. Phys. 39, 1068 (1963).
27. R. E. Peacock and P. T. Wilkinson, Proc. Phys. Soc. (London) 83, 525 (1964).
28. G. J. Hoytink, J. Appl. Chem. (London) 11, 393 (1965).
29. G. Nouchi, Compt. Rend. 262B, 27 (1966).
30. R. L. DeGroot and G. J. Hoytink, J. Chem. Phys. 46, 4523 (1967).
31. M. K. Orloff, J. Chem. Phys. 47, 235 (1967).
32. G. Wagnière, Theor. Chim. Acta 9, 312 (1968).
33. M. A. El-Sayed, M. T. Wauk, and G. W. Robinson, Mol. Phys. 5, 205 (1962).
34. D. M. Hanson and G. W. Robinson, J. Chem. Phys. 43, 4174 (1965).

35. S. D. Colson and E. R. Bernstein, J. Chem. Phys. 43, 2661 (1965).
36. See, for example, Ref. 4.
37. S. D. Colson and G. W. Robinson, J. Chem. Phys. 48, 2550 (1968).
38. I. G. Ross, J. Opt. Soc. Am. 44, 40 (1954).
39. In a recent publication (Ref. 17), Craig and Fischer also reported two weak transitions in a sample of naphthalene-d<sub>8</sub> in durene at 4.2° K, in addition to the three commonly observed intense transitions. The relative positions of these peaks are similar to those observed in Fig. 3.
40. B. -S. Sommer and J. Jortner, J. Chem. Phys. 50, 822 (1969).
41. L. E. Lyons, Proc. Chem. Soc. 1962, 71.
42. D. R. Kearns, J. Chem. Phys. 41, 581 (1964), and references therein.
43. M. Pope, J. Burgos, and J. Giachino, J. Chem. Phys, 43, 3367 (1965).
44. G. Castro and J. F. Hornig, J. Chem. Phys. 42, 1459 (1965).
45. W. L. Greer, S. A. Rice, J. Jortner, and R. Silbey, J. Chem. Phys, 48, 5667 (1968).
46. E. B. Priestley and A. Haug, J. Chem. Phys. 49, 622 (1968).

Typical first-order triplet lifetimes observed using purified crystals at room temperature are of the order of 130 msec. Recently, a particularly good crystal has yielded a lifetime of 395 msec. However, even in the event that the first-order triplet lifetime is

long in the crystal, second-order effects play a dominant role in establishing the steady-state concentration of triplets in a pure or isotopic mixed crystal. Thus, even though few triplets are lost via first-order decay, the steady-state concentration of triplets can be very low due to rapid second-order depletion of the triplet population.

PART III

AN INVESTIGATION OF DELAYED LIGHT EMISSION  
FROM Chlorella Pyrenoidosa

SECTION A

MEASUREMENT OF RAPID PHOTOPROCESSES USING  
A MODULATED cw LASER

The following is the text of a paper accepted for publication in the  
Review of Scientific Instruments

[B. E. Kohler, A. Haug, E. B. Priestley and G. W. Robinson,  
Rev. Sci. Instr. 40, 0000 (1969)]

## 1. INTRODUCTION

The fluorescence lifetimes of electronic transitions in molecules fall in the range between  $10^{-9}$  sec and about  $10^{-6}$  sec. Several methods have been used for measuring such short times. The phase fluorometric technique<sup>1-3</sup> requires that the intensity of the excitation light be modulated periodically at a frequency comparable to the decay constant of the excited state. As a consequence, the resultant emitted light intensity is modulated at the same frequency as the exciting light but delayed by a phase angle  $\beta$ . Under the assumption of an exponential decay, the lifetime  $\tau$  is given by  $\tan \beta = \omega\tau$ , where  $\omega$  is the modulation frequency. Lifetimes between  $10^{-7}$  sec and  $10^{-9}$  sec can be investigated with ultrasonic modulators operating in the MHz region.<sup>1, 2, 4</sup> Unfortunately, no simple relationship exists between the phase angle  $\beta$  and the decay constants of interest when the decay is non-exponential. Although it is possible to determine these constants from measurements of the phase angle as a function of frequency,<sup>5</sup> the problems associated with making the measurements as well as with interpreting the results tend to limit the usefulness of the method. This technical limitation, which hampers the study of non-exponential processes as, for example, the annihilation of excitons in molecular crystals<sup>6</sup> and the delayed emission in photosynthesis,<sup>7</sup> is a serious handicap to the phase fluorometric technique.

The other commonly used technique for measuring rapid decay processes utilizes pulsed excitation, e. g., laser pulses,<sup>7, 8</sup> incoherent

light flashes,<sup>9</sup> or electron bursts.<sup>10</sup> Ultra-short laser pulses<sup>11</sup> having a peak power of about  $10^{10}$  W and lasting approximately  $10^{-13}$  sec can be produced by mode locking, while subnanosecond incoherent light flashes<sup>12</sup> can be generated by means of electrical discharges in gaseous media. The study of decay processes based on such pulsed excitation suffers from several drawbacks. Firstly, use of low intensity pulses usually limits the time range over which the decay can be recorded to about a decade, simply due to the lack of signal amplitude. Since measurements over several decades are required for a reliable kinetic analysis in all but the simplest case of purely exponential decay, this presents a serious problem. This difficulty can sometimes be avoided by application of signal-averaging techniques, provided the pulse rate is high enough to make this practicable.<sup>13</sup> Secondly, application of high intensity pulses to organic and inorganic matter may result in complex photodecomposition as well as in nonlinear effects that can induce higher-order decay mechanisms, which in certain instances are irrelevant and unwanted. Thirdly, it is not known, a priori, whether pulsed excitation leads to the establishment of steady-state conditions, an essential requirement when measuring the decay of delayed emission during photosynthesis.

A system that circumvents the above-mentioned disadvantages has been developed for the study of optical decay processes occurring between  $5 \times 10^{-9}$  sec and  $6 \times 10^{-3}$  sec. With it, a heretofore practically unexplored region of the properties of the light emitted from photosynthetic systems is now accessible to detailed investigations. An

attractive feature in the construction of the apparatus is the availability of recently developed commercial components. The necessary instrumentation is described in detail in sections 3 and 4.

## 2. PRINCIPLE OF OPERATION

A block diagram of the apparatus is shown in Fig. 1. Light from a cw argon ion laser traverses the electro-optic shutter and impinges on the sample for a time that is greater than or approximately equal to one-half of each period depending upon the repetition rate. Figure 2 illustrates the way in which each cycle is divided between excitation and observation at the highest and lowest shutter repetition rates. Because of the long irradiation time of the sample (up to 0.25 sec), steady-state conditions are established during each cycle of the modulator. A sampling oscilloscope samples at successive points along the decay curve the amplitudes of the incoming pulses from a fast photomultiplier that views the exit slit of a monochromator used to analyze the emitted light. The time interval between samples is selected by means of a control on the sampling oscilloscope and the entire decay curve is progressively and cyclically sampled, the latter process being synchronous with the laser modulator cycle. A multi-channel analyzer digitally stores the vertical output of the sampling oscilloscope. Operating the analyzer in the signal-averaging mode and periodically exciting the system under investigation thus leads to a time integration of the signals and extracts them from any random background noise. The data stored in the memory can be read out either in



Figure 1. Block diagram of an apparatus for use in measuring nanosecond lifetimes. A detailed description of the operation is given in the text.

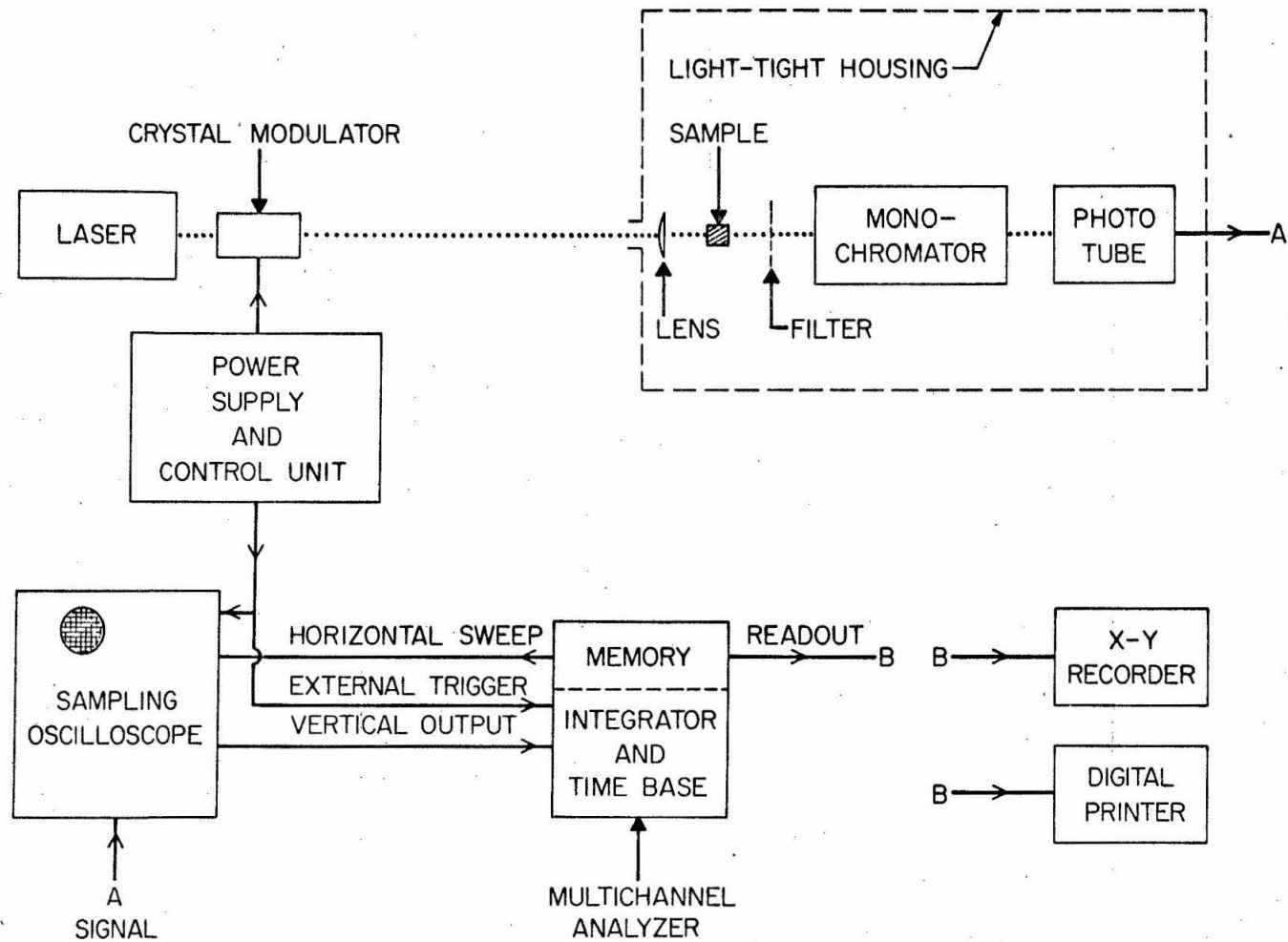
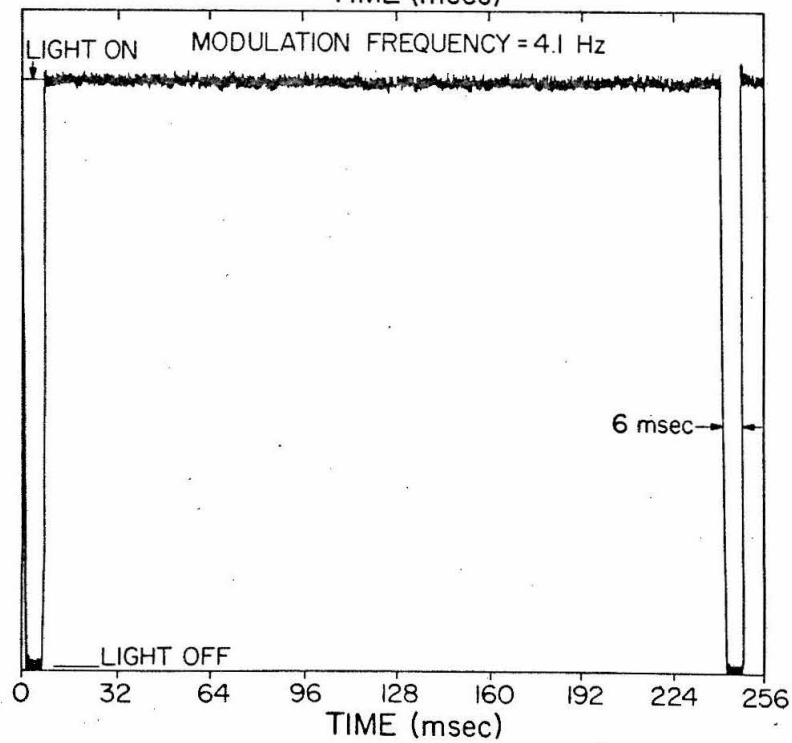
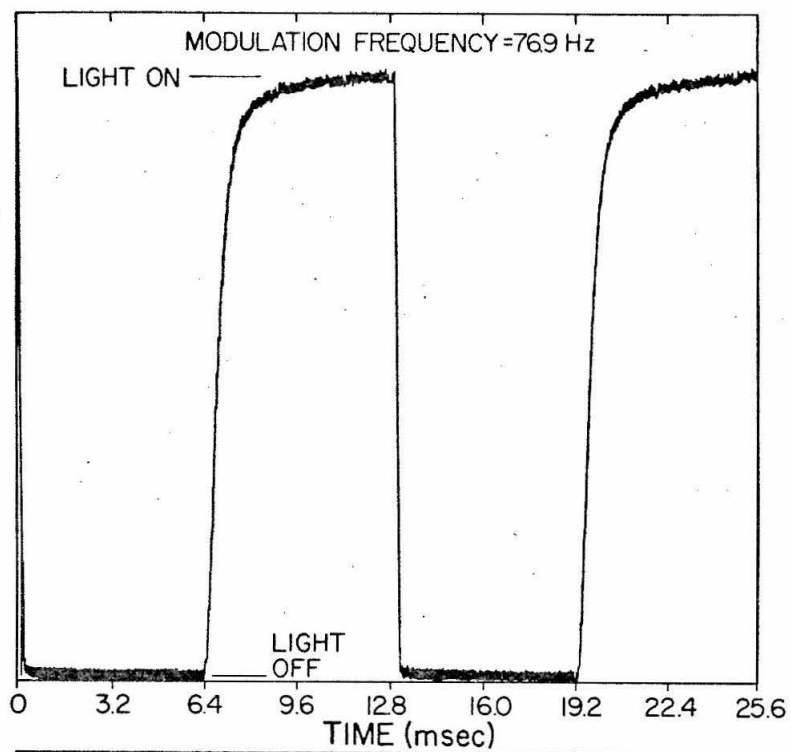


Figure 2. Distribution of the cycle time between excitation and observation at the highest repetition rate (upper curve) and the lowest repetition rate (lower curve).

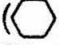
LASER LIGHT INTENSITY AT SAMPLE POSITION

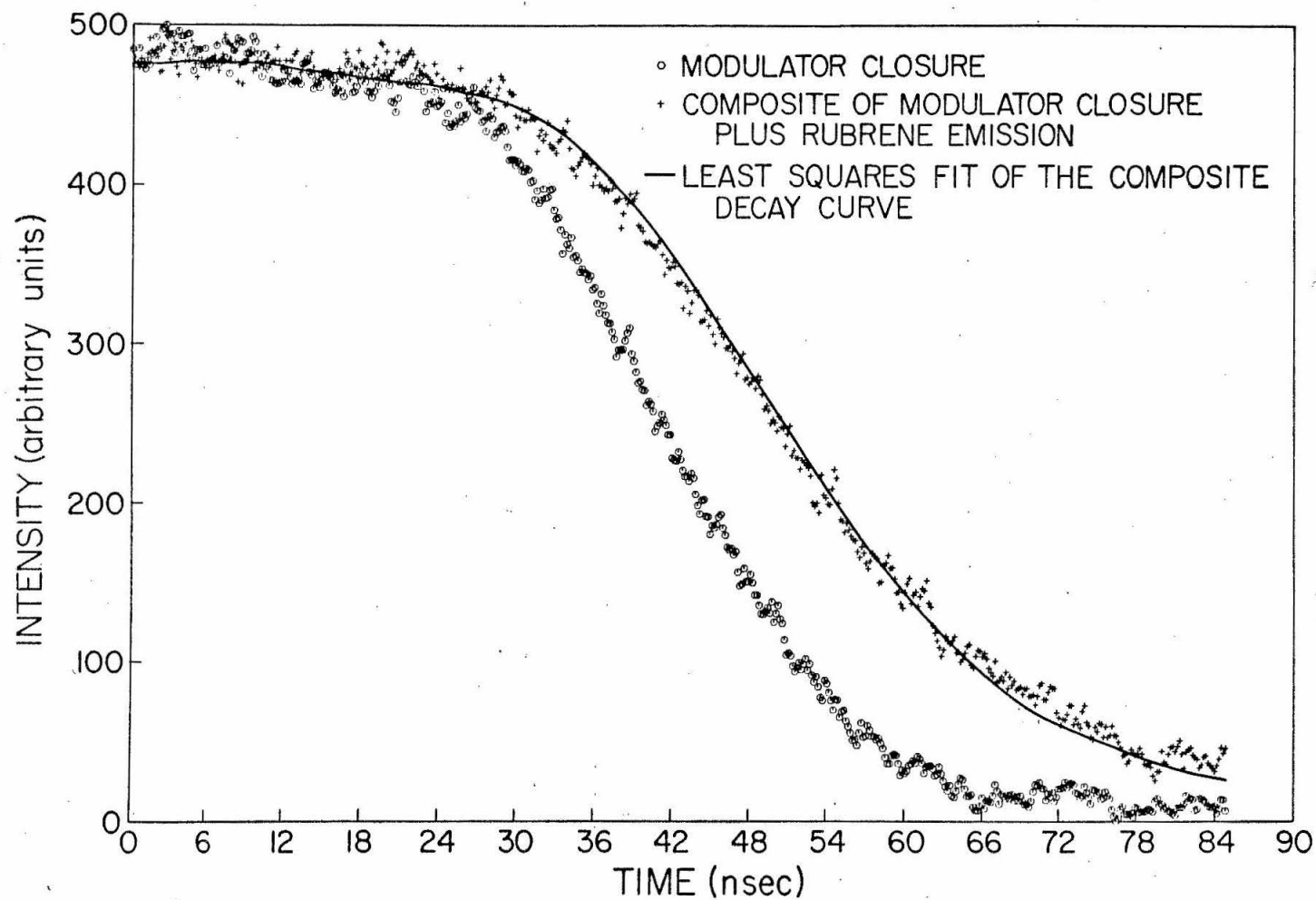


analogue or in digital form thus providing a faithful display of the decay process over several decades, even with weak signal amplitudes.

### 3. EXCITATION SYSTEM

The present light source consists of a water-cooled cw argon ion laser (Model No. LG12, Raytheon Corporation, Waltham, Massachusetts) with a total power output of 1 W distributed over several wavelengths.<sup>14</sup> Approximately 80% of the total power is shared equally by the 4880 and 5145 Å lines. Shock-free mounting of the laser head is necessary for reproducible performance. When desirable, a prism may be used to isolate the 4880 Å line from the other laser lines. Having traversed the modulator and a lens, positioned so as to produce a beam cross-section of roughly 1 cm<sup>2</sup> at the sample, this monochromatic, chopped light beam is used as the excitation source. The laser modulator (Model No. EOLM 400, Isomet Corporation, Palisades Park, New Jersey) passes all wavelengths from 2000 Å to 1.8 μ and according to the manufacturer's specifications can handle optical powers up to 100 W cw in the visible and near infrared. The 1 nsec inherent rise time of the modulator is degraded to about 30 nsec (Fig. 3) by its associated driving electronics (Model No. HVQ-2X4105, Isomet Corporation, Springfield, Virginia). This value is by no means limiting and could in principle be reduced significantly by use of more sophisticated electronic circuitry. Its relatively low operating voltage (~500 V compared to ~15-30 kV necessary for operation of a Kerr cell) makes the crystal modulator desirable from the standpoint of shielding the

Figure 3. Typical time course curves for the closure of the laser modulator () and the composite of the laser modulator closure plus emission from a solution of rubrene in benzene (+). The calculated composite curve is also shown (-). See the text for details of the calculation.



sensitive detection equipment from electrical noise. The contrast ratio (the ratio of the transmission in the "closed" condition to that in the "open" condition) is of the order of  $10^{-4}$ . For roughly 6 msec of each cycle the KD\*P crystal has no voltage applied to it so that the modulator is in the "closed" condition (Fig. 2), during which time, lifetime or spectral measurements can be performed. The remainder of each cycle is divided between recovery time ( $\sim 3$  msec) of the modulator and excitation time. Since the argon ion laser is operated at low power output, power densities at the sample are of the order of  $10 \text{ mW/cm}^2$  and can be easily measured with a calibrated Eppley thermopile.

To minimize scattered light, the sample, monochromator, and photomultiplier were enclosed in a light-tight housing (Fig. 1). Confining both the laser beam and the emitted light inside metal tubes containing the necessary optics further reduced stray light inside this housing.

#### 4. SIGNAL DETECTION AND READOUT SYSTEM

A 0.5 m Ebert scanning spectrometer (Jarrell-Ash Division, Fisher Scientific Company, Waltham, Massachusetts) was positioned at an angle of  $180^\circ$  with respect to the direction of propagation of the excitation beam (Fig. 1). The photomultiplier, coolable to dry-ice temperature, was mounted at the exit slit of the monochromator by means of a short metal pipe. One of two Amperex photomultiplier tubes (Amperex Electronic Corporation, Hicksville, Long Island, New York) was used, viz., the 56 UVP and 56 TVP. Both photomultipliers



are characterized by short time spread ( $0.5 \times 10^{-9}$  sec), fast rise time ( $2 \times 10^{-9}$  sec) and high gain. According to the manufacturer's specifications the 56 UVP has a type S13 spectral response (maximum sensitivity at 4200 Å, extending into the red to 6500 Å), and the 56 TVP has a type S20 spectral response (maximum sensitivity at 4100 Å, extending into the red to 8200 Å). The main advantage of the 56 UVP is that it has lower dark current than the 56 TVP and is therefore preferable when sensitivity to the red of 6500 Å is not required.

The negative output signal from the photomultiplier was taken through a short 50 Ω coaxial cable directly to the vertical amplifier (Type 4S1, Tektronix, Beaverton, Oregon) of a sampling oscilloscope (Type 661, Tektronix, Beaverton, Oregon). Weak photomultiplier pulses may be conveniently amplified in fast broad-band amplifiers, such as the AN 101 dual amplifier module (Edgerton, Germershausen and Grier, Salem, Massachusetts) that have a rise and fall time of less than  $2.5 \times 10^{-9}$  sec. The timing unit (Type 5T3, Tektronix, Beaverton, Oregon) of the sampling oscilloscope was externally triggered by a synchronous pulse provided by the laser modulator control unit. The signal, amplified in the sampling oscilloscope, was fed into the integrator and time base unit of the multichannel analyzer (Model ND 180, Nuclear Data, Palatine, Illinois) operated in the signal-averaging mode (Fig. 1). The time base of the oscilloscope<sup>15</sup> is proportional to the channel addresses of the multichannel analyzer, each channel corresponding therefore to a definite time after triggering the electronic system.

Readout from the memory was accomplished either by a digital

printer (Model 5050 B, Hewlett-Packard, Palo Alto, California) or by an X-Y plotter (Type 7590 CM, Hewlett-Packard, Moseley Division, Pasadena, California).

Since the laser sometimes shows variations due to vibrations and thermal changes, a drift compensation can be accomplished in the following way.<sup>16</sup> A second sampling oscilloscope is introduced that does not scan the decay curve sequentially in time but is locked to one definite point in time just prior to the start of the decay process to be investigated. The output of this second sampling oscilloscope is subtracted from that of the first and thus compensates for systematic variations in the laser output.

Occasionally, a long-lived weak emission must be measured in the presence of a short-lived intense component of emission. For a sufficiently large difference between the two intensities, it becomes necessary to gate the photomultiplier so that it comes on only after the intense "prompt" emission has decayed away. This permits the sensitivity to be increased sufficiently to detect the weak emission while preventing damage to the photocathode by the "prompt" emission. Several schemes have been reported in the literature,<sup>17</sup> slight modifications of which can be made to suit the particular tube being gated.

## 5. PERFORMANCE

To demonstrate the operation of the instrument, the decay of fluorescence emission from rubrene (5, 6, 11, 12-tetraphenylnaphthacene) dissolved in benzene has been measured at room temperature. Three samples were used in the experiments.

a. Sample PreparationSample No. 1

Commercial grade rubrene (Eastman Organic Chemicals, Rochester, New York) without further purification, and analytical reagent grade benzene (Mallinckrodt Chemical Works, St. Louis, Missouri) were used to prepare the first sample. A 1-cm pathlength of the solution had an optical density of 0.40 at 4880 Å. No attempt was made to remove air from the sample. This sample was not used immediately after preparation but stood for several days in a closed vessel with no effort being made to shield it from room light.

Sample No. 2

Analytical thin-layer chromatography (tlc) showed the commercial grade rubrene to contain at least four components besides rubrene itself. Consequently, the crude material was chromatographed on a silica gel column (E. Merckag silica gel, distributed by EM reagents Division, Brinkmann Instruments, Inc., Westbury, New York) and recrystallized from a benzene-methylcyclohexane solution. The resulting crystals were found to be free from all contaminants present in the starting material, as evidenced by tlc. Sample No. 2 was prepared by dissolving the chromatographed, recrystallized rubrene in Phillips' research grade benzene (Phillips Petroleum Company, Bartlesville, Oklahoma; minimum purity set at 99.91% by manufacturer), the optical density of 1-cm pathlength of the resulting solution being 0.58 at 4880 Å. No effort was made to degas the sample.

Sample No. 3

Sample No. 3 was prepared from the same solution as sample No. 2. However, it was carefully outgassed on a vacuum line (limiting pressure  $< 10^{-6}$  Torr with the sample at  $77^{\circ}\text{K}$ ) in a series of freeze-pump-thaw cycles.

b. Lifetime Determination

Figure 3 shows the result of a typical lifetime determination. The modulator closure was first measured by scattering a small fraction of the incident laser light onto the photomultiplier tube. The scatterer was then replaced by a rubrene sample, a Corning Glass filter C.S. 3-68 was placed over the photomultiplier window to block the exciting laser light and the measurement was repeated. The resulting curve is a composite of the modulator closure and the rubrene emission, thus necessitating numerical analysis of the data in order to extract the lifetime of the rubrene emission.

In the following brief description of the numerical analysis four quantities are to be distinguished. The functions  $s(t)$  and  $c(t)$  represent, respectively, the true time course curves of the laser modulator closure in the absence of a sample, and the composite of the laser modulator closure plus emission from a sample.  $S(t)$  and  $C(t)$  denote the measured values of  $s(t)$  and  $c(t)$ , respectively, and reflect the fact that the detector response is non-ideal, i.e., the detector response to a  $\delta$ -function input at the time  $t$  is the somewhat delocalized function  $R(t-t')$  rather than  $\delta(t-t')$ . From the superposition theorem<sup>18</sup> it follows that,

$$S(t) = \int_0^{\infty} s(t-t'')R(t'')dt'' \quad (1)$$

and

$$C(t) = \int_0^{\infty} c(t-t'')R(t'')dt'' \quad (2)$$

We wish to establish a theoretical relationship between  $S(t)$  and  $C(t)$  given Eqs. (1) and (2) and the fact that  $s(t)$  and  $c(t)$  satisfy

$$\frac{dc(t)}{dt} = Ks(t) - \beta c(t) \quad , \quad (3)$$

where  $\beta$  is the total first-order decay constant (the reciprocal of the measured lifetime of the sample emission) and  $K$  is a scaling factor between the excitation and emission intensities.  $K$  represents the product of the absorption coefficient, the reciprocal of the radiative lifetime, the volume of the sample that is excited and a geometrical factor associated with the experimental setup. Equation (3) has been written to include first-order decay only, anticipating the kinetic form of the fluorescence emission of rubrene. The analysis for arbitrary kinetic decay is treated in Section 6.

Solving Eq. (3) for  $c(t)$  yields

$$c(t) = \exp(-\beta t)K \int_{-\infty}^t s(t')\exp(\beta t')dt' \quad (4)$$

From Eqs. (1)-(4) it follows by straightforward manipulations that

$$C(t) = \exp(-\beta t)K \int_{-\infty}^t \left\{ \int_0^{\infty} s(\tau-t'')R(t'')dt'' \right\} \exp(\beta \tau)d\tau \quad (5)$$

Identifying the expression in braces in Eq. (5) as  $S(\tau)$  gives as a final result

$$C(t) = \exp(-\beta t) K \int_{-\infty}^t S(\tau) \exp(\beta \tau) d\tau . \quad (6)$$

Comparison of Eqs. (4) and (6) shows that  $C(t)$  and  $S(t)$  satisfy an equation analogous to Eq. (3), namely

$$\frac{dC(t)}{dt} = KS(t) - \beta C(t) . \quad (7)$$

Thus the measured curves are related by precisely the same equation as are the true curves so that  $C(t)$  and  $S(t)$  can be used directly in Eq. (7) to determine  $K$  and  $\beta$ , with no loss in accuracy due to the non-ideality of the detection system response. This result has the important consequence that the signal-to-noise ratio alone sets the experimental limitation on the shortest lifetime measurable. In other words, the shortest lifetime measurable is that which just results in an experimentally detectable difference between  $S(t)$  and  $C(t)$ .

Since  $S(t)$  and  $C(t)$  are known only in numerical form, Eq. (7) must be solved by numerical methods. The Runge-Kutta technique<sup>19</sup> was used for this purpose and the solution fitted, within the framework of least squares,<sup>20</sup> to the experimentally measured curve. Six separate lifetime determinations were made for each of the three samples. The mean value of the emission lifetime for each of the three samples is tabulated in Table I. Since sample No. 1 was allowed to stand in a closed vessel, unshielded from room light for several days prior to use, it is probable that some of the oxygen present

TABLE I. Results of lifetime determinations of fluorescence from three samples of rubrene in benzene. The results show the effects of impurities and oxygen on the fluorescence lifetime.

| Sample         | Mean Lifetime<br>$\bar{\tau}$ | Estimated Uncertainty |
|----------------|-------------------------------|-----------------------|
| 1 <sup>a</sup> | 11.3                          | $\pm 2.0$             |
| 2 <sup>b</sup> | 9.5                           | $\pm 2.0$             |
| 3 <sup>c</sup> | 16.3                          | $\pm 2.1$             |

<sup>a</sup>Impure rubrene; Mallinckrodt reagent grade benzene; sample not outgassed.

<sup>b</sup>Chromatographed, recrystallized rubrene; Phillips' research grade benzene; sample not outgassed.

<sup>c</sup>Chromatographed, recrystallized rubrene; Phillips' research grade benzene; sample carefully outgassed.

initially would have been consumed in the known photochemical oxidation of rubrene.<sup>21</sup> Sample No. 2 on the other hand was used immediately after preparation so that the difference in the emission lifetime of samples 1 and 2 may be due simply to a difference in their oxygen content. The increase in the emission lifetime of sample No. 3 compared to that of sample No. 1 appears to be attributable almost entirely to removal of oxygen, other impurities seeming to be of negligible consequence to the overall lifetime of the excited state.

## 6. DATA ANALYSIS FOR ARBITRARY DECAY KINETICS

A data reduction scheme applicable to emission governed by arbitrary kinetics is presented in this section. Just as for purely exponential decay, the finite response time of the detector cannot limit the accuracy of the decay constants determined from the measurements. Furthermore, the true time course curve of the emission is obtained explicitly during the calculation.

In addition to the four functions defined previously, the true time course curve of the emission, i. e., the curve that would be observed if in fact the modulator closure and detector response were infinitely fast, is represented by  $f(t)$ . It follows from the superposition theorem<sup>18</sup> that

$$c(t) = \int_0^{\infty} f(t')s(t-t')dt' \quad (8)$$

Together with Eqs. (1) and (2), Eq. (8) leads in a straightforward manner to



$$C(t) = \int_0^{\infty} f(t')S(t-t')dt' . \quad (9)$$

$S(t)$  and  $C(t)$  are the experimentally determined laser modulator closure and composite curve so that Eq. (9) can be solved numerically for  $f(t)$ . Having  $f(t)$  explicitly, it is a simple matter to least squares fit the data to whatever model seems most physically justified. The validity of the model will be evidenced by the quality of the fit.

In practice the integration in Eq. (9) can be truncated as soon as the integrand becomes negligible. Thus the upper limit on the integral poses no obstacle to the numerical calculation.

## 7. CONCLUSIONS

1. A versatile apparatus for measuring short emission lifetimes has been described. Steady-state conditions in the sample are established before the lifetime measurement is begun.
2. Signal averaging makes possible use of low intensity excitation without significant degradation in the quality of the signal.
3. Careful analysis of the data permits measurement of lifetimes that are much shorter than the time required to switch off the excitation light, the minimum being set by the signal-to-noise ratio alone.
4. Since an explicit decay curve is obtained from the measurements, no assumptions need be made about the decay kinetics. See Section 6.
5. With sufficient improvement in the electronic driving circuitry associated with the crystal modulator, and some increase in the signal-to-noise ratio, lifetimes of 1 nsec or less could be measured using the apparatus described.

REFERENCES

1. L. Brewer, C. G. James, R. G. Brewer, F. E. Stafford, R. A. Berg, and G. M. Rosenblatt, *Rev. Sci. Instr.* 33, 1450 (1962).
2. S. J. Strickler and R. A. Berg, *J. Chem. Phys.* 37, 814 (1962).
3. J. B. Birks, D. J. Dyson, and I. H. Munro, *Proc. Roy. Soc. (London)* 275A, 575 (1963).
4. A. Schmitten, *Z. Physik* 135, 294 (1953); B. D. Venetta, *Rev. Sci. Instr.* 30, 450 (1959); A. J. De Maria, R. Gagosz, and G. Barnard, *J. Appl. Phys.* 34, 453 (1963).
5. A. Müller, R. Lumry, and M. S. Walker, *Photochem. Photobiol.* 9, 113 (1969); G. M. Lawrence and B. D. Savage, *Phys. Rev.* 141, 67 (1966).
6. H. Sternlicht, G. C. Nieman, and G. W. Robinson, *J. Chem. Phys.* 38, 1326 (1963); E. B. Priestley and A. Haug, *J. Chem. Phys.* 49, 622 (1968).
7. R. K. Clayton, Molecular Physics in Photosynthesis (Blaisdell Publishing Co., New York, 1965); H. T. Witt, "Direct measurements of reactions in the  $10^{-1}$  to  $10^{-8}$  sec range by single and repetitive excitations with pulses of electromagnetic waves" in Fast Reactions and Primary Processes in Chemical Kinetics, S. Claesson, Ed. (Interscience Publishers, Inc., New York, 1967).
8. R. W. Hellwarth, Advances in Quantum Electronics, J. R. Singer, Ed. (Columbia University Press, New York, 1961).
9. G. Porter, *Z. Elektrochem.* 64, 59 (1960); P. G. Bowers and G. Porter, *Proc. Roy. Soc. (London)* 296A, 435 (1967); B. Ke, R. W. Treharne, and C. McKibben, *Rev. Sci. Instr.* 35, 296 (1964).

10. W. R. Bennett, Jr., P. J. Kindlmann, and G. N. Mercer, Appl. Opt. Suppl. 2 on Chemical Lasers, 34 (1965).
11. A. J. De Maria, D. A. Stetser, and W. H. Glenn, Science 156, 1557 (1967), and numerous references cited therein.
12. J. Yguerabide, Rev. Sci. Instr. 36, 1734 (1965).
13. H. Dreeskamp, A. K. Ghosh, and M. Burton, Rev. Sci. Instr. 32, 304 (1961); O. J. Steingraber and I. B. Berlman, Rev. Sci. Instr. 34, 524 (1963).
14. E. F. Labuda, E. I. Gordon, and R. C. Miller, IEEE J. Quant. Electr. QE-1, 273 (1965).
15. The 5T3 timing unit of the sampling oscilloscope provided the time base for all lifetime measurements. The accuracy of this unit was checked by paralleling it with a calibrated Hewlett-Packard digital counter (Model No. 5245L), using a variable frequency pulse generator (Tektronix, Type 184 Time Mark generator) to provide the input. The limiting factor in determining the frequency of the input signal with the oscilloscope was found to be the uncertainty associated with reading values from the oscilloscope screen. To within this error, the input signal frequency as determined by the oscilloscope and counter was the same. On the basis of this finding the uncertainty in the time axis of Fig. 3 is believed to be less than 0.25 nsec.
16. D. A. Thompson and H. Chang, phys. stat. sol. 17, 83 (1966).
17. R. G. Bennett and R. P. Schwenker, Rev. Sci. Instr. 30, 836 (1959); K. B. Keller and B. M. K. Nefken, Rev. Sci. Instr. 35, 1359 (1964); R. de Martini and K. P. Wacks, Rev. Sci. Instr. 38, 866 (1967).

18. R. G. Brown and J. W. Nilsson, Introduction to Linear Systems Analysis (John Wiley and Sons, Interscience, New York, 1962), p. 115.
19. See, for example, H. B. Keller, Numerical Methods for Two-Point Boundary-Value Problems (Blaisdell Publishing Co., Massachusetts, 1968), p. 26.
20. See, for example, N. Arley and K. Rander Buch, Introduction to the Theory of Probability and Statistics (John Wiley and Sons, Interscience, New York, 1950), p. 181.
21. L. F. Fieser and M. Fieser, Organic Chemistry (Reinhold Publishing Corp., New York, 1956), 3rd ed., pp. 773-775.

SECTION B

THE DECAY KINETICS OF DELAYED EMISSION FROM  
Chlorella Pyrenoidosa IN THE MILLISECOND-  
TO-SECOND TIME INTERVAL

## 1. INTRODUCTION

Light emission from illuminated green plants was first reported by Stokes<sup>1</sup> a little over 100 years ago. The emission that Stokes observed has now come to be known as fluorescence, or "prompt" emission since it is characterized by a lifetime on the order of a few nanoseconds in all systems investigated to date. It was not until the relatively recent discovery by Strehler and Arnold<sup>2</sup> in 1951, however, that it was realized that in addition to fluorescence green plants also emit light for up to several minutes after termination of the excitation. This delayed light, as it is commonly referred to, is believed to be somehow associated with one or more steps in the photosynthetic process, subsequent to the primary acts of light harvesting and transfer of energy to the reaction centers. It has been variously suggested that it could result from: reversal of certain steps along the chain of events that together constitute photosynthesis,<sup>3</sup> electron-hole recombinations occurring in quasi-crystalline regions of the photosynthetic unit,<sup>4,5</sup> or perhaps from slow release of energy from unidentified shallow, electron-trapping levels.<sup>6</sup>

Similarities between prompt and delayed emission have been noted in several instances. The spectra of the two types of emission from Chlorella pyrenoidosa are quite similar; both have maxima at 685 nm, suggesting that the emissions probably originate from electronically excited chlorophyll molecules.<sup>7</sup> There is strong evidence<sup>8</sup> that fluorescence from green plants comes primarily from pigment system

2.<sup>9</sup> This same conclusion appears to be true for delayed emission as well, since a Scenedesmus mutant lacking functional system 2 reaction centers does not exhibit delayed emission.<sup>10</sup> Furthermore, 3-(3,4-dichlorophenyl)-1,1-dimethylurea (DCMU), which inhibits the oxygen evolving capabilities of photosystem 2, also markedly reduces the intensity of delayed emission.<sup>11</sup> It has even been suggested by Arnold and Davidson<sup>12</sup> that a large part of fluorescence in vivo may in fact be nothing more than a fast component of delayed emission. Their original suggestion was based on an extrapolation of the known delayed fluorescence intensity, measured at times longer than  $10^{-5}$  sec, backward in time to a few nanoseconds after cessation of the exciting light. This extrapolation showed that it would be reasonable to expect delayed emission occurring on the same time scale as fluorescence to have an intensity comparable to that of fluorescence.

Despite numerous experiments designed to study various aspects of the problem (kinetics, quantum yields, biochemical alterations, etc.), very little is presently known about the inter-relationship between fluorescence and delayed light, nor is much understood about their quantitative involvement in photosynthesis. In order to obtain quantitative information about the behavior of fluorescence and delayed emission, accurate measurements of the time-course curve over the entire range between  $10^{-9}$  sec and roughly 1 sec are required. Such data, if subjected to rigorous kinetic analysis, may help not only to elucidate the early physical processes taking place in the photosynthetic unit, but may also provide deeper insight into the nature of the subsequent light-driven biochemical transformations that occur during photosynthesis.

As part of the larger effort, directed at obtaining the complete time-course curve of delayed emission from Chlorella, careful measurements of the decay kinetics of the emission between  $10^{-3}$  sec and 1 sec have been made. Although similar studies have been undertaken in the past,<sup>2, 6, 13</sup> the measurements reported herein are believed to be more conclusive, largely due to the fact that we have used signal averaging to improve the quality of the raw data. A further improvement in the present experiments is the use of digital data acquisition, which facilitates numerical analysis of the data. The dependence of the decay kinetics on the excitation light intensity has been investigated, and delayed emission from cells inhibited with DCMU has also been studied.

## 2. EXPERIMENTAL

### a. Materials

Cells of the Emerson strain of Chlorella pyrenoidosa were grown in test-tube cultures in Knop's medium at 26.5° C. The algal cultures were continuously aerated with a mixture of 5% CO<sub>2</sub> in 95% air. Cell suspensions from the exponential growth phase ( $k \approx 1.3$  per day) were adjusted to an optical density of 0.9 at 488 nm prior to their use in the experiments. Measurements were made using fully illuminated 1 ml samples in a quartz cuvette maintained at 26.5° C. Continuous aeration with 5% CO<sub>2</sub> in 95% air was provided so as to ensure conditions as near normal as possible during the measurements. Since a period of roughly two hours was required to collect the data for a single decay curve, it



was necessary to stir the cells to avoid settling. Negligible changes in emission due to changes in the excitation light intensity or cell concentration occurred during the measurement interval.

### b. Apparatus

The experiments were made using a phosphoroscope described in detail in Appendix A. Light from a 500 W xenon arc lamp, suitably filtered and focused, provided a broad band ( $\sim 80$  nm) of exciting light centered at 488 nm. Excitation power densities, measured with a calibrated Eppley thermopile, ranged from 10 mW/cm<sup>2</sup> down to 0.1 mW/cm<sup>2</sup>. A Bausch and Lomb 0.25 m "High Intensity" monochromator with a reciprocal linear dispersion of 64 Å/mm at the exit slit (slit-width 3 mm) served to isolate the light emitted at 685 nm. This emitted light was detected by a dry-ice cooled EMI 9558 photomultiplier. A Nuclear Data model ND180 multichannel analyzer was used to average the output of the photomultiplier over many repetitions of the decay. The decay curve was ultimately read out in digital form onto a Hewlett-Packard model 5050B digital printer. Numerical analysis of the data was accomplished using the techniques described in Appendices B and C.

## 3. RESULTS AND DISCUSSION

Figures 1 and 2 show the decay curves at each of 3 excitation power densities in the absence, and in the presence of DCMU, respectively. A brief description of these curves is given in the accompanying captions. In each case, the decay curve can be adequately described by

Figure 1. Decay of delayed emission from Chlorella pyrenoidosa cells excited by 488 nm light. The three curves correspond to incident power densities at the sample of: 10 mW/cm<sup>2</sup> (top), 1 mW/cm<sup>2</sup> (center) and 0.1 mW/cm<sup>2</sup> (bottom). The filled circles represent the experimental data points; the least-squares fit of the function  $I(t) = A \exp(-t/\tau_1) + B \exp(-t/\tau_2)$  to these points is shown as a solid line. The values of the lifetimes  $\tau_1$  and  $\tau_2$  are summarized in Table I.

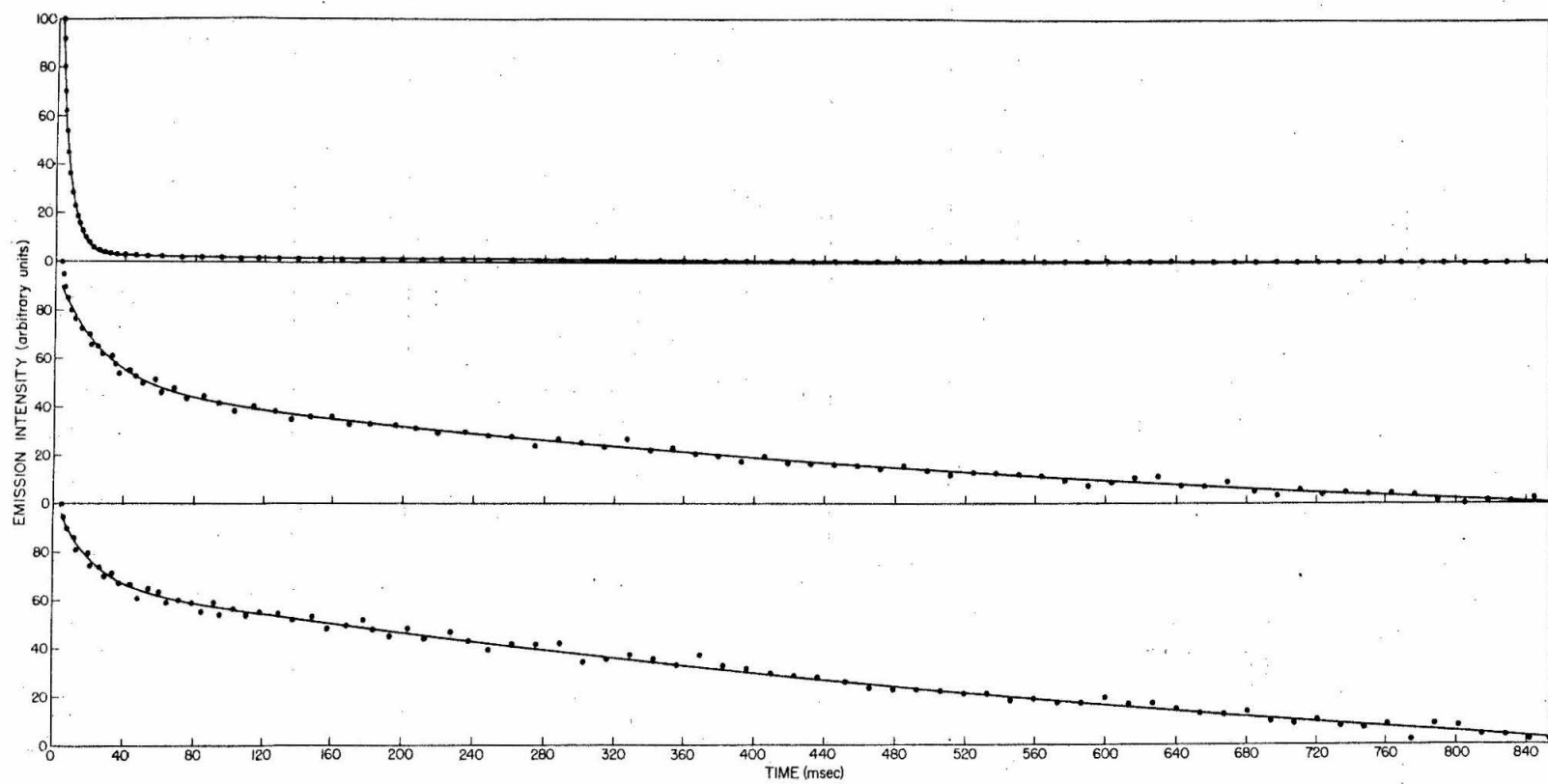
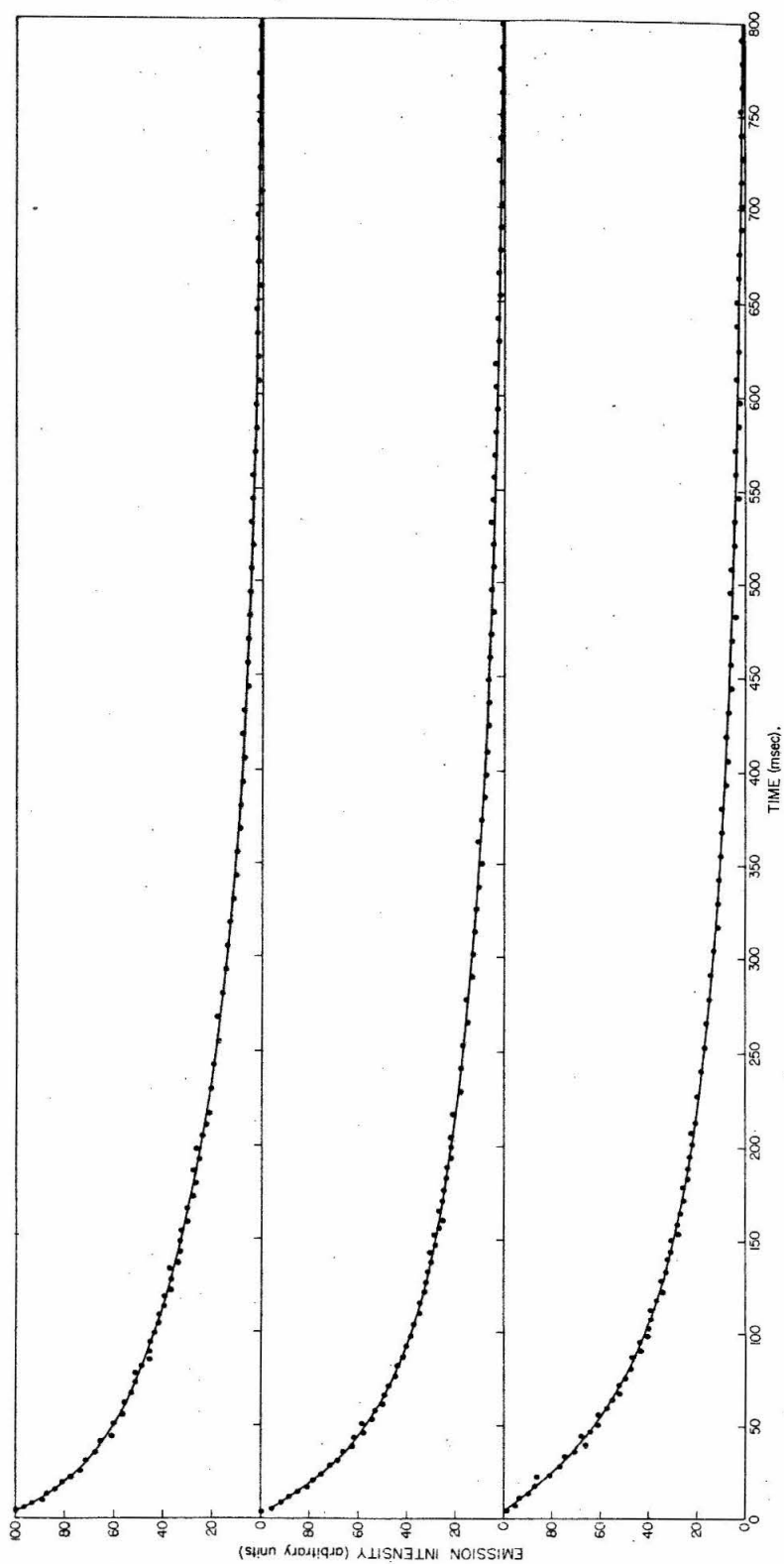


Figure 2. Decay of delayed emission from *Chlorella pyrenoidosa* cells inhibited with 3-(3,4-dichlorophenyl)-1,1-dimethylurea (DCMU). The wavelength of the exciting light was 488 nm; the incident power densities at the sample were: 10 mW/cm<sup>2</sup> (top), 1 mW/cm<sup>2</sup> (center) and 0.1 mW/cm<sup>2</sup> (bottom). The filled circles represent experimental data points; the least-squares fit of the function  $I(t) = A \exp(-t/\tau_1) + B \exp(-t/\tau_2)$  to these points is shown as a solid line. The values of the lifetimes  $\tau_1$  and  $\tau_2$  are summarized in Table II.



the sum of two exponential decays, i. e., by an expression of the form  $I(t) = A \exp(-t/\tau_1) + B \exp(-t/\tau_2)$ . Tables I and II summarize the results of the analysis of the data shown in Figs. 1 and 2, respectively.

It is seen that the lifetimes,  $\tau_1$  and  $\tau_2$ , are both dependent upon the intensity of the excitation light whether or not the cells have been inhibited with DCMU; the effect is, however, more pronounced in the absence of the inhibitor.  $\tau_1$  shows the stronger dependence on excitation light intensity in both cases, varying by more than a factor of 4, compared to somewhat less than a factor of 2 variation in  $\tau_2$ , for uninhibited cells. The variation in  $\tau_1$  for inhibited cells amounts to more like a factor of 2.5, whereas  $\tau_2$  changes by less than 25% in this case. In general, both lifetimes increase with decreasing excitation light intensity. This interesting observation, not entirely understood at present, indicates that some light-driven changes internal to the cell, such as light-induced shrinkage of the chloroplasts, effectively alter the rates of the underlying reactions. If the delayed light were indeed associated with some of these reactions, then one might expect changes in the reaction rates to be reflected in the behavior of the delayed emission.

To say more without the complete time course curve having been measured would be foolhardy. However, what has been described in this part of the thesis forms a solid basis upon which future work can be founded. The equipment has been assembled, the necessary programs for data analysis written and a start made toward collecting the data required to construct the complete emission decay curve for

TABLE I. Analysis of the decay curves shown in Fig. 1.  
Delayed emission from Chlorella pyrenoidosa at 26.5° C--  
no inhibitor.

| EXCITATION LIGHT POWER<br>DENSITY<br>(mW/cm <sup>2</sup> ) | COMPONENT LIFETIMES |                 |
|--|---------------------|-----------------|
|  | $\tau_1$ (msec)     | $\tau_2$ (msec) |
| 10   | 5.4                 | 452             |
| 1  | 23.4                | 666             |
| 0.1  | 17.1                | 839             |

TABLE II. Analysis of the decay curves shown in Fig. 2.  
Delayed emission from Chlorella pyrenoidosa at 26.5° C--  
DCMU added as an inhibitor.

| EXCITATION LIGHT POWER<br>DENSITY<br>(mW/cm <sup>2</sup> ) | COMPONENT LIFETIMES |                 |
|--|---------------------|-----------------|
|  | $\tau_1$ (msec)     | $\tau_2$ (msec) |
| 10   | 21.6                | 175             |
| 1  | 38.3                | 217             |
| 0.1  | 53.5                | 216             |

Chlorella. If these few preliminary data are any indication, there may be some unexpected results awaiting those who carry on the work. Hopefully, this type of experiment will lead to a better understanding of the photosynthetic process--a process crucial to life on our planet.



REFERENCES

1. G. G. Stokes, Proc. Roy. Soc. (London) 13, 144 (1864).
2. B. L. Strehler and W. Arnold, J. Gen. Physiol. 34, 809 (1951).
3. W. E. Arthur and B. L. Strehler, Arch. Biochem. Biophys. 70, 507 (1957).
4. G. Tollin and M. Calvin, Proc. Nat. Acad. Sci. 43, 895 (1957).
5. W. Arnold, J. Phys. Chem. 69, 788 (1965).
6. G. Tollin, E. Fujimori and M. Calvin, Proc. Nat. Acad. Sci. 44, 1035 (1958).
7. J. R. Azzi, Oak Ridge National Laboratory, TM 1534 (1966).
8. L. N. M. Duysens, Thesis, University of Utrecht (1952).
9. Photosynthesis is known to involve two light-driven reactions coupled by some sequence of oxidation-reduction reactions. System 1 refers to the long-wavelength ( $> 685$  nm) sensitive reaction centers, whereas system 2 denotes those reaction centers driven primarily by light of shorter wavelength ( $< 685$  nm). For details of these two systems see, R. K. Clayton, Molecular Physics in Photosynthesis (Blaisdell Publishing Co., New York, 1965).
10. W. Bertsch, J. R. Azzi and J. B. Davidson, Biochim. Biophys. Acta 143, 129 (1967).
11. P. B. Sweetser, C. W. Todd and R. T. Hersh, Biochim. Biophys. Acta 51, 509 (1961).

12. W. Arnold and J. B. Davidson, "The Decay of Delayed Light at Short Times" in Photosynthetic Mechanisms of Green Plants B. Kok and A. T. Jagendorf Eds. (National Academy of Sciences--National Research Council Publication 1145, Washington D.C., 1963), p. 698.
13. R. H. Ruby, Photochem. and Photobiol. 8, 299 (1968).

PART IV

APPENDICES

## APPENDIX A

## EXPERIMENTAL

This Appendix contains a more complete description of some of the experimental equipment and procedures than has been given previously. For the most part the discussion is simply an enlargement upon earlier mention of the particular procedure or piece of apparatus, although in one or two cases it is concerned with a description of equipment that was constructed but which for various reasons never found its way into any of the experiments. It is hoped that by including a brief description of these items, what might otherwise be relegated to a dusty corner in some cabinet may instead be utilized in the experiments of future generations of graduate students. The material comprising the Appendix falls logically into one of two categories, viz., "Equipment" and "Procedures".

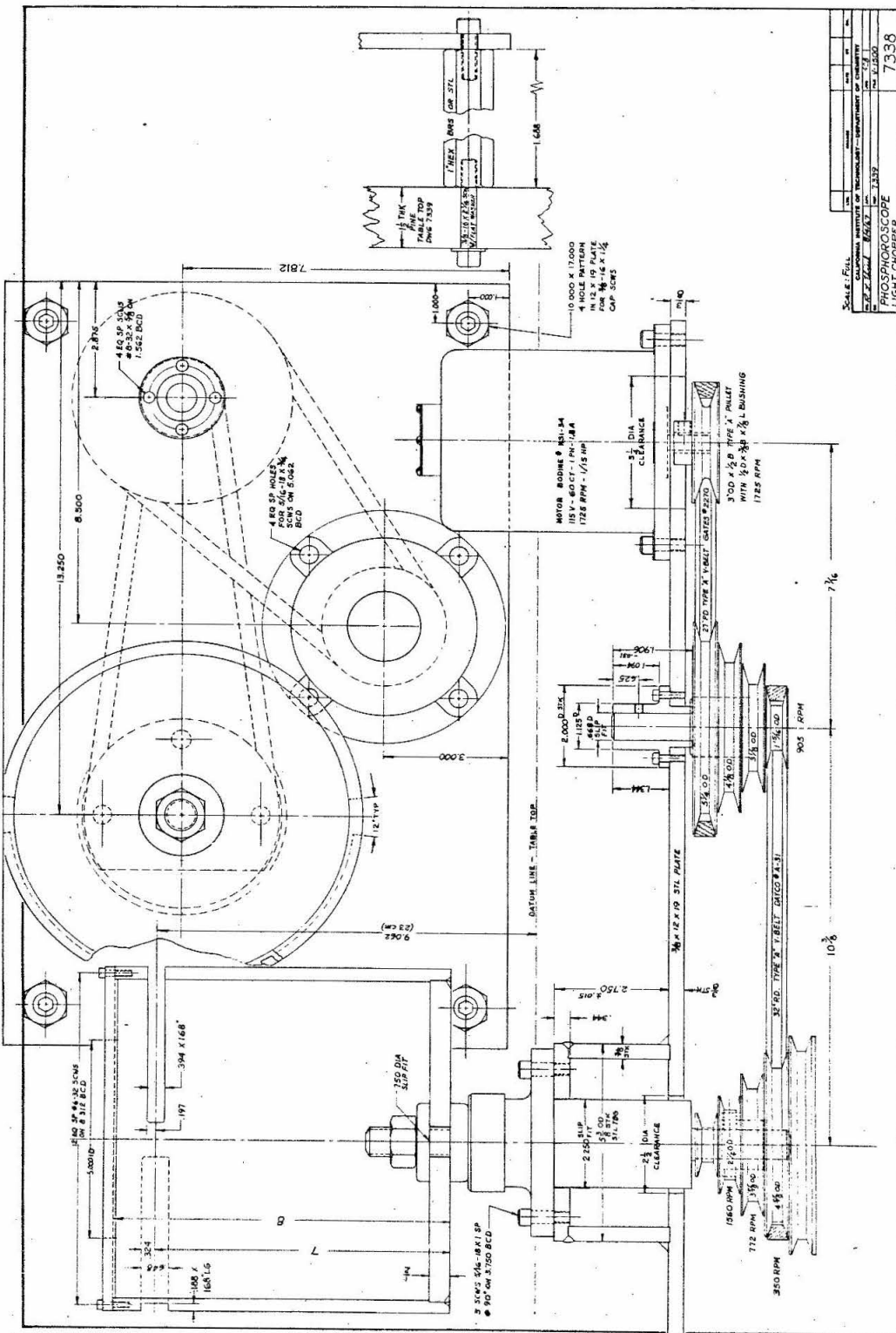
1. EQUIPMENT

Equipment described in this section was included either because it was used extensively in the experiments described in this thesis or else it is of sufficiently general applicability in optical spectroscopic experiments to warrant some comment.

a. Variable Speed Phosphoroscope

A variable speed phosphoroscope, consisting of a rotating cylindrical drum with a slot cut in its circumference, was mounted in the top of a wooden table as shown in Figs. A1 and A2. The angle

Figure A1. A drawing of the variable speed phosphoroscope.



|  |  |      |  |      |  |
|--|--|------|--|------|--|
| SCALE: Full  |  | DATE |  | PAGE |  |
| CALIFORNIA INSTITUTE OF TECHNOLOGY—DEPARTMENT OF CHEMISTRY |  | 1339 |  | 7338 |  |
| R. Z. M. 1339  |  | 1339 |  | 7338 |  |
| PHOSPHOROSCOPIC  |  | 1339 |  | 7338 |  |
| LIGHT NUMBER   |  | 1339 |  | 7338 |  |

Figure A2. A drawing of the mounting table for the variable speed phosphoroscope.



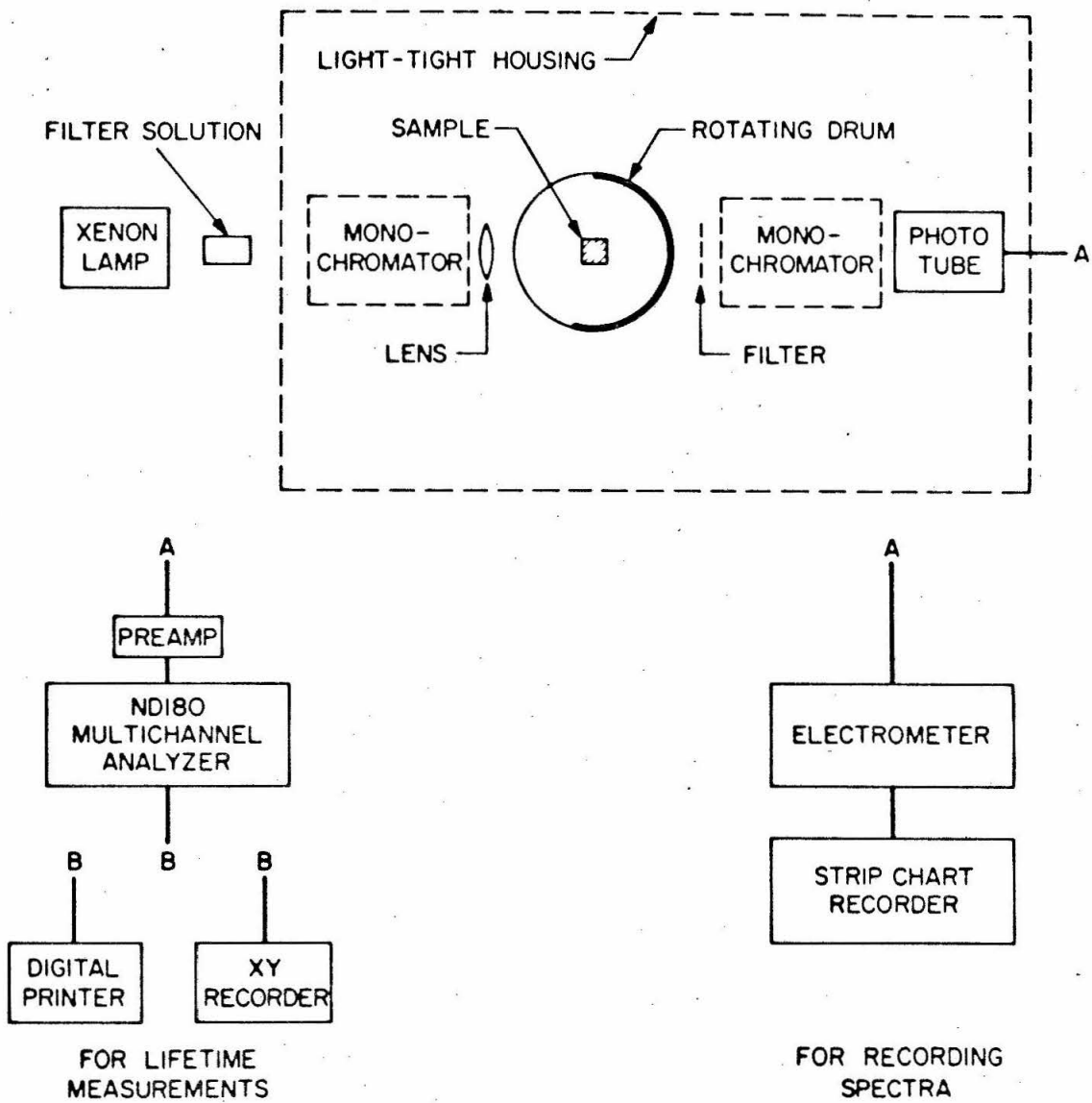


subtended at the center of the drum by the slot was  $165^\circ$ , corresponding to excitation and observation periods ranging from 0.9 sec at the lowest speed to 15.9 msec at the highest speed. Because the slot extended less than half way around the drum, a dead time existed between excitation and observation which varied from 83 to 1.4 msec depending upon the phosphoroscope speed. On the basis of these time characteristics one concludes that this phosphoroscope should be useful in the study of optical emissions having lifetimes between 2 msec and roughly 1 sec.

The experimental arrangement illustrated in Fig. A3 can be exploited for measurements of emission and excitation spectra as well as for lifetime determinations. Emission lifetimes can be studied most reliably by collecting data at different phosphoroscope speeds, chosen so that sufficient time overlap exists between successive speeds, and then fitting these data together to obtain a decay curve extending over several lifetimes. This procedure was facilitated by digital data acquisition which made numerical reduction of the data particularly straightforward. A discussion of the numerical techniques can be found in Appendix C. The best spectral measurements were obtained using the highest phosphoroscope speed together with a 1-3 sec time constant in the detection electronics. This served to average out fluctuations in the photomultiplier output due to the phosphoroscope rotation.

Replacing the cylindrical drum having the  $165^\circ$  slot by another having two opposing slots, each subtending an angle of  $85^\circ$  at the center, provided alternate access to the sample by two light beams at right

Figure A3. An illustration of the experimental arrangement used to measure emission lifetimes and spectra or excitation spectra, depending upon the position of the monochrometer. For lifetime measurements the photomultiplier output was amplified and averaged over a long period of time by the multichannel analyzer. Either analog or digital readout could be selected. In the recording of spectra, the photomultiplier output was fed directly into an electrometer and recorded on a strip-chart recorder.



angles to each other. The experimental arrangement shown in Fig. A4 was used to study triplet-triplet absorption spectra of several samples. As the drum rotates, the molecules are alternately excited (some to their lowest excited triplet state) by a 6500 W Xenon arc lamp and then subjected to a spectroscopic continuum light beam, thus permitting observation of absorptions within the triplet manifold.

#### b. Coolable Photomultiplier Housing

Many of the experiments involved detection of weak emission signals, necessitating low detector noise. EMI 6256 photomultiplier tubes, selected for low noise, were cooled to dry ice temperature ( $-78.5^{\circ}\text{C}$ ) in housings like the one illustrated in Fig. A5. Cooling the tubes reduces thermionic emission since the latter is proportional to  $T^2 \exp(-K/T)$ ,  $T$  being the absolute temperature and  $K$  a constant. Reductions of one to two orders of magnitude in dark current could be achieved by cooling, indicating that thermionic emission contributes substantially to the dark current. The main features of the housing shown are its ability to hold dry ice for up to 24 hours and complete elimination of condensation around the base and voltage divider network.

#### c. Optical Bench Support Assembly

Figures A6 through A9 exhibit details of an optical bench support assembly that was mounted on a 1.8 m Jarrell-Ash spectrometer. These supports mount rigidly on the front of the instrument, providing a sturdy base upon which optical components for a variety of experimental arrangements can be mounted. Provision is made for double-beam operation using the light tunnel described below. Figures A6 and

Figure A4. An illustration of the experimental arrangement for recording triplet-triplet absorption spectra. The sample was subjected alternately to light from the 6500 W xenon arc lamp used to create triplet-states and the continuum provided by the spectroscopic xenon lamp. Triplet-state lifetimes could be determined by measuring the rate of disappearance of the transient absorption.

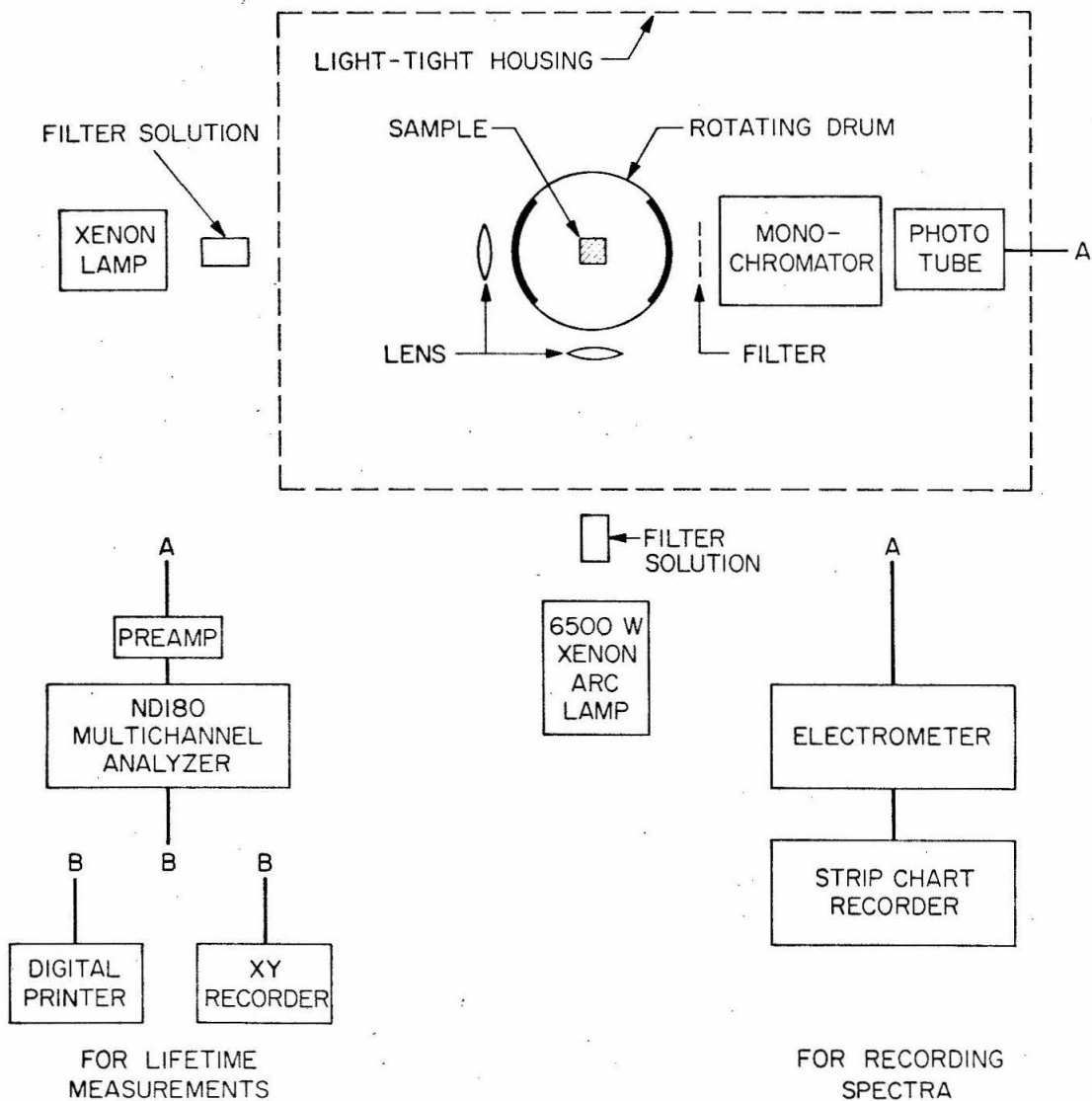
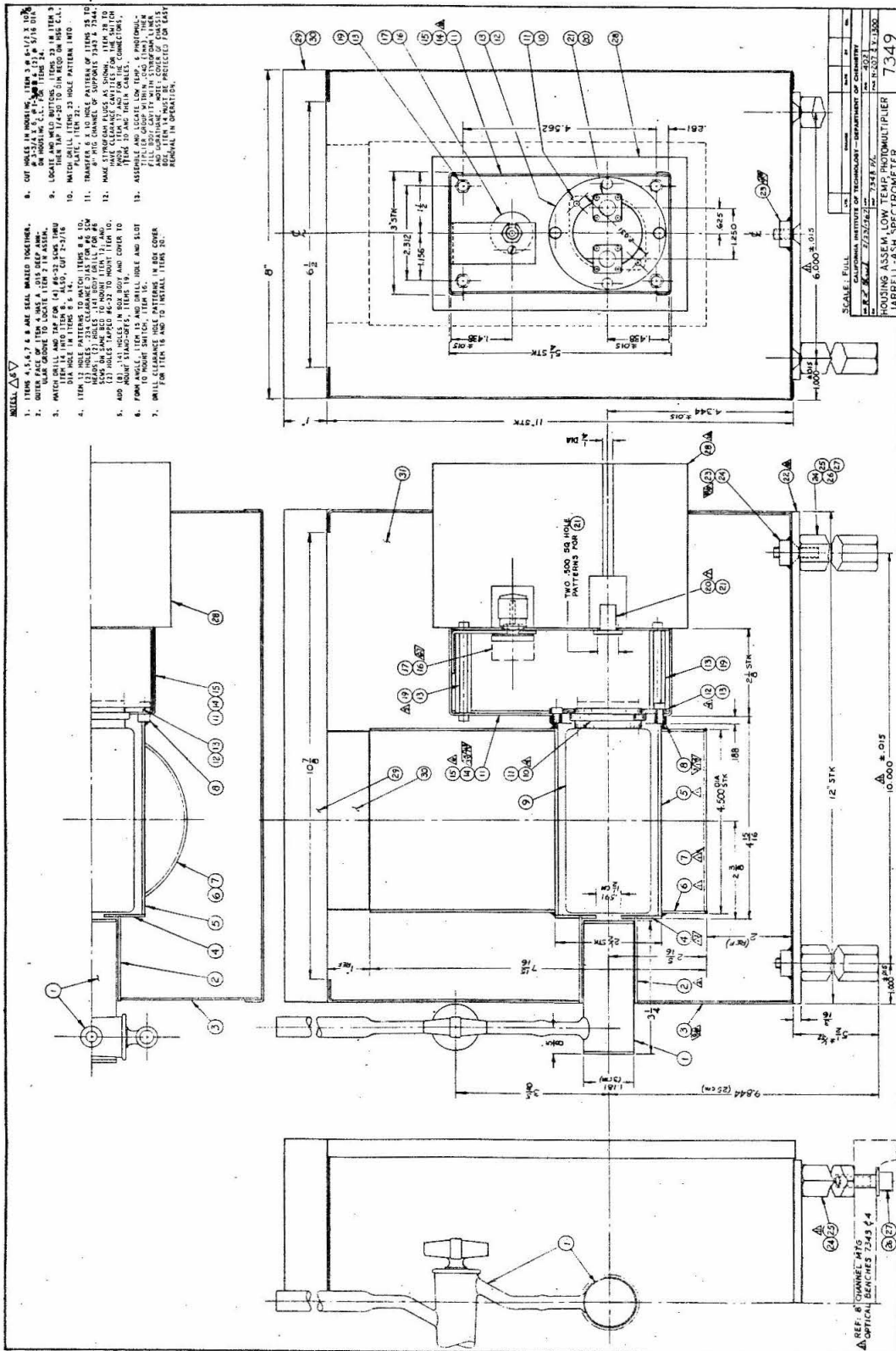


Figure A5. A drawing of the coolable photomultiplier housing designed for use with an EMI 6256 photomultiplier tube.





A7 show the left and right supports, respectively, when facing the instrument. These are constructed of 8" aluminum channel and are designed to support Ealing aluminum triangular optical benches as well as a Dewar mount (Fig. A8), coolable photomultiplier housings (Fig. A5) and a mount for a PAR model BZ-1 chopper suitable for use with a PAR model HR-8 lock-in amplifier. An extension, which mounts at right angles to the right-hand bench (Fig. A9), makes possible simultaneous utilization of the double-beam capability and the rotatory refractor plate assembly described in sub-section e. Details of the metal, liquid-helium Dewar compatible with this system have been described previously in a thesis by E. R. Bernstein, California Institute of Technology, 1968.

#### d. Light Tunnel Assembly

A light-tight system containing lenses, polarizers (before and after the sample), a beam splitter, variable apertures and two coolable EMI 6256 photomultiplier tubes is shown in Fig. A10. This system bolts directly over the exit slit of a 1.8 m Jarrell-Ash spectrometer to provide double-beam capability. The monochromatic light beam emerging from the exit slit of the spectrometer is split into reference and sample beams, the sample beam containing roughly 95% of the total intensity. The outputs from the two photomultiplier tubes are fed into a differential amplifier (Tektronix, type 1A7 or PAR type A pre-amp) which amplifies the difference signal. Nulling of the signal prior to beginning an experiment can be accomplished by adjustment of the two variable apertures, one of which is situated in each light beam.

Figure A6. A drawing of the left optical bench support (when facing the instrument) mounted on a 1.8 m Jarrell-Ash spectrometer.

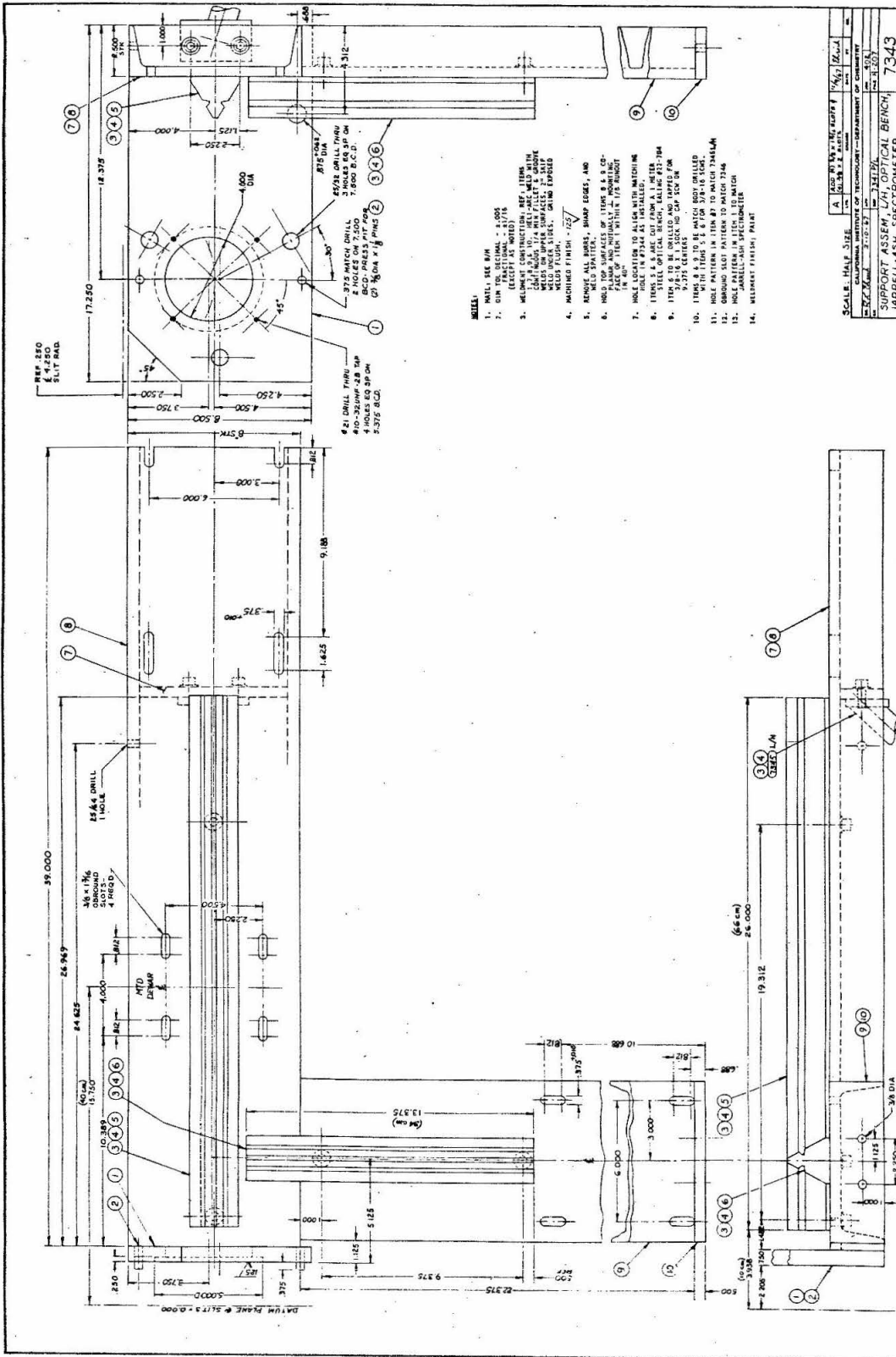


Figure A7. A drawing of the right optical bench support (when facing the instrument) mounted on a 1.8 m Jarrell-Ash spectrometer.

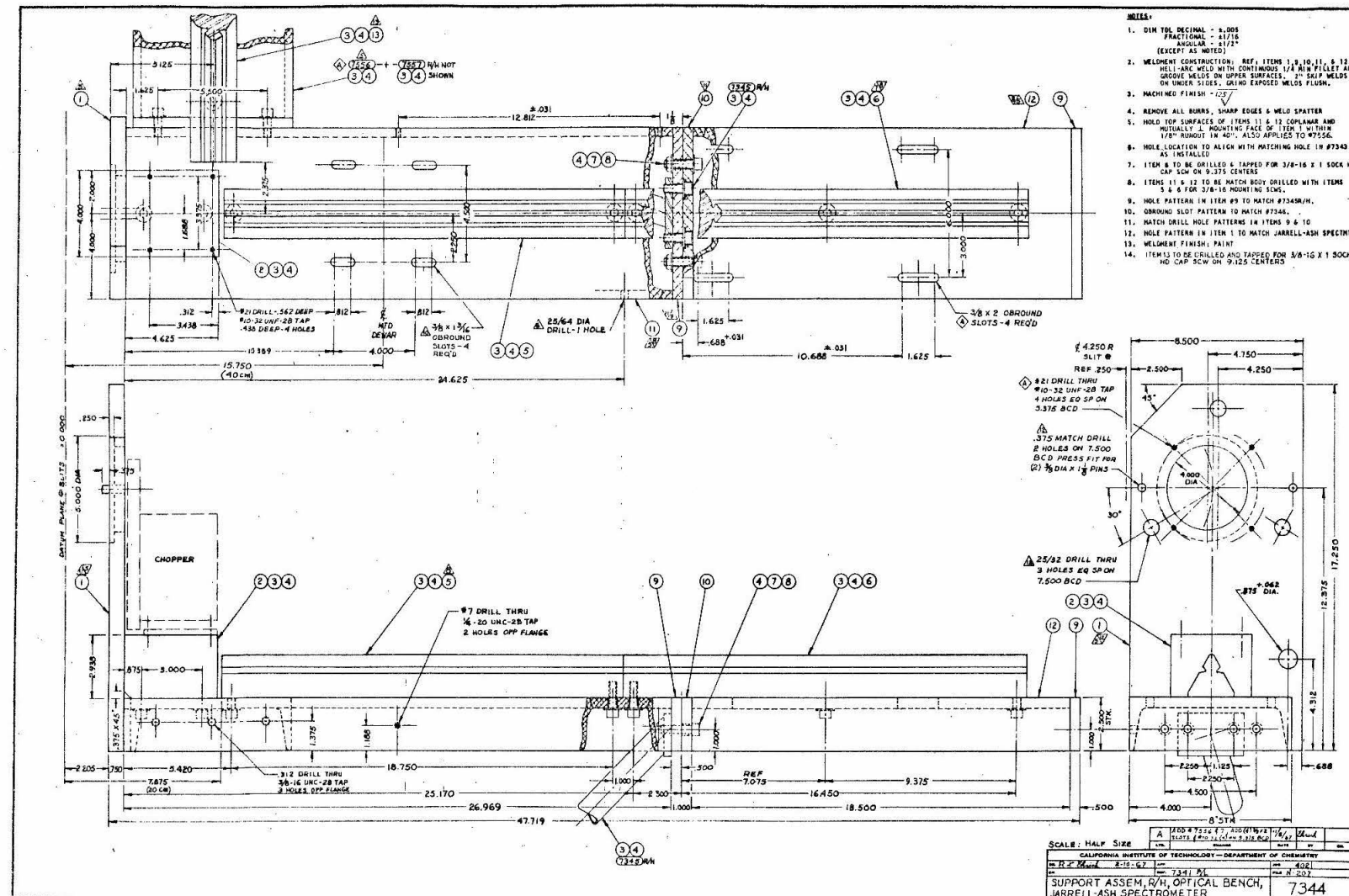
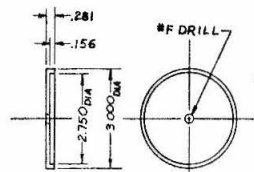
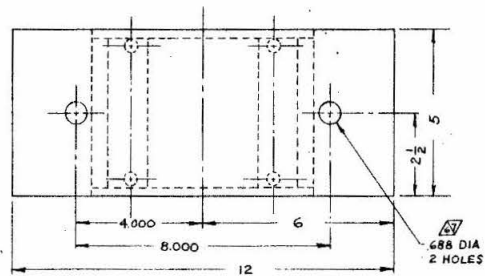
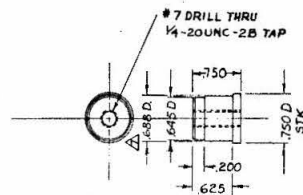


Figure A8. A drawing of a helium Dewar support weldment used to mount a metal helium Dewar on either of the optical bench supports shown in Figs. A6 and A7.



WASHER, HOLD-DOWN  
ITEM 7  
SCALE: HALF



PLUG-LOCATING  
ITEM 6  
SCALE: FULL

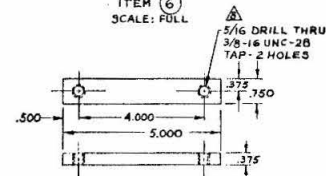
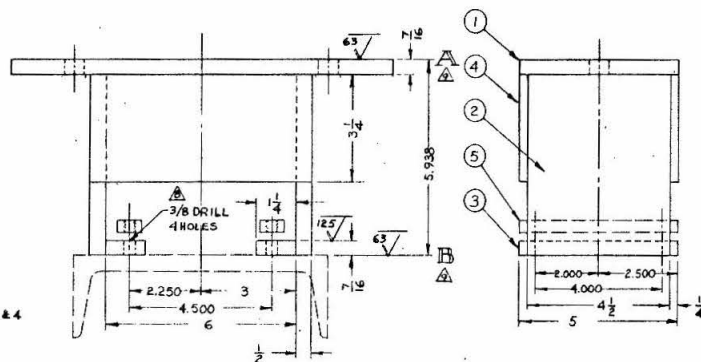


PLATE-NUT-3/8-16  
ITEM 5  
SCALE: HALF



# NOTES:

1. MATL: SEE B/M
2. CONSTRUCTION: HELI-ARC WELDED WITH 1/4 CONVEX FILLET & GROOVE WELDS
3. DIM TOL DECIMAL -  $\pm .005$   
FRACTIONAL -  $\pm 1/32$   
ANGULAR -  $\pm 1/2^\circ$   
(EXCEPT AS NOTED)
4. MACHINED FINISH -  $\sqrt{}$
5. BREAK SHARP EDGES & REMOVE WELD SPATTER
6. TRANSFER HOLE PATTERN FROM BASE OF LOWER HELIUM DEWAR #6601
7. PRESS FIT DIA HOLES FOR ITEMS 6
8. HOLE PATTERNS OF ITEMS 3, 5, 7, 3, 4 & 4 SUPPORT ASSEMBLY TO MATCH
9. HOLD SURFACES "A" II "B" WITHIN .010 IN 10.000
10. FINISH: CLEAR ANODIZE

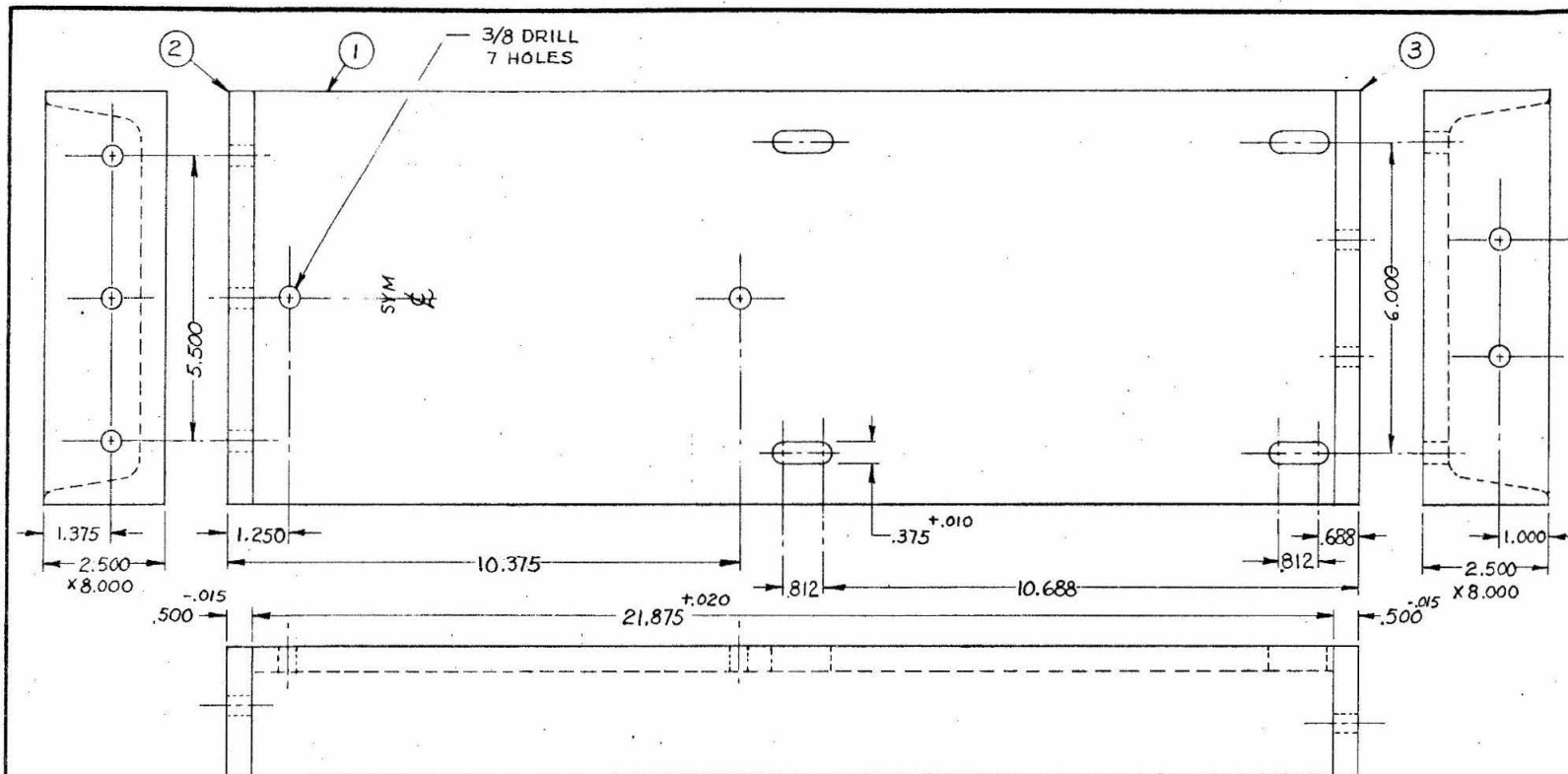
SCALE: HALF & NOTED

| DATE   | CHANGE        | BY         | CHK          |
|--|---------------|------------|--------------|
| CALIFORNIA INSTITUTE OF TECHNOLOGY—DEPARTMENT OF CHEMISTRY |               |            |              |
| REV. 2-10-62   | REV. 7-3-1-62 | REV. 4-2-1 | REV. 11-20-7 |
| SUPPORT WELDMENT, HELIUM DEWAR, JARRELL-ASH SPECTROMETER   |               |            | 7346         |

FORM CL-8

**Figure A9.** A drawing of a lateral extension to the optical bench support shown in Fig. A7.





NOTES:

1. MATL: SEE B/M
2. DIM TOL DECIMAL -  $\pm .005$   
FRACTIONAL -  $\pm 1/16$   
(EXCEPT AS NOTED)
3. WELDMENT CONSTRUCTION:  
HELI-ARC WELD WITH CON-  
TINUOUS 1/4 MIN FILLET  
& GROOVE WELDS. GRIND  
EXPOSED WELDS FLUSH.
4. MACHINED FINISH - 125
5. REMOVE ALL BURRS, SHARP  
EDGES AND WELD SPATTER.
6. WELDMENT FINISH: BLACK  
ANODIZE

SCALE: HALF SIZE

| LTR.   |               | CHANGE |  | DATE | BY    | CHK. |
|--|---------------|--------|--|------|-------|------|
| CALIFORNIA INSTITUTE OF TECHNOLOGY—DEPARTMENT OF CHEMISTRY                           |               |        |  |      |       |      |
| DR. <i>R. S. Ehrlich</i>   | 11/8/1967     | APP.   |  | JOB  | 402   |      |
| CH.  | REF. 7341 P/L |        |  | FILE | N-207 |      |
| SUPPORT WELDMENT, EXTENSION, R/H LATERAL, OPTICAL<br>BENCH, JARRELL-ASH SPECTROMETER |               |        |  |      |       | 7556 |

Figure A10. An assembly drawing of a light tunnel mounted on a 1.8 m Jarrell-Ash spectrometer. This assembly provides for double-beam operation and can be used in conjunction with a rotary refractor plate assembly (Figs. A11 and A12) to give simultaneous rapid scan of a limited spectral region.



The numbers 1-23 on the assembly drawing (Fig. A10) correspond with numbers stamped on the individual sections of the tunnel to facilitate assembly. Although the system as shown was designed for use on a Jarrell-Ash 1.8 m spectrometer in conjunction with the optical bench support assembly described in subsection c, it has also been found useful in part with a Jarrell-Ash 0.5 m spectrometer, providing coupling between the spectrometer exit slit and a coolable photomultiplier housing (Fig. A5).

#### e. Rotary Refractor Plate Assembly

Figures A11 and A12 are drawings of a rotary refractor plate installation in a 1.8 m Jarrell-Ash spectrometer. This device utilizes the refractive properties of a quartz prism to provide a repetitive rapid scan of a small region of the spectrum centered at an arbitrary wavelength, dependent upon the position of the grating. Light striking the prism, of refractive index  $n$ , at an angle  $\theta$  to the normal, suffers a linear displacement proportional to  $\sin\theta (1 - \frac{\cos\theta}{n})$  as it traverses the prism. Thus, if the prism is positioned inside the spectrometer directly behind the exit slit, as the prism rotates, the wavelength of the light intercepted by the exit slit is a function of the rotation. It can easily be shown that an observer looking into the exit slit from outside the spectrometer would see a repetitive unidirectional wavelength scan. The prism can be rotated at frequencies up to 10 KHz, making signal averaging a feasible part of data acquisition.

The extent of the spectral region scanned depends upon the reciprocal linear dispersion of the spectrometer in which the device is

Figure A11. A drawing of a rotary refractor plate assembly mounted in a 1.8 m Jarrell-Ash spectrometer (viewed from inside the instrument). This device provides for rapid scan of approximately 15 Å of the spectrum (which 15 Å interval depends upon the position of the grating) when used in conjunction with a 600 grooves/mm grating.

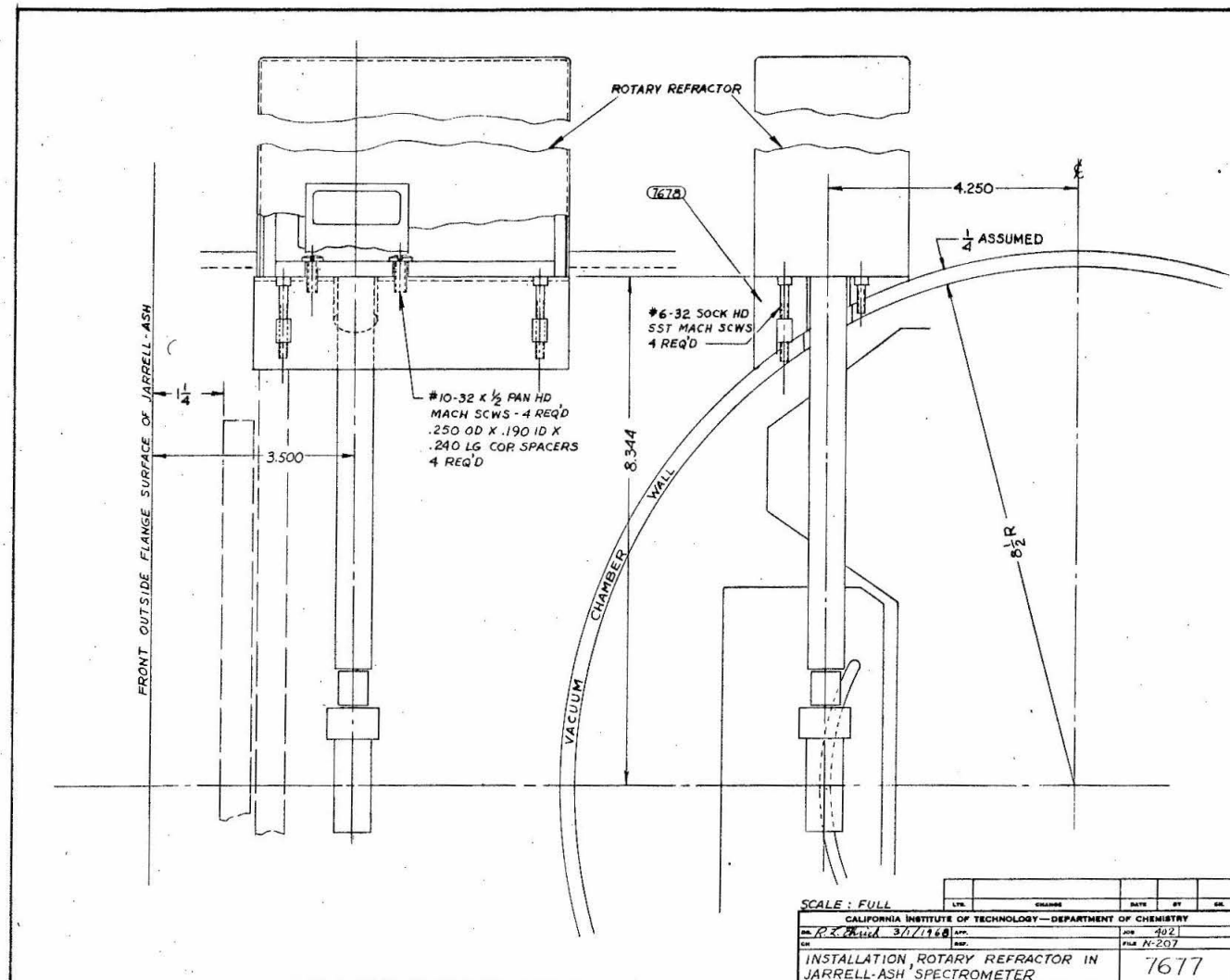
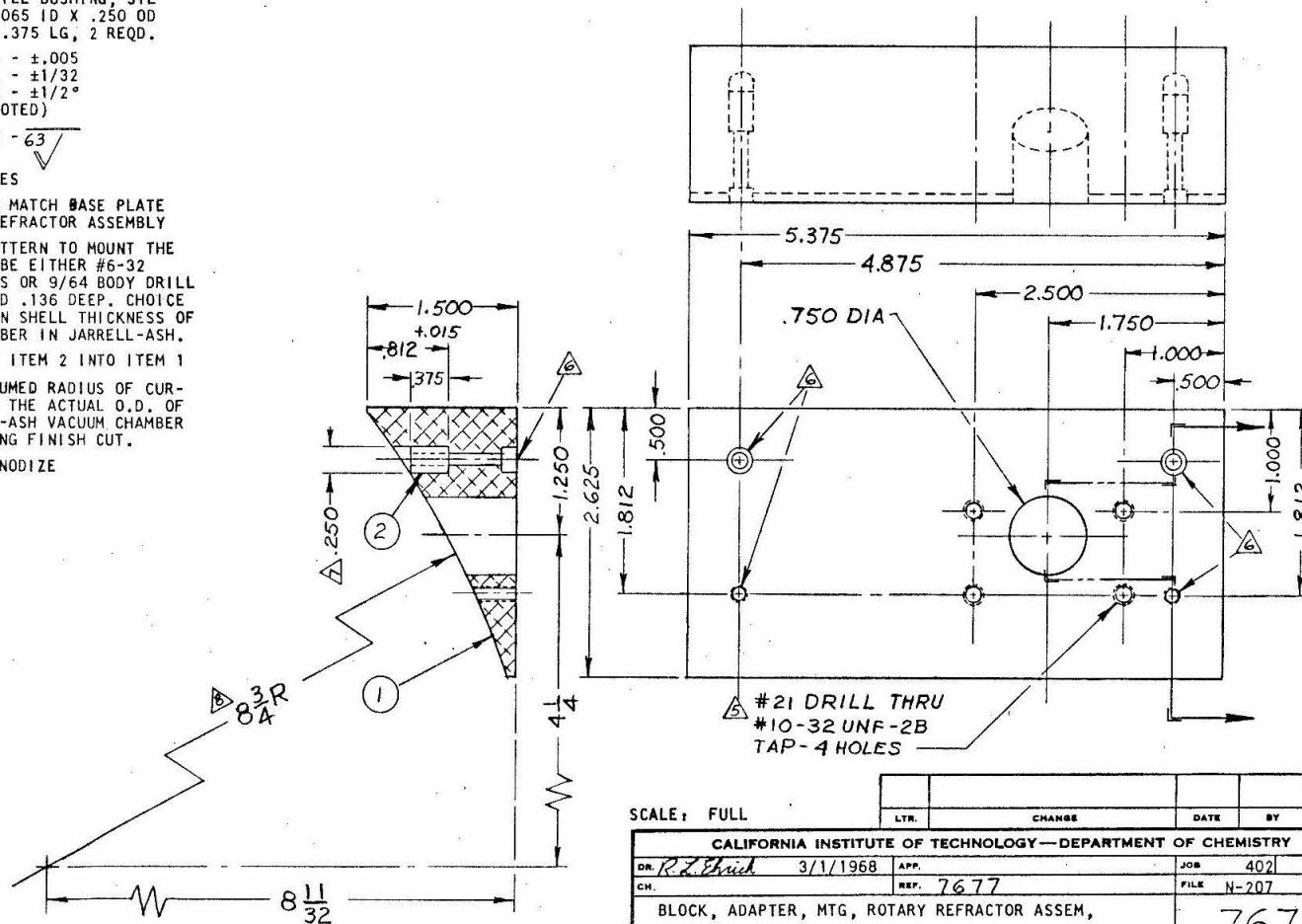


Figure A12. Details of the adapter block used in mounting the rotary refractor plate assembly.

NOTES:

1. MATL: ITEM 1 ALUM ALLOY 1024  
ITEM 2 DRILL BUSHING, STL  
.1065 ID X .250 OD  
X .375 LG, 2 REQD.
2. DIM TOL DECIMAL -  $\pm .005$   
FRACTIONAL -  $\pm 1/32$   
ANGULAR -  $\pm 1/2^\circ$   
(EXCEPT AS NOTED)
3. MACHINED FINISH -  $\sqrt{63}$
4. BREAK SHARP EDGES
5. HOLE PATTERN TO MATCH BASE PLATE  
OF ROTARY REFRACTOR ASSEMBLY
6. THE (4) HOLE PATTERN TO MOUNT THE  
BLOCK WILL BE EITHER #6-32  
TAPPED HOLES OR 9/64 BODY DRILL  
& #6 C'BORED .136 DEEP. CHOICE  
DEPENDS UPON SHELL THICKNESS OF  
VACUUM CHAMBER IN JARRELL-ASH.
7. LIGHT PRESS FIT ITEM 2 INTO ITEM 1
8. VERIFY THIS ASSUMED RADIUS OF CUR-  
VATURE WITH THE ACTUAL O.D. OF  
THE JARRELL-ASH VACUUM CHAMBER  
BEFORE MAKING FINISH CUT.
9. FINISH: BLACK ANODIZE



SCALE: FULL

CALIFORNIA INSTITUTE OF TECHNOLOGY—DEPARTMENT OF CHEMISTRY

|                        |          |           |      |       |
|------------------------|----------|-----------|------|-------|
| DR. <i>R. Z. Erick</i> | 3/1/1968 | APP.      | JOB  | 402   |
| CH.                    |          | REF. 7677 | FILE | N-207 |

BLOCK, ADAPTER, MTG, ROTARY REFRACTOR ASSEM,  
JARRELL-ASH SPECTROMETER

7678



mounted. For a 1.8 m Jarrell-Ash spectrometer, using the first order of a 600 grooves/mm grating (reciprocal linear dispersion of 13 Å/mm), an interval of approximately 15 Å is swept past the exit slit repetitively. Unfortunately, the reciprocal dispersion within the 15 Å interval is no longer linear, being most distorted near the extremities of the sweep (corresponding to large angles  $\theta$  between the normal to the prism face and direction of propagation of the light striking it). It is advantageous therefore to use only the central portion of the sweep near  $\theta = 0$  where  $\sin \theta \approx \theta$ . However, if this is not possible and it becomes necessary to use more of the sweep, corrections for the non-linearity can easily be made since the exact form of the distortion is known. The device should be particularly useful for studying line-shapes in view of the fact that the signal can be averaged over long periods of time and stored digitally.

## 2. PROCEDURES

### a. Purification of Anthracene

Attempts to purify anthracene by fusion with an alkali metal, a technique found to be effective in the purification of benzene and naphthalene, have met with failure largely because of the relatively high melting point of anthracene (217° C). At temperatures in this range, reaction between the alkali metal and anthracene is so vigorous that it results in nothing but degradation products. Consequently, purification of anthracene has been restricted to extensive zone-refining, column chromatography or a combination of the two. A modification of the fusion process has been applied to 10g of anthracene. Preliminary

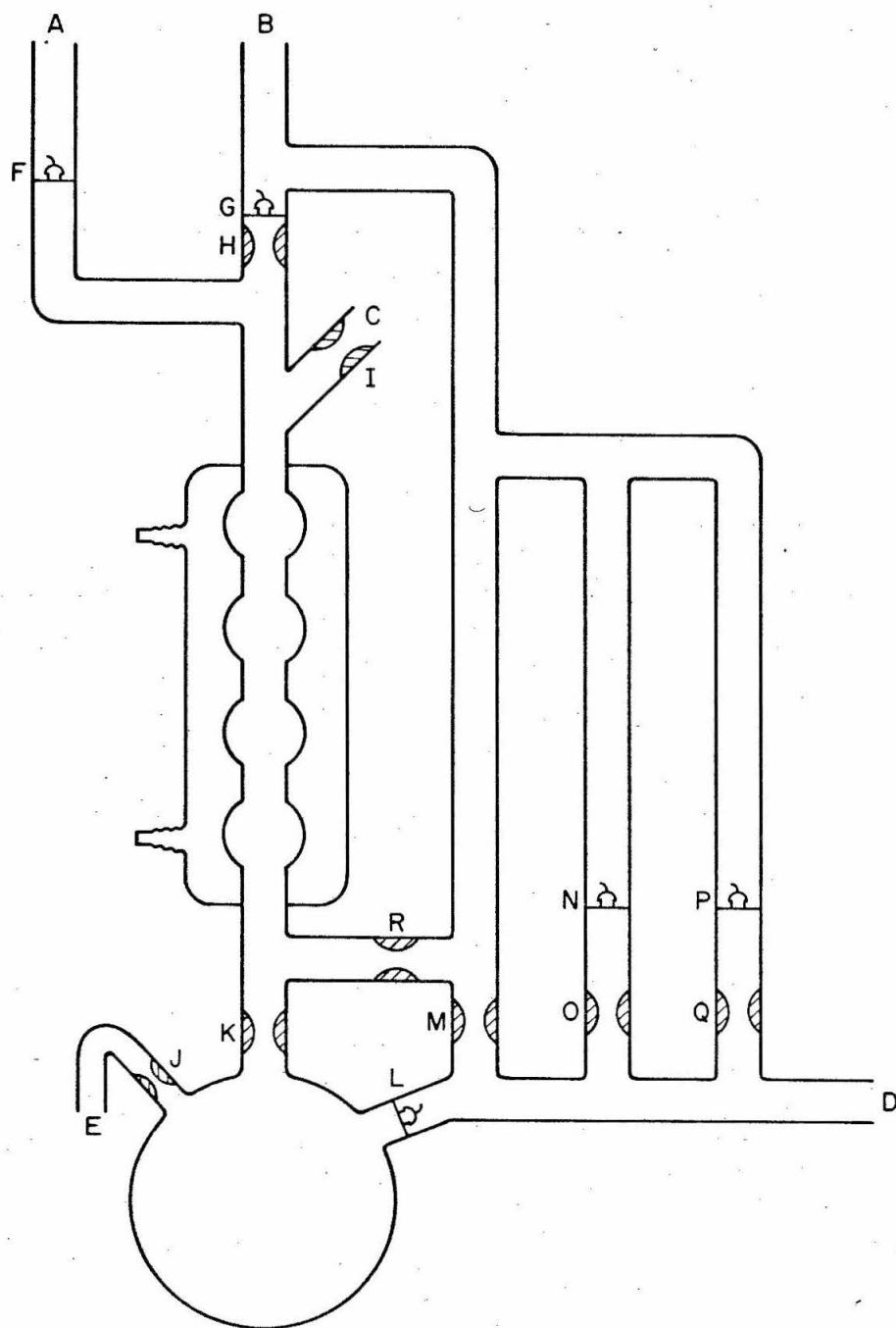
spectroscopic purity checks indicate that the impurity concentration is reduced substantially during the process.

Basically, the method consists of initial zone-refining followed by column chromatography on alumina. The purest fraction from the column is dissolved in benzene and subsequently treated with potassium metal at 80° C. Dissolving the anthracene in benzene provides the requisite mobility for effective contact with the potassium metal while obviating the need for working at temperatures near 220° C. In a final step the anthracene is once again zone-refined, care being exercised to maintain darkness around the molten zone. Since the zone-refining and chromatographic procedures are straightforward, attention will be focused on the details of the potassium treatment.

A diagram of the purification manifold is shown in Fig. A13. After initial outgassing of the manifold (limiting pressure  $\sim 4 \times 10^{-7}$  Torr), high purity potassium is introduced at E from a previously prepared break-seal tube. Constriction J is sealed and a potassium mirror formed on the walls of the reaction vessel. The initially zone-refined and chromatographed anthracene is introduced through C under a helium gas purge to avoid contaminating the potassium surface with air. Constriction I is sealed and the anthracene outgassed. Carefully dried, degassed benzene is then distilled from another part of the vacuum system into the reaction vessel through B and break-seal G. After admitting a few Torr of high purity, dry helium gas, constrictions H and R are sealed and the benzene refluxed for 24 hours. At the completion of the reaction the benzene is transferred, through break-seal F and tube A, to a vessel elsewhere on the vacuum line and

Figure A13. A drawing of the manifold used to purify anthracene. The manifold is sealed to the vacuum system at points A and B. Starting material is introduced through C. High purity potassium is admitted from a break-seal tube through E. A receiving vessel for the purified material is affixed at D.

# ANTHRACENE PURIFICATION MANIFOLD



constrictions K and M are sealed. The anthracene is transferred out of the reaction vessel through break-seal L into a receiving vessel at D. Should a pressure build-up occur during this transfer, due to liberation of trapped gases, access to the pump can be re-gained through break-seal N. After the gases have been pumped out, constriction O is sealed to re-establish the closed system necessary for continuation of the transfer. When all the anthracene has been transferred into the receiving vessel (usually a zone-refining tube), break-seal P is opened for final outgassing of the sample. A few Torr of high purity, dry helium gas is admitted to prevent sublimation during the zone-refining step, and the receiving vessel is sealed off. After the final zone-refining has been completed, the zone-refining tube is resealed to the vacuum line, access to the anthracene being through a break-seal at the upper end of the tube. The central fraction of pure anthracene is transferred under vacuum into crystal-growing tubes, outgassed once more and sealed off, thus completing the purification procedure.

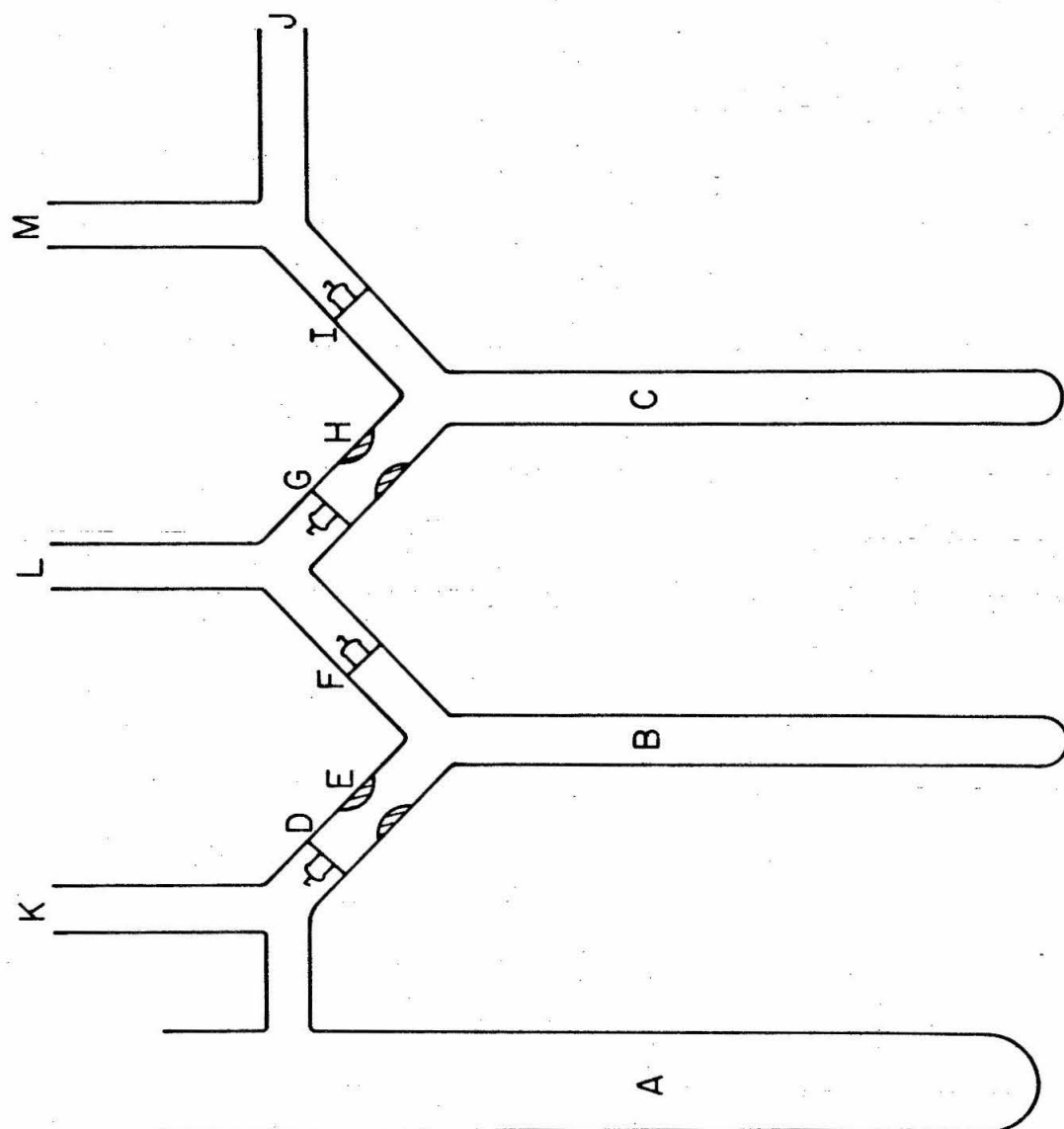
Of utmost importance is the exclusion of air during the entire process. This is particularly crucial during the time the anthracene is dissolved in benzene since anthracene is rapidly oxidized in benzene solution. Consequently, considerable time is required at each step in the purification to ensure that the system is properly degassed. One complete purification requires approximately six weeks from start to finish.

### b. Purification of Naphthalene

A brief description of the naphthalene purification procedure is included here for completeness. The manifold (Fig. A14) is initially outgassed (limiting pressure  $\sim 4 \times 10^{-7}$  Torr) and a mirror of potassium (admitted previously) formed on the walls of B and C. Zone-refined naphthalene is introduced into vessel A under a helium gas purge and subsequently transferred into vessel B through break-seal D. Constriction E is sealed and the naphthalene-potassium mixture heated to  $90^{\circ}\text{C}$  for 12 hours. The contents of B are transferred through break-seals F and G into vessel C, constriction H is sealed and a second 12 hour fusion at  $90^{\circ}\text{C}$  follows. The naphthalene is transferred from C into a receiving vessel (usually a zone-refining tube) at J and undergoes extensive zone-refining before being transferred under vacuum into crystal-growing tubes. As in the anthracene purification, air is rigorously excluded during the entire process. A complete purification can be effected in roughly one month.

Figure A14. A drawing of the manifold used to purify naphthalene. The manifold is sealed to the vacuum system at points K, L and M. Starting material is introduced into vessel A. A receiving vessel for the purified material is affixed at J.

## NAPHTHALENE PURIFICATION MANIFOLD





## APPENDIX B

## CONCERNING THE DECAY KINETICS OF EXCITED STATES

The kinetics of excited state population and depopulation are discussed for the separate cases of continuous and intermittent excitation. A comparison is made between these two types of excitation with particular reference to the experimental determination of the kinetic constants defined by the equation governing the excited state population. Provided that the periodic excitation consists of well-defined "on" and "off" intervals and the time required to switch from the "on" to the "off" condition is small compared to the lifetime of the emitting state, these constants can be determined as well with periodic as with continuous excitation. In the following, a continuous source is taken to be one that provides continuous excitation for a time that is long compared to the lifetime of the emitting state in question. Thus, steady-state conditions are reached before the source is switched off and measurements of the decay begun. A periodic source, on the other hand, is one that provides cyclically an illumination interval followed by a dark interval and steady-state conditions may not be established during a single cycle. Evidently, in the limit of vanishingly small frequency a periodic source becomes equivalent to a continuous source.

Consider the general equation for combined first- and second-order kinetics,

$$-dn(t)/dt = \beta n(t) + \gamma n^2(t) - S(t) , \quad (B1)$$

where  $n(t)$  is the excited state population as a function of time,  $\beta$  is the total first-order rate constant and  $S(t)$  is a term representing the excitation source. For a given source intensity  $I(t)$  we have

$$S(t) = CI(t), \quad (B2)$$

$C$  being the fraction of the source intensity that is effective in producing the excited states of interest. In view of the fact that  $\beta$  and  $\gamma$  may be composites of the decay constants for several first- and second-order decay channels, respectively, it is clear that Eq. (B1) is representative of the kinetics of a large number of systems. It should be noted that, except in the case that the source term is constant, Eq. (B1) cannot in general be solved analytically. Of course, if  $\gamma = 0$ , corresponding to pure first-order decay, the equation can be solved analytically for any  $S(t)$  subject only to the evaluation of the integrals involved. However, even for a non-zero  $\gamma$ , if  $S(t)$  is a square wave it is possible to solve Eq. (B1) with a constant source term during the illumination interval and with  $S(t) = 0$  throughout the dark interval of the cycle (Fig. B1). The two solutions must then be fitted together at the point in the cycle at which the illumination is interrupted, in order to obtain the complete solution. We proceed now to establish several of these results in more detail.

### 1. CONTINUOUS EXCITATION

The source term is taken to be time-independent and of magnitude  $CI_0/2$ ,  $I_0$  being the source intensity. The reason for the explicit

inclusion of the factor of 2 will become apparent later. With this source term, Eq. (B1) becomes

$$-dn(t)/dt = \beta n(t) + \gamma n^2(t) - CI_0/2 . \quad (B3)$$

Solving Eq. (B3) for  $n(t)$  with the initial value  $n(0) = 0$  yields

$$n(t) = CI_0 / \{ \beta + (\beta^2 + 2CI_0\gamma)^{\frac{1}{2}} \operatorname{ctnh} [ (\beta^2 + 2CI_0\gamma)^{\frac{1}{2}} t / 2 ] \} . \quad (B4)$$

Equation (B4) describes the approach to steady-state of a level that is being pumped by a continuous source and simultaneously depopulated by both first- and second-order processes. We note in passing that in the limit as  $t$  approaches infinity, Eq. (B4) reduces to a steady-state value of

$$n(t = \infty) = CI_0 / [ \beta + (\beta^2 + 2CI_0\gamma)^{\frac{1}{2}} ] , \quad (B5)$$

which is just the solution of Eq. (B3) with  $dn(t)/dt = 0$  and  $n(0) = 0$ , as it must be. It is a simple matter to extract from Eq. (B4) expressions appropriate to pure first- and pure second-order decay by setting  $\gamma = 0$  and  $\beta = 0$ , respectively. In the first case we obtain

$$n(t) = (CI_0/2\beta)(1 - \exp[-\beta t]) , \quad (B6)$$

whereas the approach to steady-state in the case of pure second-order decay is governed by the equation

$$n(t) = (CI_0/2\gamma)^{\frac{1}{2}} \tanh[(2CI_0\gamma)^{\frac{1}{2}} t / 2] . \quad (B7)$$

Having established Eqs. (B4), (B6) and (B7) under conditions of continuous excitation, we turn to an investigation of Eq. (B1) when the

source term  $S(t)$  is time-dependent.

## 2. PERIODIC EXCITATION

In the following discussion,  $I(t)$  is taken to be a symmetrical square wave of magnitude  $I_0$  during the first half of each cycle and 0 during the last half of each cycle (Fig. B1). This particular form for  $I(t)$  is chosen because it closely approximates the actual experimental conditions used and because it facilitates the analysis. The square wave can be represented by a Fourier series

$$I(t) = I_0 \left\{ \frac{1}{2} + \frac{2}{\pi} \sum_{k=0}^{\infty} \frac{\sin[(2k+1)\omega t]}{(2k+1)} \right\}, \quad (\text{B8})$$

with  $\omega$  equal to the frequency of the square wave excitation source. The average value of  $I(t)$  is just  $I_0/2$ , suggesting that comparison between periodic and continuous excitation is best made for a continuous source of intensity  $I_0/2$ . Hence the factor of 2 in the definition of the continuous source intensity in Eq. (B3).

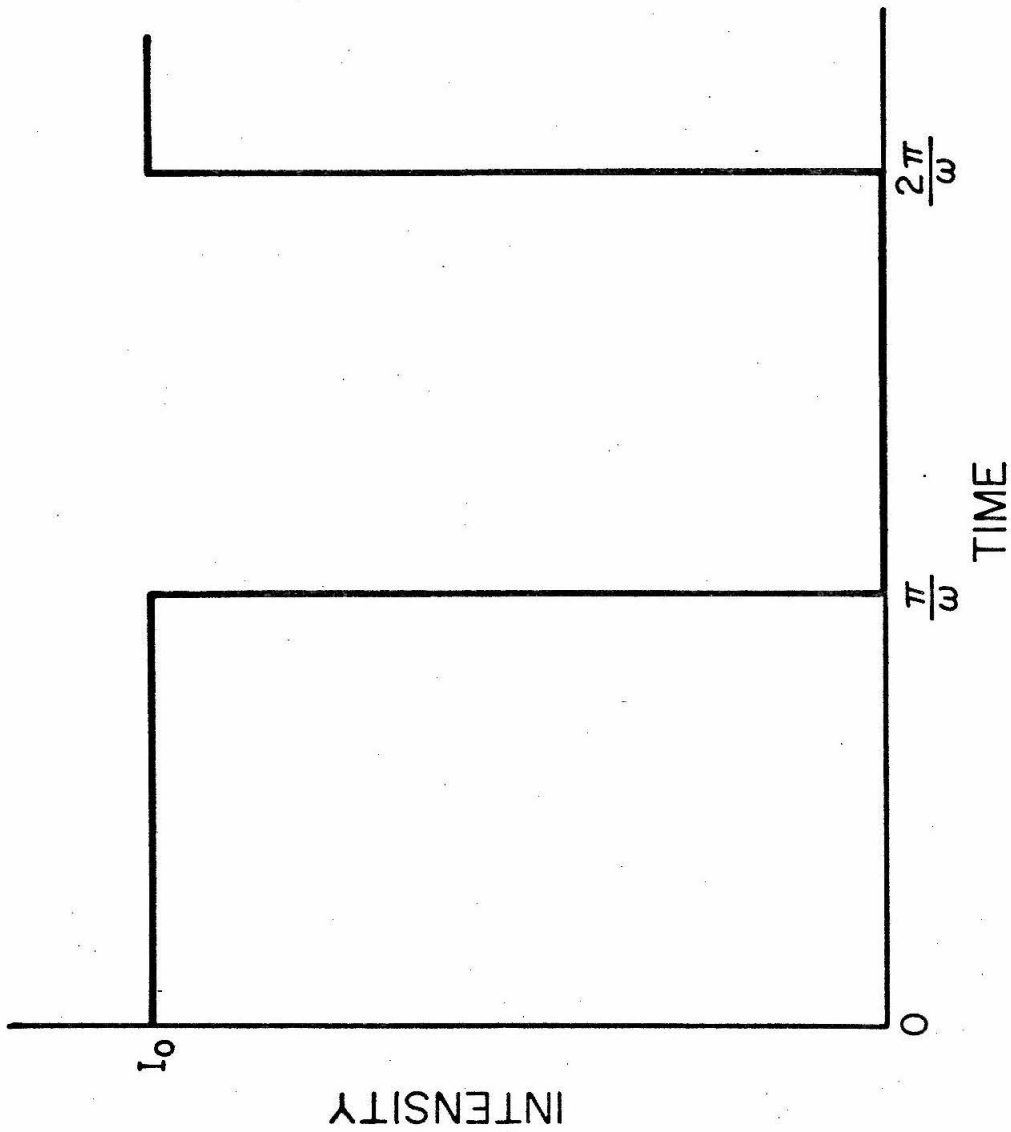
Since an analytical solution to Eq. (B1) with  $\gamma = 0$  and  $S(t)$  given by Eqs. (B2) and (B8) can be found, we consider that situation next. The equation to be solved is

$$dn(t)/dt + \beta n(t) = CI_0 \left\{ \frac{1}{2} + \frac{2}{\pi} \sum_{k=0}^{\infty} \frac{\sin[(2k+1)\omega t]}{(2k+1)} \right\}, \quad (\text{B9})$$

the solution to which is

$$n(t) = (CI_0/2\beta) + (2CI_0/\pi\beta) \{ M(\omega, \beta, t) + N(\omega, \beta) \exp[-\beta t] \}, \quad (\text{B10})$$

Figure B1. The form assumed for the source term in the analysis of the kinetics for the case of intermittent excitation. It need not be a symmetrical square wave but must be characterized by well defined "on" and "off" intervals.



when the initial value is taken to be  $n(0) = 0$ . The functions  $M(\omega, \beta, t)$  and  $N(\omega, \beta)$  are defined by

$$M(\omega, \beta, t) = \sum_{k=0}^{\infty} \left\{ \frac{\beta \sin[(2k+1)\omega t] - (2k+1)\omega \cos[(2k+1)\omega t]}{(2k+1)[\beta + (2k+1)^2\omega^2/\beta]} \right\} \quad (\text{B11})$$

and

$$N(\omega, \beta) = \sum_{k=0}^{\infty} \{1/[\beta/\omega + (2k+1)^2\omega/\beta]\} - \pi/4. \quad (\text{B12})$$

It is straightforward to show that Eq. (B10) reduces to Eq. (B6) in the limit as  $\omega$  approaches zero. That is, Eq. (B10), which contains all the time dependence of both the excited state build-up and decay under conditions of periodic excitation and first-order decay, has in it as a special case the result appropriate to continuous excitation.

For non-zero  $\gamma$  and  $S(t)$  defined by Eqs. (B2) and (B8), there exists no single analytical solution to Eq. (B1). However, due to the square wave form of  $S(t)$ , two separate analytical solutions, each valid in its respective half cycle, can be obtained. In the first half each cycle, i. e., while the excitation is "on", the appropriate equation is

$$-dn(t)/dt = \beta n(t) + \gamma n^2(t) - CI_0, \quad (\text{B13})$$

and during the latter half or "off" time of the cycle the kinetics are governed by

$$-dn(t)/dt = \beta n(t) + \gamma n^2(t). \quad (\text{B14})$$

To get the result for the first period, Eq. (B13) is solved on the

interval  $t = 0$  to  $t = \pi/\omega$  with  $n(0) = 0$ . The value  $n(\pi/\omega)$  becomes the initial value for the solution of Eq. (B14) on the interval  $t = \pi/\omega$  to  $t = 2\pi/\omega$ . For  $t$  between  $2\pi/\omega$  and  $3\pi/\omega$  one must again solve Eq. (B13) but now with an initial value given by  $n(2\pi/\omega)$  evaluated from the solution of Eq. (B14), and so on. The complete result is thus generated by a sort of bootstrap process in which Eqs. (B13) and (B14) are solved sequentially and cyclically with different initial values for each period. This technique obviously applies to any decay scheme provided the excitation has the required wave form.

In practice, it is just as simple to solve the complete equation numerically as it is to apply the bootstrap method described above. The Runge-Kutta scheme\* was used to solve Eq. (B1) with  $S(t)$  defined by Eqs. (B2) and (B3). The solution is displayed in Figs. B2-B4, the three curves corresponding to a source frequency less than, roughly equal to, and greater than the reciprocal of the lifetime of the emitting state, respectively. It can be seen that the approach to steady-state using periodic excitation parallels that for continuous excitation provided the two sources have the same average intensity.

### 3. CONCLUSIONS

- (i) With the single requirement that there be well-defined "on" and "off" intervals during the cycle, it is evident that the kinetic

---

\* See, for example, H. B. Keller, Numerical Methods for Two-Point Boundary-Value Problems (Blaisdell Publishing Co., Waltham, Massachusetts, 1968), Chap. 1.



Figure B2. Build-up and decay of excited state population under intermittent excitation when the frequency of the source is less than the reciprocal of the lifetime of the emitting state.

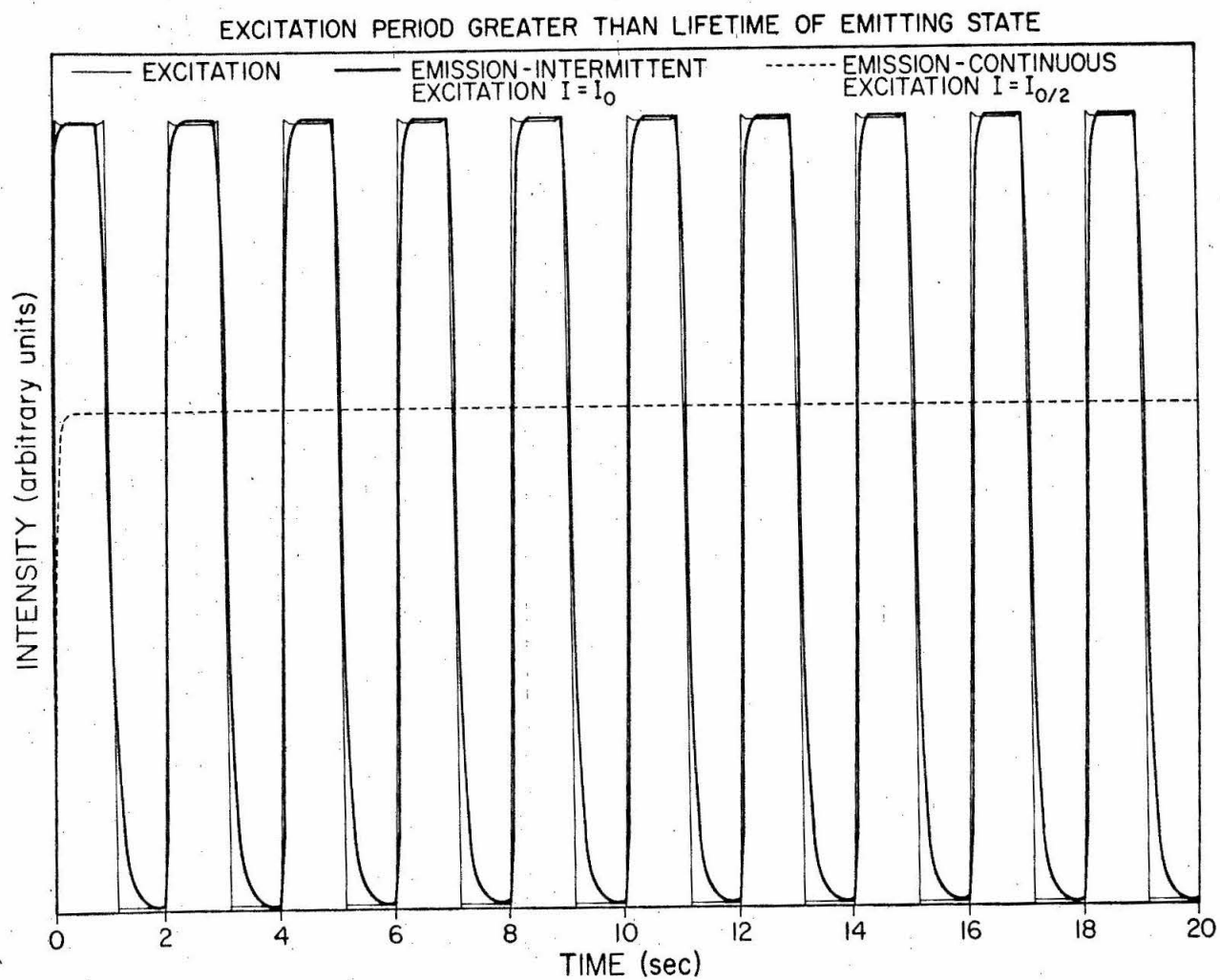


Figure B3. Build-up and decay of excited state population under intermittent excitation when the frequency of the source is roughly equal to the reciprocal of the lifetime of the emitting state.

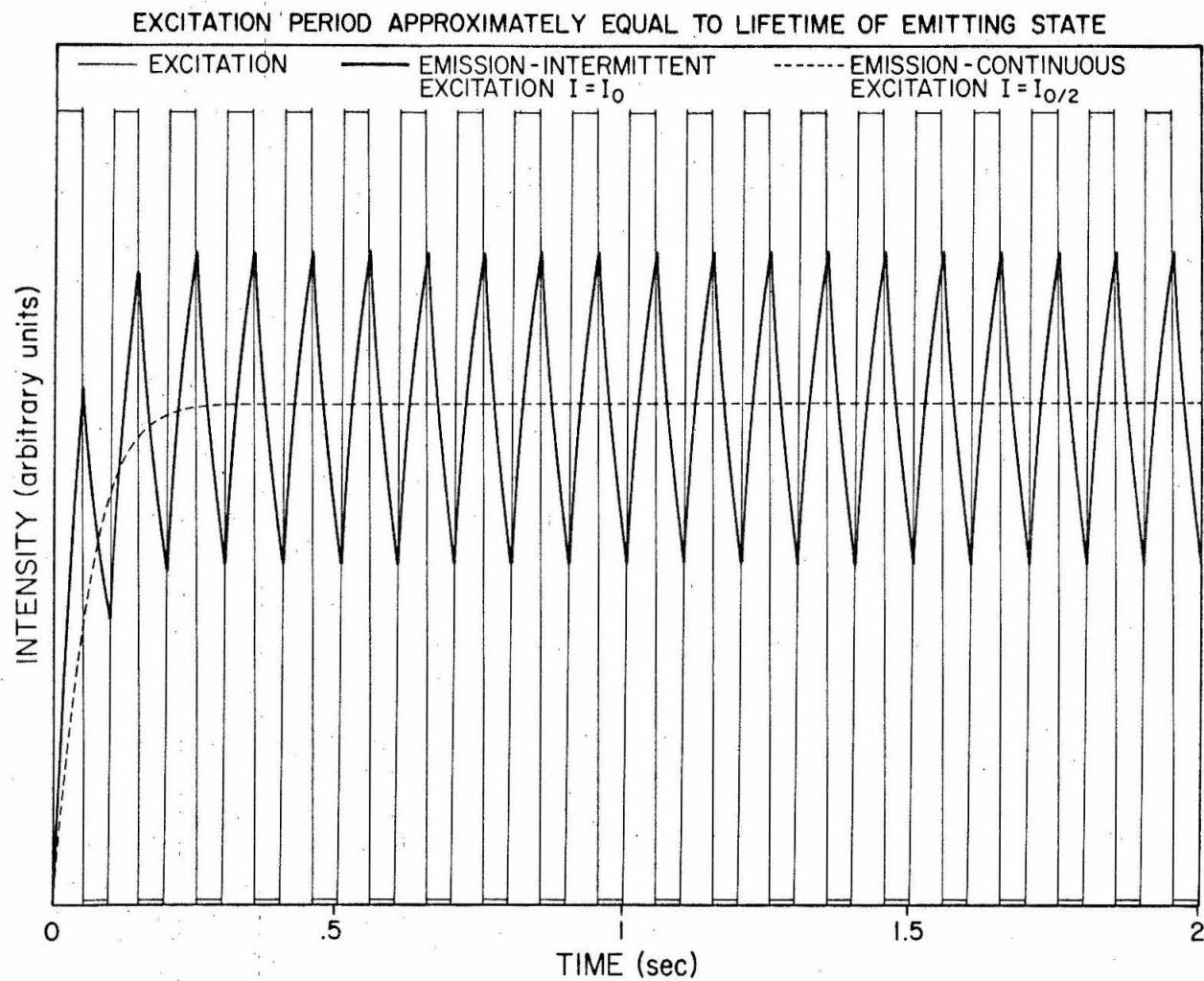
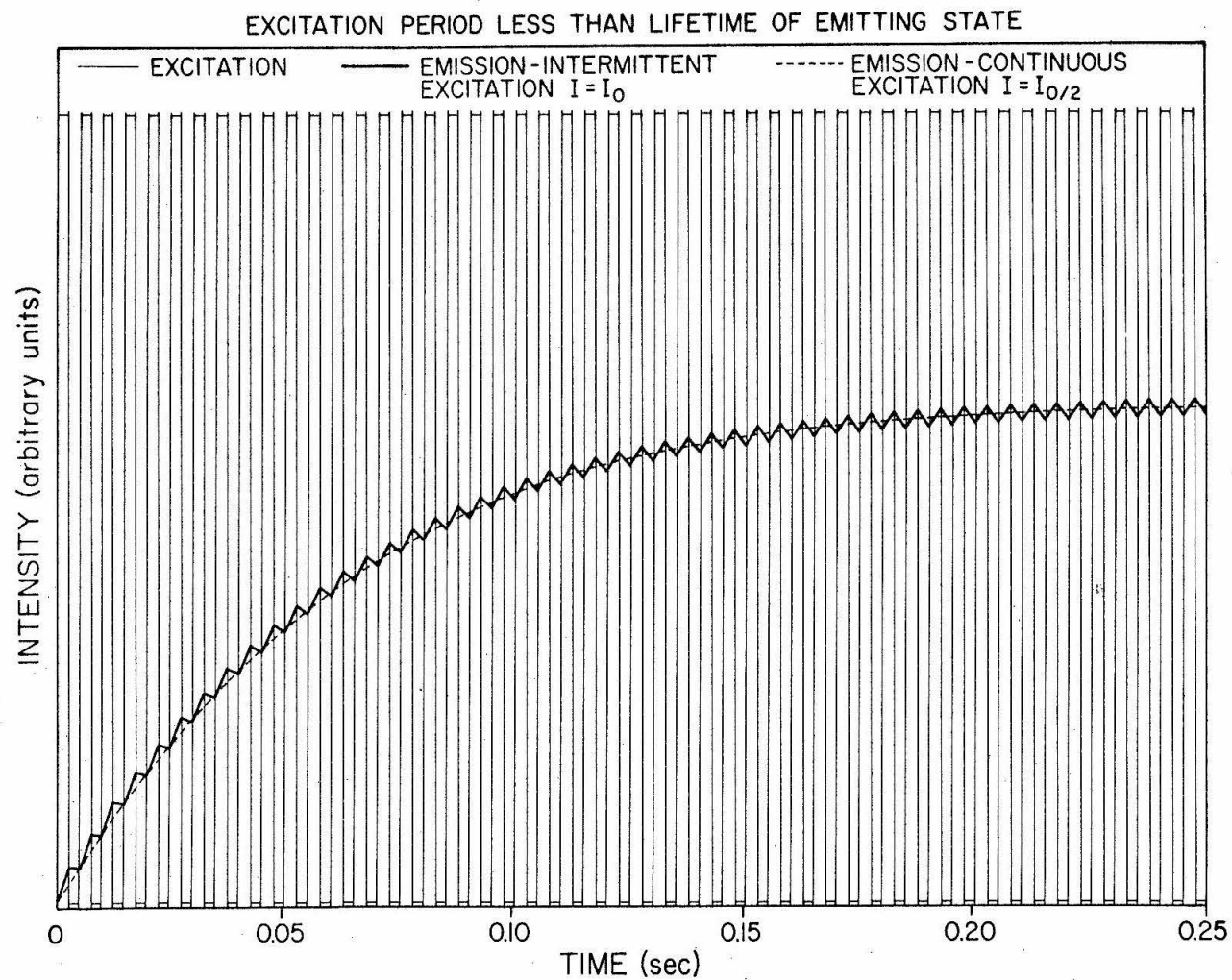


Figure B4. Build-up and decay of excited state population under intermittent excitation when the frequency of the source is greater than the reciprocal of the lifetime of the emitting state.



constants derived from experiments utilizing periodic excitation are unchanged from those obtained by use of continuous illumination. This is true for any kinetic decay scheme and is independent of any asymmetry in the source term, i.e., the source term need not be a symmetrical square wave.

- (ii) For experiments in which the period of the source term is short compared to the lifetime of the emitting state, it is a good practice to begin making measurements only after several periods have elapsed. Otherwise, the build-up to steady-state will appear as a rising background (Fig. B4). A rough estimate of the number of periods necessary prior to measurement can be obtained from the expression  $N \approx 10\omega\beta$ .
- (iii) No error is introduced into the experimental determination of the kinetic constants when a complete decay curve is "synthesized" from several pieces recorded at different frequencies.
- (iv) The approach to steady-state under conditions of periodic excitation parallels that with steady-state illumination by a source of equal average intensity. Thus, the only effect of chopping the excitation light is to reduce its average intensity by the ratio of the "off" to "on" intervals.

## APPENDIX C

## NUMERICAL METHODS

The present section is devoted to a discussion of some of the numerical methods used in analyzing various parts of the experimental data. Two books were found to be excellent reference sources for the neophyte numerical analyst. The first is "Numerical Methods for Two-Point Boundary-Value Problems" by Herbert B. Keller<sup>1</sup> which contains among other things very readable discussions of several methods for solving nonlinear differential equations. The other book is "Introduction to the Theory of Probability and Statistics" by Niels Arley and K. Rander Buch<sup>2</sup> which presents a very compact formulation of the theory of adjustment.

1. INITIALIZATION OF LIFETIME DATA

During the course of making many lifetime measurements using a variable speed phosphoroscope (see Appendix A) it became apparent that the most reliable values were obtained from measurements extending over times long compared to the lifetime being measured. This is particularly true for emission decays following non-exponential kinetics. Consequently, the following method was adopted for collecting and handling the data. In the discussion, the values used are those appropriate to the measurement of lifetimes of the order of half a second. The principles behind the method are however quite general.



The emission decay curve (intensity vs time) was recorded at four different phosphoroscope speeds chosen so that sufficient time overlap existed between successive speeds, viz., 1725, 431, 126 and 31 rpm. Absolute  $t=0$  (the time at which the excitation light ceased to strike the sample) was determined at each of the four speeds. After making the necessary baseline corrections, the data were appropriately scaled so that the four individual "pieces" fit together to form a complete decay curve. The scaling between any two successive "pieces" of the curve was accomplished by obtaining the average ratio between the two throughout the overlap region (which was determined from the known  $t=0$ ) and then multiplying one of the "pieces" by the average ratio so as to put both "pieces" on the same scale. This procedure was found to result in smooth decay curves extending over the region from roughly 2 msec to 1 sec. Acquisition of the data in digital form was found to greatly facilitate both the data initialization described above and the fitting of a kinetic scheme to the experimental decay curve.

## 2. FITTING A KINETIC SCHEME TO THE DATA

With the complete decay curve in hand, one is in a position to fit a kinetic scheme to the data as a means of extracting the decay constants. The familiar method of least squares was used for this purpose. Chapter 12 of Arley and Buch<sup>2</sup> contains an elegant presentation of the theory of adjustment as it applies both when the equation of condition are linear and when they are nonlinear. The treatment is formal but at the same time it is easily adapted to practical situations, the

compactness of the formulation making it most appealing for computer application.

A series of computer programs compatible with the IBM 360/75 has been written, listings of which can be found in Appendix D. These programs are designed to effect the data initialization and least squares fitting of any of five kinetic schemes to the experimental decay curve with a minimum of input control data.

### 3. SOLUTION OF THE TRIPLET EXCITATION DIFFUSION EQUATION

The equation to be solved has the form

$$D \frac{d^2 n(x)}{dx^2} - \beta n(x) - \gamma_e n^2(x) + m\alpha I_0 \exp(-\alpha x) = 0 \quad (C1)$$

where

$$\gamma_e = \frac{2\pi\sigma D\gamma}{\gamma + 2\pi\sigma D} \quad (C2)$$

In Eq. (C1),  $D$  is the diffusion constant,  $n(x)$  is the triplet exciton density as a function of position in the direction  $x$  perpendicular to the crystal face being irradiated,  $\beta$  and  $\gamma_e$  are the first- and effective, second-order triplet decay constants, respectively,  $m$  is the inter-system crossing efficiency,  $\alpha$  is the absorption coefficient and  $I_0$  is the incident light intensity. The constant  $\sigma$  in Eq. (C2) is the exciton-exciton "collision diameter"<sup>3</sup> and  $\gamma$  is the second-order rate constant in the limit when  $2\pi\sigma D \gg 1$ . The solution is required on the interval  $0 \leq x \leq a$  where "a" is the crystal thickness. A uniform net defined by

$$x = jh, \quad j = 0, 1, \dots, J+1, \quad h = \frac{a}{J+1} \quad (C3)$$

is constructed on the interval  $[0, a]$  and, with the aid of a centered-finite-difference approximation to the second derivative  $d^2n(x)/dx^2$ , Eq. (C1) can be cast in the form

$$-\left(\frac{n_{j+1} - 2n_j + n_{j-1}}{h^2}\right) + \frac{\beta}{D} n_j + \frac{\gamma_e}{D} n_j^2 - \frac{m\alpha I_0}{D} \exp(-\alpha jh) . \quad (C4)$$

The functional iteration is, therefore,

$$n_j^{(0)} = \text{arbitrary} , \quad 1 \leq j \leq J \quad (C5a)$$

$$n_j^{(\nu+1)} = \left(\frac{1}{1+\omega}\right) \left[ \frac{1}{2} \left( n_{j+1}^{(\nu)} + n_{j-1}^{(\nu)} \right) + \omega n_j^{(\nu)} - \frac{\beta h^2}{2D} n_j^{(\nu)} - \frac{\gamma_e h^2}{2D} n_j^{(\nu)^2} + \frac{m\alpha I_0 h^2}{2D} \exp(-\alpha jh) \right] \\ 1 \leq j \leq J ; \quad \nu = 0, 1, 2, \dots \quad (C5b)$$

$$n_0^{(\nu)} = 0 , \quad n_{j+1}^{(\nu)} = 0 \quad (C5c)$$

where  $\omega = \frac{h^2}{2} \left( \frac{\beta}{D} + \frac{2\gamma_e}{D} n_{\max} \right)$ .

After computing several iterates of the explicit scheme, Eqs. (C5), the more rapidly converging Newton iterations are used to complete the solution. The initial explicit iterations provide a first Newton iterate "close" to the solution, a necessary requirement to ensure convergence. To define the Newton iterations we first write

$$\phi_j(\underline{n}) = -\frac{1}{2}(n_{j+1} + n_{j-1}) + \left(1 + \frac{\beta h^2}{2D}\right)n_j + \frac{\gamma h^2}{2D} n_j^2 - \frac{m\alpha I_0 h^2}{2D} \exp(-\alpha j h) \quad 1 \leq j \leq J \quad (C6)$$

where

$$\underline{n} \equiv \begin{pmatrix} n_1 \\ n_2 \\ \vdots \\ n_J \end{pmatrix} \quad \text{and} \quad \underline{\Phi}(\underline{n}) \equiv \begin{pmatrix} \phi_1(\underline{n}) \\ \phi_2(\underline{n}) \\ \vdots \\ \phi_J(\underline{n}) \end{pmatrix} \quad (C7)$$

The Jacobian of  $\underline{\Phi}(\underline{n})$  is just the  $J$ th-order tridiagonal matrix

$$\underline{A}(\underline{n}) \equiv \frac{\partial \underline{\Phi}(\underline{n})}{\partial \underline{n}} = \begin{pmatrix} B_1(\underline{n}) & C_1(\underline{n}) & 0 & \dots & 0 \\ A_2(\underline{n}) & B_2(\underline{n}) & C_2(\underline{n}) & \dots & \\ \vdots & \vdots & & & \vdots \\ \vdots & & & & \vdots \\ 0 & \dots & A_{J-1}(\underline{n}) & B_{J-1}(\underline{n}) & C_{J-1}(\underline{n}) \\ & & 0 & A_J(\underline{n}) & B_J(\underline{n}) \end{pmatrix} \quad (C8a)$$

where

$$\begin{aligned} A_j(\underline{n}) &= -\frac{1}{2}, \quad 2 \leq j \leq J, \quad \nu = 0, 1, 2, \dots \\ B_j(\underline{n}) &= 1 + \frac{h^2}{2} \left( \frac{\beta}{D} + \frac{2\gamma_e}{D} n_j \right), \quad 1 \leq j \leq J, \quad \nu = 0, 1, 2, \dots \\ C_j(\underline{n}) &= -\frac{1}{2}, \quad 1 \leq j \leq J-1, \quad \nu = 0, 1, 2, \dots \end{aligned} \quad (C8b)$$

In computing  $\phi_1(\underline{n})$  and  $\phi_J(\underline{n})$  we use  $n_0 = 0$  and  $n_{J+1} = 0$  so that Eq. (C5c) is always satisfied. From Eqs. (C8) it follows that

$$\underline{n}^{(\nu+1)} = \underline{n}^{(\nu)} + \Delta \underline{n}^{(\nu)}, \quad \nu = 0, 1, 2, \dots \quad (\text{C9a})$$

where  $\Delta \underline{n}^{(\nu)}$  is the solution of

$$A(\underline{n}^{(\nu)}) \Delta \underline{n}^{(\nu)} = -\Phi(\underline{n}^{(\nu)}), \quad \nu = 0, 1, 2, \dots \quad (\text{C9b})$$

A general treatment of the method outlined here can be found in reference 1, pp. 72-90.

#### 4. CALCULATION OF THE DELAYED FLUORESCENCE AND PHOSPHORESCENCE EXCITATION SPECTRA

To calculate the delayed fluorescence and phosphorescence excitation spectra exactly, it would be necessary to know  $n(x)$  at all wavelengths for which  $\alpha$  is non-zero. However, since the problem must be solved numerically in any case, we settle for  $n(x)$  at a series of discrete wavelengths chosen so that the resolution is adequate for the present purpose. Having solved Eq. (C1) at each of these points by the method outlined in subsection iii, it remains only to determine  $I_{df}^\lambda$  and  $I_p^\lambda$  the calculated intensities of delayed fluorescence and phosphorescence, respectively, caused by excitation light of wavelength  $\lambda$ . This amounts simply to performing the following numerical integrations

$$I_{df}^\lambda = K_1 \gamma \int_0^a n_\lambda^2(x) dx \quad (\text{C10a})$$

and

$$I_p^\lambda = K_2 \beta \int_0^a n_\lambda(x) dx \quad (\text{C10b})$$

where  $K_1$  and  $K_2$  are constants. Plots of  $I_{df}^\lambda$  and  $I_p^\lambda$  versus  $\lambda$  represent a point-by-point approximation to the experimental spectra. Increasing the number of points used in the calculation will obviously result in a better approximation to the experimentally determined curve.

### 5. FITTING THE CALCULATED EXCITATION SPECTRA TO THOSE OBTAINED EXPERIMENTALLY

With both the calculated and experimental excitation spectra in hand, it appears that a logical next step would be to fit the calculated curve, allowing certain parameters to vary, to the experimental curve in order to obtain the "best estimates" of these parameters. The method of least squares provides a convenient means of accomplishing this task.

Suppose for example we wish to vary the diffusion constant  $D$  in the least squares fit of the phosphorescence excitation spectrum. This will require a knowledge of the derivative of Eq. (C10b) with respect to  $D$ ,

$$\frac{\partial I_p^\lambda}{\partial D} = K_2 \beta \cdot \int_0^a \frac{\partial n_\lambda(x)}{\partial D} dx . \quad (C11)$$

Clearly, it is necessary to know  $\partial n(x)/\partial D$  before Eq. (11) can be of any use. To obtain  $\partial n_\lambda(x)/\partial D$  we note that the derivative of Eq. (C1) with respect to  $D$  can be written in the form

$$\frac{\partial^2 Z}{\partial x^2} - \left( \frac{\beta + 2\gamma e^{n_\lambda(x)}}{D} \right) Z = - \frac{1}{D} \frac{d^2 n_\lambda(x)}{dx^2} + \frac{2\pi\sigma}{D} \left( \frac{\gamma n_\lambda(x)}{\gamma + 2\pi\sigma D} \right)^2 \quad (C12)$$

where we have replaced  $\partial n_{\lambda}(x)/\partial D$  by  $Z$ . Eq. (C12) can be solved by straightforward numerical methods<sup>1</sup> to obtain the required derivative. Eq. (C11) can then be integrated numerically to obtain a value for  $\partial I_p^{\lambda}/\partial D$ , necessary in the least squares formalism.

This same procedure is obviously applicable to other parameters that must be varied in executing the least squares fit. Details of the least squares formalism can be found in reference 2.

REFERENCES

1. H. B. Keller, Numerical Methods for Two-Point Boundary-Value Problems (Blaisdell Publishing Co., Massachusetts, 1968) pp. 21-27.
2. N. Arley and K. Rander Buch, Introduction to the Theory of Probability and Statistics (John Wiley and Sons, Interscience, New York, 1950).
3. R. M. Noyes, "Effects of Diffusion Rates on Chemical Kinetics" in Progress in Reaction Kinetics, G. Porter, Ed. (Pergamon Press, New York, 1961) Vol. 1.



## APPENDIX D

## PROGRAM LISTINGS

Program listings of a data fitting package used to analyze optical emission decay curves in the time domain from 1 msec to roughly 1 sec are included in this Appendix. Provision is made in this package for least squares fitting any of the five most commonly occurring kinetic decay schemes to the experimental data. The program can be modified very simply to cover any other time interval or decay scheme of interest. Also to be found in this Appendix is a listing of a program for extracting a first order rate constant from experimental data when the time required to switch off the excitation source is comparable to the lifetime (the reciprocal of the first order decay constant) of the emission under investigation. For convenience in visually judging the quality of the fit, the output from these programs includes a plot of the experimental data points with the least squares fitted curve superimposed.

Specific instructions for the use of these programs, including a list of required input data cards, can be found at the beginning of the appropriate program or subroutine. Details of the numerical methods upon which the programs are based have been discussed in Appendix C.

---

LEAST SQUARES DATA FITTING PACKAGE

---

THIS PACKAGE IS COMPOSED OF A CONTROL PROGRAM "SOL" AND FIVE SUB-ROUTINES--"ADONIS" FOR FIRST ORDER KINETICS\*\* "AMOR" FOR SECOND ORDER KINETICS\*\* "APOLLO" FOR THE SUM OF TWO FIRST ORDER DECAYS\*\* "EROS" FOR COMBINED FIRST AND SECOND ORDER KINETICS USING THE FIRST ORDER PART AS PROBE\*\* "HERMES" FOR COMBINED FIRST AND SECOND ORDER KINETICS USING THE SECOND ORDER PART AS PROBE. A SUBROUTINE "ICARUS" PROVIDES ONE OF TWO WEIGHT MATRICES FOR USE WITH THE DATA FITTING SUBROUTINES. INSTRUCTIONS FOR THE USE OF THIS PACKAGE, INCLUDING THE REQUIRED INPUT DATA CARDS, CAN BE FOUND IN THE PROGRAM LISTINGS WHICH FOLLOW.

```

*****
E. B. FRIESTLEY MAY 10, 1968
THIS PROGRAM INITIALIZES KINETIC DATA, MAKING IT READY FOR
TREATMENT IN THE LEAST SQUARES FITTING SUBROUTINES. IN ADDITION,
INPUT/OUTPUT IS HANDLED BY THIS MAIN PROGRAM.
THE MAXIMUM ALLOWABLE SIZE FOR THE FINAL "DATA" ARRAY IS 1450.
INPUT TO THE DATA INITIALIZATION SECTION OF THE PROGRAM CAN
CONSIST OF UP TO FOUR SETS OF DATA EACH CONTAINING 512 NUMBERS.
USING SUBROUTINES "DTAFIT", EXPONENTIAL, DOUBLE EXPONENTIAL,
SECOND ORDER, AND FIRST AND SECOND ORDER COMBINED KINETICS CAN
BE LEAST SQUARES FIT TO EXPERIMENTAL DATA POINTS.
THE NUMBER OF PARAMETERS IN THE THEORY CANNOT EXCEED FOUR.
THE PROGRAM USES NEWTONS METHOD OF LINEARIZATION DESCRIBED IN
ARLEY AND EUCH, "INTRODUCTION TO THE THEORY OF PROBABILITY AND
STATISTICS" PP181-210.
*****
*****
REQUIRED INPUT DATA CARDS
-----
*****
1. DLABEL,ICTOA,IDCA,LDCA,TINCRA (FORMAT STATEMENT EFN 2)
2. JCENO,HMSG,NDS (FORMAT STATEMENT EFN 11)
3. IDTAFT,IPLLOT,DD (FORMAT STATEMENT EFN 17)
4. 64 DATA CARDS - "ADATA" (FORMAT STATEMENT EFN 24)
5. A DLABEL,ICTO,IDC,LDCA,TINCRA CARD, FOLLOWED BY 64 DATA CARDS FOR
EACH BLOCK OF DATA TO BE READ IN (FORMAT STATEMENT EFN, S 38,
75,112)
6. A CARD WITH ESTIMATED VALUES OF THE PARAMETERS IN THE THEORY
(SEE THE APPROPRIATE SUBROUTINE "DTAFIT")
7. THE LAST DATA CARD MUST BE AN "EDTA" CARD
*****
*****
*****
DEFINITIONS
-----
*****
A-,B-,C-,DDATA =TEMPORARY STORAGE FOR BLOCKS OF 512 DATA
POINTS
CALCI =THE CALCULATED INTENSITIES
DATA =STORAGE LOCATION OF EXPERIMENTAL POINTS
DD =A MESSAGE TO BE PRINTED ON THE PLOT
DEV =CALCULATED INTENSITIES - DATA POINTS
DLABEL =A DATA IDENTIFICATION LABEL
HMSG =AN IDENTIFICATION MESSAGE, 52 COLUMNS
ICTO =THE CHANNEL FOR T=0 (A,B,C,D REFER TO THE
VARIOUS BLOCKS OF DATA TO BE PROCESSED)
IDC =THE CHANNEL FOR THE FIRST DATA POINT (A,B,
C,D REFER TO THE VARIOUS BLOCKS OF DATA
TO BE PROCESSED)
IDTAFT =A SIGNAL FOR THE TYPE OF KINETIC SCHEME
USED IN THE FITTING SUBROUTINE AS FOLLOWS-
1 SIGNIFIES FIRST ORDER KINETICS
2 SIGNIFIES SECOND ORDER KINETICS
3 SIGNIFIES THE SUM OF TWO FIRST ORDER
DECAY PROCESSES
4 SIGNIFIES COMBINED FIRST AND SECOND
ORDER KINETICS USING THE FIRST ORDER

```

PROGRAM SOL FRAME 2

```

C                                     PART AS THE EXPERIMENTAL PROBE
C                                     5 SIGNIFIES COMBINED FIRST AND SECOND
C                                     ORDER KINETICS USING THE SECOND ORDER
C                                     PART AS THE EXPERIMENTAL PROBE
C      IPLOT                          =A SIGNAL FOR PLOT OR NO PLOT AS FOLLOWS-
C                                     1 SIGNIFIES PLOT
C                                     2 SIGNIFIES NO PLOT
C      JCBNO                          =JOB NUMBER, 12 COLUMNS
C      JTEST                          =AN ERROR CHECK INDEX REGISTER SET IN
C                                     SUBROUTINE "DTAFIT"
C      LDC                            =THE CHANNEL FOR THE LAST DATA POINT (A,B,
C                                     C,D REFER TO THE VARIOUS BLOCKS OF DATA
C                                     TO BE PROCESSED)
C      NDS                            =THE NUMBER OF DATA BLOCKS TO BE PROCESSED
C      STNDEV                         =THE STANDARD DEVIATIONS OF THE PARAMETERS
C      T                              =A VECTOR CONTAINING THE TIME
C      TI                             =THE TIME OF THE FIRST DATA POINT
C      TINCX                          =THE DWELL TIME PER CHANNEL ON THE ND180
C                                     (A,B,C,D REFER TO THE VARIOUS BLOCKS OF
C                                     DATA TO BE PROCESSED)
C      TL                             =THE TIME OF THE LAST DATA POINT
C      *****
C      *****
C      *****
C      PROGRAM INITIALIZATION
C      -----
C      *****
C      DIMENSION DATA(2048),ADATA(512),BDATA(512),CDATA(512),DDATA(512)
C      DIMENSION T(1450),CALCI(1450),DEV(1450),TITLE1(3),TITLE2(9)
C      DIMENSION STNDEV(4),ADATE(2),JCBNO(3),HMSG(13),DD(3),DLABL(3)
C      EQUIVALENCE (ADATA,DATA(1)),(BDATA,DATA(513))
C      EQUIVALENCE (CDATA,DATA(1025)),(DDATA,DATA(1537))
C      COMMON/COMFLT/ITFLT,XFLT,YFLT
C      COMMON/COMFLO/ITFLO,XFLO,YFLO
C      DATA ENDD/4HEDTA/
C      DATA TITLE1/11HTIME (MSEC)/
C      DATA TITLE2/36HEMISSION INTENSITY (ARBITRARY UNITS)/
C      CALL DATE(ADATE)
C      1 READ(5,2) (DLABL(I),I=1,3),ICTCA,IDCA,LDCA,TINCRA
C      2 FORMAT (3A4,2X,I2,2X,2(I3,2X),F5.1)
C      *****
C      *****
C      *****
C      CLEAN UP AND QUIT
C      -----
C      *****
C      IF(DLABL(1)-ENDD) 10,8,10
C      8 WRITE(6,9)
C      9 FORMAT (25H1END OF INPUT ENCOUNTERED/11HEND OUTPUT)
C      STOP
C      *****
C      PROCEED IF DATA LABEL DOES NOT EQUAL "EDTA".
C      *****
C      10 READ(5,11) (JCBNO(I),I=1,3), (HMSG(J),J=1,13),NDS
C      11 FORMAT (3A4,2X,13A4,2X,I1)
C      WRITE(6,13) (JCBNO(I),I=1,3), (ADATE(J),J=1,2), (HMSG(K),K=1,13)
C      13 FORMAT (1H1/1H0/1H0/1H0,5X,7HJCBNO= ,3A4,10X,6HDATE= ,2A4/1H0,5X,
C      11HIDENTIFICATION= ,13A4)

```

PROGRAM SOL FRAME 3

```

      IF(NDS) 15,15,16
15  GO TO 2000
16  READ(5,17) IDTAFT,IFLOT,(DD(I),I=1,3)
17  FORMAT (I1,2X,I1,2X,2A4,I1)
      IF(IDTAFT) 2080,2080,18
18  IF(IFLOT) 2090,2090,22
22  WRITE(6,23) (DLABL(I),I=1,3),ICTOA,IDCA,LDCA,TINCRA
23  FORMAT (1H1/1HG/1HG/6HDATA ,3A4,21H ENCOUNTERED IN INPUT/25H0THE
1INPUT VALUES ARE.../1HG,2X,7HICTOA= ,I2,2X,6HIDCA= ,I3,2X,6HLDCA=
2 ,I3,2X,8HTINCRA= ,F8.3/36H0PROCEEDING WITH BASELINE ADJUSTMENT)
C      *****
C      *****
C      *****
C      DATA INITIALIZATION SECTION
C      -----
C      *****
C      *****
C      READ IN OF DATA BEGINS AT THIS POINT.
C      DEPENDING ON THE VALUE OF NDS (NUMBER OF DATA SETS OF 512 POINTS),
C      CONTROL PASSES SUCCESSIVELY TO INITIALIZATION OF THE VARIOUS DATA
C      BLOCKS. NDS CAN TAKE ON VALUES 1, 2, 3, OR 4.
C      IN THE INITIALIZATION OF THE DATA, THE BASELINE IS SUBTRACTED OFF,
C      THE DATA BLOCKS ARE SCALED TO EACH OTHER AND THE DATA IS
C      TRANSFERRED TO LOCATION "DATA" READY FOR FURTHER CALCULATIONS.
C      *****
      JF=-7
      JL=0
      DO 25 K=1,64
      JF=JF+8
      JL=JL+8
      READ(5,24) (ADATA(J),J=JF,JL)
      FORMAT (8(F10.1))
24  CONTINUE
C      *****
C      DATA BLOCK "ADATA" BASELINE ADJUSTMENT FOLLOWS BELOW.
C      *****
      MA=LDCA-IDCA+1
      BSUMA=0.0
      DO 26 J=9,32
      BSUMA=BSUMA+ADATA(J)
26  CONTINUE
      ABSLNE=BSUMA/24.0
      DO 28 J=1,512
      ADATA(J)=ADATA(J)-ABSLNE
28  CONTINUE
      GO TO (30,34,34,34),NDS
C      *****
C      INITIAL STORAGE OF "ADATA" IN "DATA" AND TRANSFER TO
C      THE FITTING SUBROUTINE IF NDS=1.
C      *****
30  DO 32 K=1,MA
      MT=K
      KS=IDCA+K-1
      DATA(MT)=ADATA(KS)
      T(MT)=FLOAT(KS-ICTOA)*TINCRA
32  CONTINUE
      GO TO 137
34  READ(5,35) (DLABL(I),I=1,3),ICTOB,IDCB,LDCB,TINCRB
35  FORMAT (3A4,2X,I2,2X,2(I3,2X),F5.1)

```

PROGRAM SOL FRAME 4

```

WRITE(6,36) (CLABL(I),I=1,3),ICTCB,IDCB,LDCB,TINCRB
36  FORMAT (1H1/1H0/1H0/6H0DATA ,3A4,21H ENCOUNTERED IN INPUT/25H0THE
1INPUT VALUES ARE.../1H0,2X,7HICTCB= ,12,2X,6HIDCB= ,13,2X,6HLDCB=
2 ,13,2X,8HTINCRB= ,F8.3/63H0PROCEEDING WITH BASELINE ADJUSTMENT AN
3D SCALING TO "ADATA"....)
JF=-7
JL=0
DO 40 K=1,64
JF=JF+8
JL=JL+8
READ(5,38) (BDATA(J),J=JF,JL)
38  FORMAT (8(F10.1))
40  CONTINUE
C          *****
C  DATA BLOCK "BDATA" BASELINE ADJUSTMENT FOLLOWS BELOW.
C          *****
ME=LDCB-IDCB+1
BSUMB=0.0
DO 42 J=9,32
BSUMB=BSUMB+BDATA(J)
42  CONTINUE
BESLNE=BSUMB/24.0
DO 44 J=1,512
BDATA(J)=BDATA(J)-BESLNE
44  CONTINUE
C          *****
C  SCALING OF DATA BLOCKS "ADATA" AND "BDATA" FOLLOWS BELOW.
C          *****
SUMR=0.0
SUMC=0.0
IIDCB=IDCB
46  CIA=FLOAT(IIDCB-ICTCB)*(TINCRB/TINCRA)+FLOAT(ICTCA)
IA=IFIX(CIA)
IF (CIA-FLOAT(IA)) 48,52,50
48  GO TO 2010
50  IIDCB=IIDCB+1
GO TO 46
52  IF (IA-LDCA) 54,54,56
54  SUMR=SUMR+ADATA(IA)/BDATA(IIDCB)
SUMC=SUMC+1.0
GO TO 50
56  AVRAT=SUMR/SUMC
DO 58 J=1,512
BDATA(J)=BDATA(J)*AVRAT
58  CONTINUE
C          *****
C  FINAL STORAGE OF "ADATA" IN "DATA" AFTER BASELINE ADJUSTMENT
C  AND SCALING OF "BDATA".
C          *****
DO 60 K=1,MA
MT=K
KS=IDCA+K-1
DATA(MT)=ADATA(KS)
T(MT)=FLOAT(KS-ICTCA)*TINCRA
60  CONTINUE
GO TO (62,66,70,70),NDS
62  GO TO 2020
C          *****
C  INITIAL STORAGE OF "BDATA" IN "DATA" AND TRANSFER TO
C  THE FITTING SUBROUTINE IF NDS=2.

```

PROGRAM SOL FRAME 5

```

C *****
66 DO 68 K=1,MB
   MT=MA+K
   JS=IDCB+K-1
   DATA(MT)=BDATA(JS)
   T(MT)=FLOAT(JS-ICTOB)*TINCRB
68 CONTINUE
   GO TO 137
70 READ(5,71) (DLABL(I),I=1,3),ICTOC,IDCC,LDCC,TINCRB
71 FORMAT(3A4,2X,I2,2X,2(I3,2X),F5.1)
   WRITE(6,73) (DLABL(I),I=1,3),ICTOC,IDCC,LDCC,TINCRB
73 FORMAT(1H1/1HG/1HG/6HDDATA,3A4,21H ENCOUNTERED IN INPUT/25HDTHE
1INFUT VALUES ARE.../1HG,2X,7HICTOC=,I2,2X,6HIDCC=,I3,2X,6HLDCC=
2,I3,2X,8HTINCRB=,F8.3/63HGFROCEEDING WITH BASELINE ADJUSTMENT AN
3D SCALING TO "BDATA".....)
   JF=-7
   JL=0
   DO 77 K=1,64
     JF=JF+8
     JL=JL+8
     READ(5,75) (CDATA(J),J=JF,JL)
75 FORMAT(8(F10.1))
77 CONTINUE
C *****
C DATA BLOCK "CDATA" BASELINE ADJUSTMENT FOLLOWS BELOW.
C *****
   MC=LDCC-IDCC+1
   BSUMC=0.0
   DO 80 J=9,32
     BSUMC=BSUMC+CDATA(J)
80 CONTINUE
   CBSLNE=BSUMC/24.0
   DO 82 J=1,512
     CDATA(J)=CDATA(J)-CBSLNE
82 CONTINUE
C *****
C SCALING OF DATA BLOCKS "BDATA" AND "CDATA" FOLLOWS BELOW.
C *****
   SUMR=0.0
   SUMC=0.0
   IIDCC=IDCC
84 CIB=FLOAT(IIDCC-ICTOC)*(TINCRB/TINCRB)+FLOAT(ICTOB)
   IB=IFIX(CIB)
   IF (CIB-FLOAT(IB)) 86,90,88
86 GO TO 2030
88 IIDCC=IIDCC+1
   GO TO 84
90 IF (IB-LDCB) 92,92,94
92 SUMR=SUMR+BDATA(IB)/CDATA(IIDCC)
   SUMC=SUMC+1.0
   GO TO 88
94 AVRAT=SUMR/SUMC
   DO 96 J=1,512
     CDATA(J)=CDATA(J)*AVRAT
96 CONTINUE
C *****
C FINAL STORAGE OF "BDATA" IN "DATA" AFTER BASELINE
C ADJUSTMENT AND SCALING OF "CDATA".
C *****
   DO 98 K=1,MB

```

PROGRAM SOL FRAME 6

```

      MT=MA+K
      JS=IDCB+K-1
      DATA(MT)=BDATA(JS)
      T(MT)=FLOAT(JS-ICTCB)*TINCRCB
98    CONTINUE
      GO TO (100,100,102,106),NDS
100   GO TO 204G
C
C      *****
C      INITIAL STORAGE OF "CDATA" IN "DATA" AND TRANSFER
C      TO THE FITTING SUBROUTINE IF NDS=3.
C      *****
102   DO 104 K=1,MC
      MT=MA+MB+K
      JS=IDCC+K-1
      DATA(MT)=CDATA(JS)
      T(MT)=FLOAT(JS-ICTCC)*TINCRC
104   CONTINUE
      GO TO 137
106   READ(5,107) (DLABL(I),I=1,3),ICTCD,IDCD,LDCD,TINCRC
107   FORMAT (3A4,2X,I2,2X,2(I3,2X),F5.1)
      WRITE(6,109) (DLABL(I),I=1,3),ICTCD,IDCD,LDCD,TINCRC
109   FORMAT (1H1/1HG/1HG/6HGDATA ,3A4,21H ENCOUNTERED IN INPUT/25HGTHE
1INPUT VALUES ARE..../1HG,2X,7HICTCD= ,I2,2X,6HIDCD= ,I3,2X,6HLDCC=
2 ,I3,2X,8HTINCRC= ,F8.3/63HGFROCEEDING WITH BASELINE ADJUSTMENT AN
3D SCALING TO "CDATA"....)
      JF=-7
      JL=0
      DO 115 K=1,64
      JF=JF+8
      JL=JL+8
      READ(5,112) (DDATA(J),J=JF,JL)
112   FORMAT (8(F10.1))
115   CONTINUE
C
C      *****
C      DATA BLOCK "DDATA" BASELINE ADJUSTMENT FOLLOWS BELOW.
C      *****
      MD=LDCD-IDCD+1
      BSUMD=0.0
      DO 116 J=9,32
      BSUMD=BSUMD+DDATA(J)
116   CONTINUE
      DBSLNE=BSUMD/24.0
      DO 118 J=1,512
      DDATA(J)=DDATA(J)-DBSLNE
118   CONTINUE
C
C      *****
C      SCALING OF DATA BLOCKS. "CDATA" AND "DDATA" FOLLOWS BELOW.
C      *****
      SUMR=0.0
      SUMC=0.0
      IIDCD=IDCD
120   CIC=FLOAT(IIDCD-ICTCD)*(TINCRC/TINCRC)+FLOAT(ICTCD)
      IC=IFIX(CIC)
      IF (CIC-FLOAT(IC)) 122,126,124
122   GO TO 205G
124   IIDCD=IIDCD+1
      GO TO 120
126   IF (IC-LDCC) 128,128,130
128   SUMR=SUMR+CDATA(IC)/CDATA(IIDCD)
      SUMC=SUMC+1.0

```



PROGRAM SOL FRAME 7

```

GO TO 124
130 AVRAT=SUMR/SUMC
DO 131 J=1,512
  DDATA(J)=DDATA(J)*AVRAT
131 CONTINUE
C *****
C FINAL STORAGE OF "CDATA" IN "DATA" AFTER BASELINE
C ADJUSTMENT AND SCALING OF "DDATA".
C *****
DO 132 K=1,MC
  MT=MA+MB+K
  JS=IDCC+K-1
  DATA(MT)=CDATA(JS)
  T(MT)=FLOAT(JS-ICTOC)*TINCRC
132 CONTINUE
C *****
C FINAL STORAGE OF "DDATA" IN "DATA" AFTER BASELINE ADJUSTMENT
C AND SCALING TO "CDATA".
C *****
DO 133 K=1,MC
  MT=MA+MB+MC+K
  JS=IDCD+K-1
  DATA(MT)=DDATA(JS)
  T(MT)=FLOAT(JS-ICTOD)*TINCRC
133 CONTINUE
IF (145G-MT) 134,135,135
134 NDF=MT-145G
GO TO 2G7G
135 GO TO (136,136,136,137),NDS
136 GO TO 2G6G
137 GO TO (14G,142,144,146,148),IDTAFT
C *****
C *****
C *****
C CALL TO FITTING SUBROUTINE
C -----
C *****
C *****
C FITTING SUBROUTINE "DTAFIT" CALLED AT THIS POINT
C DATA LEAST SQUARES FIT TO FIRST, SECOND, DOUBLE EXPONENTIAL,
C OR COMBINED FIRST AND SECOND ORDER KINETIC SCHEME
C *****
140 CALL DTAFIT (DK,PREXP,STNDEV,SIGMA,ITER,T,DATA,CALCI,DEV,MA,MB,MC,
  1MD,MT,NDS,TINCRA,TINCRB,TINCRC,TINCRD,RMSDV,JTEST)
GO TO (15G,1),JTEST
142 CALL DTAFIT (GAMMA,XINOT,STNDEV,SIGMA,ITER,T,DATA,CALCI,DEV,MA,MB,
  1MC,MD,MT,NDS,TINCRA,TINCRB,TINCRC,TINCRD,RMSDV,JTEST)
GO TO (15G,1),JTEST
144 CALL DTAFIT (DK1,DK2,PREXP1,PREXP2,STNDEV,SIGMA,ITER,T,DATA,CALCI,
  1 DEV,MA,MB,MC,MD,MT,NDS,TINCRA,TINCRB,TINCRC,TINCRD,RMSDV,JTEST)
GO TO (15G,1),JTEST
146 CALL DTAFIT (DK,GAMMA,XINOT,STNDEV,SIGMA,ITER,T,DATA,CALCI,DEV,MA,
  1MB,MC,MD,MT,NDS,TINCRA,TINCRB,TINCRC,TINCRD,RMSDV,JTEST)
GO TO (15G,1),JTEST
148 CALL DTAFIT (DK,GAMMA,XINOT,STNDEV,SIGMA,ITER,T,DATA,CALCI,DEV,MA,
  1MB,MC,MD,MT,NDS,TINCRA,TINCRB,TINCRC,TINCRD,RMSDV,JTEST)
GO TO (15G,1),JTEST
C *****
C *****

```

PROGRAM SOL FRAME 8

```

C *****
C *****
C PRINTOUT SECTION
C -----
C *****
150 WRITE(6,151) ITER
151 FORMAT (1H0,2X,6HITER= ,I3/1H0)
    WRITE(6,153)
153 FORMAT (78H0THE BEST ESTIMATES OF THE PARAMETERS, WITH THEIR STAND
    IARD DEVIATIONS, ARE.../1H0,20X,9HPARAMETER,32X,
    218HSTANDARD DEVIATION/1H0)
156 GO TO (157,159,162,166,170),IDTAFT
157 WRITE(6,158) DK,STNDEV(1),PREXP,STNDEV(2)
158 FORMAT (1H ,15X,4HDK= ,1FE16.8,26X,1FE16.8/1H ,12X,7HPREXP= ,
    11FE16.8,26X,1FE16.8)
    GO TO 174
159 WRITE(6,160) GAMMA,STNDEV(1),XINOT,STNDEV(2)
160 FORMAT (1H ,12X,7HGAMMA= ,1FE16.8,26X,1FE16.8/1H ,12X,7HXINOT= ,
    11FE16.8,26X,1FE16.8)
    GO TO 174
162 WRITE(6,163) DK1,STNDEV(1),DK2,STNDEV(2),PREXP1,STNDEV(3),PREXP2,
    1STNDEV(4)
163 FORMAT (1H ,14X,5HDK1= ,1FE16.8,26X,1FE16.8/1H ,14X,5HDK2= ,
    11FE16.8,26X,1FE16.8/1H ,11X,8HPREXP1= ,1FE16.8,26X,1FE16.8/1H ,
    211X,8HPREXP2= ,1FE16.8,26X,1FE16.8)
    GO TO 174
166 WRITE(6,167) DK,STNDEV(1),GAMMA,STNDEV(2),XINOT,STNDEV(3)
167 FORMAT (1H ,15X,4HDK= ,1FE16.8,26X,1FE16.8/1H ,12X,7HGAMMA= ,
    11FE16.8,26X,1FE16.8/1H ,12X,7HXINOT= ,1FE16.8,26X,1FE16.8)
    GO TO 174
170 WRITE(6,171) DK,STNDEV(1),GAMMA,STNDEV(2),XINOT,STNDEV(3)
171 FORMAT (1H ,15X,4HDK= ,1FE16.8,26X,1FE16.8/1H ,12X,7HGAMMA= ,
    11FE16.8,26X,1FE16.8/1H ,12X,7HXINOT= ,1FE16.8,26X,1FE16.8)
174 WRITE(6,175) SIGMA,RMSDV
175 FORMAT (1H0,38X,7HSIGMA= ,F12.5/1H ,38X,7HRMSDV= ,F12.5)
    WRITE(6,176)
176 FORMAT (1H1/1H0/1H0/1H0,9X,4HTIME,15X,8HEXP.INT.,30X,9HCALC.INT.,
    116X,9HDEVIATION/1H )
    DO 178 J=1,MT
    WRITE(6,177) T(J),DATA(J),CALCI(J),DEV(J)
177 FORMAT (1H ,6X,F8.3,10X,1FE15.8,23X,1FE15.8,11X,1FE15.8)
178 CONTINUE
179 GO TO (180,1),IFLOT
C *****
C *****
C *****
C *****
C PLOTTING ROUTINE
C -----
C *****
C *****
C LENGTH OF THE XAXIS IS SET, DEPENDING ON THE VALUE OF NDS.
C *****
180 CALL SYSXMX(70.0)
    ITFLT=1
    ITFLO=1
    YFLT=10.0
    YFLO=10.0
    GO TO (181,182,183,184),NDS
181 XFLT=15.0

```

PROGRAM SOL FRAME 9

```

      XFLO=15.0
      GO TO 185
182  XFLO=32.0
      XFLO=32.0
      GO TO 185
183  XFLO=48.0
      XFLO=48.0
      GO TO 185
184  XFLO=64.0
      XFLO=64.0
C
C          *****
C  SEARCH TO SET MIN AND MAX VALUES OF ORDINATE FOR PLOT
C  SUBROUTINES "XYFLT" AND "XYPLOT".
C          *****
185  YMIN=100000.0
      YMAX=1.0
      DO 200 K=1,MT
      IF (DATA(K)-YMIN) 186,186,187
186  YMIN=DATA(K)
187  IF (CALCI(K)-YMIN) 188,188,190
188  YMIN=CALCI(K)
190  IF (DATA(K)-YMAX) 194,192,192
192  YMAX=DATA(K)
194  IF (CALCI(K)-YMAX) 198,196,196
196  YMAX=CALCI(K)
198  CONTINUE
200  CONTINUE
C
C          *****
C  CALL ON "LABEL"--LABELLING OF THE X AND Y AXES OF THE PLOT PAPER.
C          *****
      NINTVL=IFIX(XFLT)
      CALL LABEL(G,G,G,G,G,T(MT),XFLT,NINTVL,TITLE1,11,G)
      CALL LABEL(G,G,G,G,G,YMIN,YMAX,10,G,10,TITLE2,36,1)
C
C          *****
C  CALL ON "XYFLT"--CONTENTS OF ARRAY "DATA" POINT PLOTTED.
C          *****
      CALL XYFLT (MT,T,DATA,G,G,T(MT),YMIN,YMAX,DD,G,3)
C
C          *****
C  GENERATION OF TEMPORARY TIME AND CALCULATED INTENSITY
C  ARRAYS FOR LINE PLOTTING
C  THE TIME AXIS IS INCREMENTED UNIFORMLY.
C          *****
      GO TO(300,215,215,215),NDS
215  TI=FLOAT(IDCA-ICTOA)*TINCRA
      DO 217 K=1,MT
      T(K)=G.0
      CALCI(K)=G.0
217  CONTINUE
      GO TO(2110,220,225,230),NDS
220  TL=FLOAT(LDCB-ICTOB)*TINCRB
      GO TO 235
225  TL=FLOAT(LDCC-ICTOC)*TINCRC
      GO TO 235
230  TL=FLOAT(LDCD-ICTOD)*TINCRD
235  DUMINT=(TL-TI)/FLOAT(MT)
      GO TO(240,250,260,270,280),IDTAFT
240  DO 245 K=1,MT
      T(K)=TI+FLOAT(K-1)*DUMINT
      CALCI(K)=PREXP*EXP(-T(K)/DK)
245  CONTINUE

```

PROGRAM SOL FRAME 10

```

      GO TO 300
250 DO 255 K=1,MT
      T(K)=TI+FLOAT(K-1)*DUMINT
      CALCI(K)=XINOT/(1.0+XINOT*GAMMA*T(K))
255 CONTINUE
      GO TO 300
260 DO 265 K=1,MT
      T(K)=TI+FLOAT(K-1)*DUMINT
      CALCI(K)=FREXF1*EXP(-T(K)/DK1)+FREXF2*EXP(-T(K)/DK2)
265 CONTINUE
      GO TO 300
270 DO 275 K=1,MT
      T(K)=TI+FLOAT(K-1)*DUMINT
      CALCI(K)=(XINOT/(EXP(T(K)/DK)+2.0*GAMMA*DK*XINOT*(SINH(T(K)/
1(2.0*DK)))**2+GAMMA*DK*XINOT*SINH(T(K)/DK)))**2
275 CONTINUE
      GO TO 300
280 DO 285 K=1,MT
      T(K)=TI+FLOAT(K-1)*DUMINT
      CALCI(K)=(XINOT/(EXP(T(K)/DK)+2.0*GAMMA*DK*XINOT*(SINH(T(K)/
1(2.0*DK)))**2+GAMMA*DK*XINOT*SINH(T(K)/DK)))**2
285 CONTINUE
C          *****
C      CALL ON "XYPLOT"---CONTENTS OF ARRAY "CALCI" LINE PLOTTED ON SAME
C      PAPER AS POINT PLOT OF EXPERIMENTALLY DETERMINED "DATA" POINTS.
C          *****
300 CALL XYPLOT(MT,T,CALCI,G,G,T(MT),YMIN,YMAX,DD,1)
310 GO TO 1
C      *****
C      *****
C      *****
C          DIAGNOSTICS
C      -----
C      *****
2000 WRITE(6,2001)
2001 FORMAT (18HERROR MESSAGE.../52HUNDS NEGATIVE OR ZERO. PROCEEDIN
1G WITH THE NEXT JOB)
      GO TO 3000
2010 WRITE(6,2011)
2011 FORMAT (45HUSCALING PROBLEMS BETWEEN "ADATA" AND "BDATA"/28HG OVER
1LAP REGION ILL-DEFINED/29H PROCEEDING WITH THE NEXT JOB)
      GO TO 3000
2020 WRITE(6,2021)
2021 FORMAT (14HERROR MESSAGE/55HUNDS=1, EXECUTION INCORRECTLY IN "BDA
1TA" INITIALIZATION/29H PROCEEDING WITH THE NEXT JOB)
      GO TO 3000
2030 WRITE(6,2031)
2031 FORMAT (45HUSCALING PROBLEMS BETWEEN "BDATA" AND "CDATA"/28HG OVER
1LAP REGION ILL-DEFINED/29H PROCEEDING WITH THE NEXT JOB)
      GO TO 3000
2040 WRITE(6,2041)
2041 FORMAT (14HERROR MESSAGE/60HUNDS=1 OR 2, EXECUTION INCORRECTLY IN
1"CDATA" INITIALIZATION/29H PROCEEDING WITH THE NEXT JOB)
      GO TO 3000
2050 WRITE(6,2051)
2051 FORMAT (45HUSCALING PROBLEMS BETWEEN "CDATA" AND "DDATA"/28HG OVER
1LAP REGION ILL-DEFINED/29H PROCEEDING WITH THE NEXT JOB)
      GO TO 3000
2060 WRITE(6,2061)

```

PROGRAM SOL FRAME 11

```

2061 FORMAT (14HERROR MESSAGE/64HNDS=1, 2, OR 3, EXECUTION INCORRECT
1Y IN "DDATA" INITIALIZATION/29H PROCEEDING WITH THE NEXT JOB)
GO TO 3000
2070 WRITE(6,2071) NDP
2071 FORMAT (14HERROR MESSAGE/81HNUMBER OF DATA POINTS AFTER BASELINE
1 CORRECTION, SCALING AND COMPACTING, EXCEEDS/69HTHE MAXIMUM ALLOW
2ABLE STORAGE (1450 DATA POINTS) IN "DATA" ARRAY BY ,I4/29H PROCEED
3ING WITH THE NEXT JOB)
GO TO 3000
2080 WRITE(6,2081)
2081 FORMAT (18HERROR MESSAGE..../55HIDTAFT NEGATIVE OR ZERO. PROCEE
1DING WITH THE NEXT JOB)
GO TO 3000
2090 WRITE(6,2091)
2091 FORMAT (18HERROR MESSAGE..../54HDIPLT NEGATIVE OR ZERO. PROCEED
1ING WITH THE NEXT JOB)
GO TO 3000
2110 WRITE(6,2111)
2111 FORMAT (18HERROR MESSAGE..../82HMISTAKE IN GENERATION OF TEMPORA
1RY TIME AND CALCULATED INTENSITY ARRAYS FOR NDS=1/29H PROCEEDING W
2ITH THE NEXT JOB)
GO TO 3000
C *****
C *****
C *****
C *****
C INTERNAL ABEND
C -----
C *****
3000 GO TO 1
C *****
C *****
C *****
END

```

## SUBROUTINE ADONIS FRAME 1

```

C *****
C *****
C E. B. PRIESTLEY MAY 3, 1969
C THIS SUBROUTINE LEAST SQUARES FITS EXPERIMENTALLY DETERMINED DATA
C POINTS TO A SINGLE EXPONENTIAL DECAY. THE LEAST SQUARES THEORY IS
C THAT OUTLINED IN ARLEY AND BUCH "INTRODUCTION TO THE THEORY OF
C PROBABILITY AND STATISTICS" CHAPTER 12.
C *****
C *****
C          REQUIRED INPUT DATA CARDS.
C          -----
C *****
C 1. DK,PREXP,IWGHT (FORMAT STATEMENT EFN 20)
C *****
C *****
C *****
C          DEFINITIONS
C          -----
C *****
C CORR          =THE BEST CORRECTIONS TO THE PARAMETERS
C DK            =THE RECIPROCAL OF THE FIRST ORDER RATE
C              CONSTANT (THE LIFETIME OF THE STATE)
C ITER          =A COUNTER FOR THE NUMBER OF ITERATIONS
C IWGHT         =A SIGNAL FOR THE TYPE OF WEIGHT MATRIX TO
C              BE USED
C              1 SIGNIFIES THE UNIT WEIGHT MATRIX
C              2 SIGNIFIES "EQUAL-TIME-EQUAL-WEIGHT"
C              WEIGHT MATRIX
C JTEST         =AN ERROR CHECK INDEX REGISTER
C PREXP         =THE PRE-EXPONENTIAL FACTOR
C *****
C *****
C *****
C          PROGRAM INITIALIZATION
C          -----
C *****
C SUBROUTINE DTAFIT (DK,PREXP,STNDEV,SIGMA,ITER,T,DATA,CALCI,DEV,MA,
1MB,MC,MD,MT,NDS,TINCRA,TINCRB,TINCRC,TINCRD,RMSDV,JTEST)
C DIMENSION DATA(2048),P(1450),T(1450),CALCI(1450),DEV(1450)
C DIMENSION AMATRX(1450,2),BMATRX(2,2),BINV(2,2),DUMMY(2)
C DIMENSION CORR(2),STNDEV(2),BDBLPR(50,2)
C COMMON/BNDCCM/EL(50,2)
C DOUBLE PRECISION BDBLPR,EL
C ITER=1
C KOUNT=0
C READ(5,20) DK,PREXP,IWGHT
20  FORMAT (F5.1,2X,F8.1,2X,I1)
C WRITE(6,25) DK,PREXP
25  FORMAT (1H1/1H0/1H0/1H0/1H0/1H0/17X,38H EXPONENTIAL FITTING SUBROU
1TINE CALLED/72H0PROCEEDING WITH THE EXPONENTIAL FIT USING THE FOLL
20WING TRIAL ESTIMATES/22H0CF THE PARAMETERS..../1H0,2X,
34HDK= ,F8.1,15X,7HPREXP= ,F8.1)
C CALL WEIGHT (P,MA,MB,MC,MD,MT,TINCRA,TINCRB,TINCRC,TINCRD,NDS,
1IWGHT)
C GO TO (30,40),IWGHT
30  WRITE(6,35)
35  FORMAT (24H0UNIT WEIGHT MATRIX USED/1H0/1H0/1H0/1H0)

```

## SUBROUTINE ADONIS FRAME 2

```

      GO TO 50
40  WRITE(6,45)
45  FORMAT (45H0"EQUAL-TIME-EQUAL-WEIGHT" WEIGHT MATRIX USED/1HG/1HG/
      11HG/1HG)
C    *****
C    *****
C    *****
C    *****
C    MAIN SECTION OF THE PROGRAM
C    -----
C    *****
50  DO 90 I=1,MT
      CALCI(I)=PREXP*EXP(-T(I)/DK)
      AMATRX(I,1)=CALCI(I)*T(I)/(DK**2)
      AMATRX(I,2)=CALCI(I)/PREXP
      DEV(I)= CALCI(I)-DATA(I)
90  CONTINUE
      SQDEV=0.0
      RMSDEV=0.0
      DO 130 K=1,2
      DO 120 J=1,2
      BMATRX(K,J)=0.0
120  CONTINUE
130  CONTINUE
      DO 160 K=1,2
      DO 150 J=1,2
      DO 140 I=1,MT
      BMATRX(K,J)=BMATRX(K,J)+AMATRX(I,K)*F(I)*AMATRX(I,J)
140  CONTINUE
      BDBLFR(K,J)=BMATRX(K,J)
150  CONTINUE
160  CONTINUE
      CALL BNDINV(BDBLFR,2,DETERM,1.0E-08,ITEST)
      DO 180 J=1,2
      DO 170 K=1,2
      BINV(J,K)=BDBLFR(J,K)
170  CONTINUE
180  CONTINUE
      DO 190 K=1,2
      DUMMY(K)=0.0
      CORR(K)=0.0
190  CONTINUE
      DO 210 K=1,2
      DO 200 I=1,MT
      DUMMY(K)=DUMMY(K)+AMATRX(I,K)*F(I)*DEV(I)
200  CONTINUE
210  CONTINUE
      DO 260 I=1,2
      DO 250 K=1,2
      CORR(I)=CORR(I)-BINV(I,K)*DUMMY(K)
250  CONTINUE
260  CONTINUE
      DO 270 I=1,MT
      SQDEV=SQDEV+DEV(I)*DEV(I)*F(I)
      RMSDEV=RMSDEV+DEV(I)*DEV(I)
270  CONTINUE
      SIGMA=SQRT(SQDEV/FLCAT(MT-2))
      RMSDV=SQRT(RMSDEV/FLCAT(MT))
      DO 280 I=1,2
      STNDEV(I)=(SQRT(BINV(I,I)))*SIGMA

```

## SUBROUTINE ADONIS FRAME 3

```

280 CONTINUE
   IF (ABS(CORR(1)/STNDEV(1))-0.01) 290,320,320
290 IF (ABS(CORR(2)/STNDEV(2))-0.01) 310,320,320
310 KOUNT=KOUNT+1
   IF (KOUNT-10) 320,315,315
315 JTEST=1
   ITER=ITER+1
   GO TO 330
320 DK=DK+CORR(1)
   PREXF=PREXF+CORR(2)
   ITER=ITER+1
   IF (ITER.GE.60) GO TO 400
   GO TO 50
*****
*****
*****
*****
                        BEAT A HASTY RETREAT
                        -----
*****
330 RETURN
*****
*****
*****
*****
                        ERROR MESSAGES
                        -----
*****
400 WRITE(6,405)
405 FORMAT (35H1LOCIFING HAS EXCEEDED 60 ITERATIONS/29H PROCEEDING WITH
1 THE NEXT JOB)
   GO TO 3000
*****
*****
*****
                        SET ERROR CHECK INDEX REGISTER
                        -----
*****
3000 JTEST=2
   GO TO 330
*****
*****
*****
*****
END

```



SUBROUTINE AMOR FRAME 1

```

C *****
C *****
C E. B. PRIESTLEY MAY 6, 1969
C THIS SUBROUTINE LEAST SQUARES FITS EXPERIMENTALLY DETERMINED DATA
C POINTS TO A PURE SECOND ORDER DECAY. THE LEAST SQUARES THEORY IS
C THAT OUTLINED IN ARLEY AND BUCH "INTRODUCTION TO THE THEORY OF
C PROBABILITY AND STATISTICS" CHAPTER 12.
C *****
C *****
C *****
C REQUIRED INPUT DATA CARDS
C -----
C *****
C 1. GAMMA,XINOT,IWGT (FORMAT STATEMENT EFN 20)
C *****
C *****
C *****
C DEFINITIONS
C -----
C *****
C CORR =THE BEST CORRECTIONS TO THE PARAMETERS
C GAMMA =THE SECOND ORDER RATE CONSTANT
C ITER =A COUNTER FOR THE NUMBER OF ITERATIONS
C IWGT =A SIGNAL FOR THE TYPE OF WEIGHT MATRIX TO
C BE USED
C 1 SIGNIFIES THE UNIT WEIGHT MATRIX
C 2 SIGNIFIES "EQUAL-TIME-EQUAL-WEIGHT"
C WEIGHT MATRIX
C JTEST =AN ERROR CHECK INDEX REGISTER
C XINOT =THE EMISSION INTENSITY AT T=0
C *****
C *****
C *****
C PROGRAM INITIALIZATION
C -----
C *****
C SUBROUTINE DTAFIT (GAMMA,XINOT,STNDEV,SIGMA,ITER,T,DATA,CALCI,DEV,
1MA,MB,MC,MD,MT,NDS,TINCRA,TINCRB,TINCRC,TINCRD,RMSDV,JTEST)
C DIMENSION DATA(2048),P(1450),T(1450),CALCI(1450),DEV(1450)
C DIMENSION AMATRIX(1450,2),BMATRIX(2,2),BINV(2,2),DUMMY(2)
C DIMENSION CORR(2),STNDEV(2),BDBLPR(50,2)
C COMMON/BNDCCOM/EL(50,2)
C DOUBLE PRECISION BDBLPR,EL
C ITER=1
C KOUNT=0
C READ(5,20) GAMMA,XINOT,IWGT
20 FORMAT (F9.1,2X,F8.1,2X,I1)
C WRITE(6,25) GAMMA,XINOT
25 FORMAT (1H1/1H0/1H0/1H0/1H0/1H0/17X,39H SECOND ORDER FITTING SUBRO
1UTINE CALLED/73HUPROCEEDING WITH THE SECOND ORDER FIT USING THE FO
2LLOWING TRIAL ESTIMATES/22HOF THE PARAMETERS..../1H0,2X,
37HGAMMA= ,F9.7,15X,7HXINOT= ,F8.1)
C CALL WEIGHT (P,MA,MB,MC,MD,MT,TINCRA,TINCRB,TINCRC,TINCRD,NDS,
1IWGT)
C GO TO (30,40),IWGT
30 WRITE(6,35)
35 FORMAT (24HUNIT WEIGHT MATRIX USED/1H0/1H0/1H0/1H0)
C GO TO 50

```

SUBROUTINE AMOR FRAME 2

```

40  WRITE(6,45)
45  FORMAT (45H0"EQUAL-TIME-EQUAL-WEIGHT" WEIGHT MATRIX USED/1H0/1H0/
11H0/1H0)
C   *****
C   *****
C   *****
C   *****
C   MAIN SECTION OF THE PROGRAM
C   -----
C   *****
50  DO 90 I=1,MT
    DENOM=1.0+GAMMA*XINOT*T(I)
    CALCI(I)=XINOT/DENOM
    AMATRX(I,1)=1.0/DENOM**2
    AMATRX(I,2)=-T(I)*(XINOT/DENOM)**2
    DEV(I)= CALCI(I)-DATA(I)
90  CONTINUE
    SQDEV=0.0
    RMSDEV=0.0
    DO 130 K=1,2
    DO 120 J=1,2
    BMATRX(K,J)=0.0
120  CONTINUE
130  CONTINUE
    DO 160 K=1,2
    DO 150 J=1,2
    DO 140 I=1,MT
    BMATRX(K,J)=BMATRX(K,J)+AMATRX(I,K)*P(I)*AMATRX(I,J)
140  CONTINUE
    BDBLPR(K,J)=BMATRX(K,J)
150  CONTINUE
160  CONTINUE
    CALL BNDINV(BDBLPR,2,DETERM,1.0E-08,ITEST)
    DO 180 J=1,2
    DO 170 K=1,2
    BINV(J,K)=BDBLPR(J,K)
170  CONTINUE
180  CONTINUE
    DO 190 K=1,2
    DUMMY(K)=0.0
    CORR(K)=0.0
190  CONTINUE
    DO 210 K=1,2
    DO 200 I=1,MT
    DUMMY(K)=DUMMY(K)+AMATRX(I,K)*P(I)*DEV(I)
200  CONTINUE
210  CONTINUE
    DO 260 I=1,2
    DO 250 K=1,2
    CORR(I)=CORR(I)-BINV(I,K)*DUMMY(K)
250  CONTINUE
260  CONTINUE
    DO 270 I=1,MT
    SQDEV=SQDEV+DEV(I)*DEV(I)*P(I)
    RMSDEV=RMSDEV+DEV(I)*DEV(I)
270  CONTINUE
    SIGMA=SQRT(SQDEV/FLOAT(MT-2))
    RMSDEV=SQRT(RMSDEV/FLOAT(MT))
    DO 280 I=1,2
    STNDEV(I)=(SQRT(BINV(I,I)))*SIGMA

```

SUBROUTINE AMOR FRAME 3

```

280 CONTINUE
   IF (ABS(CORR(1)/STNDEV(1))-0.01) 290,320,320
290 IF (ABS(CORR(2)/STNDEV(2))-0.01) 310,320,320
310 KOUNT=KOUNT+1
   IF (KOUNT-10) 320,315,315
315 JTEST=1
   ITER=ITER+1
   GO TO 330
320 XINOT=XINGT+CORR(1)
   GAMMA=GAMMA+CORR(2)
   ITER=ITER+1
   IF (ITER.GE.60) GO TO 400
   GO TO 50
C *****
C *****
C *****
C *****
C BEAT A HASTY RETREAT
C -----
C *****
330 RETURN
C *****
C *****
C *****
C *****
C ERROR MESSAGES
C -----
C *****
400 WRITE(6,405)
405 FORMAT (35H1LOOPING HAS EXCEEDED 60 ITERATIONS/29H PROCEEDING WITH
1 THE NEXT JOB)
   GO TO 3000
C *****
C *****
C *****
C *****
C SET ERROR CHECK INDEX REGISTER
C -----
C *****
3000 JTEST=2
   GO TO 330
C *****
C *****
C *****
END

```

## SUBROUTINE AFCLLG FRAME 1

```

C *****
C *****
C E. B. PRIESTLEY MAY 5, 1969
C THIS SUBROUTINE LEAST SQUARES FITS EXPERIMENTALLY DETERMINED DATA
C POINTS TO THE SUM OF TWO FIRST ORDER DECAYS. THE LEAST SQUARES
C THEORY IS THAT OUTLINED IN ARLEY AND BUCH "INTRODUCTION TO THE
C THEORY OF PROBABILITY AND STATISTICS" CHAPTER 12.
C *****
C *****
C
C          REQUIRED INPUT DATA CARDS
C          -----
C
C *****
C 1. DK1,DK2,PREXP1,PREXP2,IWGHT (FORMAT STATEMENT EFN 20)
C *****
C *****
C *****
C
C          DEFINITIONS
C          -----
C
C *****
C CORR =THE BEST CORRECTIONS TO THE PARAMETERS
C DK1,DK2 =THE RECIPROCAL OF THE TWO FIRST ORDER RATE
C          CONSTANTS (THE TWO LIFETIMES)
C ITER= =A COUNTER FOR THE NUMBER OF ITERATIONS
C IWGHT =A SIGNAL FOR THE TYPE OF WEIGHT MATRIX
C          TO BE USED
C          1 SIGNIFIES THE UNIT WEIGHT MATRIX
C          2 SIGNIFIES "EQUAL-TIME-EQUAL-WEIGHT"
C          WEIGHT MATRIX
C JTEST =AN ERROR CHECK INDEX REGISTER
C PREXP1,PREXP2 =THE TWO PRE-EXPONENTIAL FACTORS
C *****
C *****
C *****
C
C          PROGRAM INITIALIZATION
C          -----
C
C *****
C SUBROUTINE DTAFIT (DK1,DK2,PREXP1,PREXP2,STNDEV,SIGMA,ITER,T,DATA,
1CALCI,DEV,MA,MB,MC,MD,MT,NDS,TINCRA,TINCRB,TINCRC,TINCRD,RMSDV,
2JTEST)
C DIMENSION DATA(2048),P(1450),T(1450),CALCI(1450),DEV(1450)
C DIMENSION AMATRX(1450,4),BMATRX(4,4),BINV(4,4),DUMMY(4)
C DIMENSION CORR(4),STNDEV(4),BDBLPR(50,4)
C COMMON/ENDCCM/EL(50,4)
C DOUBLE PRECISION BDBLPR,EL
C ITER=1
C KOUNT=0
C READ(5,20) DK1,DK2,PREXP1,PREXP2,IWGHT
20 FORMAT (2(F5.1,2X),F8.1,2X,F8.1,2X,I1)
C WRITE(6,25) DK1,DK2,PREXP1,PREXP2
25 FORMAT (1H1/1H0/1H0/1H0/1H0/1H0/18X,44HDOUBLE EXPONENTIAL FITTING
1SUBROUTINE CALLED/79H0PROCEEDING WITH THE DOUBLE EXPONENTIAL FIT U
2SING THE FOLLOWING TRIAL ESTIMATES/22H0OF THE PARAMETERS.../1H0,
32X,5HDK1= ,F8.1,5X,5HDK2= ,F8.1,5X,8HPREXP1= ,F8.1,5X,8HPREXP2= ,
4F8.1)
C CALL WEIGHT (P,MA,MB,MC,MD,MT,TINCRA,TINCRB,TINCRC,TINCRD,NDS,
1IWGHT)
C GO TO (30,40),IWGHT

```

## SUBROUTINE AFOLLO FRAME 2

```

30  WRITE(6,35)
35  FORMAT (24HUNIT WEIGHT MATRIX USED/1HG/1HG/1HG/1HG)
    GO TO 50
40  WRITE(6,45)
45  FORMAT (45H"EQUAL-TIME-EQUAL-WEIGHT" WEIGHT MATRIX USED/1HG/1HG/
1HG/1HG)
C   *****
C   *****
C   *****
C   *****
C   MAIN SECTION OF THE PROGRAM
C   -----
C   *****
50  DO 90 I=1,MT
    CALCI(I)=PREXP1*EXP(-T(I)/DK1)+PREXP2*EXP(-T(I)/DK2)
    AMATRX(I,1)=T(I)*PREXP1*EXP(-T(I)/DK1)/DK1**2
    AMATRX(I,2)=T(I)*PREXP2*EXP(-T(I)/DK2)/DK2**2
    AMATRX(I,3)=EXP(-T(I)/DK1)
    AMATRX(I,4)=EXP(-T(I)/DK2)
    DEV(I)= CALCI(I)-DATA(I)
90  CONTINUE
    SQDEV=0.0
    RMSDEV=0.0
    DO 130 K=1,4
    DO 120 J=1,4
    BMATRX(K,J)=0.0
120  CONTINUE
130  CONTINUE
    DO 160 K=1,4
    DO 150 J=1,4
    DO 140 I=1,MT
    BMATRX(K,J)=BMATRX(K,J)+AMATRX(I,K)*F(I)*AMATRX(I,J)
140  CONTINUE
    BDBLFR(K,J)=BMATRX(K,J)
150  CONTINUE
160  CONTINUE
    CALL ENDINV(BDBLFR,4,DETERM,1.0E-08,ITEST)
    DO 180 J=1,4
    DO 170 K=1,4
    BINV(J,K)=BDBLFR(J,K)
170  CONTINUE
180  CONTINUE
    DO 190 K=1,4
    DUMMY(K)=0.0
    CORR(K)=0.0
190  CONTINUE
    DO 210 K=1,4
    DO 200 I=1,MT
    DUMMY(K)=DUMMY(K)+AMATRX(I,K)*F(I)*DEV(I)
200  CONTINUE
210  CONTINUE
    DO 260 I=1,4
    DO 250 J=1,4
    CORR(I)=CORR(I)-BINV(I,J)*DUMMY(J)
250  CONTINUE
260  CONTINUE
    DO 270 I=1,MT
    SQDEV=SQDEV+DEV(I)*DEV(I)*F(I)
    RMSDEV=RMSDEV+DEV(I)*DEV(I)
270  CONTINUE

```

## SUBROUTINE APOLLO FRAME 3

```

      SIGMA=SQRT(SQDEV/FLOAT(MT-4))
      RMSDV=SQRT(RMSDEV/FLOAT(MT))
      DO 280 I=1,4
      STNDEV(I)=(SQRT(BINV(I,I)))*SIGMA
280  CONTINUE
      IF (ABS(CORR(1)/STNDEV(1))-0.01) 290,350,350
290  IF (ABS(CORR(2)/STNDEV(2))-0.01) 310,350,350
310  IF (ABS(CORR(3)/STNDEV(3))-0.01) 320,350,350
320  IF (ABS(CORR(4)/STNDEV(4))-0.01) 340,350,350
340  KOUNT=KOUNT+1
      IF (KOUNT-10) 350,345,345
345  JTEST=1
      ITER=ITER+1
      GO TO 360
350  DK1=DK1+CORR(1)
      DK2=DK2+CORR(2)
      PREXF1=PREXF1+CORR(3)
      PREXF2=PREXF2+CORR(4)
      ITER=ITER+1
      IF (ITER.GE.60) GO TO 400
      GO TO 50
C      *****
C      *****
C      *****
C      *****
C      BEAT A HASTY RETREAT
C      -----
C      *****
360  RETURN
C      *****
C      *****
C      *****
C      *****
C      ERROR MESSAGES
C      -----
C      *****
400  WRITE(6,405)
405  FORMAT (35HILCOPIING HAS EXCEEDED 60 ITERATIONS/29H PROCEEDING WITH
1 THE NEXT JOB)
      GO TO 3000
C      *****
C      *****
C      *****
C      *****
C      SET ERROR CHECK INDEX REGISTER
C      -----
C      *****
3000 JTEST=2
      GO TO 360
C      *****
C      *****
C      *****
END

```

## SUBROUTINE EROS FRAME 1

```

C *****
C *****
C E. B. PRIESTLEY APRIL 24, 1969
C THIS SUBROUTINE LEAST SQUARES FITS EXPERIMENTALLY DETERMINED DATA
C POINTS TO COMBINED FIRST AND SECOND ORDER KINETICS USING THE
C FIRST ORDER PART AS THE PROBE. THE INITIAL RAW GUESSES ARE FIRST
C REFINED BY FITTING POINTS FOR T LESS THAN DK ALLOWING ONLY XINOT
C AND GAMMA TO VARY AND POINTS FOR T GREATER THAN DK ALLOWING
C ONLY XINOT AND DK VARY. IF DESIRED, THIS REFINEMENT OF THE
C PARAMETERS CAN BE SUPPRESSED BY SETTING KAPPA EQUAL TO 2.
C IF THE REFINEMENT IS DESIRED, KAPPA IS SET EQUAL TO 1 AND
C THESE REFINED ESTIMATES OF DK AND GAMMA ARE THEN USED AS THE
C INITIAL GUESSES FOR THE COMBINED KINETIC SCHEME. FOR THIS
C SUBROUTINE TO WORK OPTIMALLY, THEREFORE, DATA POINTS SPANNING THE
C TIME DOMAIN FROM T LESS THAN DK TO T GREATER THAN DK SHOULD BE
C USED. THE LEAST SQUARES THEORY IS THAT OUTLINED IN ARLEY AND BUCH
C "INTRODUCTION TO THE THEORY OF PROBABILITY AND STATISTICS" CH 12.
C *****
C *****
C          REQUIRED INPUT DATA CARDS
C          -----
C *****
C 1. DK,GAMMA,XINOT,KAPPA,IWGHT (FORMAT STATEMENT EFN 20)
C *****
C *****
C          DEFINITIONS
C          -----
C *****
C CORR          =THE BEST CORRECTIONS TO THE PARAMETERS
C DK            =THE RECIPROCAL OF THE FIRST ORDER RATE
C              CONSTANT (THE LIFETIME OF THE STATE)
C DKSTOR        =VALUE OF DK FROM THE PREVIOUS ITERATION
C GAMMA         =THE SECOND ORDER RATE CONSTANT
C GAMSTR        =VALUE OF GAMMA FROM THE PREVIOUS ITERATION
C ITER1,ITER2,ITER3 =COUNTERS FOR THE NUMBER OF ITERATIONS
C              REQUIRED IN THE SEPARATED THEORY
C ITER          =A COUNTER FOR THE NUMBER OF ITERATIONS
C              REQUIRED IN THE COMPLETE THEORY
C IWGHT         =A SIGNAL FOR THE TYPE OF WEIGHT MATRIX
C              TO BE USED
C              1 SIGNIFIES THE UNIT WEIGHT MATRIX
C              2 SIGNIFIES "EQUAL-TIME-EQUAL-WEIGHT"
C              WEIGHT MATRIX
C JTEST         =AN ERROR CHECK INDEX REGISTER
C KAPPA         =A SIGNAL FOR INITIAL ESTIMATE REFINEMENT
C              1 SIGNIFIES REFINEMENT
C              2 SIGNIFIES NO REFINEMENT
C XINOT         =THE INITIAL PHOSPHORESCENCE INTENSITY AT
C              T=0
C *****
C *****
C *****
C          PROGRAM INITIALIZATION
C          -----
C *****
C SUBRCUTINE DTAFIT (DK,GAMMA,XINOT,STNDEV,SIGMA,ITER,T,DATA,CALCI,

```

SUBROUTINE EROS FRAME 2

```

1 DEV,MA,MB,MC,MD,MT,NDS,TINCRA,TINCRB,TINCRD,TINCRD,RMSDV,JTEST)
  DIMENSION DATA(2048),F(1450),T(1450),CALCI(1450),DEV(1450)
  DIMENSION AMATRX(1450,3),BMATRX(3,3),BINV(3,3),DUMMY(3)
  DIMENSION CORR(3),STNDEV(3),BDBLFR(50,3)
  COMMON/BNDCCOM/EL(50,3)
  DOUBLE PRECISION BDBLFR,EL
  ITER1=1
  ITER2=1
  ITER3=1
  ITER=1
  READ(5,20) DK,GAMMA,XINOT,KAPPA,IWGT
20  FORMAT (F5.1,2X,F9.1,2X,F8.1,2X,I1,2X,I1)
  WRITE(6,25) DK,GAMMA,XINOT
25  FORMAT (1H1/1HG/1HG/1HG/1HG/17X,49H FIRST AND SECOND ORDER FIT
  1TING SUBROUTINE CALLED/83HGFROCEEDING WITH THE FIRST AND SECOND OR
  2DER FIT USING THE FOLLOWING TRIAL ESTIMATES/22HGF THE PARAMETERS.
  3.../1HG,2X,4HDK= ,F8.1,10X,7HGAMMA= ,F9.7,10X,7HXINOT= ,F8.1)
  CALL WEIGHT (F,MA,MB,MC,MD,MT,TINCRA,TINCRB,TINCRD,TINCRD,NDS,
  1IWGT)
  GO TO (30,40),IWGT
30  WRITE(6,35)
35  FORMAT (24HUNIT WEIGHT MATRIX USED/1HG/1HG/1HG/1HG)
  GO TO 48
40  WRITE(6,45)
45  FORMAT (45H"EQUAL-TIME-EQUAL-WEIGHT" WEIGHT MATRIX USED/1HG/1HG/
  1HG/1HG)
48  DO 49 K=1,MT
  DATA(K)=DATA(K)/1000.0
  T(K)=T(K)/1000.0
49  CONTINUE
  DK=DK/1000.0
  GAMMA=1.0E 06*GAMMA
  XINOT=XINOT/1000.0
  MST=MT/10
  GAMSTR=GAMMA
  DKSTOR=DK
  GO TO (50,165),KAPPA
  *****
  *****
  *****
  *****
  MAIN SECTION OF THE PROGRAM
  -----
  *****
  *****
  SECTION ONE--FIT OF THE FIRST ONE TENTH OF THE DATA POINTS USING
  THE COMPLETE THEORY BUT PERMITTING ONLY GAMMA AND XINOT TO VARY.
  *****
50  DO 60 I=1,MST
  CALCI(I)=XINOT/(EXP(T(I)/DK)+2.0*GAMMA*DK*XINOT*(SINH(T(I)/
  1(2.0*DK)))**2+GAMMA*DK*XINOT*SINH(T(I)/DK))
  AMATRX(I,1)=((CALCI(I)/XINOT)**2)*EXP(T(I)/DK)
  AMATRX(I,2)=-(CALCI(I)**2)*DK*2.0*(SINH(T(I)/(2.0*DK)))**2-
  1(CALCI(I)**2)*DK*SINH(T(I)/DK)
  DEV(I)=CALCI(I)-DATA(I)
60  CONTINUE
  SQDEV=G.0
  DO 65 K=1,2
  DO 63 J=1,2
  BMATRX(K,J)=0.0

```



SUBROUTINE EROS FRAME 3

```

63 CONTINUE
65 CONTINUE
DO 75 K=1,2
DO 73 J=1,2
DO 70 I=1,MST
BMATRX(K,J)=BMATRX(K,J)+AMATRX(I,K)*F(I)*AMATRX(I,J)
70 CONTINUE
BDBLFR(K,J)=BMATRX(K,J)
73 CONTINUE
75 CONTINUE
CALL BNDINV(BDBLFR,2,DETERM,1.0E-08,ITEST)
DO 80 J=1,2
DO 77 K=1,2
BINV(J,K)=BDBLFR(J,K)
77 CONTINUE
80 CONTINUE
DO 86 K=1,2
DUMMY(K)=0.0
CORR(K)=0.0
86 CONTINUE
DO 90 K=1,2
DO 87 J=1,MST
DUMMY(K)=DUMMY(K)+AMATRX(J,K)*F(J)*DEV(J)
87 CONTINUE
90 CONTINUE
DO 95 I=1,2
DO 93 K=1,2
CORR(I)=CORR(I)-BINV(I,K)*DUMMY(K)
93 CONTINUE
95 CONTINUE
DO 98 J=1,MST
SQDEV=SQDEV+F(J)*DEV(J)**2
98 CONTINUE
SIGMA=SQRT(SQDEV/FLOAT(MST-2))
DO 100 I=1,2
STNDEV(I)=SQRT(BINV(I,I))*SIGMA
IF(ABS(CORR(I)/STNDEV(I)).GT.0.01) GO TO 102
100 CONTINUE
GO TO 104
102 XINOT=XINOT+CORR(1)
GAMMA=GAMMA+CORR(2)
ITER1=ITER1+1
IF(ITER1.GE.20) GO TO 410
GO TO 50

C *****
C SECTION TWO--FIT OF ALL THE DATA POINTS USING THE COMPLETE THEORY
C BUT PERMITTING ONLY DK AND XINOT TO VARY.
C *****
104 XINOT=XINOT+CORR(1)
GAMMA=GAMMA+CORR(2)
105 DO 106 I=1,MT
CALCI(I)=(EXP(T(I)/DK)+2.0*GAMMA*DK*XINOT*(SINH(T(I)/
1(2.0*DK)))**2+GAMMA*DK*XINOT*SINH(T(I)/DK))
AMATRX(I,1)=((CALCI(I)/XINOT)**2)*EXP(T(I)/DK)
AMATRX(I,2)=(CALCI(I)**2)*T(I)*EXP(T(I)/DK)/(XINOT*(DK**2))-
12.0*GAMMA*(CALCI(I)*SINH(T(I)/(2.0*DK)))**2-(CALCI(I)**2)*GAMMA*
2SINH(T(I)/DK)+(CALCI(I)**2)*T(I)*GAMMA*EXP(T(I)/DK)/DK
DEV(I)=CALCI(I)-DATA(I)
106 CONTINUE
SQDEV=0.0

```

## SUBROUTINE EROS FRAME 4

```

      DO 108 K=1,2
      DO 107 J=1,2
      BMATRX(K,J)=0.0
107  CONTINUE
108  CONTINUE
      DO 112 K=1,2
      DO 111 J=1,2
      DO 110 I=1,MT
      BMATRX(K,J)=BMATRX(K,J)+AMATRX(I,K)*F(I)*AMATRX(I,J)
110  CONTINUE
111  BDBLFR(K,J)=BMATRX(K,J)
111  CONTINUE
112  CONTINUE
      CALL BNDINV(BDBLFR,2,DETERM,1.0E-08,ITEST)
      DO 118 J=1,2
      DO 116 K=1,2
      BINV(J,K)=BDBLFR(J,K)
116  CONTINUE
118  CONTINUE
      DO 123 K=1,2
      DUMMY(K)=0.0
      CORR(K)=0.0
123  CONTINUE
      DO 125 K=1,2
      DO 124 J=1,MT
      DUMMY(K)=DUMMY(K)+AMATRX(J,K)*F(J)*DEV(J)
124  CONTINUE
125  CONTINUE
      DO 130 I=1,2
      DO 128 K=1,2
      CORR(I)=CORR(I)-BINV(I,K)*DUMMY(K)
128  CONTINUE
130  CONTINUE
      DO 135 J=1,MT
      SQDEV=SQDEV+F(J)*DEV(J)**2
135  CONTINUE
      SIGMA=SQRT(SQDEV/FLCAT(MT-2))
      DO 140 I=1,2
      STNDEV(I)=SQRT(BINV(I,I))*SIGMA
      IF (ABS(CORR(I)/STNDEV(I)).GT.0.01) GO TO 150
140  CONTINUE
      GO TO 160
150  XINOT=XINOT+CORR(1)
      DK=DK+CORR(2)
      ITER2=ITER2+1
      IF (ITER2.GE.20) GO TO 420
      GO TO 105
160  XINOT=XINOT+CORR(1)
      DK=DK+CORR(2)
      IF (ABS((DKSTOR-DK)/DKSTOR).LE.0.1.AND.ABS((GAMSTR-GAMMA)/GAMSTR).
1LE.0.1) GO TO 165
      GAMSTR=GAMMA
      DKSTOR=DK
      ITER3=ITER3+1
      ITER1=1
      ITER2=1
      IF (ITER3.GE.10) GO TO 430
      GO TO 50

```

C \*\*\*\*\*  
 C SECTION THREE--FIT OF ALL THE DATA POINTS USING THE COMPLETE

SUBROUTINE EROS FRAME 5

C THEORY AND PERMITTING ALL THREE PARAMETERS TO VARY SIMULTANEOUSLY.

```

C *****
165 DO 170 I=1,MT
    CALCI(I)=XINOT/(EXP(T(I)/DK)+2.0*GAMMA*DK*XINOT*(SINH(T(I)/
    1(2.0*DK)))**2+GAMMA*DK*XINOT*SINH(T(I)/DK))
    AMATRX(I,1)=(CALCI(I)**2)*T(I)*EXP(T(I)/DK)/(XINOT*(DK**2))-
    12.0*GAMMA*(CALCI(I)*SINH(T(I)/(2.0*DK)))**2-(CALCI(I)**2)*GAMMA*
    2SINH(T(I)/DK)+(CALCI(I)**2)*T(I)*GAMMA*EXP(T(I)/DK)/DK
    AMATRX(I,2)=-(CALCI(I)**2)*DK*2.0*(SINH(T(I)/(2.0*DK)))**2-
    1(CALCI(I)**2)*DK*SINH(T(I)/DK)
    AMATRX(I,3)=((CALCI(I)/XINOT)**2)*EXP(T(I)/DK)
    DEV(I)=CALCI(I)-DATA(I)
170 CONTINUE
    SQDEV=0.0
    RMSDEV=0.0
    DO 180 K=1,3
    DO 175 J=1,3
    BMATRX(K,J)=0.0
175 CONTINUE
180 CONTINUE
    DO 195 K=1,3
    DO 190 J=1,3
    DO 185 I=1,MT
    BMATRX(K,J)=BMATRX(K,J)+AMATRX(I,K)*F(I)*AMATRX(I,J)
185 CONTINUE
    BDBLFR(K,J)=BMATRX(K,J)
190 CONTINUE
195 CONTINUE
    CALL BNDINV(BDBLFR,3,DETERM,1.0E-08,ITEST)
    DO 215 J=1,3
    DO 210 K=1,3
    BINV(J,K)=BDBLFR(J,K)
210 CONTINUE
215 CONTINUE
    DO 220 K=1,3
    DUMMY(K)=0.0
    CORR(K)=0.0
220 CONTINUE
    DO 230 K=1,3
    DO 225 I=1,MT
    DUMMY(K)=DUMMY(K)+AMATRX(I,K)*F(I)*DEV(I)
226 CONTINUE
230 CONTINUE
    DO 260 I=1,3
    DO 250 J=1,3
    CORR(I)=CORR(I)-BINV(I,J)*DUMMY(J)
250 CONTINUE
260 CONTINUE
    DO 270 I=1,MT
    SQDEV=SQDEV+F(I)*DEV(I)**2
    RMSDEV=RMSDEV+DEV(I)**2
270 CONTINUE
    SIGMA=SQRT(SQDEV/FLOAT(MT-3))
    RMSDV=SQRT(RMSDEV/FLOAT(MT))
    DO 280 I=1,3
    STNDEV(I)=SQRT(BINV(I,I))*SIGMA
280 CONTINUE
    IF (ABS(CORR(1)/STNDEV(1)).GE.0.01) GO TO 320
    IF (ABS(CORR(2)/STNDEV(2)).GE.0.01) GO TO 320
    IF (ABS(CORR(3)/STNDEV(3)).GE.0.01) GO TO 320

```

SUBROUTINE EROS FRAME 6

```

      JTEST=1
      ITER=ITER+1
      GO TO 360
320  DK=DK+CORR(1)
      GAMMA=GAMMA+CORR(2)
      XINOT=XINOT+CORR(3)
      ITER=ITER+1
      IF (ITER.GE.60) GO TO 440
      GO TO 165
360  DK=DK+CORR(1)
      GAMMA=GAMMA+CORR(2)
      XINOT=XINOT+CORR(3)
      DO 400 K=1,MT
      DATA(K)=1000.0#DATA(K)
      T(K)=1000.0#T(K)
      CALCI(K)=1000.0#CALCI(K)
      DEV(K)=1000.0#DEV(K)
400  CONTINUE
      SIGMA=1000.0#SIGMA
      RMSDV=1000.0#RMSDV
      DK=1000.0#DK
      GAMMA=(1.0E-06)*GAMMA
      XINOT=1000.0#XINOT
      STNDEV(1)=1000.0#STNDEV(1)
      STNDEV(2)=(1.0E-06)*STNDEV(2)
      STNDEV(3)=1000.0#STNDEV(3)
C *****
C *****
C *****
C *****
C BEAT A HASTY RETREAT
C -----
C *****
405 RETURN
C *****
C *****
C *****
C *****
C ERROR MESSAGES
C -----
C *****
410 WRITE(6,415) ITER3
415 FORMAT (50H1LOOPING IN SECTION ONE HAS EXCEEDED 20 ITERATIONS/
144H SECTIONS ONE AND TWO LOOP INDEX NOW EQUALS ,I2/29H PROCEEDING
2WITH THE NEXT JOB)
      GO TO 3000
420 WRITE(6,425) ITER3
425 FORMAT (50H1LOOPING IN SECTION TWO HAS EXCEEDED 20 ITERATIONS/
144H SECTIONS ONE AND TWO LOOP INDEX NOW EQUALS ,I2/29H PROCEEDING
2WITH THE NEXT JOB)
      GO TO 3000
430 WRITE(6,435)
435 FORMAT (64H1LOOPING BETWEEN SECTIONS ONE AND TWO HAS EXCEEDED 10 I
1ITERATIONS/29H PROCEEDING WITH THE NEXT JOB)
      GO TO 3000
440 WRITE(6,445)
445 FORMAT (52H1LOOPING IN SECTION THREE HAS EXCEEDED 60 ITERATIONS/
129H PROCEEDING WITH THE NEXT JOB)
      GO TO 3000
C *****

```

SUBROUTINE EROS FRAME 7

```
C *****
C *****
C *****
C          SET ERROR CHECK INDEX REGISTER
C          -----
C *****
3000 JTEST=2
      GO TO 405
C *****
C *****
C *****
      END
```

## SUBROUTINE HERMES FRAME 1

```

C *****
C *****
C E. B. PRIESTLEY MAY 5, 1969
C THIS SUBROUTINE LEAST SQUARES FITS EXPERIMENTALLY DETERMINED DATA
C POINTS TO COMBINED FIRST AND SECOND ORDER KINETICS USING THE
C SECOND ORDER PART AS THE PROBE. THE INITIAL RAW GUESSES ARE FIRST
C REFINED BY FITTING POINTS FOR T LESS THAN DK ALLOWING ONLY XINOT
C AND GAMMA TO VARY AND POINTS FOR T GREATER THAN DK ALLOWING
C ONLY XINOT AND DK VARY. IF DESIRED, THIS REFINEMENT OF THE
C PARAMETERS CAN BE SUPPRESSED BY SETTING KAPPA EQUAL TO 2.
C IF THE REFINEMENT IS DESIRED, KAPPA IS SET EQUAL TO 1 AND
C THESE REFINED ESTIMATES OF DK AND GAMMA ARE THEN USED AS THE
C INITIAL GUESSES FOR THE COMBINED KINETIC SCHEME. FOR THIS
C SUBROUTINE TO WORK OPTIMALLY, THEREFORE, DATA POINTS SPANNING THE
C TIME DOMAIN FROM T LESS THAN DK TO T GREATER THAN DK SHOULD BE
C USED. THE LEAST SQUARES THEORY IS THAT OUTLINED IN ARLEY AND BUCH
C "INTRODUCTION TO THE THEORY OF PROBABILITY AND STATISTICS" CH 12.
C *****
C *****
C          REQUIRED INPUT DATA CARDS
C          -----
C *****
C 1. DK,GAMMA,XINOT,KAPPA,IWGHT (FORMAT STATEMENT EFN 20)
C *****
C *****
C          DEFINITIONS
C          -----
C *****
C CORR          =THE BEST CORRECTIONS TO THE PARAMETERS
C DK            =THE RECIPROCAL OF THE FIRST ORDER RATE
C              CONSTANT (THE LIFETIME OF THE STATE)
C DKSTOR        =VALUE OF DK FROM THE PREVIOUS ITERATION
C GAMMA         =THE SECOND ORDER RATE CONSTANT
C GAMSTR        =VALUE OF GAMMA FROM THE PREVIOUS ITERATION
C ITER1,ITER2,ITER3 =COUNTERS FOR THE NUMBER OF ITERATIONS
C              REQUIRED IN THE SEPARATED THEORY
C ITER          =A COUNTER FOR THE NUMBER OF ITERATIONS
C              REQUIRED IN THE COMPLETE THEORY
C IWGHT         =A SIGNAL FOR THE TYPE OF WEIGHT MATRIX
C              TO BE USED
C              1 SIGNIFIES THE UNIT WEIGHT MATRIX
C              2 SIGNIFIES "EQUAL-TIME-EQUAL-WEIGHT"
C              WEIGHT MATRIX
C JTEST         =AN ERROR CHECK INDEX REGISTER
C KAPPA         =A SIGNAL FOR INITIAL ESTIMATE REFINEMENT
C              1 SIGNIFIES REFINEMENT
C              2 SIGNIFIES NO REFINEMENT
C XINOT        =THE INITIAL PHOSPHORESCENCE INTENSITY AT
C              T=0
C *****
C *****
C *****
C          PROGRAM INITIALIZATION
C          -----
C *****
C SUBROUTINE DIAFIT (DK,GAMMA,XINOT,STNDEV,SIGMA,ITER,T,DATA,CALCI,

```



## SUBROUTINE HERMES FRAME 3

```

      DO 65 K=1,2
      DO 63 J=1,2
      BMATRX(K,J)=0.0
63    CONTINUE
65    CONTINUE
      DO 75 K=1,2
      DO 73 J=1,2
      DO 70 I=1,MST
      BMATRX(K,J)=BMATRX(K,J)+AMATRX(I,K)*F(I)*AMATRX(I,J)
70    CONTINUE
      BDBLFR(K,J)=BMATRX(K,J)
73    CONTINUE
75    CONTINUE
      CALL BNDINV(BDBLFR,2,DETERM,1.0E-08,ITEST)
      DO 80 J=1,2
      DO 77 K=1,2
      BINV(J,K)=BDBLFR(J,K)
77    CONTINUE
80    CONTINUE
      DO 86 K=1,2
      DUMMY(K)=0.0
      CORR(K)=0.0
86    CONTINUE
      DO 90 K=1,2
      DO 87 J=1,MST
      DUMMY(K)=DUMMY(K)+AMATRX(J,K)*F(J)*DEV(J)
87    CONTINUE
90    CONTINUE
      DO 95 I=1,2
      DO 93 K=1,2
      CORR(I)=CORR(I)-BINV(I,K)*DUMMY(K)
93    CONTINUE
95    CONTINUE
      DO 98 J=1,MST
      SQDEV=SQDEV+F(J)*DEV(J)**2
98    CONTINUE
      SIGMA=SQRT(SQDEV/FLOAT(MST-2))
      DO 100 I=1,2
      STNDEV(I)=SQRT(BINV(I,I))*SIGMA
      IF(ABS(CORR(I)/STNDEV(I)).GT.0.01) GO TO 102
100   CONTINUE
      GO TO 104
102   XINOT=XINOT+CORR(1)
      GAMMA=GAMMA+CORR(2)
      ITER1=ITER1+1
      IF(ITER1.GE.20) GO TO 410
      GO TO 50
      C          *****
      C  SECTION TWO--FIT OF ALL THE DATA POINTS USING THE COMPLETE THEORY
      C  BUT PERMITTING ONLY DK AND XINOT TO VARY.
      C          *****
104   XINOT=XINOT+CORR(1)
      GAMMA=GAMMA+CORR(2)
105   DO 106 I=1,MT
      TVALU=XINOT/(EXP(T(I)/DK)+2.0*GAMMA*DK*XINOT*(SINH(T(I)/
      1(2.0*DK)))**2+GAMMA*DK*XINOT*SINH(T(I)/DK))
      CALCI(I)=TVALU**2
      TVALU1=((TVALU/XINOT)**2)*EXP(T(I)/DK)
      AMATRX(I,1)=2.0*TVALU*TVALU1
      TVALU2=(CALCI(I))*T(I)*EXP(T(I)/DK)/(XINOT*(DK**2))-

```



## SUBROUTINE HERMES FRAME 4

```

12. G=GAMMA*(TVALU*SINH(T(I)/(2.0*DK)))**2-(CALCI(I))*GAMMA*
2SINH(T(I)/DK)+(CALCI(I))*T(I)*GAMMA*EXP(T(I)/DK)/DK
AMATRX(I,2)=2.0*TVALU*TVALU2
DEV(I)=CALCI(I)-DATA(I)
106 CONTINUE
SQDEV=0.0
DO 108 K=1,2
DO 107 J=1,2
BMATRX(K,J)=0.0
107 CONTINUE
108 CONTINUE
DO 112 K=1,2
DO 111 J=1,2
DO 110 I=1,MT
BMATRX(K,J)=BMATRX(K,J)+AMATRX(I,K)*F(I)*AMATRX(I,J)
110 CONTINUE
BDBLPR(K,J)=BMATRX(K,J)
111 CONTINUE
112 CONTINUE
CALL BNDINV(BDBLPR,2,DETERM,1.0E-08,ITEST)
DO 118 J=1,2
DO 116 K=1,2
BINV(J,K)=BDBLPR(J,K)
116 CONTINUE
118 CONTINUE
DO 123 K=1,2
DUMMY(K)=0.0
CORR(K)=0.0
123 CONTINUE
DO 125 K=1,2
DO 124 J=1,MT
DUMMY(K)=DUMMY(K)+AMATRX(J,K)*F(J)*DEV(J)
124 CONTINUE
125 CONTINUE
DO 130 I=1,2
DO 128 K=1,2
CORR(I)=CORR(I)-BINV(I,K)*DUMMY(K)
128 CONTINUE
130 CONTINUE
DO 135 J=1,MT
SQDEV=SQDEV+F(J)*DEV(J)**2
135 CONTINUE
SIGMA=SQRT(SQDEV/LOAT(MT-2))
DO 140 I=1,2
STNDEV(I)=SQRT(BINV(I,I))*SIGMA
IF(ABS(CORR(I)/STNDEV(I)).GT.0.01) GO TO 150
140 CONTINUE
GO TO 160
150 XINOT=XINOT+CORR(1)
DK=DK+CORR(2)
ITER2=ITER2+1
IF(ITER2.GE.20) GO TO 420
GO TO 105
160 XINOT=XINOT+CORR(1)
DK=DK+CORR(2)
IF(ABS((DKSTOR-DK)/DKSTOR).LE.0.1.AND.ABS((GAMSTR-GAMMA)/GAMSTR).
1LE.0.1) GO TO 165
GAMSTR=GAMMA
DKSTOR=DK
ITER3=ITER3+1

```

## SUBROUTINE HERMES FRAME 5

```

ITER1=1
ITER2=1
IF (ITER3.GE.10) GO TO 430
GO TO 50

C          *****
C SECTION THREE--FIT OF ALL THE DATA POINTS USING THE COMPLETE
C THEORY AND PERMITTING ALL THREE PARAMETERS TO VARY SIMULTANEOUSLY.
C          *****

165 DO 170 I=1,MT
    TVALU=XINOT/(EXP(T(I)/DK)+2.0*GAMMA*DK*XINOT*(SINH(T(I)/
1(2.0*DK)))**2+GAMMA*DK*XINOT*SINH(T(I)/DK))
    CALCI(I)=TVALU**2
    TVALU1=(CALCI(I))*T(I)*EXP(T(I)/DK)/(XINOT*(DK**2))-
12.0*GAMMA*(TVALU*SINH(T(I)/(2.0*DK)))**2-(CALCI(I))*GAMMA*
2SINH(T(I)/DK)+(CALCI(I))*T(I)*GAMMA*EXP(T(I)/DK)/DK
    AMATRX(I,1)=2.0*TVALU*TVALU1
    TVALU2=-(CALCI(I))*DK*2.0*(SINH(T(I)/(2.0*DK)))**2-
1(CALCI(I))*DK*SINH(T(I)/DK)
    AMATRX(I,2)=2.0*TVALU*TVALU2
    TVALU3=((TVALU/XINOT)**2)*EXP(T(I)/DK)
    AMATRX(I,3)=2.0*TVALU*TVALU3
    DEV(I)=CALCI(I)-DATA(I)
170 CONTINUE
    SQDEV=0.0
    RMSDEV=0.0
    DO 180 K=1,3
    DO 175 J=1,3
    BMATRX(K,J)=0.0
175 CONTINUE
180 CONTINUE
    DO 195 K=1,3
    DO 190 J=1,3
    DO 185 I=1,MT
    BMATRX(K,J)=BMATRX(K,J)+AMATRX(I,K)*F(I)*AMATRX(I,J)
185 CONTINUE
    BDBLFR(K,J)=BMATRX(K,J)
190 CONTINUE
195 CONTINUE
    CALL BNDINV(BDBLFR,3,DETERM,1.0E-08,ITEST)
    DO 215 J=1,3
    DO 210 K=1,3
    BINV(J,K)=BDBLFR(J,K)
210 CONTINUE
215 CONTINUE
    DO 220 K=1,3
    DUMMY(K)=0.0
    CORR(K)=0.0
220 CONTINUE
    DO 230 K=1,3
    DO 226 I=1,MT
    DUMMY(K)=DUMMY(K)+AMATRX(I,K)*F(I)*DEV(I)
226 CONTINUE
230 CONTINUE
    DO 260 I=1,3
    DO 250 J=1,3
    CORR(I)=CORR(I)-BINV(I,J)*DUMMY(J)
250 CONTINUE
260 CONTINUE
    DO 270 I=1,MT
    SQDEV=SQDEV+F(I)*DEV(I)**2

```

## SUBROUTINE HERMES FRAME 6

```

      RMSDEV=RMSDEV+DEV(I)**2
- 270  CONTINUE
      SIGMA=SQRT(SQDEV/FLOAT(MT-3))
      RMSDV=SQRT(RMSDEV/FLOAT(MT))
      DO 280 I=1,3
      STNDEV(I)=SQRT(BINV(I,I))*SIGMA
 280  CONTINUE
      IF (ABS(CORR(1)/STNDEV(1)).GE.0.01) GO TO 320
      IF (ABS(CORR(2)/STNDEV(2)).GE.0.01) GO TO 320
      IF (ABS(CORR(3)/STNDEV(3)).GE.0.01) GO TO 320
      JTEST=1
      ITER=ITER+1
      GO TO 360
 320  DK=DK+CORR(1)
      GAMMA=GAMMA+CORR(2)
      XINOT=XINOT+CORR(3)
      ITER=ITER+1
      IF (ITER.GE.60) GO TO 440
      GO TO 165
 360  DK=DK+CORR(1)
      GAMMA=GAMMA+CORR(2)
      XINOT=XINOT+CORR(3)
      DO 400 K=1,MT
      DATA(K)=DATA(K)*1.0E 06
      T(K)=1000.0*T(K)
      CALCI(K)=CALCI(K)*1.0E 06
      DEV(K)=DEV(K)*1.0E 06
 400  CONTINUE
      SIGMA=SIGMA*1.0E 06
      RMSDV=RMSDV*1.0E 06
      DK=1000.0*DK
      GAMMA=(1.0E-06)*GAMMA
      XINOT=1000.0*XINOT
      STNDEV(1)=1000.0*STNDEV(1)
      STNDEV(2)=(1.0E-06)*STNDEV(2)
      STNDEV(3)=1000.0*STNDEV(3)
C      *****
C      *****
C      *****
C      *****
C      BEAT A HASTY RETREAT
C      -----
C      *****
 405  RETURN
C      *****
C      *****
C      *****
C      *****
C      ERROR MESSAGES
C      -----
C      *****
 410  WRITE(6,415) ITER3
 415  FORMAT (50H1LOOPING IN SECTION ONE HAS EXCEEDED 20 ITERATIONS/
144H SECTIONS ONE AND TWO LOOP INDEX NOW EQUALS ,I2/29H PROCEEDING
2WITH THE NEXT JOB)
      GO TO 3000
 420  WRITE(6,425) ITER3
 425  FORMAT (50H1LOOPING IN SECTION TWO HAS EXCEEDED 20 ITERATIONS/
144H SECTIONS ONE AND TWO LOOP INDEX NOW EQUALS ,I2/29H PROCEEDING
2WITH THE NEXT JOB)

```

SUBROUTINE HERMES FRAME 7

```

      GO TO 3000
430  WRITE(6,435)
435  FORMAT (64H1LOOPING BETWEEN SECTIONS ONE AND TWO HAS EXCEEDED 10 I
      1TERATIONS/29H PROCEEDING WITH THE NEXT JOB)
      GO TO 3000
440  WRITE(6,445)
445  FORMAT (52H1LOOPING IN SECTION THREE HAS EXCEEDED 60 ITERATIONS/
      129H PROCEEDING WITH THE NEXT JOB)
      GO TO 3000
C     *****
C     *****
C     *****
C     *****
C     SET ERROR CHECK INDEX REGISTER
C     -----
C     *****
3000  JTEST=2
      GO TO 405
C     *****
C     *****
C     *****
      END

```

## SUBROUTINE ICARUS FRAME 1

```

C *****
C *****
C E. B. PRIESTLEY MAY 14, 1969
C THIS SUBROUTINE GENERATES ONE OF TWO POSSIBLE WEIGHT MATRICES,
C DEPENDING UPON THE VALUE OF "IWGHT", TO BE USED IN THE SUBROUTINES
C "DTAFIT". THE WEIGHT MATRIX CAN BE EITHER A UNIT MATRIX OR AN
C "EQUAL-TIME-EQUAL-WEIGHT" WEIGHT MATRIX (SEE THE SUBROUTINE
C "DTAFIT" FOR THE APPROPRIATE VALUE OF IWGHT TO BE USED).
C *****
C *****
C *****
C PROGRAM INITIALIZATION
C -----
C *****
C SUBROUTINE WEIGHT(F,MA,MB,MC,MD,MT,TINCRA,TINCRB,TINCRD,TINCRD,
C INDS,IWGHT)
C DIMENSION F(1450)
C IF (IWGHT) 2010,2010,10
C *****
C *****
C *****
C MAIN SECTION OF THE PROGRAM
C -----
C *****
10 GO TO (20,40),IWGHT
C *****
C UNIT WEIGHT MATRIX GENERATED IF IWGHT=1.
C *****
20 DO 30 I=1,MT
F(I)=1.0
30 CONTINUE
GO TO 120

C *****
C "EQUAL-TIME-EQUAL-WEIGHT" WEIGHT MATRIX GENERATED IF IWGHT=2.
C *****
40 DO 50 I=1,MA
F(I)=1.0
50 CONTINUE
GO TO (120,60,60,60),NDS
60 MI=MA+1
MF=MA+MB
DO 70 I=MI,MF
F(I)=TINCRB/TINCRA
70 CONTINUE
GO TO (2000,120,80,80),NDS
80 MI=MA+MB+1
MF=MA+MB+MC
DO 90 I=MI,MF
F(I)=TINCRD/TINCRA
90 CONTINUE
GO TO (2000,2000,120,100),NDS
100 MI=MA+MB+MC+1
MF=MA+MB+MC+MD
DO 110 I=MI,MF
F(I)=TINCRD/TINCRA
110 CONTINUE
C *****
C *****
C *****

```

SUBROUTINE ICARUS FRAME 2

```

C      *****
C      BEAT A HASTY RETREAT
C      -----
C      *****
120  RETURN
C      *****
C      *****
C      *****
C      *****
C      ERROR MESSAGES
C      -----
C      *****
2000 WRITE(6,2001)
2001 FORMAT (37H0ERROR IN GENERATION OF WEIGHT MATRIX/17H0EXECUTION HAL
1TED)
GO TO 3000
2010 WRITE(6,2011)
2011 FORMAT (23H0IWGHT NEGATIVE OR ZERO/17H0EXECUTION HALTED)
GO TO 3000
C      *****
C      *****
C      *****
C      *****
C      INTERNAL ABEND
C      -----
C      *****
3000 STOP
C      *****
C      *****
C      *****
C      *****
END

```

---

**RUNGE-KUTTA NANOSECOND LIFETIME PACKAGE**

---

THIS PACKAGE CONSISTS OF A PROGRAM "RKFNDC" WHICH CAN BE USED TO EXTRACT THE FIRST ORDER RATE CONSTANT FROM EXPERIMENTAL DATA OBTAINED FROM MEASUREMENTS MADE WITH THE LASER SOURCE NANOSECOND LIFETIME MEASURING APPARATUS. SUBROUTINE "INTERP" USES LAGRANGIAN INTERPOLATION TO OBTAIN POINTS BETWEEN THE DATA POINTS IN ORDER TO INCREASE THE ACCURACY OF THE RUNGE-KUTTA SECTION OF "RKFNDC".

## PROGRAM RKFNDC FRAME 1

```

C *****
C *****
C E. B. PRIESTLEY MAR. 31, 1969
C THIS PROGRAM CAN BE USED TO OBTAIN A FIRST ORDER RATE CONSTANT FOR
C FLUORESCENCE DECAY WHEN THE LIFETIME OF THE EMITTING STATE IS
C SHORTER THAN THE TIME REQUIRED TO SWITCH OFF THE EXCITING LIGHT.
C IT SIMPLY SOLVES THE FIRST ORDER DIFFERENTIAL EQUATION FOR THE
C EMISSION INTENSITY AS A FUNCTION OF TIME, USING NUMERICAL VALUES
C FOR THE DECAYING EXCITATION TERM. THE RUNGE-KUTTA SCHEME IS USED
C TO OBTAIN THE SOLUTION, THE RESULT BEING FITTED IN A LEAST SQUARES
C SENSE TO THE EXPERIMENTAL DECAY CURVE.
C *****
C *****
C
C REQUIRED INPUT DATA CARDS
C -----
C *****
C 1. DLABL (FORMAT STATEMENT EFN 4)
C 2. JOBNO,HMSG (FORMAT STATEMENT EFN 10)
C 3. TAU,SCALE,TINCR,IFLOT (FORMAT STATEMENT EFN 12)
C 4. EXCINT (FORMAT STATEMENT EFN 15)
C 5. EMIS (FORMAT STATEMENT EFN 20)
C 6. THE LAST DATA CARD MUST BE AN "ENDDTA" CARD
C *****
C *****
C
C DEFINITIONS
C -----
C *****
C DLABL =A DATA IDENTIFICATION LABEL
C EMIS =THE EXPERIMENTAL EMISSION INTENSITY
C EXCINT =THE EXCITATION INTENSITY
C EXINOT =THE EXCITATION INTENSITY AT T=0
C FMT1,FMT2 =ONE DIMENSIONAL ARRAYS WHERE THE FORMATS
C USED IN LABELLING THE X AND Y AXES,
C RESPECTIVELY, ARE STORED
C HMSG =A JOB IDENTIFICATION MESSAGE
C IFLOT =SIGNAL FOR PLOT OR NO PLOT AS FOLLOWS....
C 1 SIGNIFIES PLOT, 2 SIGNIFIES NO PLOT
C JOBNO =THE JOB NUMBER
C LF1,LF2 =INTEGERS SPECIFYING THE FIELD LENGTHS
C OF FMT1 AND FMT2, RESPECTIVELY
C SCALE =A SCALING FACTOR BETWEEN EMISSION AND
C EXCITATION INTENSITIES
C TAU =THE LIFETIME OF THE EMITTING STATE
C TINCR =THE NET SIZE (EQUIVALENT DWELL TIME PER
C CHANNEL ON ND180 MULTI-CHANNEL ANALYZER)
C TITLE1,TITLE2 =THE X AND Y LABELS, RESPECTIVELY
C XN =THE RUNGE-KUTTA SOLUTION TO THE
C DIFFERENTIAL EQUATION FOR THE POPULATION
C OF THE EXCITED STATE WHICH IS EMITTING
C *****
C *****
C *****
C
C PROGRAM INITIALIZATION
C -----
C *****
C DIMENSION EXCINT(520),XN(520),AMATRX(512,2),EMIS(512),BMATRX(2,2)

```



## PROGRAM RKFND C FRAME 2

```

      DIMENSION F(512), DUMMY(2), CORR(2), DEV(512), BINV(2,2), STNDEV(2)
      DIMENSION HMSG(9), JOBNO(2), ADATE(2), DD(3), DLABL(4), DNDT(512)
      DIMENSION DNDSC(512), T(512), TITLE1(2), TITLE2(5)
      DIMENSION EDBLFR(50,2)
      COMMON/ENDCOM/EL(50,50)
      DOUBLE PRECISION EDBLFR, EL
      DD(1)=0
      DD(3)=1
      DATA ENDD/6HENDDTA/
      DATA TITLE1/11HTIME (NSEC)/
      DATA TITLE2/27HINTENSITY (ARBITRARY UNITS)/
      DATA FMT1,LF1,FMT2,LF2/6H(F5.2),5,6H(F6.1),6/
      CALL DATE(ADATE)
1  ITER=0
      READ(5,4) (DLABL(J), J=1,4)
4  FORMAT (4A6)
C *****
C *****
C *****
C *****
C          CLEAN UP AND QUIT
C          -----
C *****
      IF(DLABL-ENDD) 9,7,9
7  WRITE(6,8)
8  FORMAT (25H1END OF INPUT ENCOUNTERED/11HEND OUTPUT)
      STOP
C *****
C  PROCEED IF DATA LABEL DOES NOT EQUAL "ENDDTA".
C *****
9  READ(5,10) (JOBNO(I), I=1,2), (HMSG(J), J=1,9)
10 FORMAT (2A6,2X,9A6)
      READ(5,12) TAU,SCALE,TINCR,IPL0T
12 FORMAT (F8.3,2X,2(F8.5,2X),I1)
      JF=-7
      JL=0
      DO 16 K=1,64
      JF=JF+8
      JL=JL+8
      READ(5,15) (EXCINT(J), J=JF,JL)
15 FORMAT (8(F10.1))
16 CONTINUE
      JF=-7
      JL=0
      DO 24 K=1,64
      JF=JF+8
      JL=JL+8
      READ(5,20) (EMIS(J), J=JF,JL)
20 FORMAT (8(F10.1))
24 CONTINUE
      WRITE(6,25) (JOBNO(I), I=1,2), (ADATE(J), J=1,2), (HMSG(K), K=1,9)
25 FORMAT (1H1/1H0/1H0/1H0,5X,7HJOBNO= ,2A6,10X,6HDATE= ,2A6/1H0,5X,
11HIDENTIFICATION= ,9A6)
      WRITE(6,27) (DLABL(J), J=1,4)
27 FORMAT (1H0/1H0/1H0,5X,5HDATA ,4A6,21H ENCOUNTERED IN INPUT)
      WRITE(6,30) TAU,SCALE,TINCR
30 FORMAT (1H1/1H0/1H0/1H0,65HTHE VALUES ASSIGNED THE TWO PARAMETERS
1AS INITIAL GUESSES ARE.../1H0,20X,5HTAU= ,1PE15.8,5H NSEC/1H0,
220X,7HSCALE= ,1PE15.8/1H0/1H0/1H0/1H0,36HTHE TIME INCREMENT HAS TH
3E VALUE.../1H0,20X,7HTINCR= ,1PE15.8,5H NSEC)

```

## PROGRAM RKFND C FRAME 3

```

C *****
C *****
C *****
C *****
C          MAIN SECTION OF THE PROGRAM
C          -----
C *****
C          *****
C          THE AVERAGE BASELINE IS SUBTRACTED FROM EACH DATA POINT, THE TIME
C          ARRAY IS FILLED AND THE EXCITATION INTENSITY AT T=0 IS CALCULATED.
C          *****
C          BASLN=0.0
C          DO 35 J=472,512
C          BASLN=BASLN+EXCINT(J)
35  CONTINUE
C          BASLN=BASLN/40.0
C          DO 38 J=1,512
C          EXCINT(J)=EXCINT(J)-BASLN
C          EMIS(J)=EMIS(J)-BASLN
C          T(J)=TINCR*FLOAT(J-1)
38  CONTINUE
C          EXINOT=0.0
C          DO 40 J=1,40
C          EXINOT=EXINOT+EXCINT(J)
40  CONTINUE
C          EXINOT=EXINOT/40.0
C          *****
C          RUNGE-KUTTA SOLUTION TO THE DIFFERENTIAL EQUATION.
C          *****
C          HH=TINCR/10.0
45  ITER=ITER+1
C          XN(1)=SCALE*EXINOT*TAU
C          XX=XN(1)
C          DO 50 J=1,511
C          XINT=EXCINT(J)
C          DO 48 K=1,10
C          RK1=SCALE*XINT-XX/TAU
C          STEP=FLOAT(2*K-1)/20.0
C          CALL INTERF(STEP,XINT,J,EXCINT)
C          RK2=SCALE*XINT-(XX+HH*RK1/2.0)/TAU
C          RK3=SCALE*XINT-(XX+HH*RK2/2.0)/TAU
C          STEP=FLOAT(K)/10.0
C          CALL INTERF(STEP,XINT,J,EXCINT)
C          RK4=SCALE*XINT-(XX+HH*RK3)/TAU
C          XX=XX+(HH/6.0)*(RK1+2.0*RK2+2.0*RK3+RK4)
48  CONTINUE
C          XN(J+1)=XX
50  CONTINUE
C          DO 51 J=513,520
C          XN(J)=XN(512)
51  CONTINUE
C          *****
C          GENERATION OF THE DERIVATIVES OF THE EMISSION INTENSITY WITH
C          RESPECT TO THE PARAMETERS DEFINED BY THE KINETIC EQUATION.
C          *****
C          DNCT(1)=SCALE*EXINOT
C          XX=DNCT(1)
C          DO 54 J=1,511
C          XNVAL=XN(J)
C          DO 52 K=1,10

```

## PROGRAM RKFNC FRAME 4

```

      RK1=-XX/TAU+XNVAL/(TAU**2)
      STEP=FLOAT(2*K-1)/20.0
      CALL INTERF(STEP,XNVAL,J,XN)
      RK2=-(XX+HH#RK1/2.0)/TAU+XNVAL/(TAU**2)
      RK3=-(XX+HH#RK2/2.0)/TAU+XNVAL/(TAU**2)
      STEP=FLOAT(K)/10.0
      CALL INTERF(STEP,XNVAL,J,XN)
      RK4=-(XX+HH#RK3)/TAU+XNVAL/(TAU**2)
      XX=XX+(HH/6.0)*(RK1+2.0#RK2+2.0#RK3+RK4)
52  CONTINUE
      DNDT(J+1)=XX
54  CONTINUE
      DNDSC(1)=EXINOT#TAU
      XX=DNDSC(1)
      DO 58 J=1,511
      XINT=EXCINT(J)
      DO 56 K=1,10
      RK1=XINT-XX/TAU
      STEP=FLOAT(2*K-1)/20.0
      CALL INTERF(STEP,XINT,J,EXCINT)
      RK2=XINT-(XX+HH#RK1/2.0)/TAU
      RK3=XINT-(XX+HH#RK2/2.0)/TAU
      STEP=FLOAT(K)/10.0
      CALL INTERF(STEP,XINT,J,EXCINT)
      RK4=XINT-(XX+HH#RK3)/TAU
      XX=XX+(HH/6.0)*(RK1+2.0#RK2+2.0#RK3+RK4)
56  CONTINUE
      DNDSC(J+1)=XX
58  CONTINUE
C      *****
C      LEAST SQUARES FIT OF THE CALCULATED TO THE EXPERIMENTAL
C      EMISSION DECAY CURVE.
C      *****
      SQDEV=0.0
      RMSDEV=0.0
      DO 60 J=1,512
      F(J)=1.0
60  CONTINUE
      DO 70 J=1,2
      DO 65 K=1,2
      BMATRIX(J,K)=0.0
65  CONTINUE
70  CONTINUE
      DO 75 K=1,2
      DUMMY(K)=0.0
      CORR(K)=0.0
75  CONTINUE
      DO 80 J=1,512
      DEV(J)=XN(J)-EMIS(J)
      AMATRIX(J,1)=DNDT(J)
      AMATRIX(J,2)=DNDSC(J)
80  CONTINUE
      DO 95 K=1,2
      DO 90 J=1,2
      DO 85 I=1,512
      BMATRIX(K,J)=BMATRIX(K,J)+AMATRIX(I,K)*F(I)*AMATRIX(I,J)
85  CONTINUE
90  CONTINUE
95  CONTINUE
      DO 97 I=1,2

```

PROGRAM RKFND C FRAME 5

```

DO 96 J=1,2
  BDBLFR(I,J)=BMATRIX(I,J)
96 CONTINUE
97 CONTINUE
  CALL BNDINV(BDBLFR,2,DETERM,1.0E-08,ITEST)
DO 105 J=1,2
  DO 100 K=1,2
    BINV(J,K)=BDBLFR(J,K)
100 CONTINUE
105 CONTINUE
DO 115 K=1,2
  DO 110 J=1,512
    DUMMY(K)=DUMMY(K)+AMATRIX(J,K)*F(J)*DEV(J)
110 CONTINUE
115 CONTINUE
DO 125 I=1,2
  DO 120 K=1,2
    CORR(I)=CORR(I)-BINV(I,K)*DUMMY(K)
120 CONTINUE
125 CONTINUE
DO 130 J=1,512
  SQDEV=SQDEV+F(J)*DEV(J)**2
  RMSDEV=RMSDEV+DEV(J)**2
130 CONTINUE
  SIGMA=SQRT(SQDEV/FLOAT(510))
  RMSDV=SQRT(RMSDEV/FLOAT(512))
DO 135 I=1,2
  STNDEV(I)=SQRT(BINV(I,I))*SIGMA
  IF (ABS(CORR(I)/STNDEV(I)).GT.0.01) GO TO 145
135 CONTINUE
  GO TO 150
145 TAU=TAU+CORR(1)
  SCALE=SCALE+CORR(2)
  IF (ITER.GE.50) GO TO 146
  GO TO 45
C *****
C *****
C *****
C *****
C PRINTOUT SECTION
C -----
C *****
146 WRITE(6,147) ITER
147 FORMAT (1H1////1H0,37HTHE SOLUTION HAS NOT CONVERGED AFTER ,I3,
166H ITERATIONS. THE PRESENT STATUS OF THE CALCULATION FOLLOWS BEL
20W.)
  WRITE(6,148)
148 FORMAT (1H0////78H0THE PRESENT VALUES OF THE PARAMETERS, WITH THEI
1R STANDARD DEVIATIONS, ARE..../1H0,20X,9HPARAMETER,32X,18HSTANDARD
2 DEVIATION/1H0)
  GO TO 155
150 WRITE(6,152)
152 FORMAT (1H0////78H0THE BEST ESTIMATES OF THE PARAMETERS, WITH THEI
1R STANDARD DEVIATIONS, ARE..../1H0,20X,9HPARAMETER,32X,18HSTANDARD
2 DEVIATION/1H0)
155 WRITE(6,157) TAU,STNDEV(1),SCALE,STNDEV(2)
157 FORMAT (1H ,16X,1PE16.8,30X,1PE16.8)
  WRITE(6,160) SIGMA,RMSDV
160 FORMAT (1H0,38X,7HSIGMA= ,F12.5/1H ,38X,7HRMSDV= ,F12.5)
  WRITE(6,165)

```

PROGRAM RKFNDC FRAME 6

```

165 FORMAT (1H1////1H0,9X,4HTIME,15X,6HEXP.INT.,3G0,9HCALC.INT.,16X,
19HDEVIATION/1H )
DO 175 J=1,512
WRITE(6,170) T(J),EMIS(J),XN(J),DEV(J)
170 FORMAT (1H ,6X,F8.3,10X,1PE15.8,23X,1PE15.8,11X,1PE15.8)
175 CONTINUE
IF (ITER.GE.50) GO TO 2000
GO TO (178,1),IFLOT

C *****
C *****
C *****
C *****
C          PLOTTING ROUTINE
C          -----
C *****
C          *****
C          SEARCH THE DATA FOR THE MAXIMUM AND MINIMUM VALUES, TO BE USED
C          IN ESTABLISHING THE SCALE ALONG THE ORDINATE.
C          *****
178 YMAX=0.0
YMIN=1.0E 20
DO 240 K=1,512
IF (YMAX-XN(K)) 180,180,185
180 YMAX=XN(K)
185 IF (XN(K)-YMIN) 190,190,195
190 YMIN=XN(K)
195 IF (YMAX-EXCINT(K)) 200,200,205
200 YMAX=EXCINT(K)
205 IF (EXCINT(K)-YMIN) 210,210,215
210 YMIN=EXCINT(K)
215 IF (YMAX-EMIS(K)) 220,220,225
220 YMAX=EMIS(K)
225 IF (EMIS(K)-YMIN) 230,230,240
230 YMIN=EMIS(K)
240 CONTINUE
CALL LABEL(0.0,0.0,T(1),90.000,15.0,15,TITLE1,11,0,FMT1,LF1)
CALL LABEL(0.0,0.0,YMIN,YMAX,10.0,5,TITLE2,27,1,FMT2,LF2)
CALL XYFLT(512,T,EMIS,T(1),90.000,YMIN,YMAX,DD,0,3)
CALL XYFLT(512,T,EXCINT,T(1),90.000,YMIN,YMAX,DD,0,1)
CALL XYFLT(512,T,XN,T(1),90.000,YMIN,YMAX,DD,1)
GO TO 1

C *****
C *****
C *****
C *****
C          ERROR MESSAGES
C          -----
C *****
2000 WRITE(6,2001)
2001 FORMAT (1H1////1H0,5X,61HSCUTICN HAS NOT CONVERGED. PLOTS SKIP
1PED, EXECUTION HALTED.)
GO TO 3000

C *****
C *****
C *****
C *****
C          INTERNAL ABEND
C          -----
C *****
3000 STOP

```

PROGRAM RKFNDC FRAME 7

C \*\*\*\*\*  
C \*\*\*\*\*  
END

## SUBROUTINE INTERF FRAME 1

```
C *****  
C E. B. PRIESTLEY APRIL 4, 1969  
C THIS SUBROUTINE IS USED TO INTERPOLATE VALUES BETWEEN KNOWN POINTS  
C ON A CURVE. IT IS USED IN CONJUNCTION WITH PROGRAM EBPREN TO  
C INTERPOLATE VALUES OF THE EXCITATION AND EMISSION INTENSITIES.  
C *****  
C *****  
C          PROGRAM INITIALIZATION  
C          -----  
C *****  
C      SUBROUTINE INTERF(XINTVL,VALUE,J,VECTOR)  
C      DIMENSION VECTOR(520)  
C      *****  
C      *****  
C          MAIN SECTION OF THE PROGRAM  
C          -----  
C *****  
C      VALUE=(XINTVL-1.0)*(XINTVL-2.0)*(3.0-XINTVL)*VECTOR(J)/6.0+  
C      1*XINTVL*(XINTVL-2.0)*(XINTVL-3.0)*VECTOR(J+1)/2.0+XINTVL*  
C      2*(XINTVL-1.0)*(3.0-XINTVL)*VECTOR(J+2)/2.0+XINTVL*(XINTVL-1.0)*  
C      3*(XINTVL-2.0)*VECTOR(J+3)/6.0  
C      *****  
C      *****  
C          BEAT A HASTY RETREAT  
C          -----  
C *****  
C      RETURN  
C      *****  
C      *****  
C      END
```

**PART V**

**PROPOSITIONS**



### PROPOSITION I

It is proposed that the phonon density of states function and dispersion law for molecular crystals be investigated using neutron-scattering spectroscopy. Naphthalene and anthracene are cited as examples of molecular crystals for which the results of such a study would be of particular interest.

It is well-known that the motion of the particles (atoms, molecules, ions) comprising a lattice can be analyzed into a set of lattice waves.<sup>1</sup> These quantized lattice waves, originally termed phonons by Frenkel,<sup>2</sup> are the fundamental entities from which sound waves are composed. Almost all of the concepts that are familiar from the study of photons, such as the wave-particle duality, are equally applicable to phonons. Thermal vibrations in crystals are thermally excited phonons analogous to the thermally excited photons of black-body electromagnetic radiation in a cavity. Again, in analogy to the electromagnetic photon field, one customarily speaks of a phonon field which is capable of absorbing or emitting quanta of vibrational excitation.

The most characteristic property of phonons is their dispersion law, that is, the relationship between their frequency and wavenumber. This relationship can be calculated from first principles in a few simple cases, a linear chain of atoms and simple cubic lattices being examples. However, for more complex crystal structures the dispersion law must be determined experimentally. A second important

characteristic of phonons is their density of states function. The best way of obtaining the dispersion curve as well as the density of states function experimentally has been found to be the study of inelastic scattering of thermal neutrons by the crystal. Unlike photons, which are scattered by the atomic or molecular electronic distribution (as in Raman scattering, for example), neutrons are predominantly scattered by atomic nuclei. If the nuclei are static only elastic scattering can occur, the frequency of the scattered wave being identical to that of the incident wave. If on the other hand the nuclei are moving, due to thermal or some other form of excitation, the scattered wave suffers a Doppler shift so that some fraction of the outgoing neutron wave will be of different energy than the incident wave. Because the neutron and atomic masses are comparable, momentum transfers between the neutrons and atoms sufficient to span the entire Brillouin zone<sup>1</sup> are experimentally accessible. This is in contradistinction to photon scattering for which momentum conservation at least in the case of one-phonon processes restricts the phonon frequency measurements to the region near the origin of the Brillouin zone.

The basic experiment consists of measuring the energy of neutrons scattered at various angles out of a nearly mono-energetic incident beam, due to collisions with moving atomic nuclei in the sample. If the sample contains strongly incoherent scattering nuclei, then the technique measures the uncorrelated motions of single atoms and this leads directly to the phonon density of states spectrum. If the scattering is predominantly coherent, the scattered waves from various lattice sites may add constructively or destructively so that

information about the correlated motions of atoms separated in the lattice by some given distance, governed by the momentum transfer, is obtained. It is thus possible to determine the frequencies and wave vectors of phonons throughout the energy-momentum space using neutron-scattering spectroscopy.

This technique has been successfully applied to metallic crystals such as Al, Pb, Na; ionic crystals of which NaI and KBr are examples; and graphite which is a covalent crystal.<sup>3</sup> However, no work has been done on a large class of crystals that appears to have the requisite properties for such a study, *viz.*, molecular crystals. Typical of this group are benzene, naphthalene and anthracene as well as the rare gas solids. Recent calculations of the dispersion curves and phonon frequencies for naphthalene and anthracene crystals<sup>4</sup> make them particularly appealing samples for an experimental investigation of this sort. Furthermore, a great deal is known about the electronic properties of these crystals<sup>5</sup> and the sort of information obtainable from neutron-scattering spectroscopy about the lattice dynamics would be entirely complimentary to existing data.

The theory of inelastic scattering of slow neutrons was first given in detail by Weinstock<sup>6</sup> using the Born approximation. The theory has since been amplified by Cassels,<sup>7</sup> Waller and Froman,<sup>8</sup> Kothari and Singwi,<sup>9</sup> and by Van Hove.<sup>10</sup> The first experiments which demonstrated that the complete dispersion diagram could be constructed from neutron scattering data were performed by Brockhouse and Stewart.<sup>11</sup> To illustrate the principles of neutron scattering,<sup>12</sup> we consider the amplitude of the total wave field scattered from a system

of moving nuclei, when a well collimated, mono-energetic neutron beam is incident. The incident neutron beam is represented by

$$\psi_0(\vec{r}, t) = \exp[i(\vec{k}_0 \cdot \vec{r} - \omega_0 t)] \quad (\text{PI-1})$$

where  $\hbar^2 k_0^2 / 2m = \hbar \omega_0$  is the neutron energy, and  $\hbar \vec{k}_0$  is the neutron momentum. In the presence of an assembly of nuclei this beam is acted on by the time-dependent Hamiltonian operator

$$H = H_0 + \sum_n \frac{2\pi\hbar^2}{m} b_n \delta\{\vec{r} - \vec{R}_n(t_0)\} \quad (\text{PI-2})$$

where  $H_0 = -\frac{\hbar^2}{2m} \nabla^2$ ,  $\vec{R}_n(t)$  is the position of nucleus  $n$  at time  $t$  and  $b_n$  is the scattering length of the nucleus at  $\vec{R}_n$  ( $\vec{R}_n$  is an operator and care must be exercised in manipulation not to violate commutation properties with other nuclear co-ordinates to which the nucleus at  $\vec{R}_n$  is dynamically coupled). The scattered wave field then develops according to the time-dependent Schrödinger equation

$$i\hbar \frac{\partial}{\partial t} \psi(\vec{r}, t)|_{t_0} = \left[ H_0 + \sum_n \frac{2\pi\hbar^2}{m} b_n \delta\{\vec{r} - \vec{R}_n(t_0)\} \right] \psi(\vec{r}, t)|_{t_0} . \quad (\text{PI-3})$$

Writing  $\psi(\vec{r}, t) = \psi_0(\vec{r}, t) + \psi_s(\vec{r}, t)$  and keeping only first order perturbation terms, yields

$$\begin{aligned} & \left( i\hbar \frac{\partial}{\partial t} + \frac{\hbar^2}{2m} \nabla^2 \right) \psi_s(\vec{r}, t)|_{t_0} \\ &= \frac{2\pi\hbar^2}{m} \sum_n b_n \delta\{\vec{r} - \vec{R}_n(t_0)\} \psi_0(\vec{r}, t_0) . \end{aligned} \quad (\text{PI-4})$$

Thus, the total scattered wave field is the result of the superposition

of the solutions representing waves originating at all earlier times from the source terms on the right hand side of Eq. (PI-4). The solution is readily obtained using the Green's function method.<sup>13</sup> Restricting the solution to large  $\vec{r}$  and Fourier transforming it with respect to time yields a scattering amplitude

$$f(\vec{k}, \omega_1) = \frac{1}{rT} \int_0^T dt_0 \exp[-i\omega t_0] \sum_n b_n \int d\vec{r}' \delta\{\vec{r}' - \vec{R}_n(t_0)\} \times \exp[i\vec{Q} \cdot \vec{r}'] \quad (\text{PI-5})$$

where  $\vec{Q} = \vec{k}_0 - \vec{k}$  and  $\omega = \omega_0 - \omega_1$  and where  $T$  is some long time used as the period for the Fourier transformation. The differential scattering cross-section is proportional to the square of  $f(\vec{k}, \omega_1)$  and has the form

$$\frac{\partial^2 \sigma}{\partial \Omega \partial \omega} = \frac{\vec{k}}{k_0} \frac{1}{2\pi} \iint d\tau \exp[-i\omega\tau] \sum_{m,n} b_m^* b_n \times \exp[i\vec{Q} \cdot (\vec{r} - \vec{r}'')] \delta\{\vec{r}'' - \vec{R}_m(0)\} \delta\{\vec{r} - \vec{R}_n(\tau)\} d\vec{r}'' d\vec{r} \quad (\text{PI-6})$$

$$= \frac{\vec{k}}{k_0} \frac{1}{2\pi} \int_{-\infty}^{\infty} d\tau \exp[-i\omega\tau] \sum_{m,n} b_m^* b_n \exp\{i\vec{Q} \cdot [\overline{\vec{R}_n(\tau)} - \vec{R}_m(0)]\} \quad (\text{PI-7})$$

where the bar denotes the time average. This differential scattering cross-section describes the experimentally observable intensity distribution of the scattered neutrons, as a function of the energy transferred ( $\hbar\omega$ ) and the solid angle of scatter, provided the incident neutron beam is nearly mono-energetic.

The two  $\delta$ -functions in Eq. (PI-6) define a space-time correlation function<sup>10</sup>

$$G(\vec{r}, \tau) = \frac{1}{N} \sum_{m,n} \int d\vec{r}' \overline{\delta\{\vec{r} + \vec{R}_m(0) - \vec{r}'\} \delta\{\vec{r}' - \vec{R}_n(\tau)\}} \quad (\text{PI-8})$$

where  $N$  is the number of scatterers in the sample. The sum in Eq. (PI-8) contains two types of terms; those for which  $n$  is equal to  $m$  and those for which  $n$  is not equal to  $m$ . The correlation function can thus be split into two parts, the "self" correlation function  $G_s(\vec{r}, \tau)$  concerned with the positions and time-dependent motion of the same scatterer and the "distinct" correlation function  $G_d(\vec{r}, \tau)$  which describes the time dependence of the correlated motions of two scatterers. The differential scattering cross-section can be separated into two terms which involve the double Fourier transforms of these two correlation functions. Before displaying these equations which describe coherent and incoherent scattering, it seems appropriate to consider the origin of the two types of scattering. For nuclei without nuclear spin the scattering length is the same for every nucleus and neutrons incident on different atoms in the lattice are scattered coherently. When the scattering nucleus has spin, however, there are different scattering lengths associated with the different relative orientations of the nuclear and neutron spins. This can lead to amplitude differences in the scattering from neighboring atoms and hence to an overall incoherent scattering. More generally, the interference effects giving rise to the coherent scattering depend only on the average scattering length

whereas the mean square deviation from this average governs the incoherent scattering. Making use of the above considerations, the differential cross-sections for coherent and incoherent scattering can be written as

$$\frac{\partial^2 \sigma^{\text{coh.}}}{\partial \Omega \partial \omega} = \frac{b_c^2 N}{2\pi} \frac{\vec{k}}{k_0} \int d\vec{r} d\tau \exp[i(\vec{Q} \cdot \vec{r} - \omega\tau)] G_d(\vec{r}, \tau) \quad (\text{PI-9})$$

and

$$\frac{\partial^2 \sigma^{\text{incoh.}}}{\partial \Omega \partial \omega} = \frac{b_i^2 N}{2\pi} \frac{\vec{k}}{k_0} \int d\vec{r} d\tau \exp[i(\vec{Q} \cdot \vec{r} - \omega\tau)] G_s(\vec{r}, \tau) \quad (\text{PI-10})$$

respectively, where  $b_c$  is the coherent scattering length and  $b_i$  is the incoherent scattering length.

The differential cross-section for incoherent scattering can be re-written in terms of a scattering law  $S(\vec{Q}, \omega)$

$$\frac{\partial^2 \sigma^{\text{incoh.}}}{\partial \Omega \partial \omega} = b_i^2 \frac{\vec{k}}{k_0} \exp[-(\hbar\omega/kT)] S(\vec{Q}, \omega) \quad (\text{PI-11})$$

The density of states function  $Z(\omega)$  is related to  $S(\vec{Q}, \omega)$  through Eq. (PI-12),

$$Z(\omega) = \frac{4M\omega}{\hbar} \sinh(\hbar\omega/2kT) \lim_{Q \rightarrow 0} [S(\vec{Q}, \omega)/Q^2] \quad (\text{PI-12})$$

where  $M$  is the mass of the scattering atom and  $T$  is the absolute temperature. From Eqs. (PI-11) and PI-12) it is evident that the density of phonon states can be determined directly from a measurement of the differential cross-section for incoherent neutron scattering.

To see that the dispersion law can be obtained from the differential cross-section for coherent scattering, the nuclear position vectors  $\vec{R}_n$  are written as the sum of equilibrium position vectors  $\vec{P}_n$  and small displacements  $\vec{\mu}_n$ ,

$$\vec{R}_n = \vec{P}_n + \vec{\mu}_n \quad (\text{PI-13})$$

Expansion of the  $\vec{\mu}_n$  in terms of the phonon normal modes makes it possible by means of some rather lengthy but straightforward manipulations to write Eq. (PI-7) in the form

$$\begin{aligned} \frac{\partial^2 \sigma^{\text{coh.}}}{\partial \Omega \partial \omega} &= \frac{\hbar b_c^2 (2\pi)^3}{V} \sum_{\vec{q}} \frac{\vec{k}}{k_0} \delta(\hbar\omega \mp \hbar f) \sum_{\vec{\tau}} \delta(\vec{Q} \mp \vec{q} - 2\pi\vec{\tau}) \\ &\times |\vec{Q} \cdot \vec{U}|^2 \frac{\hbar(n + \frac{1}{2} \pm \frac{1}{2})}{2Mf} \exp(-2W) \end{aligned} \quad (\text{PI-14})$$

where  $V$  is the crystal volume,  $f$  and  $\vec{q}$  are the frequency and wave vector of a phonon,  $\vec{\tau}$  is a reciprocal lattice vector and  $W$  is given by

$$W = \sum_{\vec{q}} \frac{|\vec{Q} \cdot \vec{U}|^2 \hbar(n + \frac{1}{2})}{2NfM} \quad (\text{PI-15})$$

The vectors  $\vec{U}$  are polarization vectors and take account of the various polarizations and amplitudes of vibration for atoms excited in the phonon motion. The factor  $\exp(-2W)$ , known as the Debye-Waller factor, evidently gives the dependence of the intensity of scattering upon the momentum transfer and the thermal vibration amplitudes. The first  $\delta$ -function in Eq. (PI-14) is an expression of the law of conservation of energy and the second  $\delta$ -function defines the so-called crystal



momentum conservation law. Because of these stringent conditions for phonon excitation, it is possible by the correct choice of crystal orientation, incident and outgoing neutron wave vectors, and hence the direction of momentum transfer, to excite only phonons of selected frequencies along chosen crystallographic directions.

Equations (PI-11) and (PI-14) apply specifically to one-phonon changes in the state of a crystal having a single molecule per unit cell. Generalizations of the equations to include multi-phonon processes in crystals with more than one molecule per unit cell can be made in a straightforward manner. The phonon spectrum in crystals having more than one molecule per unit cell shows some additional features. For each polarization in a given propagation direction the dispersion relation has two branches known as the acoustical and optical branches. Two characteristics of the spectrum are noteworthy, viz., acoustical branches always pass through the origin (i. e.,  $\omega(0) = 0$ ) and optical branches always approach  $|q| = 0$  with zero slope (i. e.,  $d\omega(\vec{q})/d\vec{q}|_{|q|=0} = 0$ ).

In conclusion, we consider the requisite properties<sup>3</sup> that a crystal should have in order that it can be conveniently studied by neutron-scattering spectroscopy.

1. Large single crystals (from 1 to 10 cubic centimeters in volume) must be obtainable.
2. The crystal should be as free from defects as possible.
3. It is desirable that the melting point be high and that no low temperature phase transitions occur. The crystal can then be studied at a convenient temperature and storage is no problem.

4. The crystal structure should be simple so that the number of branches is not too large. Crystals having as many as fifteen branches have been successfully studied in the past.
5. The phonon frequencies should be neither too high nor too low compared to the mean neutron frequency. For thermal neutrons ( $\sim 0.025$  eV in energy),  $\nu \approx 6 \times 10^{12}$  sec<sup>-1</sup>.
6. The neutron capture and incoherent scattering cross-sections should be small compared to the coherent cross-section for dispersion law measurements. For density of states measurements, of course, a large incoherent scattering cross-section is desirable.

The first two criteria in the above list can be met if sufficient care is exercised in growing either naphthalene or anthracene crystals. The third criterion presents no problem since naphthalene (m. p. 80°C) and anthracene (m. p. 217°C) can be conveniently handled at room temperature. With two molecules per unit cell, six branches are expected in the phonon dispersion relation for both crystals. Phonon frequencies in these crystals are known to lie in the range from 0.5 -  $6 \times 10^{12}$  sec<sup>-1</sup> which is very close to the frequency of thermal neutrons. Scattering by hydrogen is almost completely incoherent while that from deuterium is almost entirely coherent.<sup>14</sup> Carbon has a negligible incoherent scattering cross-section and the capture cross-section<sup>15</sup> for all three atoms is very small. It seems most practical, therefore, to use perdeuterated naphthalene and anthracene for the dispersion law measurements (coherent scattering) and the perprotonated analogs for the density of states determinations (incoherent scattering).

On the basis of the above considerations it is concluded that neutron-scattering spectroscopy could be used to obtain the phonon dispersion relation and density of states function for crystalline naphthalene and anthracene. In view of the importance of a good understanding of phonons in these crystals, this type of experimental study is considered to be very worthwhile.

# REFERENCES

1. See, for example, C. Kittel, Introduction to Solid State Physics (John Wiley and Sons, Inc., New York, 1966), 3rd ed.; or J. M. Ziman, Electrons and Phonons (Oxford University Press, 1960).
2. J. Frenkel, Wave Mechanics, Elementary Theory (Oxford University Press, 1932), 1st ed., p. 265.
3. Recent reviews have been given by B. N. Brockhouse, "Phonons and Neutron Scattering" in Phonons and Phonon Interactions, Thor A. Bak Ed. (W. A. Benjamin, Inc., New York, 1964); and W. M. Lomer and G. G. Low, Thermal Neutron Scattering, P. A. Egelstaff, Ed. (Academic Press, Inc., New York, 1965).
4. G. S. Pawley, Phys. stat. sol. 20, 347 (1967).
5. D. P. Craig and S. H. Walmsley, Excitons in Molecular Crystals (W. A. Benjamin, Inc., New York, 1968).
6. R. Weinstock, Phys. Rev. 65, 1 (1944).
7. J. M. Cassels, Progress in Nuclear Physics, O. Frisch, Ed. (Academic Press, Inc., New York, 1950), Vol. 1.
8. I. Waller and P. O. Froman, Arkiv Fysik 4, 183 (1952).
9. L. S. Kothari and K. S. Singwi, Solid State Physics, F. Seitz and D. Turnbull, Eds. (Academic Press, Inc., New York, 1958), Vol. VIII.
10. L. Van Hove, Phys. Rev. 95, 249 (1954).
11. B. N. Brockhouse and A. T. Stewart, Phys. Rev. 100, 756 (1955); Rev. Mod. Phys. 30, 236 (1958).

12. The treatment follows reference 3 for the most part.
13. J. Mathews and R. L. Walker, Mathematical Methods of Physics (W. A. Benjamin, Inc., New York, 1965).
14. Neutron Cross-Sections, USAEC (McGraw-Hill Book Co., Inc., New York, 1955).
15. Atlas of X-ray Spectra from Radiative Capture of Thermal Neutrons (Pergamon Press, New York, 1959).

## PROPOSITION II

Conventional one-photon triplet-triplet absorption spectroscopy has been used to study highly excited triplet states in most of the polyacenes. Several of the more interesting polyacene molecules are centrosymmetric so that only transitions between states of opposite parity are allowed. Consequently, many excited triplet states having the same parity as the lowest triplet state have not been experimentally observed. It is proposed that two-photon triplet-triplet absorption spectroscopy be used to study these states since the selection rules for two-photon absorption require that transitions occur between states of the same parity.

One-photon triplet-triplet absorption has been used extensively to investigate the excited triplet states of many of the polyacene molecules.<sup>1-11</sup> However, in centrosymmetric molecules dipole selection rules require that the initial and final states in a one-photon transition have opposite parity. Consequently, for molecules such as benzene, naphthalene and anthracene many of the excited triplet states cannot be studied using this technique. It is proposed that these states be observed using two-photon triplet-triplet absorption spectroscopy since the selection rules for two-photon absorption require that transitions occur between states of the same parity. By analogy with the well documented one-photon transitions, these two-photon transitions should

be characterized by an oscillator strength near unity and give rise to an intense absorption spectrum containing information that is largely complementary to that derived from the one-quantum spectrum.

The areas in which this type of investigation could be of potential value are too numerous to enumerate here. Suffice it to cite one example, namely the problem of determining at what point, as one considers higher and higher excited states of a molecular crystal, the Frenkel tight-binding approximation ceases to be a valid description of the exciton state. There may in fact be no sharp demarcation, but it will not be possible to draw any conclusion until the complete excited state manifold has been studied. Perhaps the most equitable way of evaluating the proposed experiments is to say that they have the potential of providing new input to a number of existing problems and, like any other untried experiment, they may even hold some unexpected surprises.

The theory of two-photon transitions was formulated many years ago by Göppert-Mayer<sup>12</sup> and has been reconsidered in light of the present availability of high powered lasers in two recent papers by Kleinman<sup>13</sup> and Braunstein.<sup>14</sup> The derivation, based on well-known results from time-dependent perturbation theory, is considered below.

The electromagnetic field is treated classically and enters the problem only via the perturbation Hamiltonian. Consequently, as far as the quantum mechanical treatment is concerned, the system consists of the molecules of interest and perhaps their environment and, in the absence of the radiation field, is described by a Hamiltonian  $H_0$  and eigenfunctions  $u_n$ , which satisfy

$$H_0 u_n = E_n u_n . \quad (\text{PII-1})$$

In the presence of an electromagnetic field of frequency  $\omega$ , the system is perturbed so that the appropriate Hamiltonian describing the system is then

$$H = H_0 + H'(t) . \quad (\text{PII-2})$$

The solution  $\psi(t)$  of the time-dependent Schrödinger equation

$$\frac{\partial \psi(t)}{\partial t} = -\frac{i}{\hbar} H\psi(t) \quad (\text{PII-3})$$

can be expanded, at any time  $t$ , in terms of the complete orthonormal set  $u_n$ , which are the solutions of Eq. (PII-1), according to

$$\psi(t) = \sum_n a_n(t) u_n e^{-iE_n t/\hbar} . \quad (\text{PII-4})$$

Substitution of Eq. (PII-4) in Eq. (PII-3) leads straightforwardly to an alternate but entirely equivalent form for the Schrödinger equation [Eq. (PII-3)], given by

$$\dot{a}_k = -\frac{i}{\hbar} \sum_n a_n H'_{kn}(t) e^{i\omega_{kn}t} \quad (\text{PII-5})$$

where  $\dot{a}_k$  stands for the time derivative of  $a_k$ ,  $H'_{kn}(t)$  is the matrix element  $\langle u_k | H'(t) | u_n \rangle$  and  $\omega_{kn}$  is defined by

$$\omega_{kn} = (E_k - E_n)/\hbar .$$

Substitution of the usual perturbation expansion for the  $a_n$  into Eq. (PII-5) results in the following identities:



$$\begin{aligned}
\dot{a}_k^{(0)} &= 0 \\
\dot{a}_k^{(1)} &= -\frac{i}{\hbar} \sum_n a_n^{(0)} H'_{kn}(t) e^{i\omega_{kn}t} \\
\dot{a}_k^{(2)} &= -\frac{i}{\hbar} \sum_n a_n^{(1)} H'_{kn}(t) e^{i\omega_{kn}t} \\
&\vdots \\
\dot{a}_k^{(S)} &= -\frac{i}{\hbar} \sum_n a_n^{(S-1)} H'_{kn}(t) e^{i\omega_{kn}t} .
\end{aligned} \tag{PII-6}$$

Assuming a harmonic perturbation, we can write the perturbation matrix elements as

$$H'_{km}(t) = \frac{H'_{km}}{2} (e^{i\omega t} + e^{-i\omega t}) . \tag{PII-7}$$

Combining Eq. (PII-7) with the first two of Eqs. (PII-6), performing the necessary integration and substituting the result into the third of Eqs. (PII-6) yields, for  $\dot{a}_\ell^{(2)}(t')$

$$\begin{aligned}
\dot{a}_\ell^{(2)}(t') &= \frac{i}{4\hbar^2} \sum_n H'_{nm} H'_{\ell n} \left[ \frac{1 - e^{i(\omega - \omega_{mn})t'}}{\omega_{mn} - \omega} + \frac{1 - e^{-i(\omega_{mn} + \omega)t'}}{\omega_{mn} + \omega} \right] \\
&\times (e^{i\omega t'} + e^{-i\omega t'}) e^{-i\omega_{n\ell}t'} .
\end{aligned} \tag{PII-8}$$

Integration of Eq. (PII-8) gives numerous terms, most of which are negligible. Keeping only terms for which the denominator may become small, we obtain for  $a_\ell^{(2)}(t)$

$$a_{\ell}^{(2)}(t) = \frac{i}{4\hbar^2} H'_{mn} H'_{\ell n} \left\{ \frac{e^{i(\omega_{\ell n} - \omega)t} - 1}{(\omega_{\ell n} - \omega)(\omega - \omega_{nm})} + \frac{e^{-i(2\omega - \omega_{\ell m})t} - 1}{(2\omega - \omega_{\ell m})(\omega - \omega_{nm})} \right\} \quad (\text{PII-9})$$

where  $\omega_{nm} + \omega_{\ell n} = \omega_{\ell m}$  has been used.

Resonant absorption occurs when  $2\omega = \omega_{\ell m}$  so that only the second term in Eq. (PII-9) is important. The absolute square of this term, which is the probability that between  $t=0$  and  $t$  the system makes a transition from the state  $m$  to the state  $\ell$ , is

$$|a_{\ell}^{(2)}(t)|^2 = \frac{|H'_{nm} H'_{\ell n}|^2}{16\hbar^4(\omega - \omega_{nm})^2} \frac{\sin^2 \frac{1}{2}(2\omega - \omega_{\ell m})t}{[\frac{1}{2}(2\omega - \omega_{\ell m})]^2} \quad (\text{PII-10})$$

Assuming that due to "smearing" of level  $\ell$ ,  $m$  or both, only the probability of finding the difference frequency  $(2\omega - \omega_{\ell m})$  is meaningful and describing this probability per unit frequency interval by  $\rho(2\omega - \omega_{\ell m})$ , it is easy to derive a rate expression for two-photon transitions that is analogous to Fermi's "Golden Rule". This expression has the form

$$W = \frac{\pi}{8\hbar^4} \frac{|H'_{nm} H'_{\ell n}|^2}{(\omega - \omega_{nm})^2} \rho(2\omega = \omega_{\ell m}) \quad (\text{PII-11})$$

If both matrix elements  $H'_{nm}$  and  $H'_{\ell n}$  are of the electric dipole type, then, for an electric field in the  $x$  direction,

$$\begin{aligned} H'_{nm} &\sim e x_{nm} E \\ H'_{\ell n} &\sim e x_{\ell n} E \end{aligned} \quad (\text{PII-12})$$

where  $E$  is the amplitude of the electric field. Consequently, according to Eq. (PII-11), the transition rate from  $m$  to  $l$  should be proportional to  $E^2$ , i. e., to the second power of the intensity.

We turn now to a discussion of an experimental arrangement suitable for performing the proposed two-photon absorption measurements. In the early two-quantum absorption experiments,<sup>15</sup> both photons were obtained from a narrow-band laser source. However, Hopfield *et al.*<sup>16</sup> have demonstrated that one of the photons can just as well come from a continuous broad-band source such as a xenon arc lamp. This allows for investigation of a broad spectral region.

For the present purpose, a giant-pulse neodymium laser (1.06  $\mu$  radiation) is suggested since two laser photons would not provide sufficient energy to cause two-quantum absorption from the ground state to the lowest excited singlet state of any of the smaller polyacene molecules. A high intensity ultraviolet light source could be used to populate the lowest triplet state via intersystem crossing from the singlet manifold. Absorption of photons from a weak continuum light passing through the sample, that could be correlated with the presence of both the laser pulse and the xenon excitation source, would be identified as the sought after transitions. Further confirmation of the two-photon nature of these absorptions would result from a demonstration that the transition rate was linearly dependent upon the intensity of both the laser and the spectroscopic continuum. Thus, there should be no problem in verifying either the triplet-triplet, or the two-photon nature of the observed absorptions.

REFERENCES

1. D. S. McClure, J. Chem. Phys. 19, 670 (1951).
2. D. P. Craig and I. G. Ross, J. Chem. Soc. 1589 (1954).
3. G. Porter and M. W. Windsor, Disc. Faraday Soc. 17, 178 (1954).
4. G. Porter and F. J. Wright, Trans. Faraday Soc. 51, 1205 (1955).
5. G. Porter and M. W. Windsor, Proc. Roy. Soc. (London) A245, 238 (1958).
6. M. A. El-Sayed and T. Pavolopoulos, J. Chem. Phys. 39, 834 (1963).
7. G. Porter and F. Wilkinson, Proc. Roy. Soc. (London) A264, 1 (1964).
8. R. M. Hochstrasser and S. Lower, J. Chem. Phys. 40, 1041 (1964).
9. D. P. Craig and G. Fischer, Proc. Chem. Soc. 176 (1964).
10. D. P. Craig and G. Fischer, Trans. Faraday Soc. 63, 530 (1967).
11. E. B. Priestley and G. W. Robinson, J. Chem. Phys. (to be published).
12. M. Göppert-Mayer, Ann. Physik 9, 273 (1931).
13. David A. Kleinman, Phys. Rev. 125, 87 (1962).
14. Rubin Braunstein, Phys. Rev. 125, 475 (1962).
15. W. Kaiser and C. G. B. Garrett, Phys. Rev. Letters 7, 229 (1961).
16. J. J. Hopfield, J. M. Worlock and K. Park, Phys. Rev. Letters 11, 414 (1963).

### PROPOSITION III

An experimental investigation of charge carrier production resulting from direct transitions between the lowest triplet state and the conduction band of pure crystalline naphthalene is proposed. If observable, these direct transitions would provide the first means for making a detailed study of the conduction band. Furthermore, the results of such an investigation would be of great help in interpreting certain features in the triplet-triplet absorption spectrum of isotopic mixed naphthalene crystals at 4.2° K.

Certain generalizations concerning the photoconductive properties of molecular crystals may be drawn from studies of their electrical properties.<sup>1</sup> One of these generalizations is that a large photocurrent with a spectral response identical to the singlet absorption spectrum of the crystal can be generated.<sup>2,3</sup> The frequency threshold for photoconductivity is roughly equivalent to the first singlet excitation frequency of the isolated molecule. Since the lowest conduction band in these crystals lies at a higher energy than the first excited singlet state, it is apparent that light of wavelength near the photoconductivity threshold cannot produce charge carriers directly. It is now widely accepted that, in fact, this light merely produces singlet excitons and that exciton-exciton interactions are responsible for the ultimate

production of free charge carriers.<sup>4-6</sup> It is also evident that if direct transitions from the ground state to the conducting state did occur, they would be masked by the strong singlet-singlet absorption. Consequently, it has not been possible to determine the width or shape of the conduction band in any of the molecular crystals. Clearly, what is needed is a method for direct photoproduction of charge carriers using light of a wavelength that is too long to cause singlet-singlet transitions. Such a method is suggested by the results of a recent investigation of triplet-triplet absorption in isotopic mixed naphthalene crystals at 4.2° K.<sup>7</sup>

Except for a broad, structureless, continuum absorption, the triplet-triplet absorption spectrum of mixed crystals of naphthalene-h<sub>8</sub> in naphthalene-d<sub>8</sub> at 4.2° K<sup>7</sup> correlates well with that of naphthalene-h<sub>8</sub> in glassy media at 77° K.<sup>7-9</sup> The existence of this broad continuum absorption is of considerable interest since it seems to indicate that states of the host crystal may be participating in the triplet-triplet transition. On the basis of energy considerations, and the overall character of the absorption, it appears that the host states most likely to be involved are the conduction and charge-transfer states. If this were true, one would have a means of producing charge carriers by direct absorption of a photon and, furthermore, the energy of the photon necessary to produce these carriers would be too low to cause singlet-singlet absorption.

It is proposed that an experimental search be made for charge carrier production as a result of light absorption by triplet excitons in pure crystalline naphthalene at room temperature. Since the light

required to effect this transition cannot cause singlet-singlet absorption, the spectral response of the photocurrent thus produced would reflect only the structure of the initial and final states in the direct transition. Compared with the triplet exciton (initial state) bandwidth, the width of the conduction band (final state) is very large so that, to a first approximation, the spectral response of the photocurrent so generated could be taken as a measure of the conduction band shape. The results of such experiments would also be useful in interpreting the triplet-triplet absorption spectrum of isotopic mixed naphthalene crystals at 4.2° K.

The following experimental arrangement is suggested. Light from a continuously operated dc xenon arc lamp could be used to populate the lowest triplet state of the crystal via the singlet state by means of intersystem crossing. This light would have to be filtered so as to contain only wavelengths in the region of the first singlet absorption edge. Light from a second dc xenon arc lamp (the photogeneration light), passed through a suitable scanning monochromator, could then be used to scan the region in which photogeneration of charge carriers is expected. The sample cell could be any of the commonly used transparent electrode types.<sup>10</sup> There would be singlet excitons generated in the process of populating the triplet state, and these would give rise to a dc photocurrent through the exciton-exciton interaction mechanism.<sup>4-6</sup> Consequently, it would be necessary to chop the photogeneration light and use lock-in detection in order to single out the process of interest. As a final note we include a numerical estimate of the number of carriers expected and compare this to the minimum number of carriers detectable.

The steady-state concentration of triplet excitons in the crystal is given by

$$n = (m\alpha I_0/\gamma)^{\frac{1}{2}} \quad (\text{PIII-1})$$

provided

$$I_0 \gg \beta^2/4m\alpha\gamma \quad (\text{PIII-2})$$

where  $m$  is the intersystem crossing efficiency,  $\alpha$  is the singlet-singlet absorption coefficient,  $I_0$  is the incident photon flux,  $\gamma$  is the triplet-triplet annihilation rate constant, and  $\beta$  is the reciprocal of the triplet-state lifetime. Photon fluxes of  $10^{16} \text{ cm}^{-2} \text{ sec}^{-1}$ , distributed in a narrow band of frequencies around the singlet absorption edge, are readily obtainable from commercially available dc xenon arc lamps. The values of the other parameters appearing in Eqs. (PIII-1) and (PIII-2) are known to be of the following order of magnitude:

$$m \approx 0.25 ,$$

$$\alpha \approx 10 ,$$

$$\gamma \approx 10^{-11} ,$$

$$\beta \approx 10 .$$

Substituting these values into Eq. (PIII-1), which can be seen to be valid according to the criterion set down in Eq. (PIII-2), gives a steady-state triplet concentration of

$$n \approx 5 \times 10^{13} \text{ cm}^{-3} .$$



If even 1 in  $10^{10}$  of these gave rise to a free charge carrier during a 1 sec time interval, the resulting photocurrent could be detected using presently available lock-in amplifiers. On the basis of the isotopic mixed crystal triplet-triplet absorption spectrum, one would expect several orders of magnitude more charge carrier production by this sort of direct conduction band  $\leftarrow$  triplet state absorption. The experiments therefore appear to be well within the realm of feasibility.

REFERENCES

1. C. G. B. Garrett, Semiconductors, H. B. Hannay Ed., (Reinhold Publishing Corporation, New York, 1959), p. 634.
2. R. G. Kepler, Phys. Rev. 119, 1226 (1960).
3. A. Bree and L. E. Lyons, J. Chem. Phys. 22, 1630 (1954).
4. M. Silver, D. Olness, M. Swicord, and R. C. Jarnagin, Phys. Rev. Letters 10, 12 (1963).
5. S. -I. Choi and S. A. Rice, J. Chem. Phys. 38, 366 (1963).
6. R. G. Kepler and F. N. Coppage, Phys. Rev. 151, 610 (1966).
7. See Part II, Section C of the foregoing thesis.
8. D. S. McClure, J. Chem. Phys. 19, 670 (1951).
9. D. P. Craig and I. G. Ross, J. Chem. Soc. 1954, 1589.
10. G. Castro, Thesis, University of California, Riverside (1964).

#### PROPOSITION IV

Theoretical and experimental values of the Kapitza resistance of a wide range of solids are in disagreement by as much as two orders of magnitude in some cases. Experiments are proposed that would help to elucidate the cause of this large discrepancy.

When heat is conducted from a solid into a liquid, there exists a discontinuity in the temperature at the interface, i. e., there is a small difference in temperature ( $\Delta T$ ) across the boundary. Provided the heat flow ( $\dot{Q}$ ) is small,  $\Delta T/\dot{Q}$  is effectively a thermal resistance, characteristic of the boundary. Since  $\dot{Q}$  is proportional to the interfacial area  $A$ , it is customary to define the boundary resistance in terms of the heat flow per unit area,  $\dot{Q}/A$ . Kapitza resistance ( $R_K$ ) is the thermal resistance at the boundary between a solid and liquid helium,<sup>1,2</sup> and is defined as

$$R_K = A \Delta T / \dot{Q} \quad (\text{PIV-1})$$

Since it provides a prototype study in surface physics, and since it plays an essential role in all low-temperature (below 1° K) experiments, Kapitza resistance has stimulated the interest of many researchers since its discovery nearly 30 years ago.<sup>1</sup>

The presently accepted model used to explain the phenomenon is based on the large acoustic impedance mismatch that exists at the

boundary between most solids and liquid helium. The efficiency of phonon transmission at an interface depends critically on how well the acoustic impedances of the two materials forming the interface are matched. A typical solid may have a density  $\rho$  of 5 gm/cm<sup>3</sup> and transmit sound at a velocity  $v_s$  on the order of  $5 \times 10^5$  cm/sec, whereas at ordinary pressures  $\rho$  and  $v_s$  for liquid helium are 0.14 gm/cm<sup>3</sup> and  $2.4 \times 10^4$  cm/sec, respectively. This means that the acoustic impedance, i. e., the product  $\rho v_s$ , of the solid may be two or three orders of magnitude greater than that of liquid helium. As a result of this acoustic mismatch, a large fraction of the phonons impinging on the interface from both sides cannot pass through.

Khalatnikov<sup>3</sup> was the first to develop a detailed theoretical treatment of Kapitza resistance, based on this model; recent theoretical work<sup>4,5</sup> has been limited mostly to refinements of Khalatnikov's original theory. However, it is generally found that theoretical  $R_K$  values are from one to two orders of magnitude greater than the corresponding experimentally measured values. In other words, the energy flux across the interface that can be accounted for by the acoustic mismatch theory<sup>3</sup> is much smaller than the energy flux actually observed. It has been suggested,<sup>4,5</sup> that improved acoustic impedance matching would result if a film of dense helium were to form at the interface. Theoretical estimates of the thickness of the film necessary to obtain reasonable agreement between theoretical and experimental  $R_K$  values range from 15 Å to several microns. The binding between the film and substrate has been analyzed by Franchetti<sup>6</sup> in terms of van der Waals forces. Although there is good theoretical basis for

suspecting such a film, there have been no reports of experiments designed specifically to investigate the region very near the solid-liquid interface. It is the purpose of this proposition to suggest two experiments that would help to elucidate the physical structure of the region near solid-helium interfaces.

The first experiment utilizes optical reflectance techniques<sup>7</sup> to determine the thickness of the helium film. When light is reflected at normal incidence from the interface between two non-conducting media, the reflection coefficient is

$$R_0 = \left[ (n_0 - n_1) / (n_0 + n_1) \right]^2 \quad (\text{PIV-2})$$

where  $n_0$  and  $n_1$  are the refractive indices of the two media.  $R_0$  is defined as the ratio of the reflected intensity to the incident intensity. If a thin film is present on a substrate, light will be reflected from both the film surface and the film-substrate interface. For light of wavelength  $\lambda$ , normally incident on a layer of thickness  $d_1$  and refractive index  $n_1$  which is on a substrate of refractive index  $n_2$ , the reflection coefficient is

$$R = \frac{r_1^2 + 2r_1r_2 \cos 2\delta_1 + r_2^2}{1 + 2r_1r_2 \cos 2\delta_1 + r_1^2r_2^2} \quad (\text{PIV-3})$$

where  $r_1 = (n_0 - n_1) / (n_0 + n_1)$ ,  $r_2 = (n_1 - n_2) / (n_1 + n_2)$ , and  $\delta_1 = 2\pi n_1 d_1 / \lambda$ . From a measurement of  $R$  at two different wavelengths, both the refractive index  $n_1$  and the thickness  $d_1$  of the film can be found.

Most experimental measurements of  $R_K$  have involved the use

of metals as the solid, and, of the metals used, copper has been by far the most common. However, the reflection theory outlined above is valid only for non-conducting media. Therefore, a non-conductor with an affinity for helium atoms similar to that of copper is required for the proposed experiment. On the basis of Franchetti's<sup>6</sup> work, diamond is suggested as the best material for these reflectance measurements. It is expected to bind helium atoms with roughly 80% of the efficiency with which copper binds them, and its high index of refraction ensures relatively strong reflection signals. If evidence for the helium film were found from these initial experiments using diamond, it would then be of great interest to study other materials such as boron carbide, sapphire, and quartz.

The second experiment involves measuring the Kapitza resistance of a molecular crystal like anthracene. Franchetti's theory<sup>6</sup> predicts that this sort of crystal should be much less efficient than copper and diamond at binding helium atoms so that the helium film at the interface is expected to be much less significant. On this basis, one would anticipate better agreement between the measured  $R_K$  and that calculated from Khalatnikov's theory for anthracene than is typically obtained for metal-helium interfaces.

These experiments are not totally without drawback. In the reflection coefficient measurements, the film, if it exists, would undoubtedly be inhomogeneous. In this case the theory becomes somewhat more complex and interpretation of the results more difficult. In addition, if the helium film were more "liquid-like" than "solid-like", the difference in the refractive indices of the film and the bulk liquid

helium might be small enough to cause difficulty. However, this is not expected to be a problem since the indications are that film will be sufficiently "solid-like". Low thermal conductivity may cause some difficulty in measuring  $\Delta T$  across the anthracene-helium interface. Also, since anthracene is a comparatively soft solid, it may be difficult to prepare good surfaces whose area can be accurately determined. This latter difficulty is present to some extent in all Kapitza resistance measurements. The results of these experiments and others of a similar nature should help in deciding whether a "solid-like" helium film at the interface is in fact responsible for the anomalously large thermal transport across the interface, or whether some other unknown mechanism is operative.

REFERENCES

1. P. L. Kapitza, Zh. Eksp. Teor. Fiz. 11, 1 (1941), [J. Phys. U.S.S.R. 4, 181 (1941)]. This paper has also been reprinted in Collected Papers of P. L. Kapitza, D. ter Haar Ed. (Pergamon Press Ltd., Oxford, 1967), Vol. II.
2. The subject of Kapitza resistance has been reviewed recently by G. L. Pollack, Rev. Mod. Phys. 41, 48 (1969).
3. I. M. Khalatnikov, Zh. Eksp. Teor. Fiz. 22, 687 (1952).
4. L. J. Challis, K. Dransfeld, and J. Wilks, Proc. Roy. Soc. (London) A260, 31 (1961).
5. L. J. Challis and J. Wilks, Physica Suppl. 24, 145 (1958).
6. S. Franchetti, Nuovo Cimento 4, 1504 (1956).
7. O. S. Heavens, Optical Properties of Thin Solid Films, (Academic Press, Inc., Butterworths Scientific Publications, London, 1955).



### PROPOSITION V

Pulsed EPR measurements are proposed as a means of elucidating the role of paramagnetic metal ions in the enzymatic activity of metal-containing enzymes. The proposed experiments would provide a direct measure of  $T_1$ , the longitudinal relaxation time, and thus constitute a sensitive means for correlating environmental changes in the vicinity of the ion with changes in enzymatic behavior.

Of all the functions performed by protein molecules in living systems, perhaps the most remarkable is their catalytic role in almost all of the biochemical reactions basic to the life process. Proteins exhibiting such catalytic activity are called enzymes.<sup>1-3</sup>

Enzymes are rather exceptional catalysts in four respects. First, they are extraordinarily efficient; a typical enzymatic reaction, under optimal conditions, will proceed at a rate as much as  $10^8$  to  $10^{11}$  times that of the corresponding nonenzymatic reaction. Many reactions that ordinarily occur only under extreme conditions of temperature or pH proceed rapidly and quantitatively in nearly neutral solutions and at room temperature in the presence of the appropriate enzymes. Second, most enzymes are highly specific with regard to the nature of the reaction catalyzed and the structure of the substrate employed. Third, a broad spectrum of biologically important reactions is subject to

enzymatic catalysis; hydrolytic reactions, polymerizations, redox reactions, dehydrations, aldol condensations and free radical reactions are examples. Evidently, proteins are exceptionally versatile catalysts. Finally, enzymes are themselves subject to a variety of cellular controls. The rate at which they are synthesized, the final enzyme concentration, presence of both active and inactive forms of the enzyme as well as the rate and extent of interconversion between the two, are all controlled either genetically or by environmental factors.

The unquestionable importance of enzymes to the life process has stimulated vigorous research activity directed toward gaining a greater understanding of the manner in which they perform their catalytic function. The basic questions that must be answered concern the structure of the transition state and the nature of the intermediates formed during an enzymatic reaction. This in turn necessitates a knowledge both of the geometry of the substrate molecule and of the three-dimensional conformation of the enzyme. In view of the structural complexities of the enzymes, this appears to be a formidable task. However, the fact that the substrates utilized in most enzymatic reactions are small compared with the enzymes themselves, renders the problem somewhat more tractable since only a small fraction of the enzyme molecule can be near, or in direct contact with the substrate molecule in the enzyme-substrate complex. This leads to the concept of an active site which is envisioned as being the seat of enzymatic activity.

There is a growing body of evidence that some, and perhaps even

large portions, of the protein can be removed without impairment of the catalytic activity.<sup>3</sup> On the other hand, it has also been shown that certain changes in the bulk of the protein (e. g., denaturation) can completely destroy the enzymatic activity. This suggests that although the major part of the enzyme molecule is not directly involved in bond-breaking and bond-making, it is responsible for providing the "right" environment in the vicinity of the active site and for maintaining the structural integrity of the enzyme as a whole. Thus, the principal key to an understanding of the way in which enzymes function is a knowledge of the nature and behavior of the active site.

The remainder of the discussion will be limited to enzymes having paramagnetic metal ions at their active site, and to experimental techniques that utilize the paramagnetism, thus making them applicable specifically to this group of enzymes. Included in this group are many of the oxygenases, the cuproprotein enzymes and the metalloflavoproteins, to name a few. The importance of metals in enzymes has been recognized for many years<sup>4,5</sup> and the paramagnetic nature of many of the ions associated with the active sites of enzymes has been exploited in studies of their behavior using electron paramagnetic resonance spectroscopy.<sup>6-8</sup> A good deal of valuable information has been gained from these steady-state EPR studies and undoubtedly much more will be learned as additional resonances are found and investigated. The principal quantities available from these measurements are the g-value and information obtainable from the fine structure and hyperfine structure. It is proposed that additional information concerning the coupling of the ion to its environment and its relationship

to enzyme activity could be obtained from pulsed EPR measurements. These experiments would provide a direct measurement of  $T_1$ , the spin-lattice or longitudinal relaxation time, and would complement the above-mentioned steady-state experiments.

To demonstrate the principles<sup>9-12</sup> involved in such a study, we consider the behavior of an ion, in a state of total angular momentum  $J$ , subjected simultaneously to a static magnetic field,  $\vec{k} H_0$ , and to an rf field,  $\vec{i} H_1 \cos \omega t + \vec{j} H_1 \sin \omega t$ , which corresponds to a field  $H_1$  with a counterclockwise circular polarization. The static magnetic field splits the state  $J$  into  $2J+1$  levels labelled by  $M$  and the rf field induces transitions between these levels.

We begin by calculating the probability per second  $W_{M \leftrightarrow M+1}$  that the rf field causes a transition between any two levels  $M$  and  $M+1$ . The time-dependent perturbation felt by the ion as a result of the rf field is given by

$$\mathcal{H}'(t) = -\gamma \vec{J} \cdot \vec{H}_{\text{rf}} = -\gamma H_1 (J_x \cos \omega t + J_y \sin \omega t) \quad (\text{PV-1})$$

$$= \frac{\gamma H_1}{2} [J_+ \exp(-i\omega t) + J_- \exp(i\omega t)] \quad (\text{PV-2})$$

with

$$\gamma = g_J \beta / \hbar$$

and

$$J_{\pm} = J_x \pm i J_y$$

where  $g_J$  is the Lande' g-factor and  $\beta$  is the Bohr magneton. It follows from the golden rule that the transition rate is given by

$$W_{M \leftrightarrow M+1} = \frac{\pi \gamma^2 H_1^2 \hbar}{2} [J(J+1) - M(M+1)] \rho(E) \quad (\text{PV-3})$$

or, replacing  $\rho(E)$  by  $g(\nu - \nu_0)/2\pi\hbar$  where  $g(\nu - \nu_0)$  is the lineshape function,

$$W_{M \leftrightarrow M+1} = \frac{\gamma^2 H_1^2}{4} [J(J+1) - M(M+1)] g(\nu - \nu_0) \quad (\text{PV-4})$$

Equation (PV-4) has been derived for a circularly polarized field of the form  $\vec{H}_{\text{rf}} = (H_1 \cos \omega t, H_1 \sin \omega t, 0)$ . However, in the majority of experimental situations the field is linearly polarized in the form  $\vec{H}_{\text{rf}} = (H_1 \cos \omega t, 0, 0)$ . This field can be decomposed into two circularly polarized fields of opposite polarization

$$\vec{H}^+ = \left( \frac{H}{2} \cos \omega t, \frac{H}{2} \sin \omega t, 0 \right)$$

and

$$\vec{H}^- = \left( \frac{H}{2} \cos \omega t, -\frac{H}{2} \sin \omega t, 0 \right).$$

In the presence of a static magnetic field  $\vec{H} = \vec{k} H_0$ , the polarization of  $\vec{H}^-$  is opposite to the direction of precession of the ion's magnetic moment  $\vec{\mu}$  so that, if  $\omega = \omega_0$ , the torque exerted by  $\vec{H}^-$  or  $\vec{\mu}$  changes sign four times per cycle and to first order averages to zero when observed over times long compared to  $2\pi/\omega$ . Thus, by replacing  $H_1$  by  $H_1/2$ , Eq. (PV-4) becomes valid for a linearly polarized rf field of the form  $\vec{H}_{\text{rf}} = \vec{i} H_1 \cos \omega t$ .

In deriving Eq. (PV-4) it has been implicitly assumed that the levels  $M$  and  $M+1$  are homogeneously broadened. The treatment is only

slightly different for inhomogeneously broadened levels and, since the broadening mechanism is not of particular importance to the present discussion, we omit the details of that treatment.

Now imagine an ensemble of ions each like the one discussed above. Since the induced transition rate from M to M+1 is identical to that from M+1 to M, the population densities,  $N_M$  of level M and  $N_{M+1}$  of level M+1, are governed by the equations

$$\frac{dN_M}{dt} = -W(N_M - N_{M+1}) \quad (\text{PV-5})$$

and

$$\frac{dN_{M+1}}{dt} = W(N_M - N_{M+1}) \quad (\text{PV-6})$$

where  $W \equiv W_{M \leftrightarrow M+1}$ . Combining Eqs. (PV-5) and (PV-6) and defining  $n = N_M - N_{M+1}$  leads to

$$\frac{dn}{dt} = -2Wn \quad (\text{PV-7})$$

Equation (PV-7) describes the behavior of the population density difference  $n$  under the influence of an applied rf field in the absence of any coupling between the spin system and its environment.

Next, let us consider the effect of including some form of coupling between the spin system and its environment without dealing specifically with the mechanism by which it occurs. At thermal equilibrium,  $N_M^0$  and  $N_{M+1}^0$  are related by

$$\frac{N_{M+1}^0}{N_M^0} = \exp(-\gamma H_0 \hbar / kT) \quad . \quad (PV-8)$$

Denoting the probability per second that this "spin-lattice" coupling induces a transition from  $M$  to  $M+1$  by  $W\uparrow$  and from  $M+1$  to  $M$  by  $W\downarrow$ , the rate equation for  $N_M$ , in the absence of the rf field, is

$$\frac{dN_M}{dt} = W\downarrow N_{M+1} - W\uparrow N_M \quad . \quad (PV-9)$$

When the spin system is in thermal equilibrium with its surroundings,  $dN_M/dt = 0$ , so that

$$\frac{N_{M+1}^0}{N_M^0} = \frac{W\uparrow}{W\downarrow} \quad (PV-10)$$

or, using Eq. (PV-8) for the ratio  $N_{M+1}^0/N_M^0$ , we find

$$\frac{W\uparrow}{W\downarrow} = \exp(-\gamma H_0 \hbar / kT) \quad . \quad (PV-11)$$

Introducing  $N = N_M + N_{M+1}$ , and using the previous definition of  $\underline{n}$  allows us to rewrite Eq. (PV-9) in the form

$$\frac{dn}{dt} = N(W\downarrow - W\uparrow) - n(W\downarrow + W\uparrow) \quad . \quad (PV-12)$$

Upon defining  $n_0$  and  $T_1$  as

$$n_0 = N \left( \frac{W\downarrow - W\uparrow}{W\downarrow + W\uparrow} \right) \quad \text{and} \quad \frac{1}{T_1} = (W\downarrow + W\uparrow) \quad , \quad (PV-13)$$

Eq. (PV-12) becomes

$$\frac{dn}{dt} = - \frac{(n - n_0)}{T_1} . \quad (\text{PV-14})$$

$T_1$  is the spin-lattice, or longitudinal, relaxation time, i. e., the time constant with which the population density difference  $n$  regains its equilibrium value  $n_0$  after the spin system has been disturbed from equilibrium.

Now suppose the system is simultaneously undergoing transitions due to an applied rf field,  $H_1 \cos \omega t$ , and due to coupling with its environment. The difference in the population densities of levels  $M$  and  $M+1$  is then due to a competition between the thermal relaxation processes and the transitions induced by the applied field. This situation is described by the equation that results from combining Eqs. (PV-7) and (PV-14), viz.,

$$\frac{dn}{dt} = - \frac{(n - n_0)}{T_1} - 2Wn \quad (\text{PV-15})$$

which can be solved for  $n$  as a function of time. The solution is of the form

$$n(t) = n(0) \exp \left[ - \left( 2W + \frac{1}{T_1} \right) t \right] + \frac{n_0}{1 + 2WT_1} \left\{ 1 - \exp \left[ - \left( 2W + \frac{1}{T_1} \right) t \right] \right\} , \quad (\text{PV-16})$$

and contains a description of both the transient and the steady-state behavior of the system. By transient behavior we mean the response



of the system to sudden changes away from its dynamic equilibrium or steady-state condition.

The steady-state solution, obtained from Eq. (PV-16) in the limit as  $t \rightarrow \infty$ , has the form

$$n = \frac{n_0}{1 + 2WT_1} \quad (\text{PV-17})$$

which is just the solution of Eq. (PV-15) with  $dn/dt = 0$ , as it must be. It is easy to see that the net power density absorbed by the system is given by

$$\frac{P(t)}{V} = n(t) W \hbar \omega \quad (\text{PV-18})$$

where  $V$  is the volume of the sample. Substitution of Eqs. (PV-4) and (PV-17) into Eq. (PV-18) yields, for the steady-state power absorption per unit volume,

$$\frac{P}{V} = \frac{n_0 \hbar \omega \gamma^2 H_1^2 [J(J+1) - M(M+1)] g(\nu - \nu_0)}{16 + 2\gamma^2 H_1^2 T_1 [J(J+1) - M(M+1)] g(\nu - \nu_0)} \quad (\text{PV-19})$$

where  $H_1$  has been replaced by  $H_1/2$  to be consistent with the assumed linear polarization of the applied rf field. We observe that as  $H_1$  is increased the power absorption eventually levels off. This effect, known as saturation, occurs since increases in the transition rate  $W$  with increasing  $H_1$  [see Eq. (PV-4)] are accompanied by decreases in  $n$  [see Eq. (PV-17)]. Another phenomenon that sets in at sufficiently high power levels is the so-called power broadening of a transition.

As the incident rf power is increased the line begins to broaden due to the fact that the spins spend less and less time in the energy levels as a result of the greater and greater number of transitions that they make per second. When these two effects are combined, we conclude that the power absorbed at a particular value of the static field  $H_0$  must decrease as  $H_1$  is made larger and larger. That this is so, can be seen from the fact that the total power absorbed becomes constant and is spread over an increasingly broad line.

From Eqs. (PV-16) and (PV-18) it is a simple matter to obtain an equation for the power absorption per unit volume, including the transient behavior,

$$\begin{aligned} \frac{P(t)}{V} = n(0) W \hbar \omega \exp \left[ - \left( 2W + \frac{1}{T_1} \right) t \right] \\ + \frac{n_0 W \hbar \omega}{1 + 2W T_1} \left\{ 1 - \exp \left[ - \left( 2W + \frac{1}{T_1} \right) t \right] \right\} \quad (\text{PV-20}) \end{aligned}$$

where  $W$  is given by Eq. (PV-4) with  $H_1/2$  in place of  $H_1$ , and  $n(0)$  is the difference in population densities of levels  $M$  and  $M+1$  at  $t=0$ .

Evidently, if a perturbation is applied and then removed quickly (the time of removal will be designated as  $t=0$ ), the system will regain its state of dynamic equilibrium with a characteristic time constant  $\left( 2W + \frac{1}{T_1} \right)$ . This suggests a good way for measuring  $T_1$ .<sup>13, 14</sup> The resonance of interest is located and the dc field held constant at the resonant value. With the sample receiving a steady influx of low intensity microwaves at the frequency  $(\gamma H_0/\hbar)$ , a short intense pulse of microwaves of exactly the same frequency is applied. If the pulse is of

high enough intensity to cause saturation and power broadening of the transition, a sudden decrease in the intensity of the steady-state EPR signal will be observed. The relaxation of the system back to its original state of dynamic equilibrium will then result in the reappearance of the steady-state EPR signal with a time constant equal to  $T_1/(2WT_1 + 1)$ . By keeping the steady-state microwave intensity low, the denominator can be made equal to unity and the time constant is then just  $T_1$ .

The technique just described requires saturation of the transition of interest. The power necessary to achieve saturation depends upon the magnitude of  $T_1$ , more power being required when  $T_1$  is small than when it is large. With presently available microwave pulses<sup>14</sup> the technique can be straightforwardly applied to systems having spin-lattice relaxation times down to  $10^{-6}$  to  $10^{-7}$  sec. Somewhat more effort directed toward obtaining shorter, more intense microwave pulses might well be repaid in terms of increased time resolution, making it possible to measure even shorter  $T_1$  values.

In general,  $T_1$  depends upon the environment of the spin system and is thus sensitive to environmental changes. In the case of enzymes, where the local environment is probably provided by the bulk of the protein molecule,  $T_1$  might be expected to be sensitive to changes in temperature, pH, ionic strength, etc. of the surrounding medium since these are known to change the protein conformation. Enzymatic activity is strongly dependent upon the conformation of the protein also so that the likelihood that some correlation could be found between the magnitude of  $T_1$  and enzyme behavior seems pretty high.

REFERENCES

1. See, for example, P. D. Boyer, H. Lardy and K. Myrback, The Enzymes (Academic Press Inc., New York, 1959).
2. H. R. Mahler and E. H. Cordes, Biological Chemistry (Harper and Row, Publishers, New York, 1966).
3. J. B. Neilands and P. K. Stumpf, Outlines of Enzyme Chemistry (John Wiley and Sons, Inc., New York, 1955), 2nd ed.
4. O. Warburg, Heavy Metal Prosthetic Groups (Oxford University Press, Oxford, 1949).
5. Metals and Enzyme Activity, E. M. Crook, Ed. (Cambridge University Press, 1958).
6. G. Schoffa, Elektronenspinresonanz in der Biologie (Verlag G. Braun Karlsruhe, 1964).
7. Magnetic Resonance in Biological Systems, A. Ehrenberg, B. G. Malmström and T. Vänngård, Eds. (Pergamon Press, Oxford, (1967).
8. H. Beinert, "Complexities in Metal-Flavoprotein Function Revealed by EPR Spectroscopy" in Flavins and Flavoproteins, E. C. Slater, Ed. (Elsevier Publishing Co., New York, 1966), pp. 37-48.
9. See, for example, C. P. Slichter, Principles of Magnetic Resonance (Harper and Row, Publishers, New York, 1963).
10. M. Bersohn and J. C. Baird, An Introduction to Electron Paramagnetic Resonance (W. A. Benjamin, Inc., New York, 1966).

11. A. Carrington and A. D. McLachlin, Introduction to Magnetic Resonance (Harper and Row, Publishers, New York, 1967).
12. A. Yariv, Quantum Electronics (John Wiley and Sons, Inc., New York, 1967).
13. K. D. Bowers and W. B. Mims, Phys. Rev. 115, 285 (1959).
14. O. S. Leifson and C. D. Jeffries, Phys. Rev. 122, 1781 (1961).